



BUILDING A LOW EMISSIONS FUTURE

Great Artesian Basin Authigenic Carbonates as Natural Analogues for Mineralisation Trapping

CO2CRC Project 1.5.2

ANLEC Project 7-1011-0189

Authors: S.D. Golding¹, G.K.W. Dawson¹, J.K. Pearce¹, F. Farrajota¹, T. Mernagh², C.J. Boreham³, L.S. Hall³, T.J. Palu³ and S. Sommacal⁴

24 February 2016, CO2CRC Report No: RPT16-5497



¹ The University of Queensland, ² Australian National University, ³ Geoscience Australia, ⁴ FEI Australia

CO2CRC acknowledges and appreciates the strong relationships it has with industry, community, government, research organisations, projects and agencies in Australia and around the world.

Industry

ANLEC R&D (on behalf of ACALET)

Chevron Australia

Coal 21

Global CCS Institute

INPEX Browse Ltd

Shell Development (Australia) Pty Ltd

Community

Landowners near site

Moyne Shire

Nirranda South

Government

Australian Government:
Department of Education and Training

Australian Government:
Department of Industry, Innovation and Science

CarbonNet Project

NSW: Department of Industry

SA: The Department for Manufacturing, Innovation, Trade, Resources and Energy (DMITRE)

Victoria: Department of Economic Development, Jobs, Transport and Resources

WA: Department of Mines and Petroleum

Research

Australian National University
Charles Darwin University

CSIRO

Curtin University

Federation University Australia

Geoscience Australia

GNS Science

Imperial College London

Korea Institute of Geosciences & Mineral Resources

Lawrence Berkeley National Laboratory (LBNL)

UK CCS Research Centre

University of Adelaide

University of Edinburgh

University of Melbourne

University of NSW

University of Queensland

University of Western Australia

CO2CRC Limited

Level 1, 700 Swanston Street, bldg. 290

The University of Melbourne

Victoria 3010 Australia

www.co2crc.com.au

Reference: Golding, S, Dawson, G, Pearce, J, Farrajota, F, Mernagh, T, Boreham, C, Hall, L, Palu, T and Sommacal, S, 2016. Great Artesian Basin Authigenic Carbonates as Natural Analogues for Mineralisation Trapping. CO2CRC Limited, Melbourne, Australia, CO2CRC Publication Number RPT16-5497

© CO2CRC 2016

Unless otherwise specified, CO2CRC Ltd retains copyright over this publication. You must not reproduce, distribute, publish, copy, transfer or commercially exploit any information contained in this publication that would be an infringement of any copyright, patent, trademark, design or other intellectual property right.

Requests and inquiries concerning copyright should be addressed to Chief Operating Officer, PO Box 1182, Carlton VIC 3053 Australia. **p:** +61 3 8595 9600 | **e:** info@co2crc.com

Acknowledgements

The authors wish to acknowledge financial assistance provided to the CO2CRC by the Australian Government through its CRC program and through Australian National Low Emissions Coal Research and Development (ANLEC R&D). ANLEC R&D is supported by Australian Coal Association Low Emissions Technology Limited and the Australian Government through the Clean Energy Initiative.

Executive Summary

This project aims to support CO₂ storage projects in Australian onshore sedimentary basins through investigation of the controls on the formation of authigenic carbonates in low salinity, siliciclastic aquifers of the Great Artesian Basin (GAB) as a natural analogue of mineralisation trapping. Differentiating between carbonate formed via different mechanisms, and determining controls on the extent of authigenic carbonate formation could lead to options for engineered accelerated mineralisation in reservoirs. Key parameters derived from petrological and geochemical analyses of the carbonates were fed into a model for carbonate authigenesis within the GAB and the laboratory experiments designed to demonstrate processes of enhanced carbonate mineral trapping of CO₂ in Precipice and Hutton sandstone core.

More than 250 well completion reports were selected from among tens of thousands of publically available petroleum, coal seam gas and stratigraphic drilling records on the basis of spatial and geological coverage, the detail of included information, and type and availability of associated samples. The selected reports have been assessed in detail for the presence of significant carbonate mineralisation and samples of carbonate cemented sandstone as well as carbonate fracture mineralisation were taken from 50 localities. All Mesozoic units within the chosen wells were subject to sampling whether the strong carbonate cement was sporadic or extensive. The samples include both chipped and cored intervals.

Most of the 145 GAB cement and vein samples analysed for carbonate stable isotopes samples were calcite, with only 8 samples of siderite and 3 of dolomite in sufficient abundance for measurement. Overall, the samples defined very broad ranges of $\delta^{13}\text{C}$ and $\delta^{18}\text{O}$ values reflecting a variety of fluid origins and temperatures of precipitation. The main population of samples precipitated at a temperature of close to 80°C from high latitude meteoric groundwater, most likely during the Mesozoic Era when Australia was positioned much closer to the South Pole. A subset of Surat Basin carbonates likely precipitated from evolved meteoric fluids at temperatures well in excess of 120°C based on the oxygen isotope compositions and limited fluid inclusion data. Six of the wells containing the majority of these high temperature clastic vein and cement samples either lie on or adjacent to the Moonie-Goondiwindi and Burunga-Leichhardt thrust fault systems and subsidiary faults in the eastern Surat Basin. Movement on these older faults is thought to have continued throughout deposition of the Surat Basin succession and would have provided pathways for relatively hot fluid migration from the underlying Bowen Basin. A subset of Eromanga Basin carbonate samples from SW Queensland and NE South Australia also have fluid inclusion homogenisation temperatures that indicate formation at temperatures $\geq 120^\circ\text{C}$. Calculated oxygen isotope compositions of Eromanga mineralising fluids are consistent with mixing between groundwater of meteoric origin and evolved basinal brines possibly sourced from the underlying Cooper Basin, which is supported by the variable salinities up to 14.7 wt% NaCl equivalent.

The majority of Surat and Eromanga carbonates have calculated carbon isotope fluid compositions that are consistent with inorganic sources, specifically marine carbonate ($\delta^{13}\text{C}$ value of $\sim 0\text{‰}$) and magmatic/mantle carbon dioxide ($\delta^{13}\text{C}$ value of $\sim -5\text{‰}$). Twenty two samples from the Eromanga Basin and five samples from the Surat Basin are more depleted in ^{13}C , with calculated carbon fluid compositions less than -10‰ across the model temperature range. This necessarily requires an organic carbon source most likely associated with

local microbial degradation processes or thermal maturation and hydrocarbon generation at deeper levels. Six Surat Basin carbonates have ^{13}C -enriched fluid isotopic compositions $\geq 1\text{‰}$ that may suggest they have incorporated ^{13}C -enriched residual CO_2 from methanogenesis.

Cement and vein carbonates (mainly calcite) were tested for their elemental concentrations using partial leach methods. Rare earth element and Y abundances (REEY), fractionation between LREE and HREE, and anomalous concentrations of specific REE's can be indicative of mineral precursor compositions, mineralising fluid composition (including ligands involved) and the conditions of the environments through which the fluid migrated prior to precipitation. The majority of the cement and vein carbonates have at least two orders of magnitude greater total REE than biogenic marine carbonate and plot within the field of hydrothermal veins on a variation diagram of Yb/Ca versus Yb/La. High heat flux associated with basin extension is a possible reason for the apparent hydrothermal signatures of the majority of cements and vein samples tested. Convecting groundwater in such a regime can obtain hydrothermal characteristics, and extension also opens multiple fluid-flow pathways from depth up into shallow formations.

This study examined 76 doubly polished thin sections for fluid inclusions in carbonate cements and veins that would be suitable for fluid inclusion microthermometry. Although most samples contained abundant fluid inclusions in the quartz grains only 37 samples contained suitable inclusions in the carbonate cement. The study of fluid inclusions in diagenetic environments requires a great deal of caution as there are several problems commonly encountered that may lead to post-entrapment modification such as nucleation metastability and thermal equilibration. Where two-phase inclusions were observed we are confident that the homogenisation temperatures reflect true trapping temperatures. Fluid inclusion data provide evidence of relatively high temperatures of formation water for a subset of samples in the eastern Surat Basin, and the Eromanga Basin in the vicinity of the Queensland-South Australia border.

Our findings support the original hypothesis of this research that significant carbonate cementation in shallow clastic aquifer systems may form where fluids migrating vertically from deeper source rocks or leaky hydrocarbon traps mix with local formation water. However, the carbon isotope evidence for mixed carbon sources in the majority of cases may indicate that calcite precipitation occurs in the more basic and dilute region of the mixing zone where the migrating CO_2 is associated with hydrocarbons. The origin of the fluid inclusion CO_2 in Eromanga Basin carbonates is likely to be a combination of Permian overmature coals and inorganic sources based on carbon isotope composition. Gaseous hydrocarbons found in fluid inclusions in several Eromanga Basin samples are sourced from the underlying Cooper Basin. Eromanga fluid inclusion homogenisation temperatures are generally higher than maximum temperatures of the host strata and within the underlying sedimentary column, suggesting that the source of the fluids are deeper and hotter. Hydrothermal fluids from beneath the Cooper Basin entrain Permian-sourced gaseous hydrocarbons and CO_2 along the migration pathway to the Eromanga Basin host formations. Fluid inclusion homogenisation temperatures within Eromanga Basin carbonate cements are generally lower away from the Cooper Basin edge that may indicate longer fluid migration distances and more cooling. In a similar way, higher temperature carbonate cements in the eastern Surat are largely restricted to the Precipice Sandstone, Evergreen Formation sandstones and Hutton Sandstone that suggests the Walloon Subgroup acted as a regional seal

with hydrothermal fluids sourced from the underlying Bowen Basin focused into the more permeable sandstone-dominated units.

The availability of aqueous divalent cations for precipitation of dissolved CO₂ as carbonate minerals and the dissolution of CO₂ can be rate-limiting steps in the process of mineral trapping, in addition to (for example) processes that produce sufficient local alkalinity for precipitation to occur. Experiments and modelling work indicate the reaction of muscovite/biotite from the mudstone baffle in the Precipice Sandstone would provide Fe and Mg for mineral trapping of CO₂ as siderite and ankerite with precipitation of kaolinite. The co-injection of low concentrations of SO₂ with CO₂ enhanced silicate dissolution and subsequent carbonate mineral precipitation. In a chlorite-rich section of the Hutton Sandstone, co-injection of SO₂ with CO₂ resulted in mainly alteration of chlorite with precipitation of siderite, ankerite, magnesite/dolomite and kaolinite. Alternatively, direct addition of dissolved ions would both increase the available cations for precipitation and potentially buffer the pH to near-neutral or even alkaline conditions if the brine was of sufficient bicarbonate content. Experiments reacting a quartzose Precipice Sandstone core with CO₂ and a Ca-bicarbonate rich saline brine resulted in mineral trapping as calcite and dolomite precipitation in the pore space. Both brine mixing and SO₂ co-injection experiments indicate mineral precipitation might be enhanced if fluids moved rapidly to lower temperature and pressure regions.

Simulations of CO₂ injection either with groundwater or with coal seam gas (CSG) brine diluted in groundwater and two different quartzose Precipice Sandstone reservoir mineralogies (with either minor K-feldspar or andesine plagioclase) were performed. The CO₂-sandstone-groundwater simulations produced an overall net increase in dissolved CO₂ relative to that originally injected, due to dissolution of minor calcite, with some precipitation of ankerite. Both of the CO₂-sandstone-brine models resulted in calcite precipitation. With the andesine plagioclase mineralogy in place of K-feldspar, five times more calcite and almost an order of magnitude more kaolinite was precipitated.

Possible avenues for further investigation include the co-injection of CO₂ with coal seam gas waste water or desalination brine-concentrate to accelerate carbonate formation and the effects of gas compositions with low levels of impurities.

Table of Contents

Executive Summary	ii
Table of Contents.....	v
Index of Figures	vii
Index of Tables	xii
1. Introduction	14
1.1. Overview of work program.....	14
1.2. Background.....	14
1.3. Parameters affecting carbonate precipitation.....	16
1.3.1. CO ₂ -fluid-rock interaction processes.....	16
2. Methods	23
2.1. Sampling strategy	23
2.2. Sample types.....	23
2.3. Analytical methods.....	26
2.3.1. X-ray diffraction (XRD)	26
2.3.2. Carbonate stable isotopes	26
2.3.3. Partial leaching methods.....	26
2.3.4. Major element analysis.....	27
2.3.5. Trace and minor element analysis.....	27
3. Analytical Results and Discussion.....	28
3.1. XRD analyses.....	28
3.2. Carbonate stable isotopes.....	31
3.3. Carbonate acid leaching results	43
3.3.1. Major elements	44
3.3.2. Rare earth elements and yttrium (REEY).....	53
3.4. Fluid inclusion studies.....	68
3.4.1. Fluid inclusion temperatures and salinity analyses.....	68
3.4.2. Fluid inclusion gases	74
3.4.3. Bulk crush-leach analyses	77
3.5. Eromanga Basin burial history model.....	82
3.5.1. Geological model.....	82
3.5.2. Burial history and thermal maturity modelling.....	82
3.5.3. Fluid inclusion homogenisation temperatures and host rock maturity	98
3.6. Summary discussion	100
3.6.1. Discussion of results of natural analogues study	100
3.6.2. Model for carbonate authigenesis in the GAB	102
4. Laboratory corroboration of accelerated carbonate mineralisation.....	106
4.1. Core characterisation	108
4.1.1. Fluid-rock interaction experiments.....	108
4.1.2. Brine mixing experiment.....	111
4.2. Experimental methods	112
4.2.1. Fluid-rock interaction experiments.....	112
4.2.2. Brine mixing experiment.....	113
4.3. Post-reaction core characterisation	113
4.3.1. Fluid-rock experiments	113
4.3.2. Brine mixing experiment.....	116
4.4. Water chemistry	118
4.4.1. Fluid-rock interaction experiments.....	118
4.4.2. Brine mixing experiment.....	123
4.5. Discussion.....	125
5. Model Scenarios of CO₂ Injection with Mineralisation Trapping.....	127
6. Conclusions.....	130
7. Recommendations for Future Work.....	132
8. References	133
Appendix 1: Samples collected.....	149

Appendix 2: Core sample photographs.....	158
Appendix 3: XRD mineralogy.....	178
Appendix 4: Normalised REEY data	183
Appendix 5: Fluid inclusion results.....	190
Appendix 6: FEI characterisation of samples WW1_Precipice_1212m and WW1_Hutton_724m pre and post batch reactor experiments.....	206
1 Executive summary	209
2 Project workflow	211
3 Results and Discussion	212
3.1 Scoping scan imaging in 3D by μ CT	212
3.2 Before reaction imaging of sub-plug in 3D by μ CT at the pore-scale	213
3.3 Segmentation of before reaction tomograms into X-ray distinct components and quantification in 3D	215
3.4 SEM imaging and mineral mapping by automated quantified SEM-EDS before reaction	217
3.5 Geochemical reactivity studies at University of Queensland	220
3.6 After reaction imaging of sub-plug in 3D by μ CT at the pore-scale and mineral segmentation into X-ray distinct components.	221
3.7 After reaction SEM imaging and mineral mapping by automated quantified SEM- EDS..	223
3.8 Investigation and quantification in 3D of changes due to CO ₂ :brine:rock interactions	225
4 Conclusions	228

Index of Figures

Figure 1: Schematic representation of the change of trapping mechanisms and increasing CO ₂ storage security over time (modified after Class <i>et al.</i> , 2009; IPCC, 2005).	18
Figure 2: SEM examples of A) plagioclase (labradorite), 1043.7m and B) biotite/chlorite, 981.24 m, in the Evergreen Formation, West Wandoan 1 core, Surat Basin.	19
Figure 3: SEM image of associated chlorite and siderite, in the Evergreen Formation at 897 m, Chinchilla 4 core, Surat Basin.	19
Figure 4: Examples of the difference in dissolved cation concentrations due to aqueous reactions with pure CO ₂ or mixed high concentration CO ₂ -SO ₂ in A) Berea Sandstone (Dawson <i>et al.</i> , 2015) and B) dissolved Fe from Chinchilla 4 Precipice Sandstone core from 1092 m (modified after Pearce <i>et al.</i> , 2013a; Pearce <i>et al.</i> , 2015c).	20
Figure 5: SEM image of plagioclase corroded after reaction with impure CO ₂ (high impurity concentrations), the Evergreen Formation 1043.7 m, West Wandoan 1 core.	21
Figure 6: Maps of the Eromanga (A) and Surat (B) basins showing locations of sampled sites.	24
Figure 7: For significantly calcite-cemented zones (>100 m thick), there is an inverse correlation between the proportion of cemented samples containing calcium-plagioclase minerals and their calcite content as determined by semi-quantitative XRD analysis.	29
Figure 8: a) Carbon and oxygen isotope compositions of Surat and Eromanga carbonate cements and veins; b) samples from significant carbonate cemented intervals (>100m net thickness of calcite cement). Modified after Golding <i>et al.</i> (2014).	36
Figure 9: Calcite cement (grey) with congruent twinning (straight lines) and extinction across section when viewed with cross-polarised light in quartzose sandstone sample #86, Surat Basin. The majority of the grains cemented by the calcite are quartz.	53
Figure 10: Two examples of ligands (N) bound to a metal cation (M) in solution. Modified after Bhalgat <i>et al.</i> (2006).	54
Figure 11: The different kinds of carbonate collected from A) the Eromanga Basin and B) the Surat Basin. Variation diagram modified after Möller (1983).	59
Figure 12: Similar normalised REE concentrations of two cements sampled up to 42m apart (vertically) within a given formation of four different wells: A) Westbourne Formation calcites from Connemara 1, Eromanga Basin, B) Murta Formation mixed carbonates from Dullingari 37, Eromanga Basin, C) Cadna-Owie Formation calcites from Mirintu 1, Eromanga Basin, and D) Walloon Coal Measures mixed carbonates from Moonie Corner 1, Surat Basin.	60
Figure 13: Two cement samples from different formations, one a calcite and the other mixed carbonate, displaying similar normalised REE concentrations to each other, in wells: A) Strathpine 1 - the REE concentrations progressively diverge from each other with increasing REE atomic number; B) West Wandoan 1 - the concentrations of Lu, Yb, and Tm are identical but then REE concentrations diverge with decreasing atomic number.	60
Figure 14: Veins from different formations with very similar normalised REE patterns: A) mixed carbonate veins of the Evergreen Formation and Walloon Coal Measures from Chinchilla 4, Surat Basin; B) calcite and mixed carbonate veins of the Allaru Mudstone, Mackunda Formation, and Wallumbilla Formation from Connemara 1, Eromanga Basin.	62
Figure 15: Two different calcite samples, one a vein and one a cement, from different formations of the same well and yet displaying similar PAAS-normalised REE patterns. The samples have similar La concentration, +ve Eu anomalies and are MREE-enriched, but the REE patterns diverge towards the HREE.	63

Figure 16: Normalised REE concentration patterns of calcite and mixed carbonate veins from Blackall 2 that show overlapping partial similarities to each other.....	63
Figure 17: Calcite samples, one cement the other a vein, from different formations in wells separated by 750km, displaying similar normalised REEY concentration patterns.	65
Figure 18: Fluid inclusion homogenisation temperatures for GAB carbonate cements and veins. 73	
Figure 19: Locations of sample sites plotted on a map of thermal anomalies at 5 km depth; modified after Chopra and Holgate (2005).	74
Figure 20: Location map showing the majority of the wells sampled for fluid inclusion gases in the Eromanga Basin. Note: open circles show wells used in 1D modelling; colour scale is depth in metres to base of Cooper Basin. Cooper Basin outline is from Stewart <i>et al.</i> (2013).	75
Figure 21: Carbon isotopes for CO ₂ and C ₁ -C ₅ for FI gases, together with representative natural gases from the Cooper Basin and a natural gas from the Eromanga Basin.....	78
Figure 22: Plot of carbon isotopes of ethane versus methane (C2-C1 bottom curve) and ethane versus propane (C2-C3 top curve). The calculated curves are the modelled carbon isotopic composition of instantaneously generated natural gas from Type III kerogen typical of Cooper source rocks (Kuske <i>et al.</i> , 2015) at a modelled heating rate of 2°C per million years used as 'defaults' in the GORIsotopes2 version 2.4.9.0 software. Note: the samples plotting below the C2-C1 isotope curve most likely reflect an additional and variable input of isotopically light biogenic methane.	78
Figure 23: Plot of hydrogen isotopes of ethane versus methane (C2-C1 bottom curve) and ethane versus propane (C2-C3 top curve). The calculated curves are the modelled hydrogen isotopic composition of instantaneously generated natural gas at a modelled heating rate of 2°C per million years. GORIsotopes2 version 2.4.9.0 software defaults were used except for a user-defined hydrogen isotopic composition of precursors to methane, ethane and propane of -190 ‰, -190 ‰ and -180 ‰, respectively.	79
Figure 24: Successful bulk crush-leach results showing basin-dependent trends of increasing Na and K with dissolved Ca concentration.	81
Figure 25: Stratigraphy of the Cooper Basin showing depositional facies, conventional petroleum occurrences and identified source rocks (modified after Carr <i>et al.</i> , 2016; Hall <i>et al.</i> , 2015c). 85	
Figure 26: Eromanga Basin stratigraphy, depositional environment, thickness and petroleum occurrences (from DSD, 2015). Stratigraphy based upon Moussavi-Harami (1996b). Refer to DSD for further information on shows and indications.	86
Figure 27: Stratigraphy and Genesis-derived 1D burial history model for Dullingari-36 showing low maturity for whole of well succession.	91
Figure 28: Eromanga and Cooper stratigraphy, temperature and vitrinite reflectance used to constrain the Genesis-derived 1D model for Dullangari-1. Note: modelled temperature is the black line (middle); modelled vitrinite reflectance (right) using the two default models; blue line is the kinetic model of LLNL and the black line is an ARCO empirical model. Note: Hall <i>et al.</i> (2015a,b,c,d) generally observed that the LLNL model gave a better fit between observed and calculated (modelled) vitrinite reflectance for Ro _{calc} < 2-3% while the ARCO model was used in wells at much higher maturities (also refer to Figure 33).	92
Figure 29: Modelled vitrinite reflectance through time for the base of Cooper Basin (top) and base of Murta Formation, Eromanga Basin (bottom) in Dullingari-1.	93
Figure 30: Temperature map at present day for base of Cooper Basin derived from the from multi-1D petroleum model.....	94
Figure 31: Temperature map at 90 Ma for base of Cooper Basin derived from the from multi-1D petroleum model.	95

Figure 32: Temperature map at 0 Ma for Top Westbourne Formation derived from the from multi-1D petroleum model.	96
Figure 33: Temperature map at 90 Ma for Top Westbourne Formation derived from the from multi-1D petroleum model.	97
Figure 34: Modelled vitrinite reflectance versus temperature for Dullingari-1 and Merrimelia-32 using the Genesis-derived 1D burial history model and the calculated vitrinite reflectance. Note: Kinex-derived model for a simple burial history 3°C/Ma and the calculated vitrinite reflectance using the LLNL kinetic model.	99
Figure 35: Chlorite and siderite alteration of probable biotite grain (1), adjacent to much less altered phlogopite grain (2) with a sample of the Evergreen Formation, 897 m, Chinchilla 4 core, Surat Basin. Modified after Dawson <i>et al.</i> (2014).	101
Figure 36: Upper Precipice Sandstone (1165 m), West Wandoan 1 core, Surat Basin. Plagioclase feldspar grains, bottom one almost completely altered to clay and centre grain undergoing replacement by calcite with congruent twinning (bright colours). Calcite is also present as cement between framework grains, precipitated amongst clay palettes. XPL x100 (Dawson <i>et al.</i> , 2014).	101
Figure 37: A) Structural elements map of the Surat Basin showing sample locations relative to major faults, subsurface solid geology of the Bowen Basin beneath the Surat Basin, and the location of conceptual cross-section A-A'. B) Conceptual cross-section A-A' of the Moonie area showing the proposed fault pathway for ascending brines. Structural elements map and basement faults (red lines) modified from Babaahmadi <i>et al.</i> (2015, 2016). Dashed red line=inferred fault. 25x vertical exaggeration. Modelled horizons are from Sliwa (2015).	105
Figure 38: Schematic of an ideal reservoir system optimised for CO ₂ storage, showing CO ₂ rich fluid (blue) baffled in an area of low vertical permeability. Modified after Watson and Gibson-Pool (2005).	107
Figure 39: Selected SEM images of Precipice 1207.6 m. A) Surface view of cube A1, B) surface view of cube A2 both with dark organic matter and bright muscovite/biotite. C) Fe-rich muscovite/biotite and sphalerite (cube A1), D) Fe-rich muscovite and kaolinite (cube A1), E) fine grained kaolinite (cube A2).	109
Figure 40: Selected SEM images of Hutton 724 m. A) Surface view with bright zircon and Ti-oxide (rutile) grains and some open porosity, B) kaolin, C) bright zircon and Fe-rich silicate, D) Fe-Mg chlorite.	109
Figure 41: Pre reaction QEMSCAN images of A) Hutton 724 m, and B) Precipice 1212 m, and colour key. Modified from Appendix 6.	111
Figure 42: Selected SEM images of Precipice 1212 m. A) Surface view with quartz framework grains and open porosity (and bright zircon). B) Muscovite with traces of Fe and Mg signature. S, Na and Cl elemental signatures were also present. C) Muscovite and Ti-oxide. D) Amorphous silica/altered quartz and bright KCl.	112
Figure 43: Precipice 1207.6 m core block photos, left before reaction, centre post reaction with CO ₂ -brine (block A1), right post reaction with SO ₂ -CO ₂ -brine (block A2), note red-brown colouration.	114
Figure 44: SEM images of Precipice 1207.6 m after reaction A-B) with CO ₂ -brine, and C-D) with SO ₂ -CO ₂ brine. Note fine-grained bright Fe-rich precipitates on clays after reaction with SO ₂ -CO ₂ -brine in C-D.	114
Figure 45: Hutton 724 m sample photos, left block and sub-plug before reaction, right offcut and block post reaction with SO ₂ -CO ₂ -brine, note brown colouration.	115

Figure 46: SEM-EDS of Hutton 724 m post reaction. A) Zircon, quartz and Fe-rich silicate surfaces. B) Fe-rich chlorite booklets appeared altered with a reduced Fe elemental signature. C) Fe-rich precipitates with Cr and Ni signatures on kaolinite and D) EDS spectrum of bright precipitate in D (note technical issues resulted in no carbon peak).....	115
Figure 47: High resolution SEM image (left) and associated QEMSCAN mineral maps (center) at the same scale, with the colour legend (right). Hutton 724 m post reaction (modified from Appendix 6).....	116
Figure 48: SEM-EDS of Precipice 1212 m post reaction. A) and B) muscovite with fine-grained bright precipitates. C) and D) EDS spectra of precipitates in A) and B) indicating Ca content (note C peak low intensity due to technical issues).....	117
Figure 49: High resolution SEM image and QEMSCAN mineral map of Precipice 1212 m post reaction with calcite and dolomite in pore space (modified from Appendix 6).....	117
Figure 50: Water chemistry during CO ₂ -brine or SO ₂ -CO ₂ -brine reaction of Precipice 1207.6 m. A) Solution pH, B) solution electrical conductivity, C) dissolved concentrations of total carbon (TC), inorganic carbon (IC), and total organic carbon (TOC), D) dissolved inorganic carbon converted to bicarbonate concentration.....	118
Figure 51: Water chemistry during CO ₂ -brine or SO ₂ -CO ₂ -brine reaction of Precipice 1207.6 m. A) Dissolved Ca concentration, B) dissolved Mg concentration, C) dissolved Fe concentration, D) dissolved Mn concentration.....	119
Figure 52: Concentrations of As and Pb during A-B) CO ₂ -brine or SO ₂ -CO ₂ -brine reaction of Precipice 1207.6 m, and C-D) SO ₂ -CO ₂ -brine reaction of Hutton 724 m and blank experiment, note the different scales on the y axis.....	120
Figure 53: Modelled mineral volume change during reaction of Precipice 1207.6m with A) pure CO ₂ -brine, B) SO ₂ -CO ₂ -brine over 10 years.....	121
Figure 54: Water chemistry during SO ₂ -CO ₂ -brine reaction of Hutton 724 m and blank experiment. A) Solution pH, B) solution electrical conductivity, C) dissolved concentrations of total carbon (TC), inorganic carbon (IC), and total organic carbon (TOC), D) dissolved IC converted to bicarbonate concentration.....	122
Figure 55: Water chemistry during SO ₂ -CO ₂ -brine reaction of Hutton 724 m, and blank experiment. A) Dissolved Ca concentration, B) dissolved Mg concentration, C) dissolved Fe concentration, D) dissolved Mn concentration.....	122
Figure 56: Modelled mineral volume change over 10 years reaction of Hutton 724 m core with SO ₂ -CO ₂ -brine.....	123
Figure 57: Water chemistry during CO ₂ -complex brine reaction of Precipice 1212 m core, and last point after depressurisation. A) Dissolved Ca concentration, B) dissolved Mg concentration, C) dissolved Fe concentration, D) dissolved Sr concentration, E) dissolved Al concentration, and F) dissolved Cr concentration.....	124
Figure 58: CO ₂ reacted in groundwater with A) Precipice Sandstone model mineralogy and B) the same Precipice mineralogy in (A) with andesine plagioclase (labelled Al ₄₀ An ₆₀) instead of K-feldspar. Vertical scale is truncated for clarity, and the y-axis scales are different to make the mineral components legible.....	128
Figure 59: CO ₂ reacted in a mixture of brine and groundwater with A) Precipice Sandstone model mineralogy with K-feldspar and B) the same Precipice mineralogy in (A) but with andesine plagioclase in place of K-feldspar. The y-axis scales are different to make the mineral components legible.....	128

Figure 60: Tomogram images (X, Y, Z, left to right) from scoping scans of 724 (top) and 1212 (bottom) samples; red polygon indicates approximate location and size of sub-plug extracted for high resolution imaging study.	212
Figure 61: Vertical (X-top, Y-bottom) and horizontal (Z-right) plane images from high resolution 3D μ CT tomograms of sub-plugs 724 and 1212, before reaction.	214
Figure 62: Sample 724 and 1212 vertical (X-left) and horizontal (Z-right) images from high resolution tomograms (row 1 & 3) and mineral segmented images (row 2 & 4), before reaction.	216
Figure 63: SEM-registered images of samples 724 and 1212 from (left to right): tomogram, mineral segmentation, SEM and QEMSCAN® (see Table 40 for QEMSCAN® legend), before reaction.	218
Figure 64: Sample 724: SEM image (left) and zoom-in area (centre) showing an altered K-feldspar grain; image to the right shows the grain's mineral map as analysed by QEMSCAN® (see Table 40 for mineral map legend); red polygon in left image shows location of zoom-in area.	219
Figure 65: Diagram of the interior of the batch reactor vessel (Modified from Pearce <i>et al.</i> , 2015).	221
Figure 66: Sample 724 and 1212 vertical (X-left) and horizontal (Z-right) images from high resolution tomograms (row 1 & 3) and mineral segmented images (row 2 & 4), after reaction.	222
Figure 67: SEM-registered images of samples 724 and 1212 from (left to right): tomogram, mineral segmentation, SEM and QEMSCAN® (see Table 42 for QEMSCAN® legend), after reaction.	224
Figure 68: Sample 724: horizontal selected plane images (left) of before and after reaction tomograms and (right) zoom-in areas highlighting differences caused by reaction experiments; red polygon in left images shows location of zoom-in areas.	226
Figure 69: Sample 1212: horizontal selected plane images (left) of before and after reaction tomograms and (right) zoom-in areas highlighting differences caused by reaction experiments; red polygon in left images shows location of zoom-in areas.	226

Index of Tables

Table 1: Solution chemistry effects on calcite precipitation rates and composition.	22
Table 2: Coordinates of Eromanga Basin samples.	25
Table 3: Coordinates of Surat Basin samples.	25
Table 4: Summary of the number and type of carbonate-bearing samples versus samples lacking carbonate analysed via semi-quantitative XRD.	29
Table 5: Distribution of carbonates other than calcite.	29
Table 6: Feldspar distribution amongst the XRD-screened samples.	30
Table 7: Ca-bearing plagioclase feldspar distribution amongst the XRD-screened samples.	30
Table 8: Ca-bearing plagioclase feldspar distribution amongst XRD-screened samples taken from significantly carbonate cemented intervals (>300 feet or 100 metre net thickness of cemented units).	30
Table 9: Quartz, kaolin, and total phyllosilicate distribution amongst the XRD-screened samples.	30
Table 10: Mica/illite and chlorite/smectite distribution amongst the XRD-screened samples.	31
Table 11: Carbonate carbon and oxygen stable isotopes for Eromanga Basin calcites, dolomites and siderites – both cemented sandstone and fault-mineralisation intervals.	32
Table 12: Carbonate carbon and oxygen stable isotopes for Surat Basin calcites and siderites from cemented and veined sandstone intervals.	37
Table 13: Carbonate stable isotope modelling for Eromanga Basin samples. Grey shading shows most likely fluid oxygen and carbon isotope compositions based on modelling and available fluid inclusion data; horizontal green shading highlights ¹⁸ O-enriched samples.	39
Table 14: Carbonate stable isotope modelling for Surat Basin samples. Grey shading shows most likely fluid oxygen and carbon isotope compositions based on modelling and available fluid inclusion data; horizontal green shading highlights ¹⁸ O-enriched samples.	41
Table 15: Cemented sandstones elemental concentrations* (ppm) and Co/Ni within acid-leached portions. For colour coding refer to the legend at the bottom of the table.	45
Table 16: Vein elemental concentrations* (ppm) within acid-leached portions. For colour coding refer to the legend at the bottom of the table.	47
Table 17: Carbonate cement relative elemental abundances (% _{Ca+x}). Grey shading denotes high relative abundances for individual elements (% _{Ca+x}) with respect to the overall data population for that element.	49
Table 18: Carbonate vein relative elemental abundances (% _{Ca+x}). Grey shading denotes high relative abundances for individual elements (% _{Ca+x}) with respect to the overall data population for that element.	50
Table 19: Cement rare earth element (REE) concentrations* (ppm), Total Ln, and Eu/Sm within acid-leached portions. Colour legends are at the bottom of the table.	56
Table 20: Vein rare earth element (REE) concentrations* (ppm), Total Ln, and Eu/Sm within acid-leached portions. Colour legends are at the bottom of the table.	57
Table 21: Interpretations of cement sample normalised REE ratio and anomaly data. The top row indicates the significance of the shaded sections*.	66
Table 22: Interpretations of vein sample REE ratio and REE anomaly data.	67
Table 23: Eromanga Basin summary fluid inclusion data (temperature and salinity). Grey-shaded samples contain calcite veins.	69
Table 24: Surat Basin summary fluid inclusion data (temperature and salinity). Grey-shaded samples contain calcite veins.	71
Table 25: Summary of carbonate fluid inclusion data for 35 drill core and chip samples of carbonate cements and veins ¹	74
Table 26: Carbon isotope composition of Eromanga fluid inclusion samples; * $\delta^{13}\text{C}$ calcite - $\delta^{13}\text{C}$ CO ₂	76
Table 27: Calculated maturity at base of selected formations and fluid inclusion gas maturity.	80
Table 28: Bulk crush-leach results (ppb) normalised per gram of powder for a 10 mL water-soak per sample.	81

Table 29: Cooper–Eromanga–Lake Eyre regional 3D model horizons with associated ages. As lithostratigraphic units have been used, some horizons are time transgressive and as a result assigned ages are an approximate estimate only. In the 3D model, the Cuddapan Formation is included in the base Eromanga succession as it is not present over large parts of the study areas and only reaches a maximum thickness of ~ 50 m.....	83
Table 30: Cooper–Eromanga–Lake Eyre stratigraphy and associated lithologies. All formations are included in the 1D burial history models. However some simplifications have been made when grouping stratigraphic units in the Eromanga Basin in the 3D model that do not take into consideration the time transgressive nature of deposition. Lithology mixes also vary spatially.	87
Table 31: Major unconformities with estimated age ranges and erosion amounts, included in the burial history modelling. Note the top Namba and Eyre unconformities are not included in the 3D model as the 1D modelling results show they have negligible impact on the burial and thermal histories.....	89
Table 32: Mineral components of polished sub-plug slices by QEMSCAN (area %) pre and post reaction, modified from Silvano <i>et al.</i> , Appendix 6.	110
Table 33: Initial brine composition for the groundwater mixing experiments (TDS was not measured).....	113
Table 34: Input mineral volume % and surface areas used in Geochemist Workbench (version 9) models.	121
Table 35: Fluid parameters of the input groundwater and brine–groundwater mixtures used for GWB modelling, with the undiluted brine composition for comparison.	129
Table 36: Mineral parameters used in the GWB models.	129
Table 37. Description of samples selected for geochemical reactivity study from scoping scan images.	213
Table 38. Description of samples selected for geochemical reactivity study from high resolution sub-plug images.	214
Table 39. Volume percentages of X-ray distinct components derived from segmentation of before reaction sub-plug scale images; where, Framework grain_1: mostly quartz + Na-plagioclase for 724, quartz for 1212; Framework grain_2: mostly K-feldspar; Lower density clay: mostly kaolinite; Higher density ‘clays’: mostly chlorite for 724, illite + muscovite for 1212; High density grain_1: mostly rutile; High density grain_2: mostly zircon.....	217
Table 40. Modal mineralogies (area%) of investigated polished sections of samples 724 and 1212, before reaction. QEMSCAN® legend is shown in the second column from left.....	219
Table 41. Volume percentages of X-ray distinct components derived from segmentation of before and after reaction same volume of sub-plug scale images; where, Framework grain_1: mostly quartz + Na-plagioclase for 724, quartz for 1212; Framework grain_2: mostly K-feldspar; Lower density clay: mostly kaolinite; Higher density ‘clays’: mostly chlorite for 724, illite + muscovite for 1212; High density grain_1: mostly rutile; High density grain_2: mostly zircon.	223
Table 42. Modal mineralogies (area%) of investigated polished sections of samples 724 and 1212, before and after reaction. QEMSCAN® legend is shown in the second column from left. Note that the section investigated after reaction is not the same that was investigated before reaction.	225

1. Introduction

1.1. Overview of work program

The primary focus of this project is development of a better understanding of the controls on the formation of authigenic carbonates in low salinity, siliclastic aquifers of the Great Artesian Basin (GAB) as a natural analogue of mineralisation trapping in CO₂ sequestration. The objective is to determine whether there are differences in groundwater composition or reservoir conditions that encourage mineralisation of CO₂, and if so, then what are the key parameters that we may be able to use to engineer carbonate precipitation on observable timescales. This would maximise the security of long-term storage within CO₂ reservoirs and also could serve as a mitigation option in the event of CO₂ leakage from the primary storage reservoir.

Following a literature study on the general controls on carbonate mineral precipitation (Golding *et al.*, 2013b), well completion reports were assessed for the presence of significant carbonate cement and veins available for sampling. Sampling was spread spatially across the GAB, with carbonate mineralisation found within the majority of geological formations present. Sample depths given in this report are those that were written on the cores or sample storage bags in the case of drill cuttings and so are therefore driller's depths, with the datum used (e.g., KB or RT) varying slightly from well to well due to changing standards throughout time and between operators. The work program has included stable and radiogenic isotopes, trace elements, and fluid inclusion analyses of carbonate and other cements, in addition to whole-rock XRD and microscopic (petrographic and SEM) studies. Parameters derived from analyses of the carbonates feed into an overall model of carbonate authigenesis within the GAB, and inform the laboratory based exploratory experiments that seek to demonstrate processes of enhanced carbonate mineral trapping of CO₂.

1.2. Background

The Queensland and South Australian regions of the Mesozoic Surat-Eromanga basin system plus overlying Cenozoic basins collectively form the major part of what has historically been called the Great Artesian Basin. This group of basins overlie the Pennsylvanian to Early Triassic Bowen-Galilee and Cooper basins as well as older sedimentary basins, metamorphic and igneous units. Abundant coal, oil, and gas accumulations occur within the entire basin system. Coal units are generally thin and not laterally continuous, thermogenic and biogenic gas is derived from both coals and conventional sources, and oil tends to be associated with structures that have been reactivated since primary migration. Whilst mostly a relatively closed intracratonic system, the basins have experienced marine incursions at times, most significantly during the Cretaceous; limestone occurs alongside paralic coal measures in some areas (Adamson and Dorsch, 1988; Anon., 1964, 1982, 1984, 1991, 1994, 2001; Baily, 1996; Battrick *et al.*, 1985; Brown, 1984; Burnett and Darling, 1986; Dabney, 1965; Espiritu and James, 1999; Estensen *et al.*, 1986; Freeman, 1967; French, 1989; Green, 1963; Haak, 1999; Hall and Gagen, 1989; Harrison and Higginbotham, 1964; Jenkins, 1984; Knauer and Delbaere, 1992; Kyranis, 1963; Laing, 1966, 1967; Longley and Batt, 1985a, b; Lowman, 2003a, b; Moore, 1981; Nguyen *et al.*, 1996; O'Neill, 1985; Ostler, 1989; Pyle, 1965a, b, 1966a, b; Pyle *et al.*, 1963; Pyle and Dabney,

1963; Robbie and Mitchell, 1996; Salomon *et al.*, 1990; Slijderink, 1998; Surka and Rouse, 1984; Taylor, 1985; Thornton, 1984; Thornton and Elliott, 1982; Titheridge, 2010; Tolliday and How, 1986).

With the exception of petroleum and coal seam gas fields, structures (especially faults) tend to be poorly mapped throughout the basin system due to deep Cenozoic sediments covering most of the basin units, young faults tending to be too discontinuous to effectively resolve by seismic surveys (when available), and a general lack of seismic data in currently non-resource prospective areas. Whilst large-scale structural geologic data (e.g., folds and faults) are available in digital format for Queensland, digitized smaller-scale company structure maps have not been made publically available online, and are even less easily compiled digitized regional structural information is available for South Australia. Low amplitude folding and faulting has occurred throughout the GAB a number of times including recently during the Cenozoic (e.g., Etheridge *et al.*, 1991; Fergusson, 1991; Finlayson, 1993; Foster *et al.*, 1994; Mathur, 1983; Shaw, 1991). Localised intrusions and related mineralisation also occur in places, with the most significant possibly associated with a line of Oligocene-Miocene hot spot volcanoes along the eastern-most margin of the Surat Basin (Cohen *et al.*, 2007; Knesel *et al.*, 2008) as well as Cretaceous magmatism in some places.

Prior to this study, little was known about the genesis of calcite-cemented zones that occur in the Eromanga and Surat basins. Early workers considered calcite-rich sequences in the Hutton Sandstone to be near-surface low temperature calcrete horizons formed between intermittent sedimentation episodes (Gravestock *et al.*, 1983), or hydrocarbon-related diagenetic zones (HRDZ) formed via microbial activity around natural oil-seeps similar to what is currently observed occurring on offshore Australia's Northwest Shelf (Boetius *et al.*, 2000; O'Brien *et al.*, 1999; Rollet *et al.*, 2006). On the basis of oxygen isotope data, however, it has been suggested that the carbonate cements precipitated at elevated temperatures of 55–121°C (Wall, 1987). Furthermore, the carbon isotope composition of the carbonates was similar to that of Cooper Basin carbon dioxide (Rigby and Smith, 1981; Vincent *et al.*, 1985) and different from the expected carbon isotope composition of CO₂ derived from microbial oxidation of hydrocarbons (Schulz-Rojahn, 1993). Some explorationists have hypothesised that seemingly localised zones of calcite cementation (perhaps around formerly leaky faults) in sandstones at depth could have formed as a result of a process akin to “pipe-scaling” in production wells, due to higher-pressure CO₂-laden fluids from depth migrating rapidly up into lower-pressure shallower aquifers (Rob Heath, personal communication).

A previous apatite fission-track study of samples from the Bowen and Surat basins indicates that certain samples of the Precipice Sandstone experienced paleotemperatures > 80°C (Raza *et al.*, 2009). The Hutton Sandstone experienced paleotemperatures ≥ 110°C and the Injune Creek Group had paleotemperatures ≥ 70°C based on samples from the Cabawin-1, Wandoan-1, Flinton-1 and Macintyre 1 wells. The thermal history modelling of the apatite fission-track parameters suggests that cooling occurred during the interval 100–80 Ma. The magnitude of cooling was in the order of 25–60°C, being the greatest in the northern part of the trough and relatively less in the southern part of the trough. The fluid inclusion investigations of the current study provide better constraints on the paleotemperatures estimated from other indirect methods and at the same time measure the salinity of the fluids associated with carbonate precipitation. The origin of carbonates can be inferred indirectly from the carbon isotopic composition of CO₂ trapped within the fluid inclusions and directly from the carbon isotope composition of the authigenic carbonates.

1.3. Parameters affecting carbonate precipitation

Natural mineral trapping processes occur on timescales that range from days to thousands of years, with the time frame dependent upon what processes are operating in a given area. If it is possible to differentiate between carbonate formed via different mechanisms, and determine what controlled the extent of authigenic carbonate formation, this could lead to options for engineered accelerated mineralisation in reservoirs. Our ability to influence what proportion of injected CO₂ will be fixed in carbonate minerals, and to potentially decrease the time required for mineral sequestration, is limited in part by our knowledge of subsurface mineralisation processes. The primary focus of this project is a better understanding of the controls on the formation of authigenic carbonates in low salinity, siliciclastic aquifers of the GAB as a natural analogue of mineralisation trapping in CO₂ geosequestration.

1.3.1. CO₂-fluid-rock interaction processes

1.3.1.1. Introduction

Parameters determining the extent of mineral trapping in sedimentary formations include dissolved cation concentrations, temperature, pH, alkalinity, and the partial pressure (p) of CO₂. Solution temperature strongly affects both ion solubility and precipitation rates. Calcite solubility is inversely proportional to temperature and directly proportional to p CO₂. Aside from the influence of system pressure upon p CO₂, it is not as important as the other factors affecting calcite precipitation. In natural systems, pH is strongly affected by p CO₂ and the combination of high pH and alkalinity favour carbonate precipitation. For example, CO₂-saturated fluid moving up a fault may encounter a shallower sandstone, and as the CO₂ disperses within the aquifer the local p CO₂ could become sufficiently low for precipitation of carbonates to occur, if sufficient dissolved cations were available. Supercritical CO₂ dissolved in water causes acidic conditions unless the aqueous phase is initially highly basic. In spite of the addition of a base to the solution, carbonic acid interactions with both dissolved and solid species can still drive pH lower if high partial pressures of CO₂ are maintained, unless the solution is buffered.

The process of mineral trapping of CO₂ as carbonates such as calcite, siderite, ankerite and dolomite has occurred naturally in high CO₂ reservoirs through fluid-rock interaction processes (Baker *et al.*, 1995; Golding *et al.*, 2013c; Higgs *et al.*, 2013; Watson *et al.*, 2004). A rate limiting step is often the dissolution of silicate minerals to provide the necessary cations (e.g., Ca²⁺) unless an evolved basinal brine, primary magmatic fluid, or paleo-marine fluid is involved. Greater acidity (i.e., lower pH) increases silicate dissolution (Gislason *et al.*, 2010). Dissolution of silicate minerals may occur as a result of interaction with CO₂-rich fluids, present as a result of natural accumulations or due to anthropogenic CO₂ storage, which provide acidity (carbonic acid). Dissolution of CO₂ in formation water is dependent on temperature, brine salinity, flow rate, and to a lesser extent total pressure; CO₂ solubility is greatest with high partial pressures of CO₂ and low salinity waters (Duan *et al.*, 2006; Spycher and Pruess, 2005; Spycher *et al.*, 2003).

All groundwater contains dissolved metal cations (e.g., Ca, Mg, etc.) in a range of concentrations, which could potentially combine with carbonate anions to form carbonate minerals irrespective of whether reactive mineral phases exist or not. The extent of carbonate precipitation tends to be proportional to the square of

apparent solution supersaturation with respect to a given carbonate mineral (Wajon *et al.*, 1985). If two carbonate-bearing groundwaters that are individually saturated with respect to carbonate minerals are mixed, the resultant fluid may either be supersaturated or strongly undersaturated depending upon the original partial pressures of CO₂, the temperatures, and the chemical compositions of the individual waters (Chong and Sheikholeslami, 2001; Dawe and Zhang, 1997; Domingo *et al.*, 2006; Wigley and Plummer, 1976; Zuddas and Mucci, 1998). The system may also evolve with time and the degree of mixing such that undersaturation prevails in more acidic and saline parts of the system and supersaturation in the more basic and dilute region of the system.

Dissolved CO₂ provides bicarbonate and carbonate ions through reaction with water:



If there is a very high partial pressure ('concentration') of CO₂ in contact with water, an acidic system containing dissolved CO₂ and resultant carbonic acid (H₂CO₃) predominates within the groundwater system. As the proportion of CO₂ relative to water decreases, bicarbonate anions (HCO₃⁻) form with the loss of a proton. At the periphery of interaction between a CO₂ plume and groundwater, the concentration of CO₂ is sufficiently low for carbonate anions (CO₃²⁻) to exist in solution, which is necessary for carbonate mineralisation. Alkaline groundwater often naturally contains dissolved bicarbonate and to a lesser extent carbonate anions resulting from past CO₂-fluid-rock interaction processes, and in situations of high fluid flux through areas of significant changes in conditions, e.g., depressurization at production wells, even waters containing low concentrations of cations can undergo sufficient mass transfer to result in rapid carbonate mineralisation. Natural analogues include rapid migration of fluids containing CO₂ up faults and fractures into shallower formations during tectonic and/or hydrothermal activity, where the primary control on precipitation of carbonates is the reduction in partial pressure of CO₂ under high fluid-flux conditions.

Sequestered CO₂ is generally thought to be trapped within geological reservoirs via a variety of mechanisms, with the proportional contribution of each evolving over time (Figure 1). Precipitation of carbonate minerals within the pore space of the storage reservoir provides the greatest certainty of long-term storage and eliminates the risk of CO₂ leakage. Several parameters may govern the precipitation of carbonate minerals. In sedimentary systems, these mainly include pH, pCO₂, alkalinity, sufficient concentrations of dissolved cations, and temperature.

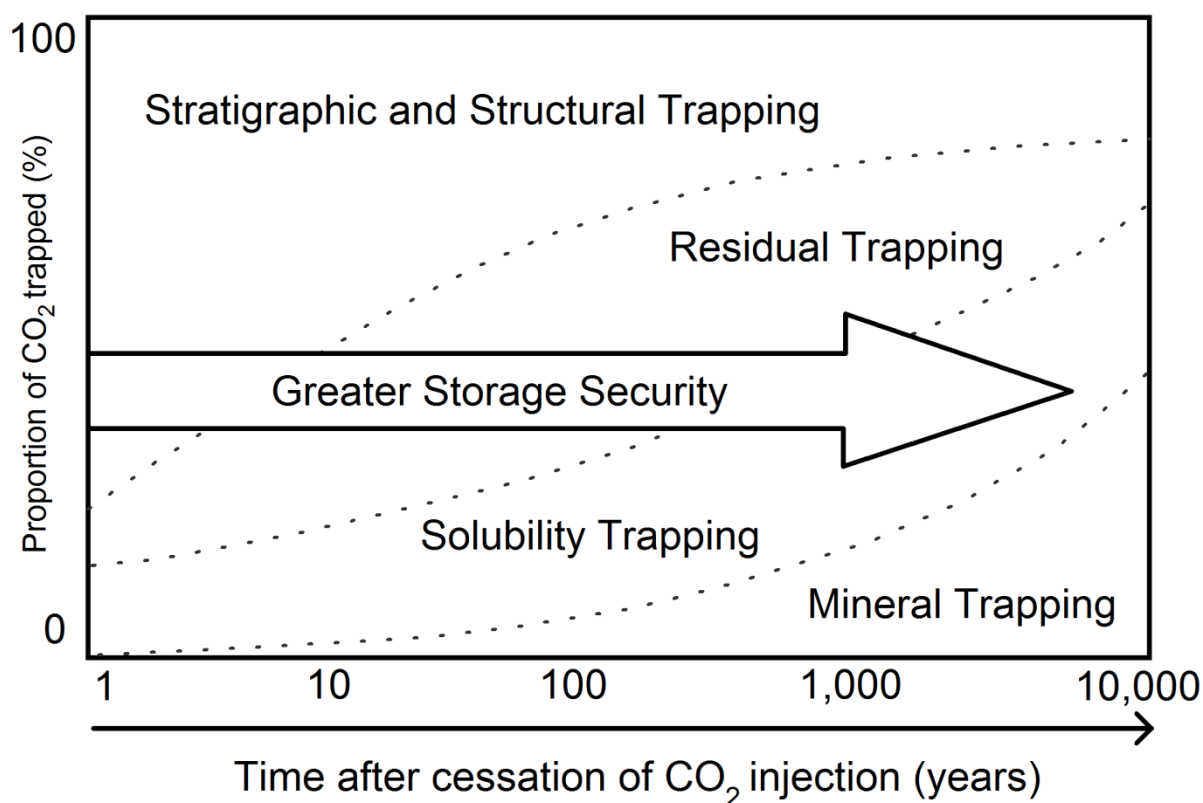


Figure 1: Schematic representation of the change of trapping mechanisms and increasing CO₂ storage security over time (modified after Class *et al.*, 2009; IPCC, 2005).

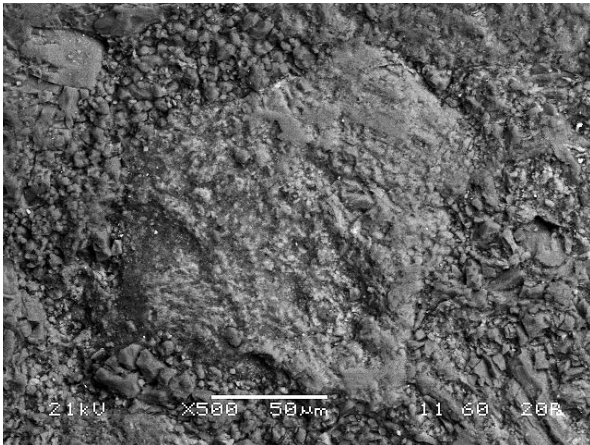
1.3.1.2. Carbonate diagenesis in sandstones

Divalent cations (e.g., Ca²⁺, Fe²⁺, Mg²⁺) are often sourced from reaction of CO₂-acidified water with aluminosilicate minerals (e.g., Figure 2 and equation 6). Previous laboratory work has shown the potential for this to occur over relatively short timescales – weeks and months (e.g., Dawson *et al.*, 2014a; Dawson *et al.*, 2013b; Dawson *et al.*, 2014b; Farquhar *et al.*, 2014; Lin *et al.*, 2008; Matter *et al.*, 2007; Rosenbauer *et al.*, 2005; Wigand *et al.*, 2008). This is consistent with observed increases in cations including Fe, Ca and Cr at the Frio I brine pilot injection of pure CO₂ in Texas, USA (Kampman *et al.*, 2014; Kharaka *et al.*, 2006).

Divalent cations may react with dissolved carbonate anions to form a variety of carbonate minerals (equation 7 and Figure 3). The process of transformation of dissolved CO₂ from carbonic acid to carbonate anions can be locally accelerated via fluid-rock interactions, which help to drive the system towards a sufficiently pH-buffered solution for carbonate formation. By way of example, siderite (and ankerite) cementation have been observed in the Westgrove Ironstone Member (Evergreen Formation, Chinchilla 4 core), interpreted to have been formed by CO₂-rich fluid infiltration (Farquhar, 2015). Siderite is closely associated with or rimming both chlorite and Fe-rich biotite, suggesting these silicates were the source of Fe²⁺ (e.g., Equation 6).

Note – The following section attempts to simplify carbonate precipitation for the understanding of the general reader; precipitation mechanisms are more varied and more complex than those described here.

A)



B)

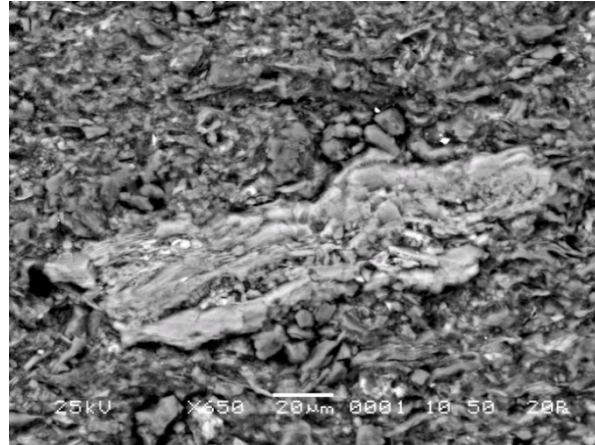


Figure 2: SEM examples of A) plagioclase (labradorite), 1043.7m and B) biotite/chlorite, 981.24 m, in the Evergreen Formation, West Wandoan 1 core, Surat Basin.

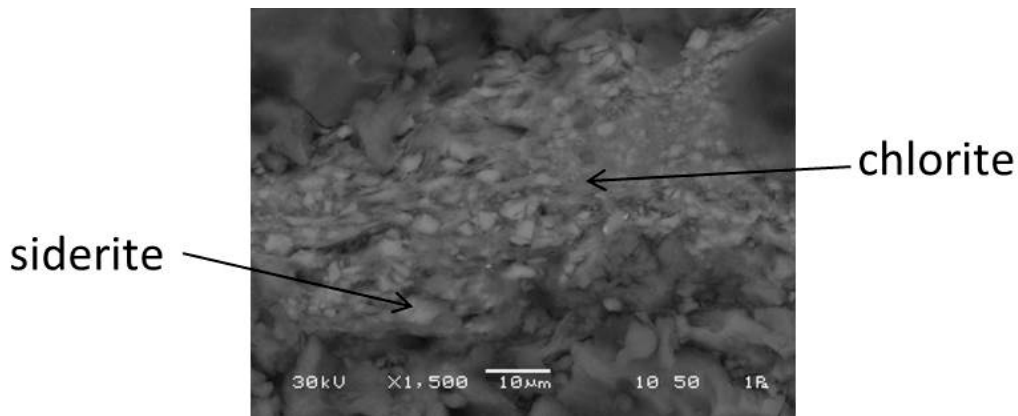
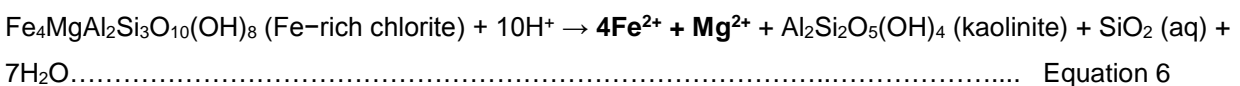


Figure 3: SEM image of associated chlorite and siderite, in the Evergreen Formation at 897 m, Chinchilla 4 core, Surat Basin.

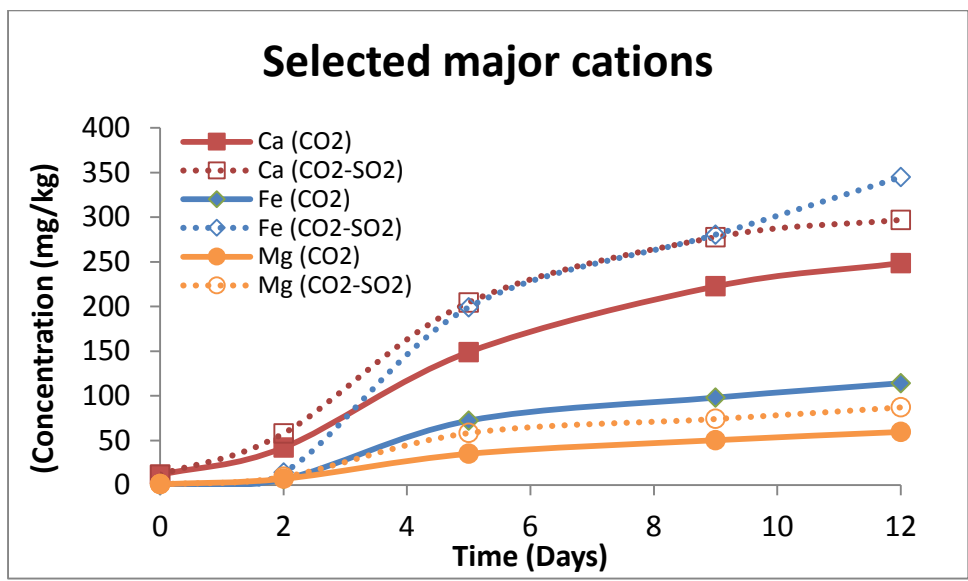


Natural CO₂ accumulations, especially those of igneous origin, often have associated impurity gases such as sulfur oxide species (SO_x). As demonstrated during the CO₂CRC reactive rocks project, impurity gases that may be present in CO₂ (e.g., SO₂ ± O₂) have been shown (at relatively high SO₂ concentrations) to enhance silicate dissolution and ion leaching (Figure 4) from samples of West Wandoan 1 core, Chinchilla 4 core and Berea Sandstone (Dawson *et al.*, 2015; Pearce *et al.*, 2013b; Pearce *et al.*, 2015b; Pearce *et al.*, 2015c). The formation of sulphuric acid, which is stronger than carbonic acid, enhances reactive silicate dissolution and ion leaching resulting in higher concentrations of divalent ions available to trap more CO₂. Impurities such as SO₂

and H₂S have also been predicted to reduce dissolved Fe³⁺ to Fe²⁺ making it available for siderite formation (Palandri and Kharaka, 2005). Dissolved sulphate from SO₂ is also predicted to complex with dissolved Al³⁺ further increasing Al silicate dissolution (Flaathen *et al.*, 2010).

Different silicate minerals (e.g., Mg vs Fe rich chlorite or albite vs labradorite) have different dissolution rates (Palandri and Kharaka, 2004); those with the fastest rates and highest reactive surface areas are generally the most reactive. The most reactive silicates in the West Wandoan 1 core and Chinchilla 4 cores (eastern Surat Basin) have been observed to be mainly Fe-rich chlorite and Ca-rich plagioclase (e.g., Figure 5 and Dawson *et al.*, 2015; Farquhar *et al.*, 2015; Pearce *et al.*, 2015c).

A)



B)

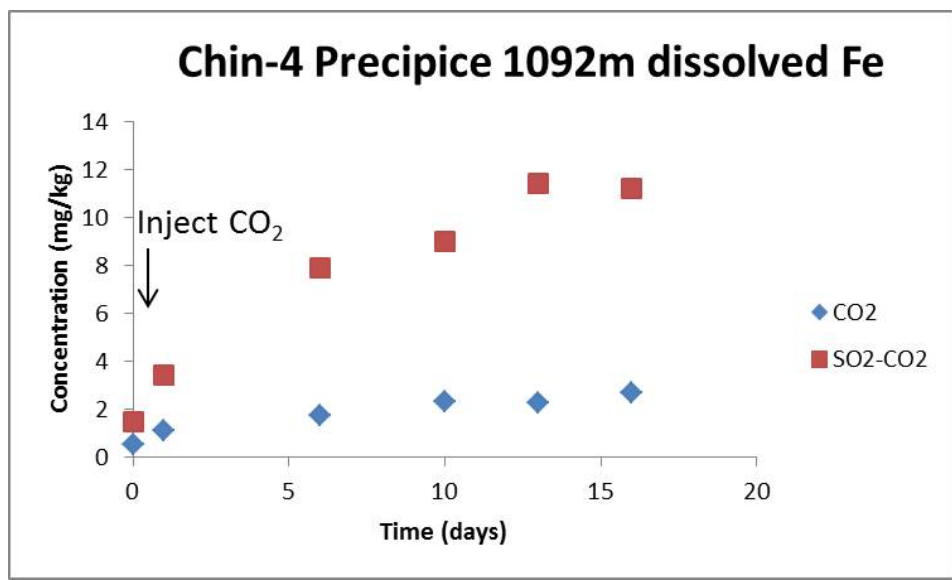


Figure 4: Examples of the difference in dissolved cation concentrations due to aqueous reactions with pure CO₂ or mixed high concentration CO₂-SO₂ in A) Berea Sandstone (Dawson *et al.*, 2015) and B) dissolved Fe from Chinchilla 4 Precipice Sandstone core from 1092 m (modified after Pearce *et al.*, 2013a; Pearce *et al.*, 2015c).

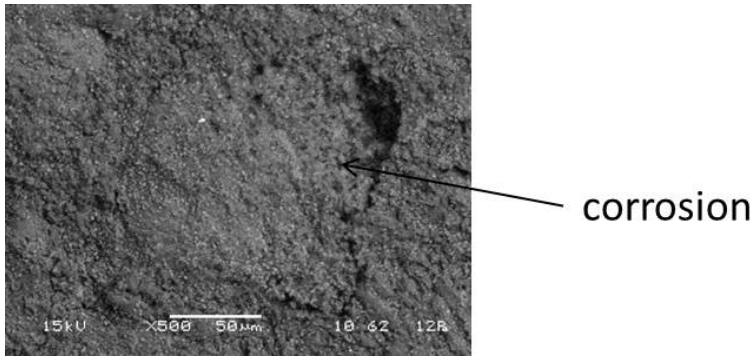


Figure 5: SEM image of plagioclase corroded after reaction with impure CO₂ (high impurity concentrations), the Evergreen Formation 1043.7 m, West Wandoan 1 core.

1.3.1.3. Brine composition effects upon carbonate mineral precipitation

The ionic composition of brines can significantly affect both the potential for carbonate precipitation and the rate at which this occurs. It is possible that influxes of highly concentrated brines (from depth) could have played a role in fluid mixing leading to massive carbonate precipitation in the past. A summary of some of the key species and their effects upon carbonate mineralisation is provided in Table 1. Calcite solubility increases with NaCl concentration up to 2 molar but decreases with further increases of NaCl concentration (Duan and Li, 2008), at which point calcite precipitation rate can increase by two orders of magnitude in response to the ionic strength of solution being increased by just 50% (Zuddas and Mucci, 1998). This is likely due to the solubility enhancement effect of chloride complexation being dominant at lower concentrations of NaCl, and the reduced solubility of CO₂ having a greater effect upon calcite solubility at higher solution molarities (Dawson, 2012). Aqueous iron, if three orders of magnitude more saturated than calcium, significantly decreases calcite formation kinetics (Van Lith *et al.*, 2003; Vasconcelos *et al.*, 1995; Wright, 1999; Zuddas *et al.*, 2003). Otherwise, the precipitation rate of siderite is generally eight orders of magnitude slower than for calcite (Vasconcelos *et al.*, 1995).

Both magnesium (Mitchell *et al.*, 2010) and sulphate ions in solution can greatly inhibit the precipitation rate of calcite at a given ionic strength (Mucci, 1988). In fact, the presence of aqueous sulphate can increase the solubility product of calcite by at least an order of magnitude (Dromgoole and Walter, 1990), and also inhibits magnesium incorporation into calcite (Mackenzie *et al.*, 2006). Similarly, aqueous strontium can marginally slow the precipitation rate of calcite (Lumsden *et al.*, 1989). Manganese negatively affects strontium but positively influences sodium incorporation in calcite (Jimenez-Lopez and Romanek, 2004), and manganese incorporation into calcite is affected by magnesium concentration (Zuddas *et al.*, 2003). Manganese can reduce the precipitation rate of dolomite (Duan and Li, 2008; Dupraz *et al.*, 2009). Humic acid inhibits calcite precipitation via interference with active crystal growth (Wright and Wacey, 2005)

Table 1: Solution chemistry effects on calcite precipitation rates and composition.

Species	Effects		
	Inhibition of precipitation rate	Other impacts	
Fe ²⁺	If three orders of magnitude more saturated than calcium (Van Lith <i>et al.</i> , 2003; Vasconcelos <i>et al.</i> , 1995; Wright, 1999; Zuddas <i>et al.</i> , 2003)		
Humic acid	Via interference with active crystal growth (Wright and Wacey, 2005)		
Mg ²⁺	Yes (Mitchell <i>et al.</i> , 2010)	Affects incorporation of Mn into calcite (Zuddas <i>et al.</i> , 2003)	
Mn ²⁺	Probable given that it definitely inhibits dolomite (Duan and Li, 2008; Dupraz <i>et al.</i> , 2009)	Negatively affects strontium incorporation into calcite (Jimenez-Lopez and Romanek, 2004)	Positively influences sodium incorporation into calcite (Jimenez-Lopez and Romanek, 2004)
NaCl	N/A	Up to 2M (~117,000 ppm NaCl or 46,000 ppm Na ⁺) concentration increases calcite solubility (Duan and Li, 2008)	NB: At greater than 2M NaCl concentration, calcite precipitation rates can increase by up to two orders of magnitude in response to solution ionic strength being increased by 50% (Zuddas and Mucci, 1998)
SO ₄ ²⁻	Yes (Mucci, 1988)	Inhibits magnesium incorporation into calcite (Mackenzie <i>et al.</i> , 2006)	May increase the solubility product of calcite by at least an order of magnitude (Dromgoole and Walter, 1990)
Sr ²⁺	Marginal impact (Lumsden <i>et al.</i> , 1989)		

2. Methods

2.1. Sampling strategy

Sampling of drill core and cuttings was spread as broadly as possible across the basin system to capture the greatest degree of variability in sandstone carbonate cementation conditions (Figure 6). Samples from different intervals of the same or adjacent wells were also taken in selected areas to help account for local variability. More than 250 well completion reports were selected from among tens of thousands of publically available (via QDEX and PEPS) petroleum, coal seam gas and stratigraphic drilling records (Dawson *et al.*, 2013). Selection was mainly on the basis of spatial and geological coverage, detail of included information, and type and availability of associated samples. The short-listed reports have been assessed in detail for the presence of significant carbonate mineralisation with samples taken from some 50 localities (Tables 2 and 3 and Appendix 1).

For cored wells, sampling intervals were chosen mainly on the basis of mudlogs and core descriptions, whereas for wells with drill cuttings samples downhole geophysics data were also used, particularly sonic logs, to locate significantly cemented intervals. All Mesozoic units within the chosen wells were subject to sampling whether the strong carbonate cement was sporadic or extensive. This was in order to obtain a sufficiently wide spread of analytical results for various lithologies and styles of cementation to be able to draw holistic interpretations of the conditions of carbonate mineralisation. There is little or no relevant existing carbonate mineralisation data available for comparison within the Surat and Eromanga basins.

Fault and vein carbonate mineralisation was also taken wherever this was found during sampling of carbonate cemented sandstones as it is postulated that faults played a key role in conveying parent fluids involved in significant carbonate cementation of sandstone units throughout the GAB.

2.2. Sample types

Brief descriptions of the samples taken are given in Appendix 1, with core sample photographs provided in Appendix 2. Samples are classified according to a hierarchy, i.e., basin, geological formation, depth, core or cuttings, carbonate cement and/or vein (if core), and so forth. Cemented, vein, and un-cemented samples are subdivided (where possible) into those occurring in sandstone units, interbedded lithologies, and mudstone/siltstone dominated intervals. XRD analysis (Appendix 3) allowed further subdivision of samples on the basis of mineralogy. Ultimately, the goal was to be able to distinguish the differences between carbonate cements that occur in 'clean' sandstones versus other lithologies, and most importantly determine what distinguishes significantly or widely cemented intervals from sporadic cementation. When discussed in the text, individual sample numbers are given either the prefix E or S to denote whether they are from the Eromanga or Surat basins, and tabulated data are sorted by basin.

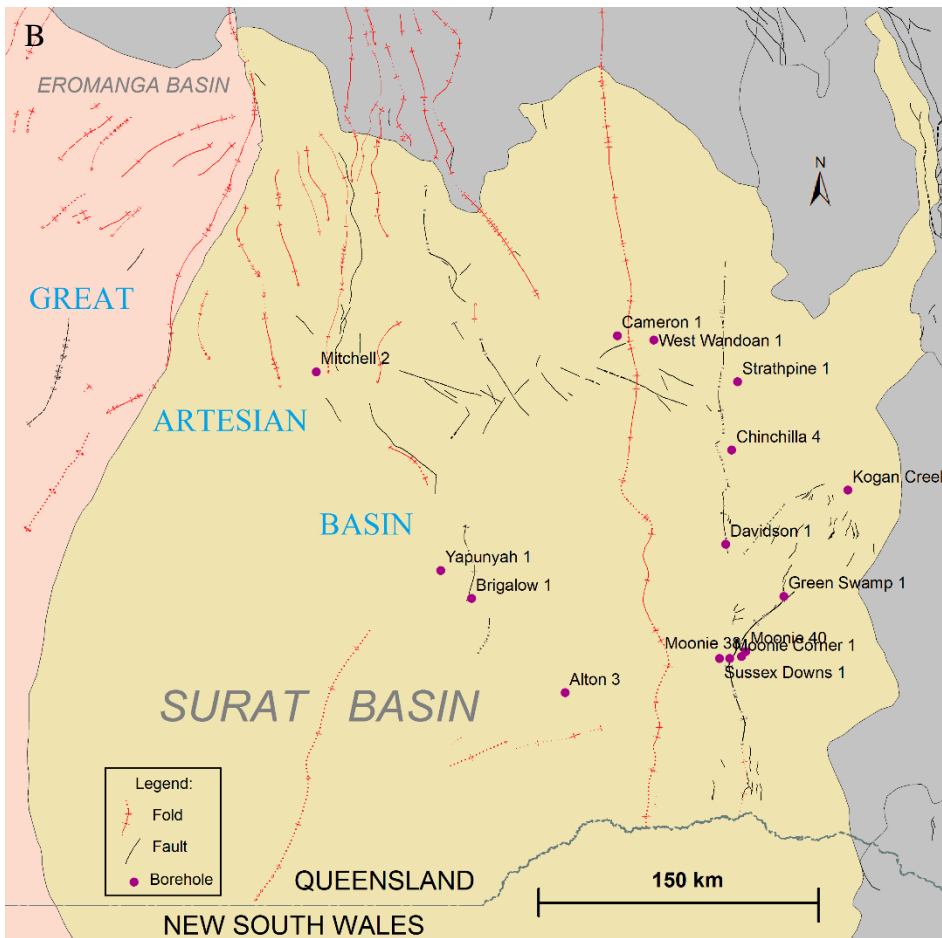
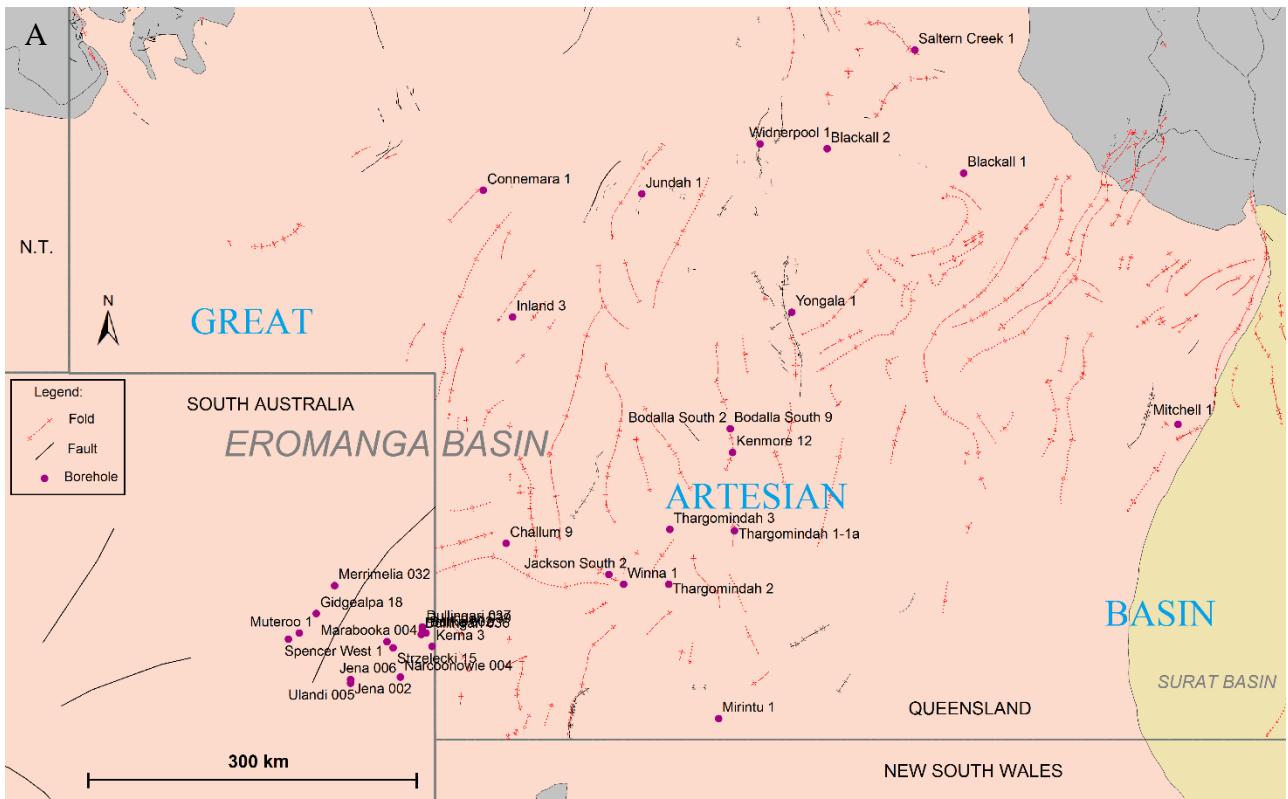


Figure 6: Maps of the Eromanga (A) and Surat (B) basins showing locations of sampled sites.

Table 2: Coordinates of Eromanga Basin samples.

Eromanga QLD			Eromanga SA		
Sample Site	Latitude	Longitude	Sample Site	Latitude	Longitude
Blackall 1	-24.36	145.34	Burke 002	-28.13	140.93
Blackall 2	-24.16	144.22	Dullingari 036	-28.14	140.89
Bodalla South 2	-26.46	143.43	Dullingari 037	-28.08	140.9
Bodalla South 9	-26.45	143.42	Dullingari 039	-28.1	140.9
Challum 9	-27.39	141.59	Gidgealpa 18	-27.97	140.03
Connemara 1	-24.50	141.40	Jena 002	-28.51	140.31
Inland 3	-25.54	141.64	Jena 006	-28.51	140.31
Jackson South 2	-27.65	142.43	Kerna 3	-28.24	140.98
Jundah 1	-24.53	142.70	Marabooka 004	-28.2	140.61
Kenmore 12	-26.65	143.44	Merrimelia 032	-27.74	140.18
Mirintu 1	-28.83	143.33	Muteroo 1	-28.13	139.89
Mitchell 1	-26.42	147.12	Narcoonowie 004	-28.49	140.72
Saltern Creek 1	-23.35	144.94	Spencer West 1	-28.18	139.8
Thargomindah 1-1a	-27.29	143.46	Strzelecki 15	-28.25	140.66
Thargomindah 2	-27.73	142.92	Ulandi 005	-28.54	140.31
Thargomindah 3	-27.28	142.93			
Widnerpool 1	-24.12	143.67			
Winna 1	-27.73	142.55			
Yongala 1	-25.5	143.93			

Table 3: Coordinates of Surat Basin samples.

Surat QLD		
Sample Site	Latitude	Longitude
Alton 3	-27.94	149.37
Brigalow 1	-27.47	148.9
Cameron 1	-26.16	149.63
Chinchilla 4	-26.73	150.2
Davidson 1	-27.2	150.17
Green Swamp 1	-27.46	150.46
Kogan Creek	-26.93	150.78
Mitchell 2	-26.34	148.13
Moonie 38	-27.76	150.25
Moonie 40	-27.73	150.27
Moonie corner 1	-27.77	150.19
Strathpine 1	-26.39	150.23
Sussex Downs 1	-27.77	150.14
Yapunyah 1	-27.33	148.75
West Wandoan 1	-26.18	149.81

2.3. Analytical methods

The thin section petrology, XRD and SEM mineralogy, trace elements, and stable isotope analyses of samples were undertaken at the University of Queensland using facilities in the Centre for Geoanalytical Mass Spectrometry and Isotope Science (CGMSIS) and the Centre for Microscopy and Microanalysis (CMM).

2.3.1. X-ray diffraction (XRD)

Semi-quantitative X-ray diffraction (XRD) analysis was undertaken for the majority of samples collected. Some vein samples were omitted from XRD analysis due to small sample size. The samples were prepared by grinding in an agate ball mill. Powders were then scanned on a Bruker D8 Advance diffractometer, from 2° to 70° 2 θ , operated at 40 kV and 40 mA. Minerals were identified and quantified using Bruker Eva Diffraclus V3 software.

2.3.2. Carbonate stable isotopes

Oxygen and carbon stable isotopic analyses were conducted using gas source isotope ratio mass spectrometry (IRMS) by the University of Queensland Earth Sciences Stable Isotope Geochemistry Laboratory. The powdered samples were reacted offline using the McCrea (1950) phosphoric acid digestion method. Calcite was reacted at 25°C for 1 day, dolomite/ankerite at 50°C for two days, and siderite at 75°C for 3 days. Sample gases were analysed on an Isoprime dual inlet isotope ratio mass spectrometer. Known acid fractionation factors were used to calculate the $\delta^{18}\text{O}$ values of calcite, dolomite/ankerite, and siderite respectively (Rosenbaum and Sheppard, 1986; Sharma and Clayton, 1965). Stable isotope analyses are reported in per mil (‰) relative to V-SMOW for oxygen and V-PDB for carbon. Analytical uncertainties better than $\pm 0.1\%$ (1σ) are established through replicate analyses of international (NBS-18 and NBS-19) and in-house standards.

2.3.3. Partial leaching methods

Partial leaching was undertaken on the samples using dilute acetic acid to dissolve carbonate cements and veins. The reasons for using dilute acetic acid (a weak acid) instead of 2% nitric acid (a strong acid) are that even when nitric acid is dilute it is still strong enough to attack non-carbonate minerals, whereas acetic acid only dissolves weak-acid-soluble minerals. Selection for partial leaching and subsequent geochemical analyses was biased towards samples with a single phase of authigenic carbonate, and samples that contain two carbonate phases but are clearly dominated by one. Carbonate mineralogy was determined primarily by XRD analysis. Veins were picked primarily using a strong scalpel, and cemented sandstones were wrapped in paper to limit transfer of metals to samples as they were carefully broken up into <5 mm chips using a hammer.

Samples were powdering in an agate ball mill followed by rinsing with deionised water to reduce the quantity of colloidal material (e.g., clay fines). Samples were oven-dried at $\sim 100^\circ\text{C}$ for about a week and then weighed out into acid-cleaned falcon tubes. The samples were dissolved in approximately 8 mL distilled 1 N acetic acid per 300 mg of carbonate then sonicated for one hour, with periodic agitation to break up powder clumps, and then reacted overnight with loose tube lids in a fume cupboard. The masses of the clean powders used were mostly up to ~ 3 g and generally did not contain more than 300 mg carbonate. Once the samples had stopped bubbling

after about one day reaction, centrifugation was undertaken to settle solid impurities and then supernatants were transferred to acid-cleaned Teflon beakers via pipetting. The residual solid samples were then rinsed with 4 mL pure water, centrifuged, and the rinse solutions added to the supernatants three times. The dissolved samples were evaporated then refluxed with double distilled 15.8 N nitric acid. Stock solutions were made in ~7 % double distilled nitric acid.

2.3.4. Major element analysis

Inductively coupled plasma optical emission spectroscopy (ICP-OES) analysis was primarily used to measure major element concentrations within the dissolved carbonates, but for samples that were deemed “too dirty” for ICP-MS analysis minor and some trace element concentrations are also reported. Samples were analysed using a Perkin Elmer Optima 3300 DV ICP-OES in the Geochemistry Laboratory at the University of Queensland. Aliquots of the samples were taken from the stock solutions prepared by partial leaching methods (see above) and diluted 1,500 times in 2 % double distilled nitric acid for analysis. An internal standard containing Y, Sc and Lu was co-injected with each sample solution into the OES nebuliser at a defined rate. An external drift solution (monitor) with similar matrix was used for further instrument and matrix correction. We ran repeats of multiple standards to assess accuracy and precision with analyses better than 2 % relative standard deviation (RSD).

2.3.5. Trace and minor element analysis

Inductively coupled plasma mass spectroscopy (ICP-MS) analysis was originally undertaken just for trace elements, but was found to be able to satisfactorily measure minor and some major element (e.g., calcium) concentrations as well. This was due to the fact that some high-concentration elements have low natural abundance stable isotopes, and these can be accurately measured via highly sensitive MS without damaging the detector. Therefore, wherever possible, the ICP-MS concentration data has been reported in preference to ICP-OES data. Some elements such as iron couldn't be analysed satisfactorily via ICP-MS though.

Samples were analysed on a Thermo Scientific X series 2 ICP-MS in the Radiogenic Isotope Facility at the University of Queensland. Aliquots of the samples were taken from the stock solutions and diluted in 2% double distilled nitric acid, such that the total dilution factor for each sample was roughly 3000 times relative to the original solid sample mass. Six ppb ^6Li , ^{103}Rh , ^{115}In , Re, Bi, ^{235}U was used as an internal standard. An external drift solution with similar matrix (monitor) was used for further instrument and matrix correction. US Geological Survey diabase standard W2a-1 was used as a calibration standard. W2a-3, Bir-1, and BHVO-2 were run as unknowns and also used to confirm long-term precision of the instrument.

3. Analytical Results and Discussion

3.1. XRD analyses

Most clastic samples collected were screened via XRD analysis (sample summary in Table 4) prior to any additional testing. Of the 193 XRD analyses, 130 were for carbonate cemented samples (14 of which also contained veins), 33 were carbonate veined samples lacking significant cement, and 30 were samples that did not contain carbonate but were from carbonate-bearing intervals. The majority of carbonate cement and vein samples collected were calcite, in spite of well logs sometimes indicating dolomite (which XRD subsequently found present as a major phase within only a single sample - #162). Similarly, 50 samples taken from well intervals logged as having abundant carbonate cement were found to contain less than 5 % when assessed using semi-quantitative XRD. Perusal of the XRD data has not revealed any significant differences between core-only and cuttings-only data, and so although it is possible that some of the wellbore cuttings samples may have contained unrecognised vein material this is unlikely to have adversely affected the overall statistics.

Close examination of the XRD data for carbonate cemented samples (excluding those known to contain veins) versus non-cemented samples has revealed potentially diagnostic features of heavily cemented units (> 10 % carbonate). Only one in five samples with > 10 % calcite cement contained any other carbonate minerals, with the proportion of other carbonate minerals present generally decreasing with increasing calcite content (Table 5). Conversely, samples with > 10 % calcite were also the most likely to contain > 5 % siderite cement (one in five samples) compared with samples containing less calcite.

Overall, the presence of feldspars of any type was strongly associated with carbonate cement (Table 6), although calcium-bearing plagioclase presence and abundance only sometimes correlated with type and amount of carbonate cementation (Table 7). When all non-veined samples are considered, presence of Ca-plagioclase is not a discriminating factor between non-calcite carbonate-bearing samples and those which lack carbonates, though samples containing Ca-plagioclase are more likely to have calcite cement than those without Ca-plagioclase. In contrast, when only significantly carbonate cemented intervals are considered (> 300 feet or 100 metre net thickness of cemented units), the presence of calcite cement is inversely correlated with the proportion of samples containing Ca-plagioclase (Figure 7), which may be coincidental given the smaller number of samples (Table 8).

Only 4 % of heavily calcite-cemented samples were quartz arenites and less than 12 % contained more than 80 % quartz relative to other non-carbonate minerals (Table 9). Over 96 % of samples with abundant calcite contained phyllosilicates, with kaolin being most often associated with calcite cement. The presence of clays may have helped initiate carbonate mineral nucleation, although it is likely that some of the clay-sized minerals present were produced via acidic groundwater alteration of other minerals. In the case of kaolin, the most abundant clay in the GAB, its association with calcite cement may be coincidental. Carbonate-cemented samples were also more likely to contain fine mica grains (including illite) than samples lacking carbonates. Chlorite/smectite content is more weakly associated with carbonate cementation than mica content (Table 10). The absence of any chlorite detected within samples cemented with carbonates other than calcite may be due to the small sample size (n = 11) and the detection limit of the XRD technique (about 1 %). However, natural

analogue studies of CO₂-rich reservoirs have shown that Fe-bearing chlorites are particularly reactive in the presence of CO₂-rich fluids and commonly replaced by smectite and ferroan carbonates in such situations (Higgs *et al.*, 2013; Higgs *et al.*, 2015).

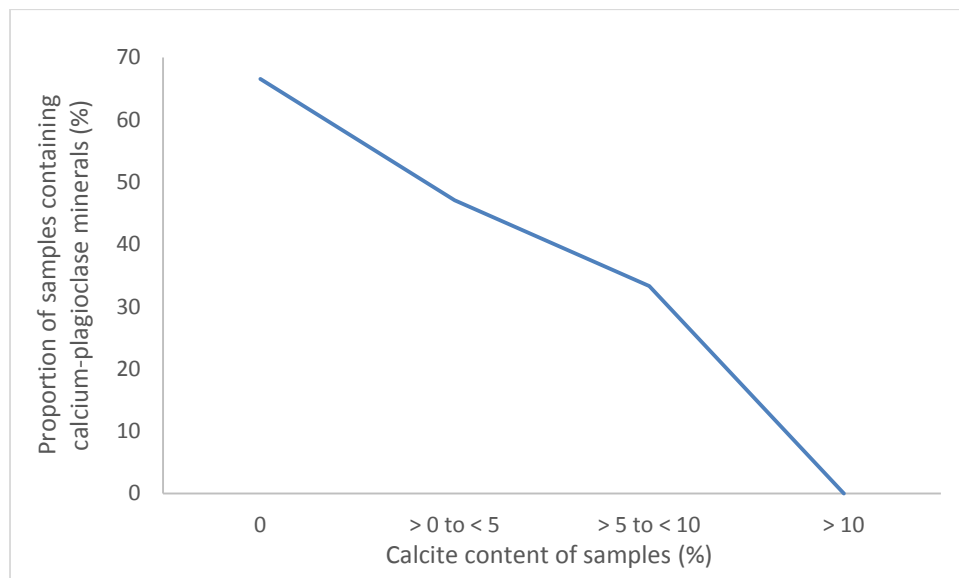


Figure 7: For significantly calcite-cemented zones (>100 m thick), there is an inverse correlation between the proportion of cemented samples containing calcium-plagioclase minerals and their calcite content as determined by semi-quantitative XRD analysis.

Table 4: Summary of the number and type of carbonate-bearing samples versus samples lacking carbonate analysed via semi-quantitative XRD.

Samples containing carbonates								Related samples with no carbonates
Total	Cement only			Cement & veins		Veins only		Total
	Calcite only	Calcite & others	Others only	Calcite only	Calcite & others	Calcite only	Calcite & others	
163	58	47	11	8	6	28	5	30

Table 5: Distribution of carbonates other than calcite.

Samples cemented with:	Abundance (%)	Number of samples	Carbonates other than calcite	Percentage of samples containing:			
				Dolomite/Ankerite		Siderite	
				Any	> 5%	Any	> 5%
Calcite	> 10	26	23.1	15.4	0	23.1	19.2
	> 5 to < 10	21	47.6	28.6	0	33.3	4.8
	> 0 to < 5	58	53.4	20.7	0	41.4	0
Carbonates other than calcite	Any	11	100	72.7	9.1	54.5	0
No carbonates	N/A	30	0	0	0	0	0

Table 6: Feldspar distribution amongst the XRD-screened samples.

Samples cemented with:	Abundance (%)	Number of samples	Percentage of samples containing feldspars:					
			Any	> 10%	> 20%	> 30%	> 40%	> 50%
Calcite	> 10	26	88.5	73.1	46.2	15.4	7.7	0
	> 5 to < 10	21	81.0	38.1	19	14.3	9.5	0
	> 0 to < 5	58	84.5	60.3	44.8	27.6	5.2	1.7
Carbonates other than calcite	Any	11	63.6	9.1	9.1	0	0	0
No carbonates	N/A	30	46.7	23.3	16.7	6.7	3.3	0

Table 7: Ca-bearing plagioclase feldspar distribution amongst the XRD-screened samples.

Samples cemented with:	Abundance (%)	Number of samples	Percentage of samples containing Ca-feldspars:					
			Any	> 10%	> 20%	> 30%	> 40%	> 50%
Calcite	> 10	26	65.4	42.3	15.4	7.7	3.8	0.0
	> 5 to < 10	21	28.6	9.5	9.5	9.5	4.8	0.0
	> 0 to < 5	58	60.3	44.8	27.6	13.8	1.7	1.7
Carbonates other than calcite	Any	11	18.2	9.1	0	0	0	0
No carbonates	N/A	30	23.3	16.7	6.7	3.3	3.3	0.0

Table 8: Ca-bearing plagioclase feldspar distribution amongst XRD-screened samples taken from significantly carbonate cemented intervals (>300 feet or 100 metre net thickness of cemented units).

Samples cemented with:	Abundance (%)	Number of samples	Percentage of samples containing Ca-feldspars:					
			Any	> 10%	> 20%	> 30%	> 40%	> 50%
Calcite	> 10	2	0	0	0	0	0	0
	> 5 to < 10	6	33.3	0	0	0	0	0
	> 0 to < 5	17	47.1	47.1	0	0	0	0
Carbonates other than calcite	Any	14	50	28.6	0	0	0	0
No carbonates	N/A	3	66.6	33.3	0	0	0	0

Table 9: Quartz, kaolin, and total phyllosilicate distribution amongst the XRD-screened samples.

Samples cemented with:	Abundance (%)	Number of samples	Percentage of samples containing:					
			Quartz abundance relative to other non-carbonate minerals		Phyllo-silicates	Kaolin		
			> 80%	> 90%	Any	Any	> 5%	> 10%
Calcite	> 10	26	11.5	3.8	96.2	96.2	46.2	15.4
	> 5 to < 10	21	66.7	57.1	61.9	57.1	9.5	0
	> 0 to < 5	58	36.2	27.6	79.3	75.9	50.0	5.2
Carbonates other than calcite	Any	11	81.8	54.5	54.5	54.5	18.2	18.2
No carbonates	N/A	30	86.7	80.0	46.7	46.7	23.3	6.7

Table 10: Mica/illite and chlorite/smectite distribution amongst the XRD-screened samples.

Samples cemented with:	Abundance (%)	Number of samples	Percentage of samples containing:						
			Micas (including Illite)				Chlorite &/or Smectite		
			Any	> 5%	> 10%	> 20%	Any	> 5%	> 10%
Calcite	> 10	26	46.2	42.3	19.2	0	26.9	11.5	0
	> 5 to < 10	21	38.1	23.8	9.5	0	14.3	4.8	4.8
	> 0 to < 5	58	60.3	56.9	48.3	6.9	37.9	19	3.4
Carbonates other than calcite	Any	11	36.4	9.1	0	0	0	0	0
No carbonates	N/A	30	16.7	16.7	13.3	6.7	10	10	0

3.2. Carbonate stable isotopes

Carbon and oxygen isotopic compositions were determined for 94 calcites, 3 dolomites and 3 siderite cements and veins in Eromanga Basin borehole samples and 40 calcite and 5 siderite cements and veins in Surat Basin borehole samples (Tables 11 and 12; Figure 8). Eromanga cements and fault veins exhibit a wide range of $\delta^{18}\text{O}$ and $\delta^{13}\text{C}$ values from 6.58 to 25.73 ‰ and -21.37 to 1.13 ‰ (n=100), respectively. The range of $\delta^{18}\text{O}$ values for Eromanga samples becomes 6.58 to 19.84 ‰ (n=93) when samples 58, 63, 66, 94, 95, 98 and 102 (with high values) are excluded. The Surat cements and veins exhibit a broad and overlapping range of $\delta^{18}\text{O}$ and $\delta^{13}\text{C}$ values from 4.90 to 24.70 ‰ and -11.11 to 9.97 ‰ (n=45), respectively. The range of $\delta^{18}\text{O}$ values for the Surat samples becomes 4.90 to 16.98 ‰ (n=42) when samples 10, 86 and 87 are excluded.

In order to determine the fluid source, we used a range of model temperatures from 40°C to 200°C and the oxygen isotope fractionation curves for calcite-water, dolomite-water and siderite-water to calculate the oxygen isotope compositions of the fluid in equilibrium with the Eromanga and Surat cements and veins (Tables 13 and 14) (Carothers *et al.*, 1988; O'Neil *et al.*, 1969; Sheppard and Schwarcz, 1970). The modelling approach is necessary because there are two variables, fluid composition and temperature, and we only have fluid inclusion data for some samples. Low temperature formation (<80°C) is unlikely for the majority of Surat and Eromanga carbonates because this would require unrealistically low fluid oxygen isotope compositions. A model temperature of 80°C gives more realistic calculated fluid oxygen isotope compositions from -12.82 to -0.66 ‰ (n=93) and -15.41 to -2.42 ‰ (n=42) for the main populations of Eromanga and Surat carbonates, respectively (Tables 13 and 14). It is likely the main population of carbonates formed in the temperature range 80 to 120°C based on this modelling and the fluid inclusion data reported in section 3.4.

The calculated fluid oxygen isotope compositions are much lower than those reported for most mid to low latitude sedimentary basins (Clayton *et al.*, 1966) and to those attained during burial diagenesis in many sedimentary basins (Clauer and Chaudhuri, 1995). This suggests meteoric dominated ^{18}O -depleted waters were involved in the precipitation of the majority of carbonates that is consistent with the mid to high latitude position of eastern Australia during the Early Jurassic to mid-Cretaceous (Veevers and Conaghan, 1984). It is likely that the Eromanga and Surat carbonates with calculated fluid oxygen isotope compositions < -12 ‰ at 80°C (samples 8, 11, 12, 13, 14, 15, 67, 70, 74, 76, 161a and 161b) were deposited at the higher temperature end of the model temperature range ($\geq 120^\circ\text{C}$).

Table 11: Carbonate carbon and oxygen stable isotopes for Eromanga Basin calcites, dolomites and siderites – both cemented sandstone and fault-mineralisation intervals.

Sample	Well	Formation	Depth (m unless marked ft)	Some notes	Carbonate cemented zone thickness (m)	$\delta^{18}\text{O}_{\text{VSMOW}} \text{‰}$	$\delta^{13}\text{C}_{\text{VPDB}} \text{‰}$
127a	Blackall 1	Hooray (Namur) Sandstone	622.35-622.6	Calcite vein/s within subvertical fractures in calcite cemented zone, coalified plant fossils.	20m (8m net)	12.53	-4.8
127b	Blackall 1	Hooray (Namur) Sandstone	622.35-622.6	Calcite vein/s within subvertical fractures in calcite cemented zone, coalified plant fossils.	20m (8m net)	12.46	-4.82
89	Blackall 1	Hooray (Namur) Sandstone	622.79-622.89	Subvertical fractures in calcite cemented zone, coalified plant fossils.	20m (8m net)	11.59	-6.13
90	Blackall 1	Birkhead Formation	773.16-773.24	Calcite vein/fault fill.	Veins & sporadic fault associated cement	13.88	-13.1
91	Blackall 2	Allaru Mudstone	311.68-611.94	4 cm thick calcite fault infill. Interval has cone-in-cone (?), calcite frags, shells.	Sporadic and frac associated	14.29	-4.64
92a	Blackall 2	Allaru Mudstone	313.54-313.61	Calcite vein and cement.	Sporadic and frac associated	13.09	-4.13
92b	Blackall 2	Allaru Mudstone	313.54-313.61	Calcite vein and cement.	Sporadic and frac associated	13.56	-4.05
93	Blackall 2	Allaru Mudstone	314.6-314.61	Calcite vein 5 mm, near horizontal.	Sporadic and frac associated	15.39	-2.21
94	Blackall 2	Allaru Mudstone	443.7-443.77	Calcite faults/veins.	Sporadic and frac associated	23.93	-0.05
95	Blackall 2	Allaru Mudstone	444.51-444.565	Contorted "fibrous" calcite veins, also veining in frags. Shells present in interval.	Sporadic and frac associated	21.5	-1.93
96	Blackall 2	Allaru Mudstone	474.19-474.36	1.5 cm thick fault calcite with radiating veins. Interval has concretions and possibly cone-in-cone.	Sporadic and frac associated	15.29	-3.06
125	Blackall 2	Allaru Mudstone	474.93-475.08	Large calcite fault/veins.	Sporadic and frac associated	16.39	-10.58
97	Blackall 2	Allaru Mudstone	475.88-476.02	Calcite fault fill, veins, other mineralised fractures with minor offsets, possibly cone-in-cone and concretion calcite? Maybe ammonite shells in interval, mainly pyritised.	Sporadic and frac associated	15.3	-2.89
98	Blackall 2	Toolebuc Formation	660.38-660.54	Large veins with shiny black minerals (phosphates etc.) and calcite. Shells mostly pyritised. Some fish spines, pyritised worm burrows, pyrite nodules.	110m (98m net carbonate presence, 28m net sandstone laminations) and also frac associated (starting above this depth)	25.73	-21.37
99	Blackall 2	Wallumbilla Formation	665.71-665.73	Large calcite veins.	Sporadic and frac associated	13.9	-14.95
155	Blackall 2	Wallumbilla Formation	809.5-809.56	Calcite veins/fault?	Sporadic calcite fracture fill and cement.	14.28	-12.28
100	Blackall 2	Wallumbilla Formation	811.46-811.47	Calcite vein horizontal? Near huge fault/small intrusion?	Sporadic and frac associated	12.32	-8.15
63	Bodalla South 2	Winton Formation	150	Very abundant calcite.	64m (30.5m net) (210 ft (100 ft net))	22.32	-10.29
51	Bodalla South 9	Hutton Sandstone	1596	Common brown calcite cement.	73m (59.5m net)	8.38	-4.66
52	Bodalla South 9	Hutton Sandstone	1617	Common brown calcite cement.	73m (59.5m net)	13.87	-7.38

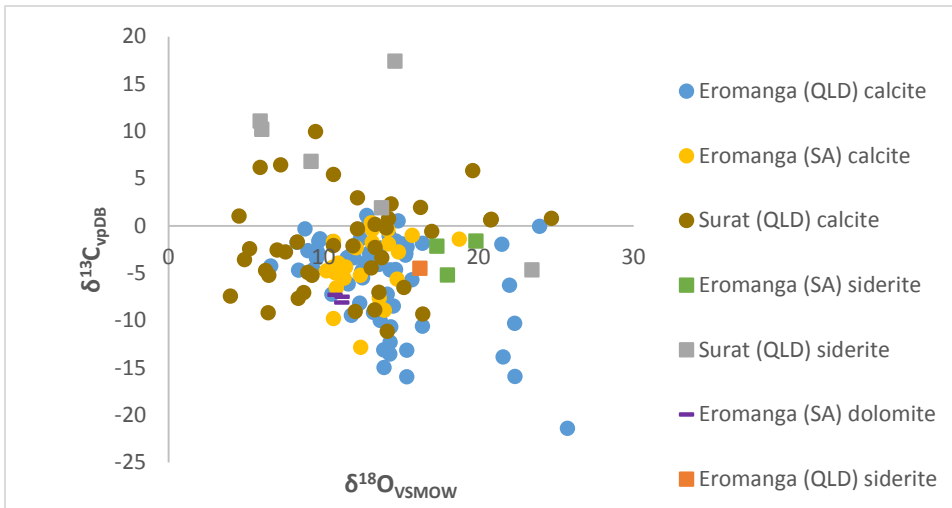
Sample	Well	Formation	Depth (m unless marked ft)	Some notes	Carbonate cemented zone thickness (m)	$\delta^{18}\text{O}_{\text{VSMOW}}\text{‰}$	$\delta^{13}\text{C}_{\text{VPDB}}\text{‰}$
169	Burke 002	Murta Formation	5063'7"	Oil show, calcite cement, microfaulting.	131m (52m net) (430 ft (170 ft net))	15.71	-0.99
102	Connemara 1	Winton Formation	119.76-119.87	Calcite cement & sporadic mud rip-up clasts, minor coal at 130 m.	Sporadic	21.99	-6.24
124	Connemara 1	Mackunda Formation	310.71-311	Calcite veins.	Sporadic and frac associated	14.65	-4.58
148	Connemara 1	Mackunda Formation	311.75-311.82	Calcite veins.	Sporadic and frac associated	16.37	-1.81
123	Connemara 1	Allaru Mudstone	371.72-371.83	Calcite veining and cone-in-cone, cement, shells.	Sporadic and frac associated	15.03	-2.61
149	Connemara 1	Allaru Mudstone	390-390.18	Calcite veins, microfaults?	Sporadic and frac associated	15.07	-1.89
150	Connemara 1	Allaru Mudstone	391.88-392	Calcite veins.	Sporadic and frac associated	13.56	-2.29
126a	Connemara 1	Allaru Mudstone	395.4-395.5	Calcite veins, cement, microfaults?	Sporadic and frac associated	14.63	-1.61
126b	Connemara 1	Allaru Mudstone	395.4-395.5	Calcite veins, cement, microfaults?	Sporadic and frac associated	14.67	-1.58
158	Connemara 1	Allaru Mudstone	448.83-448.87	Calcite veins.	Sporadic and frac associated	14.8	0.53
159	Connemara 1	Wallumbilla Formation	673.45-673.48	Calcite infill? Cone-in-cone.	Sporadic and frac associated	15.37	-13.11
103	Connemara 1	Westbourne Formation	942.17-942.37	Calcite cement, mud rip-up clasts.	40m (30m net)	9.61	-2.74
104	Connemara 1	Westbourne Formation	945.04-945.16	Calcite cement.	40m (30m net)	11.75	-3.12
105	Connemara 1	Westbourne Formation	946.24-946.34	Calcite cement.	40m (30m net)	12.94	-2.85
165	Dullingari 036	Murta Formation	4883'3"	Oil, calcite cement, 350 feet below limestone.	21m (6m net) (70 ft (20 ft net))	10.95	-3.92
167a	Dullingari 037	Murta Formation	5065'8.5"	Calcite cement.	91 m (61 m net) (300 ft (200 ft net))	11.42	-4.31
173-cal	Dullingari 037	Murta Formation	5068'8"	Calcite cement.	91m (61m net) (300 ft (200 ft net))	14.82	-2.74
173-sid	Dullingari 037	Murta Formation	5068'8"	Siderite cement.	91m (61m net) (300 ft (200 ft net))	17.3	-2.12
171	Dullingari 039	Murta Formation	5024'9"	Calcite cement, 70 feet above limestone.	76m (43m net) (250 ft (140 ft net))	13.6	-7.6
187	Gidgealpa 18	Namur Sandstone	5510	Calcite cement, coal frags.	Sporadic	13.07	0.32
189	Gidgealpa 18	Namur Sandstone	5580	Calcite cement, minor coal frags.	97.5m (73m net) (320 ft (240 ft net))	10.64	-1.63
1	Inland 3	Birkhead Fm.	4430'-4440'	Calcite & apparently siderite cement, some siliceous.	19m (13m) (62 ft (43 ft net))	12.87	0.04
64	Inland 3	Hutton Sandstone	5570'-5580'	Siderite and calcite cement, siliceous in part.	65m (61.5m net) (214 ft (202 ft net))	13.65	-9.98
78-cal	Jackson South 2	Westbourne Formation	4279'6.5"-4279'9"	Oil stained, calcite cement, veins, some siderite.	Sporadic	10.53	-7.21
78-sid	Jackson South 2	Westbourne Formation	4279'6.5"-4279'9"	Oil stained, calcite cement, veins, some siderite.	Sporadic	16.22	-4.45
166	Jena 2	Murta Formation	3882'9"	Oil show, calcite cement & veins.	135.5m (42.5m net) (445 ft (140 ft net))	13.91	-8.89
170-cal	Jena 6	Murta Formation	3934'1"	Oil show, calcite cement.	99m (33.5m net) (325 ft (110 ft net))	12.37	-5.19
170-sid	Jena 6	Murta Formation	3934'1"	Oil show, calcite cement.	99m (33.5m net) (325 ft (110 ft net))	19.84	-1.58
107	Jundah 1	Cadna-Owie Formation	795.59-795.75	Calcite veins.	Sporadic and frac associated	11.96	-3.36

Sample	Well	Formation	Depth (m unless marked ft)	Some notes	Carbonate cemented zone thickness (m)	$\delta^{18}\text{O}_{\text{VSMOW}}\text{‰}$	$\delta^{13}\text{C}_{\text{VPDB}}\text{‰}$
108	Jundah 1	Hooray (Namur) Sandstone	905.67-905.673	Strong calcite cement associated with calcite filled faults and other fractures. Also cone-in-cone calcite. Coalified plant fossils.	50m (34m net), fault-zone	9.78	-1.35
109	Jundah 1	Hooray (Namur) Sandstone	906.46-906.58	Strong calcite cement associated with calcite filled faults and other fractures. Also cone-in-cone calcite. Coalified plant fossils.	50m (34m net), fault-zone	12.72	-3.84
110	Jundah 1	Hooray (Namur) Sandstone	939.62-939.68	Calcite cement. Interval has 20 cm fault zone at 953.69 m.	50m (34m net), fault zone	11.53	-3.33
111	Jundah 1	Hooray (Namur) Sandstone	940.48-940.58	Calcite cement. Interval has 20 cm fault zone at 953.69 m.	50m (34m net), fault zone	13.06	-3.98
112	Jundah 1	Hooray (Namur) Sandstone	941.52-941.7	Calcite veins, cement.	50m (34m net), fault zone	12.51	-4.63
65	Kenmore 12	Mackunda Formation	510	Strong calcite cement, but apparently frequent limestone layers.	410m (60m net)	15.69	-5.68
66	Kenmore 12	Wallumbilla Formation	920	Strong calcite cement, some siliceous, glauconite.	30m (8m net)	21.59	-13.83
56	Kenmore 12	Cadna-Owie Formation	1075	Strong calcite cement, apparently dolomite frags.	90m (55m net)	13.56	-2.91
57	Kenmore 12	Birkhead Formation	1350	Strong calcite cement below minor limestone, minor siliceous.	195m (135m net)	12.37	-1.36
212-dol	Kerna 3	Namur Sandstone	5480	Dolomite cement & some coal frags.	73m (240 ft)	11.169	-8.07
181-dol	Kerna 3	Namur Sandstone	5500	Dolomite cement & coal frags.	73m (240 ft)	11.2	-7.46
182	Kerna 3	Namur Sandstone	5640	Calcite cement.	73m (240 ft)	13.14	-0.37
183	Kerna 3	Namur Sandstone	5700	Calcite cement & coal frags.	73m (240 ft)	10.18	-4.74
163	Marabooka 004	Oodnadatta Formation	3433	Calcite cement and veins, 100 feet above and 350 feet below limestone.	15m (9m net) (50 ft (30 ft net))	12.4	-12.83
3	Mirintu 1	Cadna-Owie Formation	677	Two layers of calcite fault-fill.	30m (15m net), with veins and faults	9.69	-1.59
4	Mirintu 1	Cadna-Owie Formation	677	Two layers of calcite fault-fill.	30m (15m net), with veins and faults	10.58	-1.64
2	Mirintu 1	Cadna-Owie Formation	696	Faults filled with calcite, sometimes two or possibly more layers.	30m (15m net), with veins and faults	8.8	-0.3
6	Mirintu 1	Cadna-Owie Fm: Wyandra Sandstone	675.29-675.33	Calcareous cement probably associated with faults.	30m (15m net), with veins and faults	9.54	-3.41
5a	Mirintu 1	Cadna-Owie Formation	680.36-680.395	Calcite fault fill, veins, and associated calcite cemented sandstone.	30m (15m net), with veins and faults	9.51	-2.79
203	Muteroo 1	Namur Sandstone	5240	Calcite cement & apparently siderite (not in XRD), coal frags.	65.5m (58m net) (215 ft (190 ft net))	11.32	-5.51
201	Muteroo 1	Namur Sandstone	5290	Calcite cement & apparently siderite (not in XRD).	65.5m (58m net) (215 ft (190 ft net))	18.75	-1.4
202	Muteroo 1	Namur Sandstone	5350	Calcite cement & apparently siderite (not in XRD).	65.5m (58m net) (215 ft (190 ft net))	14.14	-0.4
228	Muteroo 1	Namur Sandstone	5400	Calcite cement, coal and apparently siderite (not in XRD).	65.5m (58m net) (215 ft (190 ft net))	10.82	-6.53

Sample	Well	Formation	Depth (m unless marked ft)	Some notes	Carbonate cemented zone thickness (m)	$\delta^{18}\text{O}_{\text{VSMOW}}\text{‰}$	$\delta^{13}\text{C}_{\text{VPDB}}\text{‰}$
232-dol	Muteroo 1	Hutton Sandstone	6170	Dolomite, siderite and rare coal frags.	Sporadic	10.73	-7.26
164	Narcoonowie 004	Murta Formation	4395	5 feet below oil, calcite cement and veins.	430 ft (200 ft net)	10.64	-9.77
7	Saltern Creek 1	(Hooray Equiv.) Namur Sandstone	1651'2"-4"	Calcite cement.	Sporadic	8.98	-2.62
194	Spencer West 1	Namur Sandstone	4870	Calcite cement.	129.5m (97.5m net) (425 ft (320 ft net))	14.18	-1.88
195	Spencer West 1	Namur Sandstone	4910	Calcite cement.	129.5m (97.5m net) (425 ft (320 ft net))	12.11	-2.31
197	Spencer West 1	Namur Sandstone	5000	Calcite cement.	129.5m (97.5m net) (425 ft (320 ft net))	11.96	-2.18
198	Spencer West 1	Namur Sandstone	5050	Calcite cement.	129.5m (97.5m net) (425 ft (320 ft net))	10.75	-4.93
178	Strzelecki 015	Namur Sandstone	5300	Calcite cement, near trace oil show.	134m (128m net) (440 ft (420 ft net))	13.13	-1.73
179	Strzelecki 015	Namur Sandstone	5380	Calcite cement.	134m (128m net) (440 ft (420 ft net))	10.59	-4.38
152	Thargomindah 1A	Adori Sandstone	966.86-967.12	Calcite veins/faults? and cement.	10m (5m net)	11.8	-9.42
113	Thargomindah 1A	Adori Sandstone	970.18-970.28	Calcite cement cut by subvertical calcite veins, also heavy mineral concentrations present along bedding laminations.	10m (5m net)	8.29	-1.71
114	Thargomindah 2	Mackunda Formation	409.02-409.12	Some cone-in-cone nearby.	Sporadic calcite fracture fill and cement.	14.22	-1.06
153	Thargomindah 2	Mackunda Formation	409.66-409.73	Calcite veins.	Sporadic calcite fracture fill and cement.	14.49	-8.46
151	Thargomindah 2	Allaru Mudstone	454-454.03	Calcite veins.	Sporadic calcite fracture fill and cement.	12.51	-5.49
115	Thargomindah 2	Allaru Mudstone	544.14-544.26	Brecciated zones, calcite cemented sandstone and fractures and cone-in-cone, shells. Calcite mixed with grey mud. Pyrite present.	Sporadic calcite fracture fill and cement.	15.36	-15.94
116	Thargomindah 2	Allaru Mudstone	556.31-556.37	Cone-in-cone? Calcite faults and veins in frags, concretions, shells. Calcite mixed with grey mud.	Sporadic calcite fracture fill and cement.	13.39	-8.89
117	Thargomindah 2	Allaru Mudstone	560.86-560.96	Clay fault fill? Calcite veins.	Sporadic calcite fracture fill and cement.	13.22	-9.12
157	Thargomindah 2	Allaru Mudstone	576.18-576.29	Calcite veins.	Sporadic and frac associated	14.28	-13.54
118	Thargomindah 2	Cadna-Owie Formation	956.38-956.44	Calcite cement.	25m (16m net)	10.93	-4.21
119	Thargomindah 2	Cadna-Owie Formation	998.44-998.52	Calcite cement sporadic and/or frac associated, bounded by faults over 1.3 m at 997 m.	Sporadic calcite fracture fill and cement.	12.79	1.13
120	Thargomindah 3	Hooray (Namur) Sandstone	1115.47-1115.53	Calcite cement associated with slicks and microfaults.	15m (7m net)	9.33	-4.62
121	Thargomindah 3	Hooray (Namur) Sandstone	1171.58-1171.74	Calcite cement associated with slicks and faults.	10m (5m net)	14.11	-7.21
168-cal	Ulandi 5	Cadna-Owie Formation	3914'10"	Oil show, calcite cement.	61m (24m net) (200 ft (80 ft net))	14.74	-5.61
168-sid	Ulandi 5	Cadna-Owie Formation	3914'10"	Oil show, calcite cement.	61m (24m net) (200 ft (80 ft net))	17.99	-5.18
58	Widnerpool 1	Wallumbilla Formation	559'-562'	Calcite cement, near thin limestone.	Sporadic	22.35	-15.88

Sample	Well	Formation	Depth (m unless marked ft)	Some notes	Carbonate cement zone thickness (m)	$\delta^{18}\text{O}_{\text{VSMOW}} \text{‰}$	$\delta^{13}\text{C}_{\text{VPDB}} \text{‰}$
59	Widnerpool 1	Westbourne Formation	862'-865'	Calcite cement.	75m (60m net)	13.28	-3.23
8	Winna-1	(Hooray Equiv.) Murta Formation		Good oil shows, moderate siliceous and strong calcite cement.	42m (11 m net)	6.58	-4.21
9	Yongala 1	Mackunda Formation	2500'-2510'	Very calcite cemented.	128m (82m net) (420 ft (270 ft net))	14.33	-10.65

A)



B)

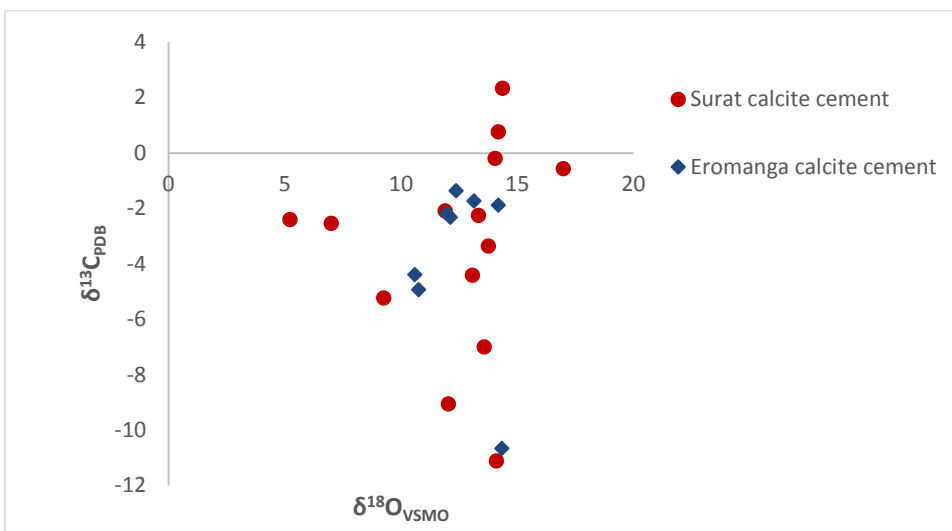


Figure 8: a) Carbon and oxygen isotope compositions of Surat and Eromanga carbonate cements and veins; b) samples from significant carbonate cemented intervals (>100m net thickness of calcite cement). Modified after Golding *et al.* (2014).

Table 12: Carbonate carbon and oxygen stable isotopes for Surat Basin calcites and siderites from cemented and veined sandstone intervals.

Sample	Well	Formation	Depth (m unless marked ft)	Some notes	Carbonate cemented zone thickness (m)	$\delta^{18}\text{O}_{\text{VSMOW}}$ ‰	$\delta^{13}\text{C}_{\text{VPDB}}$ ‰
82	Alton 3	Evergreen Formation	6066'-6066'6"	Calcite cement, oil show, 100 feet above minor coal.	Sporadic	7.54	-2.75
35	Brigalow 1	Rolling Downs Group	890	Calcite and glauconite cement.	73m (23.5m net) (240 ft (77 ft net))	15.17	-6.5
85	Cameron 1	Springbok Sandstone	147.91-148	Calcite cement. Interval has siderite nodules up to 1 cm (though not in this sample), 10 m below and 15 m above coal.	5m (4.5m net)	16.25	1.95
156	Cameron 1	Walloon Coal Measures	230.7-230.92	Fault calcite cement/veins?	Sporadic and fracture associated	9.47	9.97
84	Cameron 1	Walloon Coal Measures	230-230.22	Calcite cement and veins. Lots of solid calcite and reactive clays present.	Sporadic calcite fracture fill and cement.	10.64	5.46
74-cal	Chinchilla 4	Gubberamunda Sandstone	120.27	Minor coal containing thin sandstone.	Sporadic	7.24	6.48
74-sid	Chinchilla 4	Gubberamunda Sandstone	120.27	Minor coal containing thin sandstone.	Sporadic	9.19	6.82
161a-cal	Chinchilla 4	Walloon Coal Measures	650.30-650.48	Black minerals. Interval has calcite, siderite, micro-faults, veins, cone-in-cone, coal cleat, and sandstone cement	Sporadic and fracture associated.	5.9	6.2
161b1-sid	Chinchilla 4	Walloon Coal Measures	650.30-650.48	Siderite-rich subsample of interval.	Sporadic and fracture associated.	5.9	11.1
161b3-sid	Chinchilla 4	Walloon Coal Measures	650.30-650.48	Siderite-rich subsample of interval.	Sporadic and fracture associated.	6.0	10.2
10	Chinchilla 4	Hutton Sandstone	799m	Calcite cement, 10 m above micro-faulted veined interval.	Sporadic, probably fault related.	24.7	0.8
76-cal	Chinchilla 4	Evergreen Formation	1032.68-1032.73	Calcite in fault plane and cement.	Sporadic calcite fracture fill and cement.	6.46	-5.20
76-sid	Chinchilla 4	Evergreen Fm	1032.68-1032.73	Calcite in fault plane and cement.	Sporadic calcite fracture fill and cement.	13.74	1.91
36	Davidson 1	Hutton Sandstone	5440'-5450'	Strong calcite cement, some coal.	73m (20m net) (240 ft (66 ft net))	10.64	-2.05
11	Davidson 1	Precipice Sandstone	5840'-5850'	Strong calcite cement.	55m (21.5m net) (180 ft (71 ft net))	4.90	-3.56
12	Davidson 1	Precipice Sandstone	6010'-6020'	Extreme calcite cement.	49m (18m net) (160 ft (60 ft net))	6.43	-9.15
37	Green Swamp 1	Walloon CM	1000	Abundant calcite cement, apparently dolomite, abundant coal, some tuff layers.	670m (342m net)	14.18	0.77
13	Green Swamp 1	Hutton Sandstone	1500	Abundant strong calcite cement, siliceous cement.	347m (276.5m net)	7.00	-2.53
38	Green Swamp 1	Hutton Sandstone	1620	Abundant calcite in aggregates, also siliceous cement, apparently oolites too.	347m (276.5m net)	13.75	-3.35
86	Mitchell 2	Bungil Formation	69.43-69.52	Calcite cement, burrows filled with pyrite, plant frags though.	Sporadic	19.62	5.86
87-cal	Mitchell 2	Bungil Fm	85.91-85.97	Siderite cement/nodule.	Sporadic	20.77	0.64
87-sid	Mitchell 2	Bungil Fm	85.91-85.97	Siderite cement/nodule.	Sporadic	23.44	-4.64
88	Mitchell 2	Gubberamunda Sandstone	292.68-292.78	"Mottled" calcite cement in minor finely laminated intervals. Abundant garnets 3 m below this.	Sporadic	13.31	-8.86
83	Moonie 38	Evergreen Formation	1727.65-1727.79	Calcite cemented conglomeritic sandstone with discontinuous	219m (91m net)	13.06	-4.41

Sample	Well	Formation	Depth (m unless marked ft)	Some notes	Carbonate cemented zone thickness (m)	$\delta^{18}\text{O}_{\text{VSMOW}}$ ‰	$\delta^{13}\text{C}_{\text{VPDB}}$ ‰
				calcite mineralised cleated coal layers. Oil shows.			
39	Moonie 40	Blythesdale Group	1000'	Common strong calcite cement, some coal.	295.5m (73m net) (970 ft (240 ft net))	16.39	-9.3
53	Moonie 40	Hutton Sandstone	4830'	Common patchy hard calcite cement.	271m (152m net) (890 ft (500 ft net))	13.57	-6.99
40	Moonie Corner 1	Walloon CM	1270	Strong calcite in aggregates, siliceous cement, some coal.	390m (240m net)	14.1	-11.11
41	Moonie Corner 1	Walloon CM	1371	Common abundant calcite, siliceous cement, and carbonaceous lithics (coal).	390m (240m net)	14.05	-0.19
42	Moonie Corner 1	Walloon CM	1437	Strong calcite cement, siliceous cement, some coal.	390m (240m net)	13.33	-2.25
55	Moonie Corner 1	Walloon CM	1497	Strong calcite cement, some dolomite.	390m (240m net)	16.98	-0.56
43	Moonie Corner 1	Evergreen Fm	1818	Strong calcite cement, siliceous cement, some coal, rare limestone.	150m (95m net)	11.9	-2.08
44	Moonie Corner 1	Precipice Sandstone	1905	Strong calcite and siliceous cement.	60m (47m net)	8.99	-4.91
45	Strathpine 1	Walloon CM	270	Calcite and siliceous cement.	60m (47m net)	12.18	2.97
47	Strathpine 1	Hutton Sandstone	390	Abundant calcite cement, some siliceous cement, coal.	195m (135m net)	14.36	2.34
14	Strathpine 1	Hutton Sandstone	500	Abundant calcite cement.	195m (135m net)	5.22	-2.40
48	Strathpine 1	Evergreen Fm	618	Abundant calcite cement, some siliceous cement, coal.	Sporadic	12.18	-0.32
49	Strathpine 1	Evergreen Fm	633	Abundant calcite cement, some siliceous cement.	Sporadic	13.32	0.18
62	Strathpine 1	Evergreen Fm	678	Abundant calcite cement.	171m (52m net)	8.72	-7.02
61	Strathpine 1	Precipice Sandstone	753	Abundant calcite cement, above oil.	171m (52m net)	8.31	-1.68
50	Strathpine 1	Precipice Sandstone	801	Abundant calcite cement, oil.	171m (52m net)	8.37	-7.64
15	Sussex Downs-1	Precipice Sandstone	6800'-6810'	Abundant white calcite and clay cement.	Sporadic	6.27	-4.71
67	West Wandoan 1	Hutton Sandstone	800.70-800.85	WC15 calcite cement.	N/A log unavailable for this depth	4.55	1.06
70	West Wandoan 1	Evergreen Formation	1056.10-1056.19	Calcite cement.	Sporadic	3.99	-7.40
80	Yapunyah 1	Evergreen Formation	4970'4"-4970'10"	Calcite cement, 15 feet above oil show. Minor coals. Core sample from base of calcite zone (rest was chipped).	283m (930 ft) spanning Hutton and Evergreen, 204m net (670 ft net)	12.04	-9.05
81	Yapunyah 1	Evergreen Formation	4993'8"-4994'4"	Calcite cement, minor coal, 10 feet above fault, 10 feet below and 50 feet above oil shows. Core sample from base of calcite zone (rest was chipped).	283m (930 ft) spanning Hutton and Evergreen, 204m net (670 ft net)	9.25	-5.22

Table 13: Carbonate stable isotope modelling for Eromanga Basin samples. Grey shading shows most likely fluid oxygen and carbon isotope compositions based on modelling and available fluid inclusion data; horizontal green shading highlights ¹⁸O-enriched samples.

Sample #	Well	Depth (m unless marked ft)	Modelled fluid isotopes at different temperatures °C									
			Oxygen					Carbon				
			40	80	120	160	200	40	80	120	160	200
127a	Blackall 1	622.35-622.6	-12.93	-6.87	-2.56	0.61	3.01	-6.82	-6.09	-6.09	-6.57	-7.34
127b	Blackall 1	622.35-622.6	-13	-6.94	-2.63	0.53	2.93	-6.84	-6.12	-6.12	-6.59	-7.37
89	Blackall 1	622.79-622.89	-13.87	-7.81	-3.51	-0.34	2.06	-8.14	-7.42	-7.42	-7.9	-8.67
90	Blackall 1	773.16-773.24	-11.58	-5.52	-1.21	1.96	4.36	-15.12	-14.39	-14.39	-14.87	-15.64
91	Blackall 2	311.68-611.94	-11.17	-5.11	-0.8	2.36	4.76	-6.66	-5.93	-5.93	-6.41	-7.18
92a	Blackall 2	313.54-313.61	-12.37	-6.31	-2.01	1.16	3.56	-6.15	-5.43	-5.43	-5.9	-6.67
92b	Blackall 2	313.54-313.61	-11.9	-5.84	-1.54	1.63	4.03	-6.07	-5.34	-5.34	-5.82	-6.59
93	Blackall 2	314.6-314.61	-10.06	-4.01	0.3	3.47	5.87	-4.23	-3.5	-3.5	-3.98	-4.75
94	Blackall 2	443.7-443.77	-1.53	4.53	8.83	12	14.4	-2.06	-1.34	-1.34	-1.81	-2.59
95	Blackall 2	444.51-444.565	-3.96	2.1	6.41	9.58	11.98	-3.95	-3.23	-3.23	-3.7	-4.47
96	Blackall 2	474.19-474.36	-10.17	-4.11	0.2	3.37	5.76	-5.08	-4.36	-4.36	-4.83	-5.61
125	Blackall 2	474.93-475.08	-9.07	-3.02	1.29	4.46	6.86	-12.6	-11.87	-11.87	-12.35	-13.12
97	Blackall 2	475.88-476.02	-10.16	-4.1	0.21	3.37	5.77	-4.91	-4.18	-4.18	-4.66	-5.43
98	Blackall 2	660.38-660.54	0.27	6.33	10.63	13.8	16.2	-23.39	-22.67	-22.67	-23.14	-23.91
99	Blackall 2	665.71-665.73	-11.56	-5.5	-1.19	1.98	4.37	-16.97	-16.25	-16.25	-16.72	-17.5
155	Blackall 2	809.5-809.56	-11.18	-5.12	-0.81	2.36	4.76	-14.3	-13.58	-13.58	-14.05	-14.82
100	Blackall 2	811.46-811.47	-13.14	-7.08	-2.77	0.4	2.8	-10.17	-9.44	-9.44	-9.92	-10.69
63	Bodalla South 2	150	-3.14	2.92	7.22	10.39	12.79	-12.31	-11.59	-11.58	-12.06	-12.83
51	Bodalla South 9	1596	-17.08	-11.02	-6.72	-3.55	-1.15	-6.68	-5.96	-5.96	-6.43	-7.2
52	Bodalla South 9	1617	-11.59	-5.53	-1.23	1.94	4.34	-9.4	-8.68	-8.67	-9.15	-9.92
169	Burke 002	5063'7"	-9.74	-3.69	0.62	3.79	6.19	-3.01	-2.29	-2.29	-2.76	-3.54
102	Connemara 1	119.76-119.87	-3.47	2.59	6.89	10.06	12.46	-8.26	-7.53	-7.53	-8.01	-8.78
124	Connemara 1	310.71-311	-10.81	-4.75	-0.45	2.72	5.12	-6.6	-5.88	-5.88	-6.35	-7.12
148	Connemara 1	311.75-311.82	-9.09	-3.03	1.28	4.45	6.85	-3.83	-3.11	-3.1	-3.58	-4.35
123	Connemara 1	371.72-371.83	-10.43	-4.38	-0.07	3.1	5.5	-4.63	-3.9	-3.9	-4.38	-5.15
149	Connemara 1	390-390.18	-10.39	-4.33	-0.03	3.14	5.54	-3.91	-3.19	-3.19	-3.66	-4.44
150	Connemara 1	391.88-392	-11.9	-5.84	-1.53	1.63	4.03	-4.31	-3.59	-3.59	-4.06	-4.84
126a	Connemara 1	395.4-395.5	-10.83	-4.77	-0.46	2.7	5.1	-3.63	-2.9	-2.9	-3.38	-4.15
126b	Connemara 1	395.4-395.5	-10.79	-4.73	-0.42	2.75	5.14	-3.6	-2.88	-2.88	-3.35	-4.13
158	Connemara 1	448.83-448.87	-10.66	-4.6	-0.29	2.88	5.28	-1.49	-0.77	-0.77	-1.24	-2.01
159	Connemara 1	673.45-673.48	-10.09	-4.03	0.27	3.44	5.84	-15.13	-14.4	-14.4	-14.88	-15.65
103	Connemara 1	942.17-942.37	-15.85	-9.79	-5.49	-2.32	0.08	-4.76	-4.04	-4.04	-4.51	-5.29
104	Connemara 1	945.04-945.16	-13.71	-7.65	-3.34	-0.17	2.23	-5.14	-4.42	-4.42	-4.89	-5.66
105	Connemara 1	946.24-946.34	-12.52	-6.46	-2.16	1.01	3.41	-4.87	-4.14	-4.14	-4.62	-5.39
165	Dullingari 036	4883'3"	-14.51	-8.45	-4.15	-0.98	1.42	-5.94	-5.22	-5.22	-5.69	-6.47
167a	Dullingari 037	5065'8.5"	-14.04	-7.98	-3.68	-0.51	1.89	-6.33	-5.61	-5.61	-6.08	-6.86
173-cal	Dullingari 037	5068'8"	-10.64	-4.58	-0.28	2.89	5.29	-4.76	-4.03	-4.03	-4.51	-5.28
173-sid	Dullingari 037	5068'8"	-11.12	-4.29	0.55	4.12	6.82	-4.13	-3.41	-3.41	-3.88	-4.66
171	Dullingari 039	5024'9"	-11.86	-5.8	-1.5	1.67	4.07	-9.62	-8.89	-8.89	-9.37	-10.14
187	Gidgealpa 18	5510	-12.39	-6.33	-2.03	1.14	3.54	-1.7	-0.97	-0.97	-1.45	-2.22
189	Gidgealpa 18	5580	-14.82	-8.76	-4.46	-1.29	1.11	-3.65	-2.92	-2.92	-3.4	-4.17
1	Inland 3	4430'-4440'	-12.58	-6.53	-2.22	0.95	3.35	-1.98	-1.25	-1.25	-1.73	-2.5
64	Inland 3	5570'-5580'	-11.81	-5.75	-1.45	1.72	4.12	-12	-11.28	-11.27	-11.75	-12.52
78-cal	Jackson South 2	4279'6.5"-4279'9"	-14.93	-8.87	-4.57	-1.4	1	-9.23	-8.51	-8.51	-8.98	-9.76
78-sid	Jackson South 2	4279'6.5"-4279'9"	-12.2	-5.38	-0.53	3.04	5.74	-6.47	-5.75	-5.75	-6.22	-6.99
166	Jena 2	3882'9"	-11.55	-5.49	-1.18	1.99	4.39	-10.91	-10.19	-10.19	-10.66	-11.44
170-cal	Jena 6	3934'1"	-13.1	-7.04	-2.73	0.44	2.84	-7.21	-6.49	-6.49	-6.96	-7.74
170-sid	Jena 6	3934'1"	-8.58	-1.76	3.09	6.65	9.35	-3.6	-2.87	-2.87	-3.35	-4.12
107	Jundah 1	795.59-795.75	-13.5	-7.44	-3.14	0.03	2.43	-5.38	-4.66	-4.66	-5.13	-5.91
108	Jundah 1	905.67-905.673	-15.68	-9.63	-5.32	-2.15	0.25	-3.37	-2.65	-2.64	-3.12	-3.89
109	Jundah 1	906.46-906.58	-12.74	-6.68	-2.38	0.79	3.19	-5.86	-5.14	-5.14	-5.61	-6.39
110	Jundah 1	939.62-939.68	-13.93	-7.87	-3.56	-0.4	2	-5.35	-4.63	-4.63	-5.1	-5.88
111	Jundah 1	940.48-940.58	-12.4	-6.34	-2.04	1.13	3.53	-6	-5.28	-5.28	-5.75	-6.53
112	Jundah 1	941.52-941.7	-12.95	-6.89	-2.59	0.58	2.98	-6.65	-5.93	-5.93	-6.4	-7.17

Modelled fluid isotopes at different temperatures °C												
Sample #	Well	Depth (m unless marked ft)	Oxygen					Carbon				
			40	80	120	160	200	40	80	120	160	200
65	Kenmore 12	510	-9.77	-3.71	0.59	3.76	6.16	-7.7	-6.98	-6.97	-7.45	-8.22
66	Kenmore 12	920	-3.87	2.19	6.49	9.66	12.06	-15.85	-15.13	-15.12	-15.6	-16.37
56	Kenmore 12	1075	-11.9	-5.84	-1.54	1.63	4.03	-4.93	-4.21	-4.2	-4.68	-5.45
57	Kenmore 12	1350	-13.09	-7.03	-2.73	0.44	2.84	-3.38	-2.66	-2.65	-3.13	-3.9
212-dol	Kerna 3	5480	-18.48	-11.44	-6.44	-2.76	0.03	-12.1	-10.98	-10.7	-10.97	-11.59
181-dol	Kerna 3	5500	-18.45	-11.41	-6.41	-2.72	0.06	-11.48	-10.37	-10.09	-10.36	-10.97
182	Kerna 3	5640	-12.32	-6.26	-1.96	1.21	3.61	-2.39	-1.66	-1.66	-2.14	-2.91
183	Kerna 3	5700	-15.28	-9.22	-4.91	-1.74	0.66	-6.75	-6.03	-6.03	-6.5	-7.28
163	Marabooka 004	3433	-13.06	-7	-2.7	0.47	2.87	-14.85	-14.12	-14.12	-14.6	-15.37
3	Mirintu-1	677	-15.77	-9.71	-5.4	-2.23	0.16	-3.61	-2.89	-2.89	-3.36	-4.13
4	Mirintu-1	677	-14.88	-8.82	-4.52	-1.35	1.05	-3.66	-2.94	-2.94	-3.41	-4.19
2	Mirintu-1	696	-16.66	-10.6	-6.29	-3.12	-0.72	-2.32	-1.59	-1.59	-2.07	-2.84
6	Mirintu-1	675.29-675.33	-15.92	-9.87	-5.56	-2.39	0.01	-5.43	-4.71	-4.71	-5.18	-5.96
5a	Mirintu-1	680.36-680.395	-15.95	-9.89	-5.58	-2.41	-0.01	-4.81	-4.09	-4.09	-4.56	-5.33
203	Muteroo 1	5240	-14.14	-8.08	-3.78	-0.61	1.79	-7.53	-6.81	-6.8	-7.28	-8.05
201	Muteroo 1	5290	-6.71	-0.66	3.65	6.82	9.22	-3.42	-2.7	-2.69	-3.17	-3.94
202	Muteroo 1	5350	-11.32	-5.26	-0.96	2.21	4.61	-2.42	-1.7	-1.7	-2.17	-2.95
228	Muteroo 1	5400	-14.64	-8.58	-4.28	-1.11	1.29	-8.55	-7.82	-7.82	-8.3	-9.07
232-dol	Muteroo 1	6170	-18.91	-11.88	-6.87	-3.19	-0.4	-11.29	-10.17	-9.89	-10.16	-10.78
164	Narcoonowie 004	4395	-14.81	-8.76	-4.45	-1.28	1.12	-11.79	-11.07	-11.07	-11.54	-12.32
7	Saltern Creek 1	1651'2"-4"	-16.48	-10.42	-6.11	-2.95	-0.55	-4.64	-3.91	-3.91	-4.39	-5.16
194	Spencer West 1	4870	-11.28	-5.22	-0.91	2.25	4.65	-3.9	-3.18	-3.18	-3.65	-4.43
195	Spencer West 1	4910	-13.35	-7.29	-2.99	0.18	2.58	-4.33	-3.61	-3.61	-4.08	-4.85
197	Spencer West 1	5000	-13.5	-7.44	-3.13	0.03	2.43	-4.2	-3.48	-3.48	-3.95	-4.73
198	Spencer West 1	5050	-14.71	-8.65	-4.35	-1.18	1.22	-6.95	-6.22	-6.22	-6.7	-7.47
178	Strzelecki 015	5300	-12.33	-6.27	-1.97	1.2	3.6	-3.75	-3.03	-3.03	-3.5	-4.28
179	Strzelecki 015	5380	-14.87	-8.81	-4.51	-1.34	1.06	-6.39	-5.67	-5.67	-6.15	-6.92
152	Thargomindah 1A	966.86-967.12	-13.66	-7.6	-3.3	-0.13	2.27	-11.44	-10.72	-10.72	-11.19	-11.96
113	Thargomindah 1A	970.18-970.28	-17.17	-11.11	-6.81	-3.64	-1.24	-3.73	-3.01	-3.01	-3.48	-4.26
114	Thargomindah 2	409.02-409.12	-11.24	-5.18	-0.87	2.3	4.69	-3.08	-2.36	-2.36	-2.83	-3.6
153	Thargomindah 2	409.66-409.73	-10.97	-4.91	-0.61	2.56	4.96	-10.48	-9.76	-9.76	-10.23	-11.01
151	Thargomindah 2	454-454.03	-12.95	-6.89	-2.59	0.58	2.98	-7.51	-6.79	-6.79	-7.26	-8.04
115	Thargomindah 2	544.14-544.26	-10.1	-4.04	0.26	3.43	5.83	-17.96	-17.24	-17.24	-17.71	-18.49
116	Thargomindah 2	556.31-556.37	-12.07	-6.01	-1.71	1.46	3.86	-10.88	-10.15	-10.15	-10.63	-11.4
117	Thargomindah 2	560.86-560.96	-12.24	-6.18	-1.88	1.29	3.69	-11.14	-10.41	-10.41	-10.89	-11.66
157	Thargomindah 2	576.18-576.29	-11.18	-5.13	-0.82	2.35	4.75	-15.56	-14.84	-14.83	-15.31	-16.08
118	Thargomindah 2	956.38-956.44	-14.53	-8.47	-4.17	-1	1.4	-6.22	-5.5	-5.5	-5.97	-6.75
119	Thargomindah 2	998.44-998.52	-12.67	-6.61	-2.31	0.86	3.26	-0.89	-0.17	-0.17	-0.64	-1.41
120	Thargomindah 3	1115.47-1115.53	-16.13	-10.07	-5.77	-2.6	-0.2	-6.64	-5.92	-5.92	-6.39	-7.17
121	Thargomindah 3	1171.58-1171.74	-11.34	-5.29	-0.98	2.19	4.59	-9.23	-8.5	-8.5	-8.98	-9.75
168-cal	Ulandi 5	3914'10"	-10.72	-4.66	-0.35	2.81	5.21	-7.63	-6.9	-6.9	-7.38	-8.15
168-sid	Ulandi 5	3914'10"	-10.42	-3.6	1.24	4.81	7.51	-7.2	-6.47	-6.47	-6.95	-7.72
58	Widnerpool 1	559'-562'	-3.11	2.95	7.25	10.42	12.82	-17.9	-17.18	-17.17	-17.65	-18.42
59	Widnerpool 1	862'-865'	-12.18	-6.12	-1.82	1.35	3.75	-5.25	-4.53	-4.52	-5	-5.77
8	Winna-1	1008.08	-18.88	-12.82	-8.51	-5.35	-2.95	-6.23	-5.51	-5.51	-5.98	-6.75
9	Yongala 1	2500'-2510'	-11.13	-5.07	-0.77	2.4	4.8	-12.67	-11.95	-11.95	-12.42	-13.19

Table 14: Carbonate stable isotope modelling for Surat Basin samples. Grey shading shows most likely fluid oxygen and carbon isotope compositions based on modelling and available fluid inclusion data; horizontal green shading highlights ¹⁸O-enriched samples.

Sample	Well	Depth (m unless marked ft)	Modelled fluid isotopes at different temperatures °C									
			Oxygen					Carbon				
			40	80	120	160	200	40	80	120	160	200
82	Alton 3	6066'-6066'6"	-17.92	-11.86	-7.56	-4.39	-1.99	-4.76	-4.04	-4.04	-4.51	-5.29
35	Brigalow 1	890	-10.29	-4.23	0.07	3.24	5.64	-8.52	-7.80	-7.79	-8.27	-9.04
85	Cameron 1	147.91-148	-9.21	-3.15	1.15	4.32	6.72	-0.07	0.66	0.66	0.18	-0.59
156	Cameron 1	230.7-230.92	-15.99	-9.93	-5.62	-2.45	-0.05	7.95	8.68	8.68	8.20	7.43
84	Cameron 1	230-230.22	-14.82	-8.76	-4.46	-1.29	1.11	3.44	4.17	4.17	3.69	2.92
74-cal	Chinchilla 4	120.27	-18.22	-12.16	-7.86	-4.69	-2.29	4.46	5.18	5.18	4.71	3.93
74-sid	Chinchilla 4	120.27	-19.23	-12.40	-7.56	-3.99	-1.29	4.80	5.52	5.52	5.05	4.28
161a-cal	Chinchilla 4	650.30-650.48	-19.6	-13.5	-9.2	-6.0	-3.6	4.2	4.9	4.9	4.4	3.7
161b-sid	Chinchilla 4	650.30-650.48	-22.5	-15.7	-10.9	-7.3	-4.6	9.1	9.8	9.8	9.3	8.6
161b-sid	Chinchilla 4	650.30-650.48	-22.4	-15.6	-10.8	-7.2	-4.5	8.2	8.9	8.9	8.4	7.7
10	Chinchilla 4	799m	-0.76	5.30	9.60	12.77	15.17	-1.22	-0.50	-0.49	-0.97	-1.74
76-cal	Chinchilla 4	1032.68- 1032.73	-19.00	-12.94	-8.63	-5.46	-3.06	-7.22	-6.49	-6.49	-6.97	-7.74
76-sid	Chinchilla 4	1032.68- 1032.73	-14.68	-7.86	-3.01	0.55	3.26	-0.11	0.62	0.62	0.14	-0.63
36	Davidson 1	5440'-5450'	-14.82	-8.76	-4.46	-1.29	1.11	-4.07	-3.35	-3.34	-3.82	-4.59
11	Davidson 1	5840'-5850'	-20.56	-14.50	-10.20	-7.03	-4.63	-5.58	-4.85	-4.85	-5.33	-6.10
12	Davidson 1	6010'-6020'	-19.03	-12.97	-8.67	-5.50	-3.10	-11.17	-10.45	-10.45	-10.92	-11.70
37	Green Swamp 1	1000	-11.28	-5.22	-0.92	2.25	4.65	-1.25	-0.53	-0.52	-1.00	-1.77
13	Green Swamp 1	1500	-18.46	-12.40	-8.10	-4.93	-2.53	-4.55	-3.82	-3.82	-4.30	-5.07
38	Green Swamp 1	1620	-11.71	-5.65	-1.35	1.82	4.22	-5.37	-4.65	-4.64	-5.12	-5.89
88	Mitchell 2	292.68-292.78	-12.15	-6.10	-1.79	1.38	3.78	-10.88	-10.16	-10.16	-10.63	-11.40
86	Mitchell 2	69.43-69.52	-5.84	0.22	4.52	7.69	10.09	3.84	4.56	4.57	4.09	3.32
87-cal	Mitchell 2	85.91-85.97	-4.69	1.37	5.67	8.84	11.24	-1.38	-0.66	-0.66	-1.13	-1.90
87-sid	Mitchell 2	85.91-85.97	-4.98	1.84	6.69	10.26	12.96	-6.66	-5.94	-5.94	-6.41	-7.18
83	Moonie 38	1727.65- 1727.79	-12.40	-6.34	-2.03	1.14	3.54	-6.43	-5.71	-5.71	-6.18	-6.96
39	Moonie 40	1000'	-9.07	-3.01	1.29	4.46	6.86	-11.32	-10.60	-10.59	-11.07	-11.84
53	Moonie 40	4830'	-11.89	-5.83	-1.53	1.64	4.04	-9.01	-8.29	-8.28	-8.76	-9.53
40	Moonie Corner 1	1270	-11.36	-5.30	-1.00	2.17	4.57	-13.13	-12.41	-12.40	-12.88	-13.65
41	Moonie Corner 1	1371	-11.41	-5.35	-1.05	2.12	4.52	-2.21	-1.49	-1.48	-1.96	-2.73
42	Moonie Corner 1	1437	-12.13	-6.07	-1.77	1.40	3.80	-4.27	-3.55	-3.54	-4.02	-4.79
55	Moonie Corner 1	1497	-8.48	-2.42	1.88	5.05	7.45	-2.58	-1.86	-1.85	-2.33	-3.10
43	Moonie Corner 1	1818	-13.56	-7.50	-3.20	-0.03	2.37	-4.10	-3.38	-3.37	-3.85	-4.62
44	Moonie Corner 1	1905	-16.47	-10.41	-6.11	-2.94	-0.54	-6.93	-6.21	-6.20	-6.68	-7.45
45	Strathpine 1	270	-13.28	-7.22	-2.92	0.25	2.65	0.95	1.67	1.68	1.20	0.43
47	Strathpine 1	390	-11.10	-5.04	-0.74	2.43	4.83	0.32	1.04	1.05	0.57	-0.20
14	Strathpine 1	500	-20.24	-14.18	-9.88	-6.71	-4.31	-4.42	-3.69	-3.69	-4.17	-4.94
48	Strathpine 1	618	-13.28	-7.22	-2.92	0.25	2.65	-2.34	-1.62	-1.61	-2.09	-2.86
49	Strathpine 1	633	-12.14	-6.08	-1.78	1.39	3.79	-1.84	-1.12	-1.11	-1.59	-2.36
62	Strathpine 1	678	-16.74	-10.68	-6.38	-3.21	-0.81	-9.04	-8.32	-8.31	-8.79	-9.56
61	Strathpine 1	753	-17.15	-11.09	-6.79	-3.62	-1.22	-3.70	-2.98	-2.97	-3.45	-4.22
50	Strathpine 1	801	-17.09	-11.03	-6.73	-3.56	-1.16	-9.66	-8.94	-8.93	-9.41	-10.18
15	Sussex Downs-1	6800'-6810'	-19.19	-13.13	-8.83	-5.66	-3.26	-6.73	-6.01	-6.00	-6.48	-7.25
67	West Wandoan 1	800.70-800.85	-20.91	-14.85	-10.55	-7.38	-4.98	-0.96	-0.24	-0.23	-0.71	-1.48
70	West Wandoan 1	1056.10- 1056.19	-21.47	-15.41	-11.10	-7.93	-5.53	-9.42	-8.70	-8.70	-9.17	-9.94
80	Yapunya 1	4970'4"- 4970'10"	-13.42	-7.36	-3.06	0.11	2.51	-11.06	-10.34	-10.34	-10.82	-11.59

The Surat carbonate cements with the least positive $\delta^{18}\text{O}$ values occur in wells Chinchilla 4, Davidson 1, Green Swamp 1, Strathpine 1, Sussex Downs 1 and West Wandoan 1 that lie on or adjacent to the Moonie-Gooniwindi and Burunga-Leichhardt thrust fault systems and subsidiary faults (Figure 6), and are largely confined to the Precipice and Hutton sandstones and Evergreen Formation. Three other samples from Chinchilla 4 and Moonie 38 (10, 75 and 83) also formed at similarly elevated temperatures based on fluid inclusion homogenisation temperatures. Movement on these older faults is thought to have continued throughout deposition of the Surat Basin succession and would have provided pathways for hot fluid migration from the underlying Bowen Basin.

In contrast with the Surat, only one Eromanga Basin carbonate has a highly ^{18}O -depleted isotopic composition; however, this sample and eight other Eromanga Basin carbonate samples from SW Queensland and NE South Australia have fluid inclusion homogenisation temperatures that may indicate formation at temperatures $\geq 120^\circ\text{C}$ (Section 3.4; samples 8, 103, 108, 152, 165, 167a, 168b, 171 and 173). Calculated oxygen isotope compositions at 120 to 160 $^\circ\text{C}$ range from -8.51 to 4.81 ‰ (n=11) (Table 13), and are consistent with mixing between low salinity groundwater of meteoric origin and evolved basinal brines possibly sourced from the underlying Cooper Basin, which is supported by the variable salinities up to 14.7 wt% NaCl equivalent (Section 3.4). Previous fluid inclusion data for the Cooper Basin sandstones indicate maximum paleotemperatures of $\leq 160^\circ\text{C}$ and also record a shift in salinity towards values similar to modern groundwater indicative of fluid mixing (Toupin *et al.*, 1997).

Carbonate samples with higher $\delta^{18}\text{O}$ values precipitated under lower temperature conditions and/or from ^{18}O -enriched fluids such as seawater or basinal brines. The seven calcite samples in the Eromanga Basin with $\delta^{18}\text{O}$ values greater than 20 ‰ are from the Queensland section of the basin and restricted to marine strata with local micritic limestone, cone-in-cone structures (Franks, 1969) and glauconite. Calcite mineralisation is fracture related (samples 94, 95 and 98) or occurs as more or less extensive calcite cement (samples 63, 102, 66 and 58) sometimes in association with silica cements and thin limestone horizons. Calculated fluid oxygen isotope compositions at 40 to 80 $^\circ\text{C}$ of -3.96 to 6.33 ‰ (Table 13) and the depositional setting may suggest that calcite mineralisation was related to marine pore waters and resulted from redistribution of biogenic carbonate in the host strata. Surat Basin calcite and siderite cements/nodules in the fluvial to shallow marine Bungil Formation (Mitchell 2 - samples 86 and 87) have overlapping calculated fluid oxygen isotope compositions at 40 to 80 $^\circ\text{C}$ of -4.98 to 1.84 ‰ (Table 14), which support a similar origin. On the other hand, the calculated fluid oxygen isotope composition for the Surat Basin Chinchilla 4-799.6 m at 120°C of 7.9 ‰ is enriched in ^{18}O relative to seawater and meteoric waters, which suggests the calcite precipitated from a deep-basin fluid composed of highly evolved meteoric water. Magmatic fluids and evaporated seawater may have similar $\delta^{18}\text{O}$ values but can be excluded on the basis of the fluid inclusion data for this sample that indicate the carbonate cement precipitated from low salinity fluids with up to 1.74 wt.% NaCl equivalent (Section 3.4).

Modelling of fluid carbon isotope composition is more complex than for oxygen isotopes as the carbon isotope fractionation under aqueous conditions depends on the pH of the fluid. Under near neutral to acidic conditions, H_2CO_3 is the dominant aqueous carbonate species at temperatures less than 200°C , whereas HCO_3^- is the dominant species under near neutral to mildly alkaline conditions (Large *et al.*, 2001). The precipitation of calcite in reservoir settings occurs under near neutral to alkaline conditions so the modelling of carbon isotope

fractionation has been undertaken for the HCO_3^- -dominant case using the fractionation equations of (Ohmoto and Rye, 1979) (Tables 13 and 14). The majority of Surat and Eromanga carbonates have calculated carbon isotope fluid compositions at model temperatures $\geq 80^\circ\text{C}$ that are consistent with inorganic sources, specifically marine carbonate ($\delta^{13}\text{C}$ value of ~ 0 ‰) and magmatic/mantle carbon dioxide ($\delta^{13}\text{C}$ value of ~ -5 ‰) (Hoefs, 1987).

Twenty two samples from the Eromanga Basin and five samples from the Surat Basin are more depleted in ^{13}C , with calculated carbon fluid compositions less than -10 ‰ across the model temperature range (Tables 13 and 14). This necessarily requires an organic carbon source most likely associated with local microbial degradation processes or thermal maturation and hydrocarbon generation at deeper levels (Hoefs, 1987). The majority of Eromanga and Surat basin carbonates with ^{13}C -depleted isotopic compositions occur in mudstone/siltstone dominated intervals and have relatively ^{18}O -enriched isotopic compositions indicative of low temperature formation conditions (Figure 8), which suggests predominantly local organic carbon sources. Only one of the Surat samples that formed under higher temperature conditions linked to hot fluid migration up the Moonie-Goondiwindi and Burunga-Leichhardt thrust fault systems and none of the Eromanga samples that formed under higher temperature conditions from evolved basinal brines has a calculated fluid carbon isotopic composition less than -10 ‰. This does not preclude a role for migration of hydrocarbons and associated CO_2 from deeper levels in the formation of these carbonates as the isotopically heaviest CO_2 in Australian natural gases with $\delta^{13}\text{C}$ values between -26.1 and -2.9 ‰ are thought to be mixtures of thermogenic and inorganic CO_2 (Boreham *et al.*, 2001). On the other hand, nine Surat Basin carbonates have ^{13}C -enriched fluid isotopic compositions (≥ 1 ‰) that may suggest they have incorporated ^{13}C -enriched CO_2 residual from methanogenesis. Another process that may explain the highly positive $\delta^{13}\text{C}$ values is fractionation effects between oxidized and reduced carbon species, i.e., CO_2 and CH_4 at elevated temperatures (Golding *et al.*, 2013a; Golding *et al.*, 2000), which is relevant to the Chinchilla 4 samples.

3.3. Carbonate acid leaching results

Carbonate cement and vein samples were selected for wet chemistry elemental analyses. These analyses provided a variety of useful data. The major element results not only help with assessment of which mineral phases actually dissolved, but can also give some indication of the mineralising fluid/s composition and can be compared with the XRD results to verify which carbonate species may be present in the samples. Minor element analyses likewise help to verify which carbonates are actually present and whether or not other mineral species dissolved and thus may have contributed to the trace element concentrations detected. Various elemental ratios can be used to investigate the potential type/s of mineralising fluid as well as the overall mineralisation regimes. The trace elements, especially the rare earths, can record information such as transport mechanisms, redox conditions, presence/absence of divalent ligands in solution, and even whether the fluid temperature may have been high or low prior to precipitation.

The ICP-OES and ICP-MS element assay results are collated in Tables 15 and 16. The calcite samples are sorted according to basin (Eromanga or Surat) and by type (cement or vein). For ease of reference, sample numbers cited in the text are preceded by a letter (E or S) referring to which basin they belong to. Most of the

acid-reactive portions of the samples are dominantly calcite. To account for variations in Ca-dominated carbonate cement/vein initial sample weight and percentage recovery via acetic acid leaching, the major and minor element results in this section are often discussed in terms of the relative abundance of a particular element normalised to calcium abundance for given samples (Tables 17 and 18). This is expressed as a mass percentage abundance of element “x” with respect to the sum of ppm calcium and ppm element:

$$(x/(x + Ca)*100)$$

The values are denoted as %_{Ca+x} in order to avoid confusion with true elemental mass percentage abundances for given rock samples. The %_{Ca+x} relative abundance data presented for individual elements are not directly comparable with other elements, as the mass of the atoms of the various elements differ and so therefore the same absolute quantity of two different elements could be expressed by different mass percentages with respect to calcium. Some samples which contain more than one carbonate (“mixed carbonates”) may have slightly exaggerated %_{Ca+x} values due to there being less calcium present than for “pure” calcites, and so these sample numbers are in **bold font** to help highlight this fact. Similarly, samples which contain almost an order of magnitude less calcium than the rest of the carbonates are italicised.

To guide the reader, colour coding has been used in the tables to show for example concentrations over 10,000ppm etc., note the legend at the bottom of the table. Similarly, high relative abundances for individual elements (%_{Ca+x}) with respect to the overall data population for that element are shaded grey in Tables 17 and 18. In this discussion, major elements are those with >1 %_{Ca+x} abundance (>10,000 ppm_{Ca+x}) in at least one tested sample, and similarly the cut-offs for minor and trace elements are >0.1 %_{Ca+x}, >0.01 %_{Ca+x}, and <0.01 %_{Ca+x} (<100 ppm_{Ca+x}) respectively.

3.3.1. Major elements

Overall, the acid-leachable portions of samples analysed contain roughly similar proportions of most major elements. There are generally two orders of magnitude more calcium than iron, magnesium and manganese, with iron being more abundant than magnesium, and manganese either greater or of similar abundance to iron in several samples. A quarter of the samples have strontium, sodium and/or aluminium concentrations of approximately the same order of magnitude as magnesium. A number of samples contain significantly elevated concentrations of one or more elements relative to the total population analysed. Al, B, Ba, Ce, Fe, Mn, Fe, K, La, Mg, Mn, Na, Nd, P, S, Si, Sn, Sr and Zn are present in greater than 500ppm abundance within the acid-leachable portion of at least some samples (Tables 15 and 16). The mixed carbonate samples are more difficult to interpret than the calcites; some of the apparent enrichment of elements in terms of %_{Ca+x} may be due to the fact that several mixed carbonates contain less calcium than the majority of samples, though overall the raw data for them still shows enrichment of several elements.

Table 15: Cemented sandstones elemental concentrations* (ppm) and Co/Ni within acid-leached portions. For colour coding refer to the legend at the bottom of the table.

Basin	Sample #	Al	B	Ba	Be	Ca	Cd	Co	Cr	Cs	Cu	Fe	Ga	Hf	K	Li	Mg	Mn	Mo	Nb	Ni	Co/Ni	
Standard	JCp1	1.37E+02	<DL	7.01E+00	2.43E-03	4.57E+05	8.62E-03	4.99E-01	3.34E-01	1.83E-03	6.71E-01	2.67E+02	5.22E-03	4.83E-03	1.05E+01	3.66E-01	9.21E+02	7.54E+00	8.80E-02	1.09E+03	1.30E-03	2.73E+00	0.18
Eromanga	5	7.53E+01	<DL	1.39E+02	3.87E-01	3.35E+05	3.97E-02	3.63E+00	1.43E-01	1.54E-02	1.64E+01	3.43E+03	3.28E-01	<DL	7.41E+02	4.56E-01	<DL	1.92E+04	1.71E-01	4.14E+02	6.05E-04	3.22E+00	1.13
	6	1.97E+02	1.98E+01	1.97E+02	6.57E-01	2.78E+05	1.03E-01	5.37E+00	<DL	2.18E-02	1.43E+01	3.45E+03	5.92E-01	1.75E-03	1.05E+03	5.16E-01	4.45E+03	1.73E+04	1.97E-01	8.42E+02	1.39E-03	7.36E+00	0.73
	7	7.37E+02	1.79E+01	1.00E+02	4.76E-01	3.73E+05	6.41E-02	1.20E+01	<DL	8.59E-03	6.08E+01	4.61E+03	3.49E-01	2.63E-03	1.25E+02	5.76E-01	1.14E+03	1.52E+04	1.33E-01	3.14E+02	1.77E-03	1.57E+01	0.76
	8	2.90E+02	4.74E-01	1.89E+02	8.31E-01	3.13E+05	2.20E-02	5.91E+00	2.67E+00	8.00E-03	2.06E+01	1.65E+04	2.71E-01	2.75E-03	1.12E+02	1.11E-01	8.86E+03	8.17E+02	1.46E-02	7.47E+01	1.76E-03	1.37E+01	0.43
	65	1.43E+04	1.13E+00	3.44E+02	8.08E+00	7.01E+05	<DL	1.94E+01	3.32E+01	n.d.	9.22E+01	4.30E+04	n.d.	n.d.	5.62E+03	2.67E+01	1.80E+04	2.06E+04	1.88E+00	2.56E+03	n.d.	2.11E+01	0.92
	79	5.57E+03	4.25E+00	2.44E+02	1.53E+00	3.35E+05	7.07E-02	8.16E+00	8.08E+00	4.14E-02	2.02E+01	6.50E+01	4.69E-01	7.61E-03	1.32E+03	1.11E+04	1.18E+04	1.48E+03	6.97E-02	2.14E+03	1.14E-02	1.32E+01	0.62
	89	2.11E+03	1.50E+00	8.63E+01	1.52E+00	5.16E+05	<DL	1.12E-01	2.91E+01	n.d.	2.15E+01	5.75E+03	n.d.	n.d.	3.69E+02	2.40E+00	1.78E+03	2.85E+03	3.13E+00	2.54E+02	n.d.	1.76E+01	0.01
	102	9.99E+03	7.05E+02	2.72E+02	3.98E+00	2.54E+05	<DL	6.72E+00	4.32E+01	n.d.	1.91E+01	1.50E+04	n.d.	n.d.	3.62E+03	8.53E+00	7.77E+03	1.31E+04	1.54E+01	2.57E+03	n.d.	5.59E+00	1.20
	103	1.34E+03	<DL	9.71E+01	4.44E-01	4.20E+05	2.23E-02	6.40E+00	1.27E+01	3.35E-03	2.21E+02	2.64E+03	3.56E-01	<DL	3.47E+02	1.20E+00	<DL	8.91E+02	2.72E-02	5.05E+02	3.11E-03	1.24E+01	0.51
	104	4.86E+03	<DL	2.67E+02	4.61E+00	8.46E+05	<DL	1.32E+01	3.36E+00	n.d.	1.55E+02	1.26E+04	n.d.	n.d.	1.09E+03	2.87E+00	4.50E+03	1.30E+04	2.95E+01	8.71E+02	n.d.	1.43E+01	0.93
	105	2.29E+04	1.33E+01	1.10E+02	9.10E-01	3.04E+05	6.15E-02	3.92E+02	3.46E+02	5.14E-02	1.45E+02	2.62E+04	2.81E+00	1.87E-02	2.20E+03	9.27E+00	5.77E+03	9.54E+02	1.02E+00	4.17E+03	2.53E-02	4.80E+01	8.16
	108	1.50E+03	4.08E+02	7.47E+01	8.00E-02	4.29E+05	9.84E-03	2.42E+00	3.91E+00	9.46E-03	3.26E+01	4.75E+03	1.38E-01	<DL	9.80E+02	4.03E+00	<DL	6.46E+03	2.67E-01	1.54E+03	6.52E-03	5.05E+00	0.48
	109	2.51E+03	<DL	5.50E+01	3.03E+00	3.42E+05	<DL	<DL	7.88E+01	n.d.	8.66E+00	9.67E+03	n.d.	n.d.	2.33E+02	6.19E+00	2.89E+03	2.58E+03	7.30E+00	1.67E+02	n.d.	4.66E+01	Co <DL
	110	1.08E+04	4.82E+02	1.05E+02	3.50E+00	7.68E+05	<DL	9.87E+00	2.52E+01	n.d.	1.85E+01	1.27E+04	n.d.	n.d.	2.87E+03	4.30E+00	5.84E+03	6.44E+03	2.50E+01	2.23E+03	n.d.	1.90E+01	0.52
	111	3.59E+03	<DL	5.56E+01	2.35E+00	3.69E+05	<DL	1.83E+00	7.35E+01	n.d.	6.32E+00	8.58E+03	n.d.	n.d.	1.30E+03	3.77E+03	3.34E+03	3.28E+00	5.53E+02	n.d.	4.08E+01	0.04	
	112	3.55E+03	<DL	1.50E+02	4.16E+00	6.96E+05	<DL	8.40E+00	6.54E+00	n.d.	2.44E+01	1.33E+04	n.d.	n.d.	1.48E+03	3.20E+00	7.07E+03	1.11E+04	2.42E+01	1.54E+03	n.d.	3.23E+00	2.60
	113	2.50E+03	<DL	1.16E+02	1.81E+00	4.15E+05	<DL	2.88E+00	3.57E+01	n.d.	3.37E+00	1.03E+04	n.d.	n.d.	3.71E+02	3.86E+00	1.35E+03	8.44E+03	1.03E+01	1.48E+02	n.d.	2.36E+01	0.12
	118	4.23E+03	<DL	3.86E+02	6.62E-01	3.49E+05	<DL	<DL	<DL	n.d.	2.68E+00	9.59E+03	n.d.	n.d.	1.08E+03	5.03E+00	3.47E+03	1.55E+04	<DL	9.46E+02	n.d.	<DL	<DL
	121	7.26E+02	<DL	1.19E+02	7.07E-01	4.32E+05	1.72E-02	1.65E+00	3.65E+00	1.36E-02	3.46E+01	8.43E+03	2.18E-01	9.01E-03	1.38E+02	1.02E+00	<DL	3.78E+03	5.60E-02	1.80E+02	1.46E-03	3.22E+00	0.51
	162	6.86E+03	3.84E+01	2.98E+02	1.28E+00	1.97E+05	3.22E-02	1.07E+01	5.10E+00	2.05E-02	1.95E+00	9.53E+04	5.36E-01	1.28E-02	9.25E+02	3.86E+00	6.86E+04	1.51E+03	9.60E-02	9.90E+02	3.73E-03	1.40E+01	0.77
167	5.52E+02	3.53E+00	2.89E+02	9.75E-01	3.10E+05	3.03E-01	5.05E+00	1.01E+01	6.69E-03	2.06E+01	1.53E+04	3.62E-01	1.92E-03	1.16E+02	4.25E-01	1.93E+03	2.16E+04	3.29E-01	<DL	1.68E-03	1.33E+01	0.38	
173	3.92E+02	<DL	2.19E+02	1.13E+00	4.30E+05	2.24E-02	2.40E+00	3.09E+00	8.44E-03	3.49E+00	1.27E+04	1.66E-01	3.22E-02	3.53E+02	2.30E+00	<DL	6.78E+03	4.04E-02	6.38E+01	1.84E-03	3.56E+00	0.67	
189	2.31E+03	2.54E+01	5.55E+02	1.69E+01	6.92E+05	<DL	2.60E+01	7.62E-01	n.d.	1.06E+02	6.78E+04	n.d.	n.d.	1.28E+03	2.53E+00	2.49E+04	4.01E+03	3.16E+01	2.75E+03	n.d.	1.41E+01	1.84	
197	7.42E+03	<DL	9.65E+00	5.63E+05	<DL	1.66E+01	2.24E+01	n.d.	6.21E+01	3.91E+04	n.d.	n.d.	2.12E+03	1.21E+01	1.97E+04	3.20E+03	<DL	3.57E+03	n.d.	5.41E+01	0.31		
201	3.42E+03	<DL	8.96E+01	2.98E-01	3.41E+04	7.94E-03	4.87E+00	4.31E+01	3.84E-02	4.08E+00	7.34E+03	1.25E-01	2.54E-03	2.53E+03	8.37E+00	<DL	4.40E+02	2.36E-02	7.03E+02	2.11E-03	7.40E+00	0.66	
202	2.16E+02	6.15E+02	2.31E+02	6.52E-01	3.76E+05	2.17E-02	4.87E+00	7.09E-01	1.12E-02	1.37E+01	2.57E+04	3.54E-02	4.25E-03	1.13E+03	1.11E+00	<DL	2.20E+03	7.00E-02	8.57E+02	1.83E-03	6.64E+00	0.73	
Surat	10	3.71E+02	<DL	1.42E+02	1.17E-01	3.66E+05	1.09E-02	4.01E+00	7.06E-01	3.06E-03	2.73E+00	6.12E+03	2.56E-01	<DL	3.01E+01	2.16E-01	<DL	1.03E+04	1.28E-01	<DL	1.28E-03	7.17E+00	0.56
	14	1.28E+03	<DL	1.62E+02	7.69E-01	3.45E+05	3.87E-02	5.89E+00	1.71E+00	1.62E-02	2.54E+01	5.88E+03	2.47E-01	<DL	3.15E+02	1.66E+00	<DL	1.04E+04	7.67E-02	3.37E+02	8.65E-04	5.92E+00	1.00
	46	1.08E+03	<DL	1.52E+03	3.07E+00	2.43E+05	2.00E-01	3.76E+01	1.93E+00	7.87E-02	7.88E+01	1.78E+04	2.33E-01	7.83E-03	9.01E+02	1.19E+01	<DL	6.99E+03	4.12E-02	1.88E+03	2.05E-03	3.04E+01	1.24
	54	7.85E+03	3.27E+01	1.19E+02	8.68E+00	3.72E+04	7.95E-01	3.19E+02	2.01E+01	1.78E-01	3.79E+02	3.77E+04	2.92E-01	6.64E-02	7.87E+04	5.49E+01	3.66E+03	1.93E+03	8.74E-01	4.34E+04	5.68E-03	3.69E+02	0.87
	55	2.03E+03	9.38E+00	2.00E+02	3.59E+00	9.55E+04	4.02E-01	6.80E+01	1.27E+00	9.86E-02	3.98E+01	1.27E+04	2.79E-01	1.13E-02	4.24E+03	1.72E+01	3.05E+03	3.30E+03	2.44E-01	7.85E+04	5.40E-03	4.32E+01	1.57
	67	1.75E+02	<DL	8.02E+01	4.80E-01	4.15E+05	1.62E-02	1.71E+00	1.42E+00	5.73E-03	6.96E+01	5.49E+03	3.28E-01	<DL	9.66E+01	2.84E-01	<DL	7.12E+03	1.20E-01	2.57E+01	2.03E-03	3.86E+00	0.44
	70	5.78E+02	<DL	2.95E+02	8.81E-01	3.75E+05	2.11E-02	7.30E+00	3.30E-01	2.28E-02	4.00E+01	7.10E+03	6.86E-01	<DL	5.75E+02	6.78E-01	<DL	1.81E+04	1.21E-01	1.70E+02	2.81E-04	6.08E+00	1.20
	80	2.25E+03	9.29E+00	2.54E+02	3.51E+00	3.38E+05	<DL	1.05E+01	<DL	n.d.	1.17E+02	1.19E+04	n.d.	n.d.	4.77E+02	3.86E+00	2.14E+03	1.13E+04	2.23E+01	4.92E+02	n.d.	4.34E+00	2.41
	81	1.38E+03	<DL	4.93E+01	1.25E-01	2.15E+05	3.86E-02	6.77E-01	1.13E+00	7.70E-03	3.11E+01	2.52E+03	1.76E-01	<DL	1.93E+02	7.24E-01	<DL	9.20E+03	5.98E-02	9.13E+01	3.07E-03	1.84E+00	0.37
	85	5.35E+02	2.24E+00	1.51E+02	7.48E-01	3.47E+05	1.23E-02	8.79E+00	1.52E+00	1.46E-02	1.10E+01	1.31E+04	2.72E-01	<DL	1.22E+02	1.15E+00	<DL	7.05E+03	6.61E-02	1.84E+02	2.84E-04	9.92E+00	0.89
	86	1.02E+04	2.50E+01	6.95E+01	3.07E-01	3.27E+05	5.57E-02	2.65E+02	3.65E+00	1.60E-01	9.51E+01	7.20E+03	1.44E+00	4.86E-02	1.66E+03	1.40E+01	1.85E+03	7.80E+03	3.89E-01	2.39E+02	9.62E-03	1.13E+01	23.39
	87	4.07E+02	<DL	7.38E+01	6.70E-01	3.77E+05	1.15E-02	9.58E-01	8.05E-01	1.52E-02	3.17E+00	4.57E+03	3.03E-01	<DL	9.86E+01	1.60E+00	<DL	2.67E+04	1.51E-01	3.45E+01	8.58E-04	2.51E+00	0.38
	88	2.26E+03	<DL	4.85E+01	1.36E+00	3.13E+05	<DL	2.22E+00	6.01E+00	n.d.	3.13E+01	9.74E+03	n.d.	n.d.	2.49E+02	2.18E+00	1.34E+03	1.34E+04	1.52E+00	1.46E+01	n.d.	<DL	Ni <DL
	263	4.36E+02	<DL	2.21E+02	8.43E-01																		

Table 15: Cemented sandstones elemental concentrations* (ppm) and Co/Ni within acid-leached portions (Continued).

Basin	Sample #	P	Pb	Rb	S	Sb	Sc	Si	Sn	Sr	Ta	Th	Ti	Tl	U	V	W	Y	Zn	Zr	Y/Ho	Zr/Hf	
Standard	Jcp1	5.08E+00	3.86E-01	4.88E-02	1.60E+03	8.58E+01	8.76E-02	<DL	3.79E-02	7.33E+03	<DL	4.83E-03	8.47E-01	1.59E-03	2.77E+00	1.92E-01	2.25E-01	2.07E-01	3.75E+00	2.15E-01	116.5	44.5	
Eromanga	5	4.69E+00	2.44E+00	7.38E-01	3.63E+02	<DL	7.36E+00	2.81E+02	4.82E-03	1.11E+03	<DL	3.96E-01	3.85E-01	7.87E-03	8.00E-02	1.10E+00	1.43E-02	1.61E+01	9.61E+01	2.45E-02	32.2		
	6	2.26E+01	4.47E+00	1.30E+00	7.05E+02	<DL	1.03E+01	3.55E+02	1.28E-01	1.32E+03	4.71E-04	4.46E-01	1.11E+00	1.44E-02	1.08E-01	2.13E-01	2.03E-02	2.09E+01	8.90E+01	4.27E-02	33.3	24.3	
	7	4.79E+01	8.37E+00	3.76E-01	7.51E+02	<DL	5.65E+00	7.49E+02	1.74E-01	1.04E+03	4.69E-04	2.74E-01	1.36E+00	7.56E-03	9.91E-02	1.76E+00	1.41E-02	2.40E+01	9.78E+01	7.63E-02	35.8	29.0	
	8	3.58E+01	3.02E+00	3.64E-01	5.04E+02	<DL	4.72E+00	3.37E+02	1.86E-01	1.47E+03	6.78E-04	3.40E+00	6.94E-01	6.81E-03	9.11E-02	4.76E+00	2.41E-02	3.31E+01	4.10E+01	5.50E-02	32.0	20.0	
	65	8.58E+01	<DL	n.d.	4.31E+02	<DL	n.d.	1.65E+03	6.16E+03	1.01E+03	n.d.	n.d.	1.08E+01	n.d.	1.25E+02	3.83E+01	n.d.	n.d.	1.54E+02	5.59E+00			
	79	6.56E+01	2.24E+00	4.00E+00	7.07E+02	<DL	7.49E+00	8.93E+02	3.72E-01	1.10E+03	1.49E-04	3.82E+00	3.18E+01	2.01E-02	8.23E-01	6.13E+00	3.85E-02	3.37E+01	4.78E+01	4.77E-01	32.1	62.7	
	89	<DL	<DL	n.d.	2.10E+02	9.09E+00	n.d.	6.14E+02	1.01E+03	1.06E+03	n.d.	n.d.	5.82E+00	n.d.	<DL	<DL	n.d.	n.d.	6.24E+01	1.20E+00			
	102	3.59E+01	<DL	n.d.	7.26E+02	<DL	n.d.	4.20E+02	2.03E+03	4.15E+02	n.d.	n.d.	3.88E+00	3.74E+00	8.28E+01	<DL	n.d.	n.d.	4.33E+01	4.48E-01			
	103	1.75E+01	1.13E+01	4.92E-01	1.57E+02	1.03E+01	1.39E+01	8.28E+02	2.73E-01	2.23E+03	<DL	8.66E-01	4.39E+00	3.53E-03	1.44E-01	7.39E+00	1.39E-02	2.25E+01	8.04E+01	3.22E-01	30.5		
	104	<DL	1.29E+01	n.d.	4.64E+02	<DL	n.d.	2.12E+03	1.89E+03	4.06E+03	n.d.	n.d.	6.90E+00	7.72E+00	4.18E+01	2.77E+01	n.d.	n.d.	1.11E+02	8.03E-01			
	105	1.02E+02	2.79E+00	7.77E+00	8.14E+02	<DL	1.04E+01	9.09E+02	1.12E+00	2.10E+03	2.13E-04	1.52E+00	3.68E+01	2.53E-02	5.33E-01	4.07E+01	4.04E+01	1.28E+01	1.01E+02	1.11E+00	31.3	59.6	
	108	4.05E+00	7.12E-01	8.92E-01	6.50E+02	<DL	6.71E-01	7.30E+02	1.55E-01	7.56E+02	<DL	2.05E-01	5.98E+00	2.45E-03	1.59E-01	1.37E+00	8.63E-03	1.32E+01	2.01E+01	1.43E-01	32.3		
	109	<DL	<DL	n.d.	1.45E+02	<DL	n.d.	2.85E+02	1.55E+03	3.70E+02	n.d.	n.d.	7.27E+00	n.d.	<DL	<DL	n.d.	n.d.	1.05E+02	7.15E-01			
	110	<DL	<DL	n.d.	5.48E+02	<DL	n.d.	8.73E+02	1.83E+03	1.28E+03	n.d.	n.d.	4.93E+01	5.42E-01	1.27E+02	2.05E+01	n.d.	n.d.	9.88E+01	1.33E+00			
	111	<DL	<DL	n.d.	2.03E+02	<DL	n.d.	5.39E+02	1.41E+03	3.68E+02	n.d.	n.d.	5.45E+00	n.d.	<DL	<DL	n.d.	n.d.	1.20E+02	1.94E+00			
	112	2.82E+01	2.09E+00	n.d.	5.17E+02	<DL	n.d.	8.89E+02	1.98E+03	1.02E+03	n.d.	n.d.	2.87E+01	4.12E+00	3.29E+01	9.28E+00	n.d.	n.d.	1.10E+02	1.24E+00			
	113	5.53E+01	<DL	n.d.	2.10E+02	<DL	n.d.	4.41E+02	1.77E+03	2.01E+03	n.d.	n.d.	3.10E+01	n.d.	<DL	3.89E+01	n.d.	n.d.	6.92E+01	1.07E+00			
	118	1.76E+01	<DL	n.d.	2.55E+02	<DL	n.d.	4.00E+02	1.50E+03	7.97E+02	n.d.	n.d.	1.64E+01	n.d.	1.79E+01	<DL	n.d.	n.d.	9.33E+01	8.35E-01			
	121	1.01E+02	4.19E+00	3.11E-01	1.30E+02	3.06E+00	5.62E+00	2.27E+02	<DL	3.63E+02	<DL	2.33E+00	1.53E+00	2.74E-03	2.00E-01	7.09E+00	1.01E-02	1.02E+01	6.02E+01	7.25E-01	31.4	80.5	
	162	8.83E+01	3.86E+00	2.12E+00	5.23E+02	<DL	5.71E+00	9.42E+02	2.79E-01	3.06E+02	3.50E-04	2.23E+00	9.98E+00	2.19E-02	2.63E-01	1.60E+01	2.65E-01	1.69E+01	5.05E+01	4.18E-01	33.7	32.5	
	167	1.28E+02	5.52E+00	4.75E-01	6.74E+02	<DL	5.41E+00	5.79E+02	2.30E-01	7.59E+02	1.30E-03	1.12E+00	6.36E-01	8.44E-03	1.24E-01	1.83E+00	1.16E-01	1.67E+01	4.52E+01	6.73E-02	34.7	34.9	
	173	9.29E+01	8.16E-01	5.62E-01	1.01E+02	7.26E-01	3.41E+00	2.89E+02	<DL	4.96E+02	<DL	1.19E+00	9.78E-01	1.00E-02	6.01E-01	1.62E+00	7.62E-03	1.14E+01	1.44E+01	3.21E+00	33.2	99.7	
	189	8.58E+01	3.94E+01	n.d.	9.94E+02	<DL	n.d.	3.38E+03	1.02E+04	1.51E+03	n.d.	n.d.	3.54E+00	1.64E+00	2.86E+02	3.05E+01	n.d.	n.d.	8.92E+01	3.19E+00			
197	1.30E+02	5.86E+01	n.d.	1.17E+03	<DL	n.d.	3.99E+03	5.85E+03	8.37E+02	n.d.	n.d.	5.70E+00	n.d.	1.48E+02	5.99E+01	n.d.	n.d.	3.52E+02	2.93E+00				
201	2.55E+00	2.23E-01	6.24E+00	2.14E+02	<DL	7.89E-01	9.23E+02	<DL	8.02E+01	<DL	6.33E-02	1.01E+00	2.90E-02	9.07E-02	4.21E-01	2.75E-02	9.78E-01	2.26E+01	1.02E-01	27.8	40.2		
202	5.73E+01	1.30E+00	1.49E+00	6.24E+02	<DL	4.93E-01	4.68E+02	<DL	4.82E+02	<DL	1.53E-01	1.01E+00	1.72E-02	1.53E-01	1.35E+00	8.69E-02	2.39E+00	3.48E+01	1.53E-01	29.6	36.0		
Surat	10	6.36E+00	2.46E+00	2.23E-01	5.70E+01	<DL	1.11E+01	1.86E+01	<DL	2.08E+03	<DL	9.55E-01	9.77E-01	7.09E-03	7.66E-02	9.93E-01	1.80E-02	3.70E+01	1.41E+01	7.18E-02	30.8		
	14	6.76E+00	2.05E+02	1.14E+00	1.31E+02	<DL	4.20E+00	4.99E+01	1.33E-02	5.96E+02	<DL	1.08E+00	8.05E-01	1.35E-02	2.61E-01	1.18E+00	5.12E-02	1.00E+01	3.89E+01	1.13E-01	30.2		
	46	2.02E+01	2.71E+01	4.52E+00	1.14E+02	<DL	1.09E+01	3.87E+02	8.39E-04	2.08E+03	<DL	1.12E+00	1.98E+00	7.25E-02	1.26E+00	1.61E+00	1.65E-02	2.56E+01	1.76E+02	3.16E-01	28.9	40.3	
	54	1.16E+02	3.02E+01	1.83E+01	5.93E+03	<DL	1.78E+01	5.01E+03	2.12E-01	8.94E+02	5.76E-04	1.95E+00	4.69E+00	5.47E-01	1.80E+00	2.31E+01	3.87E-02	1.11E+01	6.01E+02	1.75E+00	25.5	26.3	
	55	5.69E+01	2.67E+01	6.25E+00	1.06E+03	<DL	8.58E+00	2.98E+03	1.99E-01	1.63E+03	7.98E-04	1.77E+00	6.84E+00	9.11E-02	1.33E+00	1.02E+01	2.68E-01	2.11E+01	4.09E+02	3.01E-01	27.2	26.7	
	67	4.47E+01	5.87E+00	3.61E-01	1.03E+02	<DL	5.11E+00	7.11E+01	<DL	3.33E+02	<DL	2.22E+00	1.06E+00	6.20E-03	1.48E-01	1.71E+00	7.11E-03	1.19E+01	6.06E+01	3.04E-01	26.7		
	70	2.83E+01	8.00E+00	1.26E+00	1.62E+02	<DL	8.41E+00	1.38E+02	<DL	3.04E+02	<DL	6.72E-01	4.22E-01	1.11E-02	9.14E-02	1.80E+00	8.94E-03	1.96E+01	3.29E+01	3.30E-02	30.6		
	80	2.15E+01	<DL	n.d.	3.09E+02	<DL	n.d.	1.73E+02	1.78E+03	3.87E+02	n.d.	n.d.	2.07E+00	3.38E+00	3.91E+01	1.97E+01	n.d.	n.d.	1.67E+02	1.08E+00			
	81	<DL	2.49E+00	6.03E-01	1.38E+02	<DL	8.68E-01	<DL	2.75E-02	4.80E+02	<DL	5.01E-01	4.65E+00	4.39E-03	6.69E-02	9.13E-01	7.81E-03	7.13E+00	8.91E+01	6.52E-02	32.6		
	85	3.83E+01	2.19E+00	6.02E-01	7.40E+01	<DL	1.53E+01	2.14E+02	<DL	3.47E+02	<DL	9.72E-01	7.60E-01	5.88E-03	3.11E-01	7.23E+00	1.45E-02	3.03E+01	7.83E+01	1.02E-01	30.9		
	86	7.22E+01	1.45E+00	7.58E+00	1.02E+03	<DL	2.32E+00	4.74E+02	6.63E-01	4.44E+02	1.39E-03	1.63E+00	3.80E+01	1.30E-02	8.21E-01	8.52E+00	5.34E+01	1.07E+01	8.23E+01	1.82E+00	34.3	37.4	
	87	8.85E+00	1.59E-01	7.59E-01	2.62E+01	<DL	5.57E+00	1.66E+01	<DL	4.08E+02	<DL	1.68E-01	6.68E-01	4.77E-03	1.96E-01	2.42E-01	1.02E-02	2.52E+01	7.76E+00	2.65E-01	45.7		
	88	3.76E+01	<DL	n.d.	8.80E+01	<DL	n.d.	<DL	1.50E+03	3.26E+02	n.d.	n.d.	5.01E+00	n.d.	<DL	1.08E+01	n.d.	n.d.	1.67E+01	1.81E+00			
	263	6.28E+01	1.69E+00	7.71E-01	5.58E+02	<DL	1.21E+00	5.05E+02	5.37E-02	7.26E+02	1.70E-03	4.82E-01	1.21E+00	3.81E-03	1.52E-01	2.33E+00	5.94E-02	7.81E+00	2.67E+01	3.35E-01	38.5	54.6	
272	4.34E+01	1.25E+01	9.29E+00	8.69E+02	<DL	3.28E+01	1.47E+03	3.39E-01	9.05E+02	7.64E-04	1.46E+00	1.74E+00	4.08E-02	6.43E-01	1.29E+01	1.38E-01	3.27E+01	2.05E+02	1.75E-01	30.4	26.7		
278	7.22E+00	1.55E-01	7.18E-01	2.98E+02	<DL	9.06E+00	9.56E+01	<DL	3.59E+02	<DL	4.21E-01	7.95E-01	4.21E-03	1.14E-01	3.96E-01	7.02E-03	1.40E+01	8.76E+00	1.84E-01	35.3			
280	9.61E+01	2.74E+00	8.29E-01	1.69E+02	<DL	3.81E+00	3.25E+02	<DL	6.36E+02	<DL	1.99E-01	1.32E+00	1.21E-02	7.43E-02	7.75E-01	5.19E-03	1.54E+01	3.89E+01	6.42E-01	41.3	61.1		
Legend:	>10,000	5,000-10,000	1,000-																				

Table 16: Vein elemental concentrations* (ppm) within acid-leached portions. For colour coding refer to the legend at the bottom of the table.

Basin	Sample #	Al	B	Ba	Be	Ca	Cd	Co	Cr	Cs	Cu	Fe	Ga	Hf	K	Li	Mg	Mn	Mo	Na	Nb	Ni	Co/Ni
N/A	JCP1	1.37E+02	<DL	7.01E+00	2.43E-03	4.57E+05	8.62E-03	4.99E-01	3.34E-01	1.83E-03	6.71E-01	2.67E+02	5.22E-03	4.83E-03	1.05E+01	3.66E-01	9.21E+02	7.54E+00	8.80E-02	1.09E+03	1.30E-03	2.73E+00	0.18
Eromanga	2	9.35E+01	<DL	6.10E+00	1.49E-02	4.50E+05	1.98E-02	2.49E-01	1.44E-01	8.95E-03	1.28E+00	3.43E+03	5.05E-01	<DL	1.16E+01	2.06E-01	<DL	1.25E+04	7.24E-02	5.59E+01	7.09E-04	2.47E+00	0.10
	3	5.14E+00	4.07E-01	9.24E+00	3.41E-02	4.05E+05	1.94E-03	2.19E-01	8.55E-02	7.50E-03	7.20E-01	2.24E+03	2.83E-01	<DL	1.09E+01	<DL	<DL	1.32E+04	8.24E-02	8.70E+01	1.98E-04	2.36E+00	0.09
	4	9.27E+01	<DL	7.77E+00	1.75E-02	4.43E+05	2.20E-03	2.57E-01	1.32E-01	8.18E-03	1.87E+00	1.54E+03	5.80E-01	<DL	1.57E+01	<DL	<DL	1.03E+04	7.64E-02	3.04E+01	2.02E-03	2.73E+00	0.09
	90	6.27E+02	<DL	7.13E+01	5.37E-01	4.20E+05	9.17E-03	1.09E+00	4.93E-01	1.81E-02	1.93E+00	8.73E+03	2.60E-01	1.06E-03	1.49E+02	1.93E-01	<DL	3.82E+03	5.59E-02	1.38E+02	5.98E-04	2.51E+00	0.44
	91	4.37E+02	<DL	2.01E+01	2.47E-01	4.30E+05	2.56E-03	3.89E-01	3.79E-01	4.63E-03	1.32E+00	9.08E+03	4.19E-01	<DL	6.33E+01	2.56E-01	<DL	2.43E+04	1.13E-01	1.17E+02	5.24E-05	2.30E+00	0.17
	92	n.d.	n.d.	3.24E+01	<DL	3.88E+05	7.49E-03	4.78E-01	4.39E-01	9.77E-03	1.19E+00	n.d.	2.72E-01	<DL	n.d.	1.16E-01	1.23E+03	n.d.	5.41E-03	n.d.	3.78E-04	2.86E+00	0.17
	93	1.08E+01	<DL	1.83E+01	3.99E-02	4.15E+05	1.28E-03	3.78E-01	3.38E-01	4.94E-03	8.16E-01	4.02E+03	4.66E-01	<DL	2.97E+01	6.27E-02	<DL	1.58E+04	8.43E-02	3.47E+01	2.63E-03	2.53E+00	0.15
	94	n.d.	n.d.	1.04E+01	<DL	4.04E+05	5.16E-03	2.82E+01	1.27E-01	3.79E-03	2.54E+00	n.d.	2.87E-02	<DL	n.d.	9.53E-01	7.37E+03	n.d.	1.56E+00	n.d.	2.85E-04	4.50E+01	0.63
	95	6.72E+01	4.00E+00	1.88E+01	<DL	4.05E+05	5.29E-03	7.88E-01	2.11E-01	1.04E-02	2.65E+00	3.66E+03	1.80E-01	<DL	9.65E+01	8.01E-01	5.51E+03	4.98E+03	6.31E-03	1.72E+03	5.13E-04	3.35E+00	0.24
	96	4.17E+02	<DL	3.41E+01	9.82E-02	4.37E+05	1.93E-03	6.15E-01	7.26E-01	4.95E-03	1.15E+00	8.80E+03	5.65E-01	<DL	1.22E+02	3.83E-01	<DL	9.28E+03	4.91E-02	3.73E+02	4.62E-04	2.62E+00	0.24
	97	4.07E+02	<DL	3.42E+01	1.59E-01	4.22E+05	2.40E-03	5.70E-01	6.14E-01	4.23E-03	1.28E+00	1.10E+04	2.77E-01	<DL	1.48E+02	3.94E-01	<DL	1.03E+04	5.77E-02	6.85E+01	3.83E-04	2.46E+00	0.23
	98	4.08E+01	<DL	3.18E+01	9.45E-02	4.03E+05	1.01E-03	2.25E-01	3.63E-01	5.89E-03	3.48E-01	3.47E+02	8.16E-02	1.10E-03	1.48E+00	2.24E+00	<DL	8.08E+03	5.25E-02	1.63E+02	3.37E-03	2.30E+00	0.10
	99	4.63E+02	<DL	6.50E+01	7.44E-02	4.23E+05	2.12E-03	9.92E-01	1.21E+00	9.76E-03	6.87E-01	6.58E+03	6.98E-01	<DL	1.83E+02	5.98E-01	<DL	2.57E+04	1.55E-01	8.29E+00	8.32E-04	2.88E+00	0.34
	100	9.82E+01	<DL	7.57E+00	1.46E-02	4.09E+05	1.86E-03	2.77E-01	5.66E-01	5.66E-03	6.22E-01	8.78E+03	6.49E-01	<DL	5.09E+01	1.24E-01	<DL	6.59E+04	1.79E-01	<DL	1.74E-04	2.15E+00	0.13
	107	<DL	<DL	3.24E+01	4.23E-01	4.12E+05	1.08E-03	3.09E-01	3.18E-01	2.99E-03	5.40E-01	8.00E+03	1.39E-01	5.06E-04	1.39E+01	1.24E-01	<DL	1.01E+04	7.50E-02	1.40E+02	1.36E-04	2.17E+00	0.14
	115	6.31E+02	<DL	1.99E+01	<DL	4.14E+05	3.77E-03	7.72E-01	4.14E-01	7.90E-03	1.80E+00	9.68E+03	5.74E-02	3.24E-03	1.82E+02	4.18E-01	1.60E+03	4.70E+03	3.67E-03	7.51E+01	5.92E-04	2.74E+00	0.28
	116	1.03E+03	<DL	2.28E+01	2.76E-01	4.23E+05	1.87E-03	7.77E-01	9.07E-01	7.98E-03	1.75E+00	8.97E+03	8.21E-02	1.17E-02	2.97E+02	1.05E+00	<DL	1.37E+04	2.93E-02	1.82E+02	4.84E-04	2.58E+00	0.30
	117	6.32E+02	<DL	1.56E+01	1.74E-01	4.12E+05	3.00E-03	7.45E-01	9.65E-01	6.16E-03	1.95E+00	9.66E+03	3.15E-01	4.95E-03	1.47E+02	7.95E-01	<DL	1.38E+04	7.53E-02	<DL	1.07E-03	3.19E+00	0.23
	123	1.71E+02	<DL	1.86E+01	1.26E-01	4.32E+05	1.66E-03	6.11E-01	6.45E-01	6.17E-03	1.45E+00	5.72E+03	1.96E-01	3.99E-03	1.01E+02	2.58E-01	<DL	2.03E+04	1.17E-01	9.48E+01	5.41E-04	2.70E+00	0.23
	124	6.72E+02	<DL	1.87E+01	1.90E-01	4.17E+05	1.49E-03	5.75E-01	6.97E-01	5.56E-03	1.57E+00	8.32E+03	2.39E-01	4.10E-03	1.58E+02	7.23E-01	<DL	2.79E+04	1.25E-01	8.84E+01	1.13E-03	2.59E+00	0.22
	125	4.39E+02	<DL	1.57E+01	1.77E-01	4.30E+05	2.80E-02	4.42E-01	8.99E-01	5.26E-03	1.03E+00	1.17E+04	1.22E-01	1.35E-02	9.86E+01	8.16E-01	<DL	5.86E+03	5.09E-02	1.24E+02	7.40E-04	2.32E+00	0.19
	127	4.25E+03	<DL	6.57E+01	6.78E-01	4.04E+05	2.03E-02	6.24E+00	2.49E+00	8.96E-03	6.85E+00	7.97E+03	3.14E-01	5.34E-03	4.48E+02	2.05E+00	<DL	4.59E+03	4.20E-02	4.21E+02	1.46E-03	7.93E+00	0.79
	148	n.d.	n.d.	2.37E+01	<DL	3.74E+05	1.38E-02	4.80E-01	3.16E-01	9.80E-03	4.09E+00	n.d.	2.41E-01	<DL	n.d.	2.53E-01	6.61E+02	n.d.	6.20E-03	n.d.	8.94E-04	3.21E+00	0.15
	150	1.75E+02	<DL	1.12E+01	1.22E-01	4.37E+05	1.45E-03	3.96E-01	4.62E-01	3.68E-03	9.57E-01	5.62E+03	1.95E-01	3.13E-03	3.90E+01	3.53E-01	<DL	1.74E+04	1.11E-01	3.23E+01	1.04E-03	2.58E+00	0.15
	151	n.d.	n.d.	4.91E+01	<DL	3.85E+05	6.76E-02	2.53E+00	2.04E+00	2.11E-02	1.14E+01	n.d.	2.39E-01	6.45E-03	n.d.	1.23E+00	1.82E+03	n.d.	7.00E-02	n.d.	3.13E-03	5.21E+00	0.49
	152	2.02E+02	<DL	1.60E+02	8.76E-01	4.21E+05	7.80E-03	8.41E-01	2.88E+00	1.02E-02	5.50E+00	1.26E+04	1.44E-01	2.42E-03	5.87E+01	4.84E-01	<DL	9.16E+03	5.72E-02	1.27E+02	1.09E-03	2.91E+00	0.29
	153	2.71E+03	8.18E+00	7.11E+00	<DL	4.00E+05	2.67E-03	1.41E+00	1.19E-01	8.13E-02	6.35E-01	1.57E+04	1.69E-01	1.41E-03	6.48E+02	<DL	4.73E+02	1.06E+04	5.14E-03	1.67E+03	2.08E-04	2.83E+00	0.50
	154	1.52E+02	1.34E+01	2.43E+01	5.22E-02	4.40E+05	1.70E-03	4.29E-01	9.90E-01	1.14E-02	1.26E+00	8.88E+03	4.85E-01	<DL	9.61E+01	1.82E-01	<DL	3.14E+04	1.13E-01	4.47E+02	2.21E-03	2.75E+00	0.16
157	n.d.	n.d.	1.49E+01	<DL	3.85E+05	2.17E-02	7.53E-01	7.20E-01	1.85E-02	2.16E+00	n.d.	1.75E-01	4.65E-03	n.d.	4.07E-01	1.12E+03	n.d.	3.56E-02	n.d.	2.65E-03	3.27E+00	0.23	
159	n.d.	n.d.	2.01E+01	<DL	3.72E+05	2.88E-03	5.69E-01	6.59E-01	6.07E-03	3.85E+00	n.d.	2.20E-01	4.24E-04	n.d.	1.93E-01	9.92E+02	n.d.	2.86E-02	n.d.	8.25E-04	2.59E+00	0.22	
277	8.04E+01	<DL	5.75E+01	7.35E-01	4.27E+05	8.87E-03	7.36E-01	3.18E-01	8.16E-02	1.89E+02	6.09E+03	3.47E-01	<DL	7.07E+01	3.84E-01	<DL	1.57E+04	1.71E-01	2.12E+02	6.72E-04	3.89E+00	0.19	
286	1.44E+01	<DL	5.85E+01	4.52E-02	4.14E+05	5.06E-03	3.23E-01	1.29E+00	3.44E-03	1.25E+00	6.38E+03	6.65E-01	<DL	2.23E+01	2.92E-01	<DL	6.90E+03	7.66E-02	1.47E+01	7.37E-04	2.36E+00	0.14	
287	1.13E+03	<DL	4.22E+02	1.49E-01	4.21E+05	3.02E-03	1.20E+00	1.80E+00	1.15E-02	1.18E+00	6.32E+03	2.56E-01	4.06E-03	4.97E+02	1.64E+00	<DL	2.37E+04	2.99E-01	7.08E+02	8.22E-04	3.16E+00	0.38	
295	6.37E+02	<DL	8.63E+01	9.45E-02	4.25E+05	2.18E-03	8.55E-01	1.74E+00	1.07E-02	1.63E+00	6.67E+03	2.94E-01	3.04E-03	2.02E+02	7.75E-01	<DL	2.31E+04	2.10E-01	1.84E+02	1.17E-03	2.52E+00	0.34	
298	8.42E+02	<DL	6.10E+01	4.93E-01	3.96E+05	7.88E-03	1.22E+00	5.54E-01	8.84E-03	1.43E+00	6.56E+03	5.08E-01	<DL	2.09E+02	9.14E-01	<DL	1.61E+04	1.84E-01	5.76E+02	3.17E-04	2.31E+00	0.53	
Surat	76	7.40E+01	<DL	6.38E+01	1.20E+00	3.48E+05	1.90E-02	6.79E-01	7.81E-01	8.88E-03	1.74E+00	1.00E+04	1.25E-01	3.39E-03	2.04E+01	1.68E-01	<DL	1.17E+03	1.53E-02	<DL	8.59E-04	2.06E+00	0.33
	84	1.37E+02	<DL	6.08E+01	1.18E+00	4.08E+05	1.85E-03	1.02E+00	1.27E-01	3.12E-02	1.29E+00	3.77E+03	3.78E-01	<DL	1.01E+02	1.79E-01	<DL	1.35E+04	1.11E-01	4.86E+02	9.29E-04	2.67E+00	0.38
	156	3.22E+03	<DL	2.00E+01	1.57E+00	4.03E+05	7.18E-04	3.98E-01	5.09E-02	8.60E-03	6.42E-01	5.14E+03	2.49E-01	<DL	2.58E+02	4.46E-02	<DL	1.60E+04	1.16E-01	3.04E+02	1.54E-04	2.33E+00	0.17
	161	1.35E+02	<DL	1.01E+02	1.47E+00	5.16E+05	1.97E-02	8.30E-01	1.26E+00	1.36E-02	3.29E+00	1.38E+04	1.50E-01	<DL	1.69E+01	6.93E-01	<DL	2.21E+03	2.32E-02	<DL	3.40E-04	2.79E+00	0.30
	279	2.14																					

Table 16: Vein elemental concentrations* (ppm) within acid-leached portions (Continued).

Basin	Sample #	P	Pb	Rb	S	Sb	Sc	sr	Sn	Sr	Ta	Th	Ti	Tl	U	V	W	Y	Zn	Zr	Y/Ho	Zr/Hf
N/A	JCp1	5.08E+00	3.86E-01	4.88E-02	1.60E+03	8.58E+01	8.76E-02	<DL	3.79E-02	7.33E+03	<DL	4.83E-03	8.47E-01	1.59E-03	2.77E+00	1.92E-01	2.25E-01	2.07E-01	3.75E+00	2.15E-01	116.5	44.5
Eromanga	2	1.93E+01	6.66E+00	6.32E-02	6.24E+01	5.61E+00	1.36E+01	<DL	3.11E-02	2.78E+02	<DL	1.16E-01	4.65E-01	1.09E-03	1.75E-03	5.99E-01	1.09E-02	2.36E+01	9.57E+00	1.78E-02	31.1	
	3	1.32E+01	1.46E-01	6.78E-02	2.94E+01	<DL	1.32E+01	<DL	6.12E-03	2.29E+02	<DL	6.65E-02	4.09E-01	4.65E-04	1.19E-03	3.43E-01	2.85E+00	1.43E+01	6.56E+00	2.50E-02	27.7	
	4	2.64E+01	1.59E-01	6.91E-02	5.41E+01	<DL	1.24E+01	<DL	1.29E-01	2.73E+02	<DL	9.82E-02	7.40E-01	6.68E-04	1.26E-03	2.68E-01	2.96E+00	2.20E+01	3.92E+00	4.59E-02	28.8	
	90	8.57E+01	1.63E+00	9.18E-01	3.71E+01	1.60E+01	1.96E+00	4.38E+02	<DL	4.00E+02	<DL	5.23E-01	6.94E-01	6.58E-03	1.53E-01	2.82E+00	1.18E-02	2.46E+01	9.37E+00	4.14E-01	35.7	391.7
	91	1.08E+02	3.43E-01	2.66E-01	7.22E+01	<DL	2.93E+00	1.47E+02	<DL	4.31E+02	<DL	9.00E-02	5.97E-01	1.16E-03	2.83E-02	3.41E+00	1.82E-02	6.28E+01	3.42E+00	3.16E-01	38.1	
	92	<DL	4.90E-01	2.75E-01	n.d.	n.d.	1.53E+01	n.d.	1.25E-02	5.97E+02	<DL	2.30E-01	4.78E-01	1.97E-03	2.68E-02	1.78E+00	7.48E-03	3.84E+01	3.19E+00	5.84E-02	28.7	
	93	3.43E+01	9.70E-01	1.42E-01	2.24E+02	<DL	3.98E+01	2.38E+01	<DL	4.18E+02	<DL	2.97E-01	4.79E-01	6.66E-04	1.72E-02	1.27E+00	1.07E-02	2.28E+01	4.31E+00	7.46E-02	26.4	
	94	<DL	2.92E+00	2.08E-02	n.d.	n.d.	1.54E+00	n.d.	4.03E-02	1.36E+03	<DL	1.69E-01	2.85E-01	1.25E-02	1.65E-02	1.42E-01	9.14E-03	5.90E+00	5.54E+00	3.86E-02	25.3	
	95	<DL	1.13E+00	1.35E-01	7.43E+02	<DL	1.67E+01	8.92E+01	<DL	1.08E+03	1.83E-03	3.50E-01	6.36E-01	7.21E-04	3.58E-02	1.42E+01	1.11E-02	3.86E+01	6.03E+00	8.29E-02	29.7	
	96	2.59E+01	7.02E-01	2.90E-01	4.20E+02	9.24E+00	1.48E+01	2.64E+02	<DL	4.58E+02	<DL	2.99E-01	7.84E-01	1.34E-03	2.76E-02	3.39E+00	1.42E-02	4.62E+01	9.97E+00	4.50E-02	30.9	
	97	3.57E+01	3.97E-01	3.44E-01	5.95E+01	<DL	4.92E+00	2.74E+02	<DL	4.71E+02	<DL	2.51E-01	6.38E-01	1.30E-03	5.96E-02	4.27E+00	6.91E-03	2.43E+01	5.83E+00	5.19E-02	34.5	
	98	6.66E+02	5.66E-02	6.33E-01	9.19E+01	1.21E+01	1.24E-01	<DL	<DL	3.23E+02	<DL	5.60E-03	6.70E-01	5.23E-04	4.58E-04	6.44E-01	2.78E-02	8.73E-02	2.79E+00	4.08E-01	33.4	371.8
	99	2.26E+01	8.92E-01	4.98E-01	5.40E+01	<DL	1.10E+01	3.12E+02	<DL	5.65E+02	<DL	7.43E-01	1.02E+00	1.38E-03	1.63E-02	3.89E+00	1.77E-02	4.16E+01	8.66E+00	5.72E-02	29.9	
	100	2.58E+01	4.69E-01	2.05E-01	1.41E+02	<DL	1.65E+00	<DL	2.74E-02	6.75E+02	<DL	1.13E-01	3.07E-01	1.13E-03	4.41E-03	1.47E+00	1.53E-02	6.05E+01	7.76E+00	5.08E-02	38.8	
	107	1.61E+02	4.38E-01	1.30E-01	6.42E+01	<DL	6.30E-01	<DL	<DL	5.94E+02	<DL	4.52E-02	3.99E-01	1.19E-03	1.29E-02	8.55E-01	6.40E-03	3.90E+00	2.79E+00	3.85E-02	36.6	76.0
	115	<DL	1.07E+00	4.50E-01	6.99E+01	<DL	1.34E+01	2.26E+02	<DL	2.85E+02	2.29E-03	2.03E-01	7.91E-01	9.86E-04	5.12E-02	1.65E+01	4.09E-03	2.11E+00	5.12E+00	1.70E-01	33.3	52.4
	116	7.66E+01	1.07E+00	5.90E-01	3.29E+02	<DL	1.61E+00	3.57E+02	<DL	2.97E+02	<DL	2.40E-01	1.06E+00	3.15E-03	5.93E-02	4.05E+00	4.33E-03	2.79E+00	6.17E+00	3.22E-01	33.3	27.5
	117	6.18E+01	9.20E-01	4.22E-01	1.87E+02	<DL	2.60E+00	4.17E+02	<DL	3.46E+02	<DL	1.98E-01	9.38E-01	2.14E-03	7.75E-02	3.96E+00	8.39E-03	2.25E+01	5.89E+00	4.04E-01	39.0	81.5
	123	3.64E+01	2.29E-01	4.49E-01	5.08E+01	<DL	3.24E+00	1.70E+02	<DL	3.66E+02	<DL	2.37E-01	7.79E-01	1.52E-03	3.85E-02	3.15E+00	3.73E-03	3.75E+00	4.04E+00	8.47E-02	37.0	21.2
	124	5.09E+01	3.79E-01	4.93E-01	1.13E+02	<DL	1.74E+00	7.54E+02	<DL	3.72E+02	<DL	1.73E-01	1.01E+00	3.27E-03	3.14E-02	2.95E+00	1.09E-02	1.13E+01	5.38E+00	1.83E-01	36.5	44.8
	125	9.40E+01	6.76E-01	3.08E-01	8.48E+01	<DL	8.08E-01	2.73E+02	<DL	3.30E+02	<DL	1.23E-01	1.59E+00	1.40E-03	3.30E-02	3.23E+00	5.43E-03	7.11E+00	4.27E+00	4.71E-01	39.9	34.8
	127	2.45E+01	5.58E+00	1.09E+00	2.12E+02	7.75E+00	4.67E+00	1.55E+03	3.23E-02	8.20E+02	<DL	8.06E-01	3.62E+00	1.35E-02	1.06E-01	5.25E+00	3.85E-02	8.04E+00	3.87E+01	1.70E-01	29.6	31.8
	148	<DL	8.19E-01	4.64E-01	n.d.	n.d.	2.06E+00	n.d.	4.24E-02	3.27E+02	<DL	1.72E-01	6.21E-01	2.27E-03	3.73E-02	1.26E+00	1.46E-02	2.27E+01	1.43E+01	9.87E-02	32.1	
	150	4.74E+01	1.67E-01	2.51E-01	8.81E+01	<DL	2.22E+00	1.23E+02	<DL	3.48E+02	<DL	9.06E-02	8.48E-01	2.20E-03	2.64E-02	3.32E+00	8.32E-03	3.89E+00	6.45E+00	1.32E-01	33.2	42.1
	151	<DL	2.74E+00	1.02E+00	n.d.	n.d.	5.41E+00	n.d.	5.73E-01	5.19E+02	9.00E-04	6.57E-01	1.28E+00	3.52E-03	1.01E-01	7.94E+00	1.31E-02	1.45E+01	2.09E+01	3.36E-01	33.0	52.0
	152	3.72E+01	1.56E+00	2.51E-01	2.39E+02	<DL	2.04E+00	2.21E+02	8.87E-03	8.71E+02	<DL	4.61E-01	7.45E-01	5.33E-03	7.34E-02	2.74E+00	7.91E-03	4.21E+00	8.34E+01	1.10E-01	34.9	45.4
	153	<DL	8.55E-02	2.15E-01	4.54E+02	<DL	1.37E+01	1.38E+03	<DL	3.70E+02	1.30E-03	8.45E-02	2.24E-01	1.66E-03	4.38E-03	1.36E+01	6.59E-03	6.24E+00	1.57E+00	1.01E-01	29.1	71.7
	154	4.81E+01	8.18E-01	3.34E-01	4.03E+02	<DL	4.79E+01	1.03E+02	<DL	4.52E+02	<DL	3.36E-01	6.86E-01	9.90E-04	2.07E-02	1.49E+00	1.88E-02	2.31E+01	6.66E+00	1.49E-01	26.3	
157	<DL	8.10E-01	5.51E-01	n.d.	n.d.	1.32E+01	n.d.	<DL	2.87E+02	2.39E-03	2.33E-01	2.55E+00	4.24E-03	1.60E-01	1.70E+01	1.12E-02	1.30E+01	5.96E+00	2.70E-01	37.8	58.0	
159	<DL	1.11E+00	3.50E-01	n.d.	n.d.	1.24E+01	n.d.	1.58E-02	3.43E+02	1.21E-03	1.44E-01	7.26E-01	7.68E-04	1.58E-02	1.69E+01	6.42E-03	8.47E+00	5.42E+00	8.01E-02	37.8	188.9	
277	5.40E+01	9.27E+00	1.02E+00	2.75E+02	<DL	2.44E+00	1.08E+02	2.34E+00	3.36E+02	<DL	3.39E-01	3.89E-01	1.85E-02	5.34E-02	5.05E-01	2.33E-02	1.81E+01	1.03E+02	1.50E-01	33.0		
286	2.69E+01	6.64E-01	1.75E-01	7.81E+01	<DL	4.19E+01	<DL	<DL	6.04E+02	<DL	5.44E-01	3.96E-01	7.40E-04	2.06E-02	2.51E+00	3.52E-02	6.44E+01	1.44E+01	8.25E-02	28.2		
287	3.54E+01	1.34E+00	8.55E-01	6.56E+02	<DL	2.09E+00	5.01E+02	<DL	3.87E+02	<DL	2.06E-01	1.32E+00	4.26E-03	2.68E-02	5.80E+00	1.04E-02	9.59E+00	1.44E+01	1.26E-01	38.9	30.9	
295	3.93E+01	1.28E+00	6.19E-01	1.45E+02	<DL	1.37E+00	2.67E+02	<DL	5.03E+02	<DL	3.33E-01	1.32E+00	1.70E-03	2.45E-02	5.02E+00	8.61E-03	9.72E+00	1.18E+01	1.36E-01	37.2	44.8	
298	7.35E+01	2.55E+00	5.84E-01	6.32E+01	<DL	3.48E+00	3.01E+02	<DL	5.53E+02	<DL	2.08E-01	7.42E-01	3.33E-03	4.59E-02	4.01E+00	9.89E-03	2.55E+01	1.41E+01	2.14E-01	34.6		
Surat	76	7.04E+01	3.83E-01	2.59E-01	3.80E+01	9.67E+00	2.86E+00	7.85E+01	2.55E-01	2.09E+02	<DL	2.77E-01	1.05E+00	2.89E-03	1.20E-01	3.50E+00	9.26E-03	1.70E+01	7.71E+00	5.55E-01	36.3	163.7
	84	7.91E+01	4.65E-01	9.43E-01	6.34E+01	<DL	7.20E-01	4.10E+01	<DL	2.88E+02	<DL	1.14E-01	1.39E+00	8.78E-03	8.78E-02	1.29E+00	1.71E-02	3.70E+01	5.63E+00	2.19E-01	29.3	
	156	2.17E+02	1.99E-01	1.10E-01	1.40E+02	<DL	3.53E-01	9.86E+01	<DL	2.03E+02	<DL	3.46E-02	4.72E-01	1.56E-03	1.67E-02	2.60E-01	5.50E-03	1.78E+01	6.75E+00	1.13E-01	35.7	
	161	1.48E+02	6.49E-01	3.89E-01	5.10E+01	<DL	2.81E+00	7.00E+01	<DL	2.79E+02	<DL	5.33E-01	8.41E-01	4.96E-03	1.23E-01	5.99E+00	1.19E-02	1.78E+01	1.41E+01	3.42E-01	36.4	
	279	6.55E+01	2.32E+00	9.15E-01	3.74E+02	<DL	2.46E+00	2.89E+02	<DL	3.32E+02	<DL	4.86E-01	6.31E-01	6.95E-03	7.24E-02	6.88E-01	1.02E-01	3.94E+01	1.58E+01	1.48E-01	34.2	
	281	1.48E+02	3.89E+00	4.46E-01	3.27E+02	<DL	2.75E+00	1.70E+02	<DL	2.91E+02	<DL	6.03E-01	8.13E-01	5.21E-03	9.53E-02	2.55E+00	1.33E-02	2.40E+01	1.33E+01	1.88E-01	34.4	
	282	1.51E+02	2.68E+00	8.75E-01	4.05E+02	<DL	6.06E+00	3.28E+02	<DL	3.24E+02	<DL	3.80E-01	7.08E-01	8.44E-03	9.90E-02							

Table 17: Carbonate cement relative elemental abundances (%Ca+x). Grey shading denotes high relative abundances for individual elements (%Ca+x) with respect to the overall data population for that element.

Basin	Type	Sample #	Al/(Al+Ca)	B/(B+Ca)	Ba/(Ba+Ca)	Co/(Co+Ca)	Cr/(Cr+Ca)	Cu/(Cu+Ca)	Fe/(Ca+Fe)	K/(K+Ca)	Mg/(Ca+Mg)	Mn/(Ca+Mn)	Na/(Na+Ca)	Ni/(Ni+Ca)	P/(P+Ca)	Rb/(Rb+Ca)	S/(S+Ca)	Si/(Si+Ca)	Sn/(Ca+Sn)	Sr/(Ca+Sr)	Zn/(Zn+Ca)	Highlighted	
N/A	Standard	JcP1	2.99E-02	N/A	1.53E-03	1.09E-04	7.30E-05	1.47E-04	5.84E-02	2.30E-03	2.01E-01	1.65E-03	2.39E-01	5.97E-04	1.11E-03	1.07E-05	3.50E-01	N/A	8.30E-06	1.58E+00	8.22E-04	2	
Eromanga	Calcite	5	2.25E-02	N/A	4.13E-02	1.08E-03	4.26E-05	4.89E-03	1.01E+00	2.20E-01	N/A	5.40E+00	1.23E-01	9.61E-04	1.40E-03	2.20E-04	1.08E-01	8.36E-02	1.44E-06	3.30E-01	2.87E-02	3	
		6	7.08E-02	7.12E-03	7.11E-02	1.94E-03	N/A	5.15E-03	1.23E+00	3.78E-01	1.58E+00	5.86E+00	3.02E-01	2.65E-03	8.14E-03	4.69E-04	2.53E-01	1.28E-01	4.61E-05	4.73E-01	3.20E-02	6	
		7	2.21E-01	5.36E-03	3.01E-02	3.60E-03	N/A	1.82E-02	1.37E+00	3.76E-02	3.41E-01	4.35E+00	9.41E-02	4.72E-03	1.44E-02	1.13E-04	2.25E-01	2.24E-01	5.21E-05	3.12E-01	2.93E-02	3	
		65	2.00E+00	1.61E-04	4.90E-02	2.77E-03	4.73E-03	1.31E-02	5.78E+00	7.95E-01	2.51E+00	2.85E+00	3.64E-01	3.01E-03	1.22E-02	N/A	6.14E-02	2.34E-01	8.71E-01	1.44E-01	2.20E-02	8	
		89	4.07E-01	2.90E-04	1.67E-02	2.18E-05	5.63E-03	4.17E-03	1.10E+00	7.14E-02	3.44E-01	5.49E-01	4.92E-02	3.42E-03	N/A	N/A	4.06E-02	1.19E-01	1.96E-01	2.05E-01	1.21E-02	1	
		102	3.78E+00	2.77E-01	1.07E-01	2.64E-03	1.70E-02	7.53E-03	5.57E+00	1.40E+00	2.97E+00	4.92E+00	1.00E+00	2.20E-03	1.41E-02	N/A	2.85E-01	1.65E-01	7.94E-01	1.63E-01	1.70E-02	11	
		103	3.18E-01	N/A	2.31E-02	1.52E-03	3.02E-03	5.25E-02	6.25E-01	8.25E-02	N/A	2.11E-01	1.20E-01	2.96E-03	4.16E-03	1.17E-04	3.74E-02	1.97E-01	6.49E-05	5.28E-01	1.91E-02	3	
		104	5.71E-01	N/A	3.15E-02	1.56E-03	3.97E-04	1.83E-02	1.47E+00	1.29E-01	5.29E-01	1.52E+00	1.03E-01	1.69E-03	N/A	N/A	5.48E-02	2.49E-01	2.23E-01	4.78E-01	1.31E-02	3	
		105	6.99E+00	4.37E-03	3.60E-02	1.29E-01	1.13E-01	4.76E-02	7.92E+00	7.17E-01	1.86E+00	3.13E-01	1.35E+00	1.58E-02	3.36E-02	2.55E-03	2.67E-01	2.98E-01	3.69E-04	6.85E-01	3.32E-02	14	
		108	3.48E-01	9.50E-02	1.74E-02	5.65E-04	9.12E-04	7.60E-03	1.10E+00	3.28E-01	N/A	1.48E+00	3.58E-01	1.18E-03	9.44E-04	2.08E-04	1.51E-01	1.70E-01	3.63E-05	1.76E-01	4.70E-03	3	
		109	7.29E-01	N/A	1.61E-02	N/A	2.30E-02	2.53E-03	2.75E+00	6.82E-02	8.39E-01	7.48E-01	4.88E-02	1.36E-02	N/A	N/A	4.25E-02	8.32E-02	4.52E-01	1.08E-01	3.08E-02	4	
		110	1.38E+00	6.28E-02	1.37E-02	1.29E-03	3.28E-03	2.41E-03	1.63E+00	3.72E-01	7.55E-01	8.32E-01	2.89E-01	2.48E-03	N/A	N/A	7.14E-02	1.14E-01	2.38E-01	1.67E-01	1.29E-02	4	
		111	9.65E-01	N/A	1.51E-02	4.97E-04	1.99E-02	1.72E-03	2.27E+00	3.50E-01	1.01E+00	8.97E-01	1.50E-01	1.11E-02	N/A	N/A	5.52E-02	1.46E-01	3.82E-01	9.97E-02	3.25E-02	6	
		112	5.07E-01	N/A	2.15E-02	1.21E-03	9.40E-04	3.50E-03	1.88E+00	2.13E-01	1.01E+00	1.56E+00	2.21E-01	4.64E-04	4.06E-03	N/A	7.43E-02	1.27E-01	2.83E-01	1.47E-01	1.58E-02	3	
		113	6.00E-01	N/A	2.80E-02	6.96E-04	8.61E-03	8.12E-04	2.43E+00	8.95E-02	3.24E-01	2.00E+00	3.58E-02	5.69E-03	1.33E-02	N/A	5.07E-02	1.06E-01	4.25E-01	4.82E-01	1.67E-02	2	
		118	1.20E+00	N/A	1.10E-01	N/A	N/A	7.67E-04	2.67E+00	3.09E-01	9.85E-01	4.26E+00	2.70E-01	N/A	5.05E-03	N/A	7.29E-02	1.14E-01	4.28E-01	2.28E-01	2.67E-02	4	
		121	1.68E-01	N/A	2.76E-02	3.82E-04	8.43E-04	8.00E-03	1.91E+00	3.19E-02	N/A	8.66E-01	4.16E-02	7.46E-04	2.33E-02	7.20E-05	3.02E-02	5.26E-02	N/A	8.39E-02	1.39E-02	10	
		197	1.30E+00	N/A	9.67E-02	3.97E-03	1.10E-02	6.49E+00	5.65E-01	3.38E+00	5.65E-01	6.30E-01	9.61E-03	2.31E-02	N/A	2.07E-01	7.03E-01	1.03E+00	N/A	1.48E-01	6.24E-02	1	
		"Mixed" carbonates	8	9.26E-02	1.51E-04	6.03E-02	1.89E-03	8.54E-04	6.57E-03	5.00E+00	3.57E-02	2.75E+00	2.60E-01	2.39E-02	4.37E-03	1.14E-02	1.16E-04	1.61E-01	1.08E-01	5.94E-05	4.69E-01	1.31E-02	4
			79	1.63E+00	1.27E-03	7.29E-02	2.44E-03	2.41E-03	1.94E-02	5.69E+00	3.94E-01	3.22E+00	4.40E-01	6.35E-01	3.95E-03	1.96E-02	1.19E-03	2.11E-01	2.66E-01	1.11E-04	3.26E-01	1.43E-02	9
162	3.37E+00		1.95E-02	1.51E-01	5.42E-03	2.59E-03	9.90E-04	3.26E+01	4.67E-01	2.58E+01	7.62E-01	5.00E-01	7.08E-03	4.48E-02	1.08E-03	2.65E-01	4.76E-01	1.42E-04	1.55E-01	2.56E-02	11		
167a	1.78E-01		1.14E-03	9.32E-02	1.63E-03	3.25E-03	6.66E-03	4.69E+00	3.73E-02	6.18E-01	6.51E+00	N/A	4.30E-03	4.13E-02	1.53E-04	2.17E-01	1.86E-01	7.42E-05	2.44E-01	1.46E-02	4		
173	9.10E-02		N/A	5.08E-02	5.57E-04	7.19E-04	8.12E-04	2.88E+00	8.20E-02	N/A	1.55E+00	1.48E-02	8.28E-04	2.16E-02	1.31E-04	2.35E-02	6.71E-02	N/A	1.15E-01	3.34E-03	0		
189	3.33E-01		3.67E-03	8.01E-02	3.76E-03	1.10E-04	1.52E-02	8.93E+00	1.85E-01	3.47E+00	5.77E-01	3.95E-01	2.04E-03	1.24E-02	N/A	1.43E-01	4.86E-01	1.46E+00	2.18E-01	1.29E-02	7		
201	9.12E+00		N/A	2.62E-01	1.43E-02	1.26E-01	1.20E-02	1.77E+01	6.91E+00	N/A	1.27E+00	2.02E+00	2.17E-02	7.47E-03	1.83E-02	6.22E-01	2.63E+00	N/A	2.34E-01	6.61E-02	13		
202	5.74E-02		1.63E-01	6.12E-02	1.29E-03	1.88E-04	3.63E-03	6.39E+00	2.99E-01	N/A	5.82E-01	2.27E-01	1.76E-03	1.52E-02	3.97E-04	1.66E-01	1.24E-01	N/A	1.28E-01	9.24E-03	3		
Surat	Calcite	10	1.01E-01	N/A	3.87E-02	1.09E-03	1.93E-04	7.44E-04	1.64E+00	8.22E-03	N/A	2.74E+00	N/A	1.96E-03	1.74E-03	6.10E-05	1.56E-02	5.07E-03	N/A	5.64E-01	3.86E-03	1	
		14	3.69E-01	N/A	4.69E-02	1.71E-03	4.96E-04	7.35E-03	1.67E+00	9.10E-02	N/A	2.93E+00	9.74E-02	1.71E-03	1.96E-03	3.31E-04	3.79E-02	1.44E-02	3.86E-06	1.72E-01	1.13E-02	0	
		67	4.21E-02	N/A	1.93E-02	4.12E-04	3.41E-04	1.68E-02	1.30E+00	2.32E-02	N/A	1.69E+00	6.18E-03	9.30E-04	1.08E-02	8.70E-05	2.48E-02	1.71E-02	N/A	8.00E-02	1.46E-02	2	
		80	6.61E-01	2.75E-03	7.51E-02	3.09E-03	N/A	3.46E-02	3.41E+00	1.41E-01	6.28E-01	3.23E+00	1.45E-01	1.28E-03	6.36E-03	N/A	9.14E-02	5.11E-02	5.24E-01	1.14E-01	4.95E-02	4	
		81	6.36E-01	N/A	2.29E-02	3.14E-04	5.27E-04	1.45E-02	1.16E+00	8.97E-02	N/A	4.09E+00	4.24E-02	8.56E-04	N/A	2.80E-04	6.42E-02	N/A	1.28E-05	2.22E-01	4.13E-02	3	
		85	1.54E-01	6.45E-04	4.37E-02	2.53E-03	4.39E-04	3.16E-03	3.64E+00	3.53E-02	N/A	1.99E+00	5.30E-02	2.86E-03	1.10E-02	1.73E-04	2.13E-02	6.17E-02	N/A	9.99E-02	2.26E-02	1	
		86	3.04E+00	7.64E-03	2.12E-02	8.10E-02	1.12E-03	2.91E-02	2.16E+00	5.05E-01	5.64E-01	2.33E+00	7.30E-02	3.47E-03	2.21E-02	2.32E-03	3.12E-01	1.45E-01	2.03E-04	1.36E-01	2.52E-02	7	
		88	7.18E-01	N/A	1.55E-02	7.08E-04	1.92E-03	1.00E-02	3.02E+00	7.95E-02	4.26E-01	4.09E+00	4.67E-03	N/A	1.20E-02	N/A	2.81E-02	N/A	4.77E-01	1.04E-01	5.35E-03	2	
		272	1.47E+00	N/A	1.11E-01	4.50E-03	2.33E-03	3.47E-03	5.38E+00	9.99E-01	2.21E+00	2.50E+00	3.14E+00	4.58E-03	1.43E-02	3.06E-03	2.85E-01	4.81E-01	1.12E-04	2.97E-01	6.76E-02	9	
		278	1.01E-01	N/A	1.46E-02	2.83E-04	2.13E-04	4.14E-04	1.29E+00	3.54E-02	2.38E-01	4.97E+00	1.53E-02	9.10E-04	1.74E-03	1.73E-04	7.18E-02	2.31E-02	N/A	8.65E-02	2.11E-03	0	
		280	3.02E-01	N/A	2.71E-02	5.23E-04	2.04E-04	5.27E-04	2.60E+00	3.25E-02	N/A	6.81E+00	1.36E-02	8.04E-04	2.42E-02	2.09E-04	4.26E-02	8.18E-02	N/A	1.60E-01	9.80E-03	1	
		"Mixed" carbonates	46	4.40E-01	N/A	6.21E-01	1.54E-02	7.94E-04	3.24E-02	6.82E+00	3.69E-01	N/A	2.79E+00	7.68E-01	1.25E-02	8.32E-03	1.86E-03	4.67E-02	1.59E-01	3.45E-07	8.49E-01	7.24E-02	7
			54	1.74E+01	8.77E-02	3.20E-01	8.50E-01	5.40E-02	1.01E+00	5.04E+01	6.79E+01	8.95E+00	4.94E+00	5.39E+01	9.81E-01	3.11E-01	4.91E-02	1.38E+01	1.19E+01	5.68E-04	2.35E+00	1.59E+00	17
55	2.08E+00		9.81E-03	2.09E-01	7.11E-02	1.32E-03	4.17E-02	1.17E+01	4.25E+00	3.09E+00	3.34E+00	4.51E+01	4.52E-02	5.95E-02	6.54E-03	1.10E+00	3.03E+00	2.09E-04	1.68E+00	4.26E-01	13		
70	1.54E-01		N/A	7.87E-02	1.95E-03	8.81E-05	1.07E-02	1.86E+00	1.53E-01	N/A	4.60E+00	4.54E-02	1.62E-03	7.56E-03	3.36E-04	4.31E-02	3.67E-02	N/A	8.10E-02	8.78E-03	1		
87	1.08E-01		N/A	1.96E-02	2.54E-04	2.13E-04	8.39E-04	1.20E+00	2.61E-02	N/A	6.62E+00	9.15E-03	6.66E-04	2.34E-03	2.01E-04	6.95E-03	4.40E-03	N/A	1.08E-01	2.06E-03	1		
263	1.26E-01	N/A	6.42E-02	3.18E-04	N/A	6.31E-04	2.47E+00	8.92E-02															

Table 18: Carbonate vein relative elemental abundances (%_{Ca+x}). Grey shading denotes high relative abundances for individual elements (%_{Ca+x}) with respect to the overall data population for that element.

Basin	Type	Sample #	Al/(Al+Ca)	B/(B+Ca)	Ba/(Ba+Ca)	Co/(Co+Ca)	Cr/(Cr+Ca)	Cu/(Cu+Ca)	Fe/(Ca+Fe)	K/(K+Ca)	Mg/(Ca+Mg)	(Mn)/(Ca+Mn)	Na/(Na+Ca)	Ni/(Ni+Ca)	P/(P+Ca)	Rb/(Rb+Ca)	S/(S+Ca)	Si/(Si+Ca)	Sn/(Ca+Sn)	Sr/(Ca+Sr)	Zn/(Zn+Ca)	Highlighted
N/A	Standard	JCP1	2.99E-02	N/A	1.53E-03	1.09E-04	7.30E-05	1.47E-04	5.84E-02	2.30E-03	2.01E-01	1.65E-03	2.39E-01	5.97E-04	1.11E-03	1.07E-05	3.50E-01	N/A	8.30E-06	1.58E+00	8.22E-04	2
Eromanga	Calcite	2	2.08E-02	N/A	1.36E-03	5.55E-05	3.20E-05	2.84E-04	7.58E-01	2.58E-03	N/A	2.70E+00	1.24E-02	5.50E-04	4.30E-03	1.41E-05	1.39E-02	N/A	6.92E-06	6.19E-02	2.13E-03	0
		3	1.27E-03	1.01E-04	2.28E-03	5.42E-05	2.11E-05	1.78E-04	5.50E-01	2.70E-03	N/A	3.16E+00	2.15E-02	5.83E-04	3.25E-03	1.68E-05	7.28E-03	N/A	1.51E-06	5.67E-02	1.62E-03	0
		4	2.09E-02	N/A	1.75E-03	5.78E-05	2.98E-05	4.23E-04	3.47E-01	3.54E-03	N/A	2.27E+00	6.86E-03	6.15E-04	5.96E-03	1.56E-05	1.22E-02	N/A	2.92E-05	6.15E-02	8.85E-04	0
		90	1.49E-01	N/A	1.70E-02	2.60E-04	1.17E-04	4.61E-04	2.04E+00	3.56E-02	N/A	9.02E-01	3.29E-02	5.98E-04	2.04E-02	2.19E-04	8.84E-03	1.04E-01	N/A	9.52E-02	2.23E-03	0
		91	1.01E-01	N/A	4.67E-03	9.03E-05	8.81E-05	3.06E-04	2.07E+00	1.47E-02	N/A	5.35E+00	2.71E-02	5.35E-04	2.51E-02	6.17E-05	1.68E-02	3.41E-02	N/A	1.00E-01	7.95E-04	2
		92	N/A	N/A	8.35E-03	1.23E-04	1.13E-04	3.05E-04	N/A	N/A	3.16E-01	N/A	N/A	7.37E-04	N/A	7.09E-05	N/A	N/A	3.21E-06	1.54E-01	8.22E-04	0
		93	2.62E-03	N/A	4.40E-03	9.12E-05	8.16E-05	1.97E-04	9.61E-01	7.17E-03	N/A	3.67E+00	8.38E-03	6.09E-04	8.27E-03	3.43E-05	5.40E-02	5.74E-03	N/A	1.01E-01	1.04E-03	0
		94	N/A	N/A	2.58E-03	6.98E-03	3.15E-05	6.29E-04	N/A	N/A	1.79E+00	N/A	N/A	1.12E-02	N/A	5.15E-06	N/A	N/A	9.98E-06	3.35E-01	1.37E-03	1
		96	9.55E-02	N/A	7.80E-03	1.41E-04	1.66E-04	2.64E-04	1.98E+00	2.80E-02	N/A	2.08E+00	8.52E-02	5.99E-04	5.94E-03	6.64E-05	9.61E-02	6.04E-02	N/A	1.05E-01	2.28E-03	0
		97	9.64E-02	N/A	8.09E-03	1.35E-04	1.45E-04	3.03E-04	2.53E+00	3.50E-02	N/A	2.37E+00	1.62E-02	5.83E-04	8.46E-03	8.14E-05	1.41E-02	6.49E-02	N/A	1.11E-01	1.38E-03	0
		99	1.09E-01	N/A	1.54E-02	2.34E-04	2.86E-04	1.62E-04	1.53E+00	4.32E-02	N/A	5.72E+00	1.96E-03	6.80E-04	5.33E-03	1.18E-04	1.28E-02	7.37E-02	N/A	1.33E-01	2.05E-03	1
		100	2.40E-02	N/A	1.85E-03	6.77E-05	1.36E-04	1.52E-04	2.10E+00	1.25E-02	N/A	1.39E+01	N/A	5.27E-04	6.32E-03	5.02E-05	3.44E-02	N/A	6.70E-06	1.65E-01	1.90E-03	1
		107	N/A	N/A	7.86E-03	7.50E-05	7.72E-05	1.31E-04	1.90E+00	3.37E-03	N/A	2.40E+00	3.40E-02	5.26E-04	3.90E-02	3.15E-05	1.56E-02	N/A	N/A	1.44E-01	6.76E-04	1
		115	1.52E-01	N/A	4.81E-03	1.86E-04	9.99E-05	4.34E-04	2.28E+00	4.39E-02	3.84E-01	1.12E+00	1.81E-02	6.61E-04	N/A	1.09E-04	1.69E-02	5.46E-02	N/A	6.88E-02	1.24E-03	0
		116	2.43E-01	N/A	5.40E-03	1.84E-04	2.15E-04	4.14E-04	2.08E+00	7.03E-02	N/A	3.15E+00	4.31E-02	6.11E-04	1.81E-02	1.40E-04	7.79E-02	8.44E-02	N/A	7.03E-02	1.46E-03	0
		117	1.53E-01	N/A	3.80E-03	1.81E-04	2.34E-04	4.75E-04	2.29E+00	3.57E-02	N/A	3.24E+00	N/A	7.76E-04	1.50E-02	1.02E-04	4.53E-02	1.01E-01	N/A	8.41E-02	1.43E-03	0
		123	3.96E-02	N/A	4.30E-03	1.41E-04	1.49E-04	3.36E-04	1.30E+00	2.33E-02	N/A	4.49E+00	2.19E-02	6.25E-04	8.42E-03	1.04E-04	1.18E-02	3.93E-02	N/A	8.47E-02	9.34E-04	0
		125	1.02E-01	N/A	3.66E-03	1.03E-04	2.09E-04	2.40E-04	2.66E+00	2.29E-02	N/A	1.34E+00	2.87E-02	5.40E-04	2.18E-02	7.16E-05	1.97E-02	6.34E-02	N/A	7.66E-02	9.92E-04	0
		127	1.04E+00	N/A	1.63E-02	1.55E-03	6.18E-04	1.70E-03	1.94E+00	1.11E-01	N/A	1.12E+00	1.04E-01	1.97E-03	6.08E-03	2.70E-04	5.26E-02	3.83E-01	8.00E-06	2.03E-01	9.59E-03	1
		148	N/A	N/A	6.33E-03	1.28E-04	8.45E-05	1.09E-03	N/A	N/A	1.76E-01	N/A	N/A	8.56E-04	N/A	1.24E-04	N/A	N/A	1.13E-05	8.73E-02	3.82E-03	0
		150	4.01E-02	N/A	2.55E-03	9.06E-05	1.06E-04	2.19E-04	1.27E+00	8.92E-03	N/A	3.82E+00	7.39E-03	5.91E-04	1.08E-02	5.74E-05	2.02E-02	2.81E-02	N/A	7.96E-02	1.48E-03	0
		151	N/A	N/A	1.27E-02	6.58E-04	5.31E-04	2.96E-03	N/A	N/A	4.70E-01	N/A	N/A	1.35E-03	N/A	2.65E-04	N/A	N/A	1.49E-04	1.35E-01	5.44E-03	0
		152	4.79E-02	N/A	3.80E-02	2.00E-04	6.83E-04	1.30E-03	2.89E+00	1.39E-02	N/A	2.13E+00	3.01E-02	6.91E-04	8.82E-03	5.96E-05	5.68E-02	5.24E-02	2.11E-06	2.06E-01	1.98E-02	1
		153	6.73E-01	2.04E-03	1.78E-03	3.52E-04	2.98E-05	1.59E-04	3.76E+00	1.62E-01	1.18E-01	2.58E+00	4.15E-01	7.07E-04	N/A	5.37E-05	1.13E-01	3.45E-01	N/A	9.25E-02	3.93E-04	2
		154	3.46E-02	3.05E-03	5.51E-03	9.73E-05	2.25E-04	2.87E-04	1.98E+00	2.18E-02	N/A	6.66E+00	1.01E-01	6.24E-04	1.09E-02	7.59E-05	9.15E-02	2.33E-02	N/A	1.02E-01	1.51E-03	2
		157	N/A	N/A	3.88E-03	1.96E-04	1.87E-04	5.63E-04	N/A	N/A	2.90E-01	N/A	N/A	8.51E-04	N/A	1.43E-04	N/A	N/A	N/A	7.46E-02	1.55E-03	0
		159	N/A	N/A	5.40E-03	1.53E-04	1.77E-04	1.03E-03	N/A	N/A	2.66E-01	N/A	N/A	6.96E-04	N/A	9.43E-05	N/A	N/A	4.26E-06	9.22E-02	1.46E-03	0
		277	1.88E-02	N/A	1.35E-02	1.72E-04	7.43E-05	4.43E-02	1.40E+00	1.65E-02	N/A	3.55E+00	4.96E-02	9.09E-04	1.26E-02	2.39E-04	6.44E-02	2.52E-02	5.48E-04	7.85E-02	2.40E-02	2
		286	3.48E-03	N/A	1.41E-02	7.80E-05	3.13E-04	3.03E-04	1.52E+00	5.40E-03	N/A	1.64E+00	3.55E-03	5.71E-04	6.50E-03	4.23E-05	1.89E-02	N/A	N/A	1.46E-01	3.49E-03	0
		287	2.68E-01	N/A	1.00E-01	2.85E-04	4.28E-04	2.81E-04	1.48E+00	1.18E-01	N/A	5.33E+00	1.68E-01	7.52E-04	8.42E-03	2.03E-04	1.56E-01	1.19E-01	N/A	9.18E-02	3.43E-03	3
295	1.50E-01	N/A	2.03E-02	2.01E-04	4.11E-04	3.84E-04	1.55E+00	4.74E-02	N/A	5.15E+00	4.34E-02	5.93E-04	9.26E-03	1.46E-04	3.41E-02	6.29E-02	N/A	1.18E-01	2.77E-03	1		
298	2.12E-01	N/A	1.54E-02	3.09E-04	1.40E-04	3.61E-04	1.63E+00	5.27E-02	N/A	3.90E+00	1.45E-01	5.84E-04	1.86E-02	1.48E-04	1.60E-02	7.60E-02	N/A	1.39E-01	3.55E-03	0		
Surat	Calcite	95	1.66E-02	9.88E-04	4.64E-03	1.95E-04	5.22E-05	6.53E-04	8.94E-01	2.38E-02	1.34E+00	1.21E+00	4.23E-01	8.28E-04	N/A	3.32E-05	1.83E-01	2.20E-02	N/A	2.67E-01	1.49E-03	3
		98	1.01E-02	N/A	7.87E-03	5.59E-05	8.99E-05	8.63E-05	8.60E-02	3.67E-04	N/A	1.96E+00	4.03E-02	5.70E-04	1.65E-01	1.40E-05	2.28E-02	N/A	N/A	7.99E-02	7.25E-04	1
		124	1.61E-01	N/A	4.48E-03	1.38E-04	1.67E-04	3.76E-04	1.95E+00	3.79E-02	N/A	6.26E+00	2.12E-02	6.20E-04	1.22E-02	1.18E-04	2.70E-02	1.80E-01	N/A	8.91E-02	1.29E-03	1
		84	3.35E-02	N/A	1.49E-02	2.50E-04	3.11E-05	3.17E-04	9.14E-01	2.46E-02	N/A	3.20E+00	1.19E-01	6.55E-04	1.94E-02	2.31E-04	1.55E-02	1.00E-02	N/A	7.05E-02	1.38E-03	0
		156	7.91E-01	N/A	4.96E-03	9.86E-05	1.26E-05	1.59E-04	1.26E+00	6.39E-02	N/A	3.83E+00	7.53E-02	5.77E-04	5.38E-02	2.74E-05	3.48E-02	2.44E-02	N/A	5.03E-02	1.67E-03	2
		279	5.60E-02	1.81E-03	2.27E-02	2.13E-04	6.83E-04	2.22E-04	1.01E+00	7.82E-02	N/A	7.16E+00	9.86E-02	8.54E-04	1.72E-02	2.40E-04	9.81E-02	7.57E-02	N/A	8.71E-02	4.15E-03	1
		281	3.43E-02	N/A	1.44E-02	2.47E-04	1.87E-04	2.94E-04	1.17E+00	1.78E-02	N/A	6.50E+00	8.12E-03	6.87E-04	3.77E-02	1.14E-04	8.33E-02	4.32E-02	N/A	7.40E-02	3.40E-03	2
		282	7.74E-02	N/A	2.02E-02	3.87E-04	2.49E-04	7.93E-04	2.35E+00	6.33E-02	N/A	8.55E+00	9.29E-02	8.19E-04	3.74E-02	2.17E-04	1.00E-01	8.11E-02	N/A	8.01E-02	3.37E-03	3
		284	3.08E-01	N/A	3.95E-02	6.71E-04	2.18E-04	1.38E-03	4.24E+00	1.23E-01	N/A	5.40E+00	5.91E-01	1.05E-03	6.48E-02	5.64E-04	9.12E-02	1.22E-01	N/A	6.48E-02	6.26E-03	3
		76	2.13E-02	N/A	1.84E-02	1.95E-04	2.25E-04	5.01E-04	2.80E+00	5.88E-03	N/A	3.34E-01	N/A	5.93E-04	2.02E-02	7.45E-05	1.09E-02	2.26E-02	7.34E-05	6.02E-02	2.22E-03	0
Surat	"Mixed" carbonates	161	2.61E-02	N/A	1.96E-02	1.61E-04	2.44E-04	6.38E-04	2.60E+00	3.28E-03	N/A	4.26E-01	N/A	5.40E-04	2.87E-02	7.53E-05	9.87E-03	1.36E-02	N/A	5.40E-02	2.73E-03	1
		283	1.33E+01	2.77E-02	4.98E-01	4.66E-02	N/A	1.44E-02	2.36E+01	1.54E+00	1.46E+00	4.69E+00	6.00E+00	2.27E-02	3.77E+00	N/A	2.65E-01	3.01E+00	4.24E+00	8.15E-01	9.14E-01	16
Threshold:			>0.5%	>0.01%	>0.1%	>0.01%	>0.01%	>0.01%	>5%	>0.3%	>1%	>										

Fifteen of the cement samples but only one vein (S283) have relatively elevated concentrations of six or more out of nineteen considered major and minor elements in Tables 17 and 18. Overall, only three cement samples are not enriched in measured elements besides calcium (S14, S287, E173), whereas twenty-three veins are “pure” calcite and the rest are enriched in three or less elements. All of the samples with more than four relatively concentrated measured elements contain $>0.3\%$ Ca^{+x} sodium (Na), and no sample with elevated sodium has less than three elements of relatively high abundance with respect to calcium. Similarly, thirteen out of seventeen samples with $>0.3\%$ Ca^{+x} potassium (K) have $>0.3\%$ Ca^{+x} Na as well, and all of the samples with elevated K have four or more measured elements of relatively high Ca^{+x} abundance. Only one vein has elevated K, and four have elevated Na.

It is possible that non-carbonate minerals such as clays may have contributed at least some of the elements leached, especially for the samples which showed elevated aluminium (Al). Silicon was only elevated for one vein and four cements though, all of which also had relatively high concentrations of Al. Another possibility is that these samples precipitated from cation-rich brines. The majority of samples with high K and/or Na also had high Al, though two of these calcites (cement E6 and vein S284) and four mixed carbonate samples had negligible Al. These six samples, especially the calcites, are the most likely to have precipitated from relatively saline brines. Some samples with both high Al and S (+/- K or Na) could perhaps be indicative of water-soluble sodium and/or potassium aluminium sulfates (similar to baking powder precursor chemicals).

Enrichment of base metals such as Zn, Cu, Ni, Sn, Cr and Co, and elevated S levels in a number of samples (mainly cements) points to possible leaching of acid-reactive sulfides and/or sulfates. However, not every sample with base metal enrichment has high sulfur, and similarly not all samples with sulfur enrichment relative to calcium have base metal enrichment. Several base metal enriched samples do have relatively high aluminium, with five of these also being phosphate-enriched. Paragenetic association of complexing elements such as Al, Ba, Fe, Zr, REE's and ligands such as carbonate, phosphate, chloride and fluoride, indicating simultaneous presence of these in mineral forming solutions, has been documented in the literature (Humphries, 1984; Mineyev, 1963). So it is possible that the enrichment in elements other than calcium in the acid-leachable component of samples is due to a single mineralisation event, although it could also point to multiple events or contribution of elements from non-cement/vein phases within samples (e.g., detrital clays) in some cases.

Two calcite samples enriched in both base metals and sulfur that could have been the result of a single mineralisation event are cements E105 and S86. These calcite-cemented quartzose sandstones are the only two which were found to contain calcite cement with congruent twinning and extinction across section when viewed with cross-polarised light (e.g., Figure 9). This means that the calcite cement in these samples precipitated at the same time in all pores, effectively forming a “single crystal” throughout the connected pore space. These samples are also the only ones tested that have Co/Ni ratios greater than five; the majority of samples have on average $\text{Co/Ni} = 0.54$, whereas for E105 the Co/Ni is 8.16 and for S86 it is 23.39. The absolute concentrations of Co and Ni within these cements and the Co/Ni ratios (>5) fit the criteria for volcanogenic pyritic ore bodies (Bralia *et al.*, 1979), whereas Co/Ni for the rest of the samples is similar to either hydrothermal (highly variable Co/Ni) or sedimentary (average $\text{Co/Ni} = 0.63$) sulfide. The three most

abundant volatiles within magmatic fluids are water, CO₂, and dissolved/gaseous sulphur species, which could account for sulfur enrichment in at least some of the samples.

Clays (especially when dispersed organics are present) can act as nucleation points for minerals such as base metal sulfides. Several of the cement samples are from units that contain coal and/or dispersed organics, which can act as reductants promoting precipitation of reduced metals. So the high abundance of elements such as zinc in the cemented samples compared with the majority of veins could simply be due to differences in mineral nucleation potential and redox conditions, rather than due to differences in mineralising fluid composition and/or detrital minerals present.

A number of samples have elevated concentrations of elements such as Fe, Mn, Sr and/or Mg, with some also having high Na, K, and/or S. If this was due to a single event, rather than multiple mineralising fluids over time or contribution of non-carbonate detrital minerals such as clays to the acid-leach results, then some conclusions can be drawn regarding precipitation conditions (e.g., Table 1). Only one out of sixteen samples with >5 %_{Ca+x} Mn also have >1 %_{Ca+x} Mg (calcite cement E6), which is in line with the fact that the presence of aqueous Mg inhibits incorporation of Mn into calcite (Zuddas *et al.*, 2003). So for sample E6, either the parent fluid must have contained substantially more than the 5.4 %_{Ca+x} Mn that it has now, or else there was some dolomite/ankerite present which is unrelated to the calcite cement. None of the samples with 0.5 %_{Ca+x} Sr have more than >1 %_{Ca+x} Mn, which inhibits strontium incorporation into calcite. Thus, it is possible that the calcites that do contain significant Mn may have precipitated from a fluid with both high Mn and Sr concentrations, with the high Sr not seen within the calcite due to the presence of abundant Mn causing it to be retained in the fluid.

Five out of nine calcites containing relatively abundant sulphur (excluding the coral) also have a high proportion of magnesium (>1 %_{Ca+x}). This is in spite of the fact that aqueous sulphate has been noted to inhibit incorporation of Mg into calcite (Mackenzie *et al.*, 2006). The parent fluid could have contained substantially more Mg than is apparent from inspection of the cement, with the sulfate precipitating as gypsum/anhydrite or being reduced to form base metal sulfides, or else the sulphur could be unrelated to the carbonate mineralisation in those samples. Four out of five calcite cements with >5 %_{Ca+x} Fe also have >0.5 %_{Ca+x} S, implying that at least some of the Fe may be associated with sulfides, but it could also be siderite or ankerite that were not apparent in XRD. Ferroan calcite is less likely, given that high concentrations of Fe in solution inhibit the precipitation rate of calcite (Van Lith *et al.*, 2003; Vasconcelos *et al.*, 1995; Wright, 1999; Zuddas *et al.*, 2003).

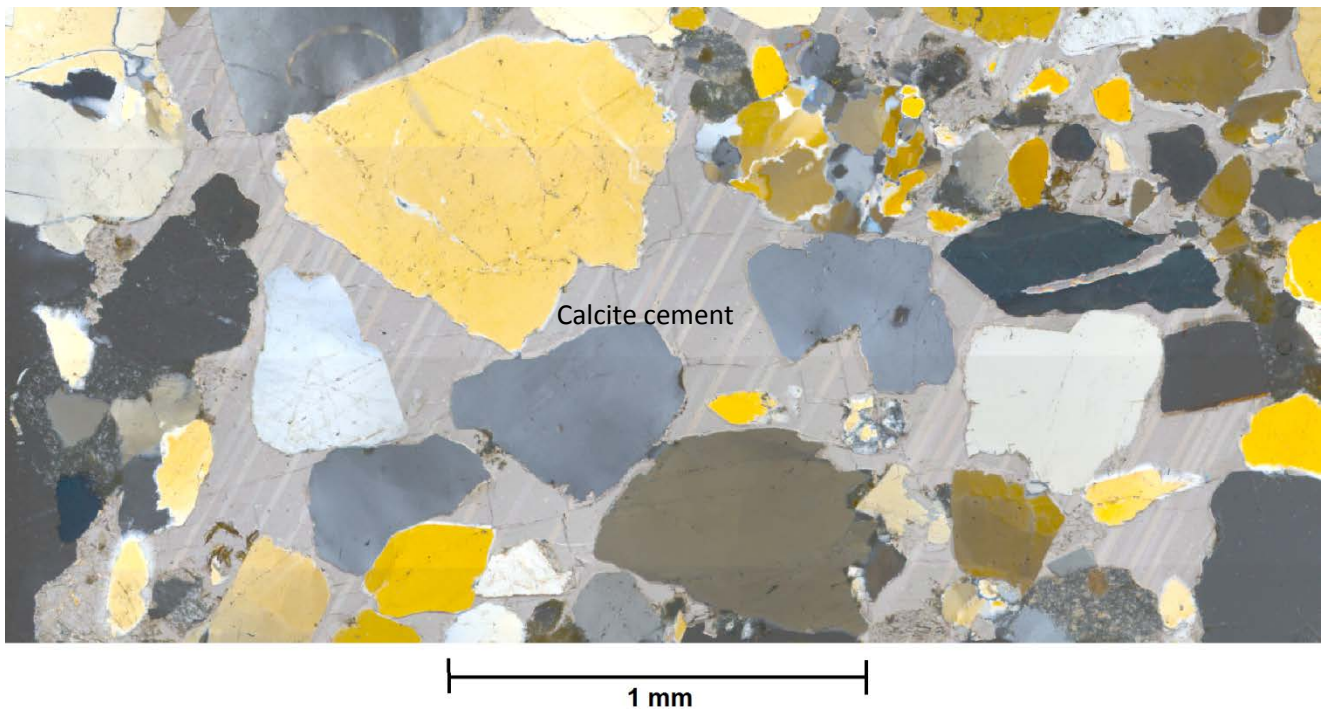


Figure 9: Calcite cement (grey) with congruent twinning (straight lines) and extinction across section when viewed with cross-polarised light in quartzose sandstone sample #86, Surat Basin. The majority of the grains cemented by the calcite are quartz.

3.3.2. Rare earth elements and yttrium (REEY)

3.3.2.1. Introduction

The lanthanides (LN), otherwise known as rare earth elements (REE), are geochemically very similar to each other, and the element yttrium (Y) is chemically similar to the REE's. They are often referred to as a single package (REEY). The REEY characteristics of carbonate cements and veins can potentially tell us about the history of the mineralising fluids and the carbonate precipitation conditions. The REE are generally transported in their 3+ oxidation state, and 3+ REE ions can substitute for Ca^{2+} , Y^{3+} , Th^{4+} , U^{4+} , Mn^{2+} , and Zr^{4+} in minerals (Henderson, 1984). Eu^{2+} can also substitute for Ca^{2+} , as well as Pb^{2+} , Sr^{2+} , and Na^+ (Henderson, 1984). Eu^{2+} is probably favoured over Eu^{3+} at higher temperatures (Saunders, 1984; Shulgin and Kozmin, 1963), and is only present in solution under reducing (anoxic) conditions.

For interpretive purposes, the REE are split into three groups: the light REE (LREE) are the elements La through to Sm, the heavy REE (HREE) are Gd through to Lu, and the middle REE (MREE) are a looser group but generally Pm through to Ho (Henderson, 1984). The REEY concentrations are usually normalised to a standard reference material, often similar to the parent rock package, in order to aid interpretation. "Shale" in terms of REE-normalisation is generally a loose synonym for aluminosilicate sedimentary rocks (Fleet, 1984), but in this report "shale normalisation" or SN refers to the Post Archean Australian Shale (PAAS) standard (Nance and Taylor, 1976; Taylor and McClennan, 1985). Another reference material that the REE have been normalised to is chondrite (CN), the primitive building block of the solar system, because this is useful for interpreting many of the processes related to mineral genesis.

Distinct differences in the normalised concentrations of individual REE's and also Y produce "REEY patterns". Oceanic sediments, both biogenic and authigenic, show similar distribution of REEY to coeval seawater (Clark, 1984). Low water-rock ratios favour the water obtaining the host-rock REE pattern (Saunders, 1984). Simple diagenesis does not affect the overall REEY patterns of sediments (Chaudhuri and Cullers, 1979; Fleet, 1984; Wildeman and Condie, 1973; Wildeman and Haskin, 1973). Normally, cerium (Ce) should be the most abundant of the REE, but La or Nd tend to dominate in marine authigenic sediments due to them having a "negative cerium anomaly". This is because aqueous Ce^{3+} readily oxidises to form insoluble Ce^{4+} in the presence of dissolved oxygen, often co-precipitating with Mn in $Mn(OH)_2$ nodules (Clark, 1984; Humphris, 1984). Cerium is the only REE that oxidises to the 4+ state in most natural environments.

The REEY patterns of carbonate cements/veins may be indicative of mineralising fluid type, source, fluid-rock interactions, and any REE-fractionation processes during fluid transport and mineral precipitation. Complexes are the major form in which the REE are transported in hydrothermal and metasomatic fluids (Humphris, 1984; Mineyev, 1963). 'Hydrothermal' temperatures generally range from 50 degrees Celsius up to granite melting temperature (Saunders, 1984), and so metasomatic fluids (generally high temperature and high water-rock ratios) can have hydrothermal element signatures (Humphris, 1984). Complexes are dissolved multivalent cations loosely bound to any of a class of anions called ligands (e.g., Figure 10). REE fluid-transport over any great distance, regardless of the kind of fluid involved, probably requires REE-complexation (Humphris, 1984). The main reason why this may be the case is the fact that free cations are more likely to become adsorbed to clay mineral surfaces (and thus lost from the solution) than ions that are bound to ligands.

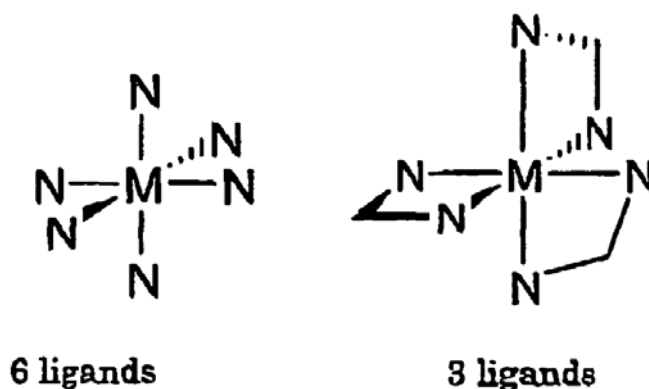


Figure 10: Two examples of ligands (N) bound to a metal cation (M) in solution. Modified after Bhalgat *et al.* (2006).

High REE concentrations, especially HREE, are associated with high concentrations of dissolved alkali metals (e.g., Li, Na and K) and volatiles (Humphris, 1984; Mineyev, 1963). Similarly, the more chloride (Cl^-) in a hydrothermal fluid, the more HREE may be in solution (Graf, 1977; Saunders, 1984). At low temperature and pressure, the HREE form stronger complexes than the LREE with Cl^- anions (Saunders, 1984). Paragenetic association of the REE with complexing cations, such as Al, Ba, Fe, and/or Zr, and the ligands fluoride, chloride, carbonate, and/or phosphate, suggests that they were simultaneously present within mineral-forming solutions (Humphris, 1984; Mineyev, 1963). For example, high zirconium within a REE-bearing mineral may indicate that the REE-transporting fluid was F-rich, especially if REE-enriched (Humphris, 1984).

The REE are extremely mobile in CO₂-rich solutions. Water-wet supercritical CO₂ tends to concentrate the REE, especially the LREE. This is due to CO₂ with dissolved water having a low pH (lower than when CO₂ is dissolved in water), which favours solution of REE and their transport either as complexes or as free ions (Humphris, 1984; Saunders, 1984). Acidic solutions apparently have a greater potential to be REE-enriched compared with alkaline solutions (Lawrence *et al.*, 2006). However, the REE do complex quite effectively, particularly with carbonate (an alkaline anion) and less so with sulphate and Cl⁻ anions (Humphris, 1984; Turner and Whitfield, 1979). Carbonate anion complexation increases with increasing REE atomic number, from La through to Lu. Similarly, greater bicarbonate anion concentration leads to greater solubility of HREE compared with LREE (Herrmann, 1978; Humphris, 1984). Overall, the HREE form more stable inorganic and organic complexes than the LREE (Humphris, 1984)(Goldberg *et al.*, 1963; Sillen and Martell, 1964).

Complexation and mineral-sorption are two processes that can fractionate the HREE from the LREE in solutions. REE complexes are sensitive to changes in the pH (Humphris, 1984; Mineyev, 1963). As the LREE complexes are the least stable, these elements would precipitate first, hence enriching the residual solutions in the HREE (Humphris, 1984; Mineyev, 1963). Loss of REE from solution due to pH increase (higher alkalinity) can be the result of exchange of REE for H⁺ in accessible mineral cation exchange sites (generally “reactive” clays), adsorption of REE onto mineral surfaces (especially clays), or co-precipitation of REE’s with other minerals such as hydroxides or carbonates (Balashov *et al.*, 1964; Humphris, 1984; Stumm and Morgan, 1970).

Phyllosilicate minerals such as clays acquire the REE mainly through surface adsorption and clays tend to hold higher REE and Y than minerals such as carbonates and quartz (Clark, 1984). REE’s can also be bound by organic matter, and at low pH metals can more effectively bind to organics than to mineral fines (Parker and Rae, 1998). Major concentrations of REE can also be present in accessory minerals and sometimes be associated with carbonate mineralisation. Certain minerals such as apatite and other phosphates can contain orders of magnitude more REE’s than more common rock-forming minerals (Humphris, 1984) if the parent fluid contained elevated concentrations of REE’s. Biogenic phosphate deposits, for example, are likely to contain much lower concentrations of REE’s than magmatic phosphates.

Most of clay REE’s are adsorbed upon mineral surfaces rather than held within the crystal lattice (Roaldset and Rosenqvist, 1971). Decreases in pH (more acidic) may cause clay REE mobilisation (Balashov and Girin, 1969), especially MREE (Fleet, 1984), with least effect upon LREE mobilisation. However, the mineralising fluid responsible for carbonate mineralisation may have imparted its element signature to the clays (especially likely if acidic fluids preceded precipitation). In addition to making similar arguments, other workers have shown that minerals such as clays and quartz/chalcedony are often precipitated at the same time as carbonates in sedimentary rocks (e.g. Uysal *et al.*, 2011).

3.3.2.2. Results

The cement and vein samples contain a similarly diverse range of REE concentrations (Tables 19 and 20). One cement (mixed carbonate S70) and seven calcite veins (E4, E96, E99, S286, S279, S282, and S284) have significantly greater total REE concentrations than common igneous rocks. The rocks that the carbonates were compared with include international standards such as BCR-2, BHVO-2, Bir-1, JG-3, and W2a.

Table 19: Cement rare earth element (REE) concentrations* (ppm), Total Ln, and Eu/Sm within acid-leached portions. Colour legends are at the bottom of the table.

Basin	Sample #	Well	Formation	Depth (m unless marked ft)	La	Ce	Pr	Nd	Sm	Eu	Gd	Tb	Dy	Ho	Er	Tm	Yb	Lu	Total Ln	Eu/Sm	
Standard	JCp1	N/A	(International coral standard)	N/A	3.88E-02	3.71E-02	6.55E-03	2.76E-02	6.34E-03	1.68E-03	8.54E-03	1.20E-03	7.83E-03	1.78E-03	5.01E-03	6.96E-04	4.81E-03	8.33E-04	0.1	0.27	
Eromanga	5	Mirintu-1	Cadna-Owie Formation	680.36-680.395	1.32E+01	3.45E+01	4.59E+00	1.96E+01	4.36E+00	1.31E+00	4.15E+00	5.98E-01	2.95E+00	5.00E-01	1.09E+00	1.24E-01	6.66E-01	8.81E-02	87.7	0.30	
	6	Mirintu-1	Cadna-Owie Formation	675.29-675.33	2.02E+01	5.22E+01	6.75E+00	2.84E+01	6.10E+00	1.64E+00	5.98E+00	7.96E-01	3.86E+00	6.26E-01	1.49E+00	1.59E-01	8.96E-01	1.20E-01	129.2	0.27	
	7	Saltern Creek 1	Namur Sandstone	1651'2"-4"	3.82E+00	1.54E+01	3.09E+00	1.84E+01	6.11E+00	3.05E+00	6.25E+00	8.39E-01	4.09E+00	6.71E-01	1.48E+00	1.56E-01	8.99E-01	1.15E-01	64.4	0.50	
	8	Winna-1	Murta Fm.	1008.08-1008.12	1.16E+01	3.57E+01	4.49E+00	1.90E+01	4.73E+00	1.14E+00	5.40E+00	8.81E-01	5.22E+00	1.04E+00	2.65E+00	3.49E-01	2.01E+00	2.69E-01	94.6	0.24	
	79	Jackson South 2	Westbourne Formation	4279'5"-2"	1.40E+01	3.95E+01	4.43E+00	1.87E+01	5.36E+00	1.40E+00	6.58E+00	1.02E+00	5.61E+00	1.05E+00	2.51E+00	3.12E-01	1.81E+00	2.43E-01	102.5	0.26	
	103	Connemara 1	Westbourne Formation	942.17-942.37	1.35E+01	3.66E+01	4.83E+00	1.93E+01	4.35E+00	2.19E+00	4.16E+00	6.83E-01	3.98E+00	7.37E-01	1.80E+00	2.27E-01	1.29E+00	1.67E-01	93.8	0.50	
	105	Connemara 1	Westbourne Formation	946.24-946.34	1.26E+01	2.84E+01	3.54E+00	1.38E+01	3.32E+00	1.23E+00	2.65E+00	3.97E-01	2.23E+00	4.08E-01	1.06E+00	1.29E-01	7.76E-01	1.04E-01	70.6	0.37	
	108	Jundah 1	Hooray (Namur) Sandstone	905.67-905.673	2.76E+00	7.06E+00	1.08E+00	5.42E+00	1.96E+00	9.16E-01	2.66E+00	3.99E-01	2.19E+00	4.09E-01	9.74E-01	1.21E-01	7.21E-01	1.00E-01	26.8	0.47	
	121	Thargomindah 3	Hooray/Namur Sandstone	1171.58-1171.74	1.33E+01	2.89E+01	3.27E+00	1.28E+01	2.66E+00	7.51E-01	2.47E+00	3.46E-01	1.80E+00	3.25E-01	7.85E-01	9.90E-02	5.67E-01	7.75E-02	68.2	0.28	
	162	Merrimelia 32	Birkhead Formation	6064'1.5"-5"	9.80E+00	2.25E+01	2.80E+00	1.20E+01	3.05E+00	1.09E+00	4.06E+00	5.78E-01	2.90E+00	5.03E-01	1.17E+00	1.40E-01	8.14E-01	1.11E-01	61.6	0.36	
	167	Dullingari 037	Murta Formation	5065'8.5"-10.5"	7.73E+00	2.06E+01	2.27E+00	9.14E+00	2.30E+00	6.04E-01	2.75E+00	4.57E-01	2.61E+00	4.83E-01	1.14E+00	1.41E-01	7.87E-01	1.05E-01	51.1	0.26	
	173	Dullingari 037	Murta Formation	5068'8"-5069	7.26E+00	1.93E+01	2.11E+00	8.25E+00	1.74E+00	4.35E-01	1.76E+00	2.92E-01	1.68E+00	3.44E-01	9.09E-01	1.23E-01	7.39E-01	9.77E-02	45.0	0.25	
	201	Muteroo 1	Namur Sandstone	5290-5300	8.19E-01	1.82E+00	2.33E-01	9.96E-01	2.26E-01	6.23E-02	2.48E-01	3.75E-02	1.91E-01	3.52E-02	8.83E-02	1.22E-02	7.18E-02	1.01E-02	4.8	0.28	
	202	Muteroo 1	Namur Sandstone	5350-5360	7.67E-01	1.84E+00	2.46E-01	1.11E+00	3.51E-01	9.06E-02	4.25E-01	7.07E-02	4.11E-01	8.06E-02	2.10E-01	2.78E-02	1.77E-01	2.50E-02	5.8	0.26	
	10	Chinchilla 4	Hutton Sandstone	799.385-799.48	8.24E+00	2.88E+01	3.59E+00	1.66E+01	5.13E+00	1.70E+00	6.31E+00	1.10E+00	6.28E+00	1.20E+00	3.05E+00	4.13E-01	2.53E+00	3.48E-01	85.2	0.33	
	14	Strathpine 1	Hutton Sandstone	500	1.00E+01	2.32E+01	2.80E+00	1.14E+01	2.59E+00	6.68E-01	2.48E+00	3.68E-01	1.85E+00	3.31E-01	7.73E-01	9.72E-02	5.63E-01	7.61E-02	57.3	0.26	
	Surat	46	Strathpine 1	Walloon Coal Measures	270	1.19E+01	3.01E+01	3.97E+00	1.85E+01	4.92E+00	1.39E+00	5.54E+00	8.16E-01	4.46E+00	8.85E-01	2.29E+00	3.11E-01	2.06E+00	3.13E-01	87.5	0.28
		54	Moonie Corner 1	Walloon Coal Measures	1455	3.65E+00	1.08E+01	1.62E+00	8.10E+00	2.63E+00	7.62E-01	3.01E+00	4.43E-01	2.39E+00	4.35E-01	1.04E+00	1.37E-01	8.57E-01	1.27E-01	36.0	0.29
		55	Moonie Corner 1	Walloon Coal Measures	1497	6.96E+00	2.36E+01	3.54E+00	1.79E+01	5.54E+00	1.46E+00	6.23E+00	9.06E-01	4.60E+00	7.76E-01	1.77E+00	2.08E-01	1.27E+00	1.80E-01	74.9	0.26
		67	West Wandoan 1	Hutton Sandstone	800.70-800.85	1.98E+01	4.92E+01	5.41E+00	2.10E+01	4.13E+00	9.65E-01	3.38E+00	5.00E-01	2.51E+00	4.45E-01	1.09E+00	1.45E-01	8.70E-01	1.13E-01	109.5	0.23
70		West Wandoan 1	Evergreen Formation	1056.10-1056.19	4.86E+01	1.06E+02	1.10E+01	4.13E+01	7.75E+00	2.25E+00	6.68E+00	9.08E-01	4.04E+00	6.41E-01	1.37E+00	1.54E-01	8.47E-01	1.06E-01	231.4	0.29	
81		Yapunya 1	Evergreen Formation	4993'8"-4994'4"	3.35E+00	9.07E+00	1.19E+00	5.01E+00	1.34E+00	4.33E-01	1.46E+00	2.16E-01	1.15E+00	2.19E-01	5.36E-01	6.98E-02	4.13E-01	5.55E-02	24.5	0.32	
85		Cameron 1	Springbok Sandstone	147.91-148	1.54E+01	3.91E+01	5.12E+00	2.18E+01	5.00E+00	1.08E+00	4.86E+00	7.81E-01	4.62E+00	9.81E-01	2.75E+00	4.06E-01	2.72E+00	3.80E-01	105.0	0.22	
86		Mitchell 2	Bungil Formation	69.43-69.52	3.33E+01	5.05E+01	5.70E+00	1.88E+01	2.76E+00	6.14E-01	2.57E+00	3.40E-01	1.77E+00	3.10E-01	8.89E-01	1.02E-01	5.98E-01	8.48E-02	118.4	0.22	
87		Mitchell 2	Bungil Formation	85.91-85.97	1.20E+01	1.69E+01	1.86E+00	7.75E+00	1.71E+00	5.91E-01	2.45E+00	3.74E-01	2.34E+00	5.51E-01	1.51E+00	2.01E-01	1.26E+00	1.92E-01	49.7	0.35	
263		Chinchilla 4	Walloon Coal Measures	580.73	9.76E+00	1.89E+01	2.18E+00	8.29E+00	1.56E+00	5.57E-01	2.14E-01	1.56E+00	1.12E+00	2.03E-01	5.56E-01	7.29E-02	4.53E-01	7.21E-02	45.5	0.36	
272		Chinchilla 4	Evergreen Formation	1143	3.17E+01	7.10E+01	9.00E+00	3.65E+01	8.43E+00	3.38E+00	1.29E+00	8.75E+00	6.53E+00	1.08E+00	2.58E+00	3.10E-01	1.94E+00	2.76E-01	182.7	0.40	
278		Mitchell 2	Bungil Formation	82.81-82.90	1.16E+01	1.88E+01	2.10E+00	8.33E+00	1.74E+00	5.34E-01	1.90E+00	2.97E-01	1.79E+00	3.96E-01	1.17E+00	1.78E-01	1.21E+00	1.81E-01	50.2	0.31	
280		Mitchell 2	Evergreen Formation	825.53-825.64	8.02E+00	1.46E+01	2.03E+00	1.03E+01	3.18E+00	6.62E-01	4.23E-01	3.48E+00	2.01E+00	3.74E-01	9.57E-01	1.25E-01	7.89E-01	1.26E-01	47.1	0.21	

*For La and Ce columns, green highlighting indicates which element is the more abundant in a given sample. Total Ln and Eu/Sm colour legend at right.

>400	>0.5
200-400	0.35-0.5
<50	<0.25

Of these standards, BCR-2 has the highest total REE (~147 ppm) and Bir-1 the lowest (~17 ppm), whereas the eight highest REE carbonates tested all have >200 ppm REE (vein S282 highest with 632 ppm). By comparison, PAAS has ~183 ppm REE, upper crustal average is 87 ppm, chondrite only has ~5 ppm, and the marine carbonate coral standard JCp-1 has up to ~0.45 ppm.

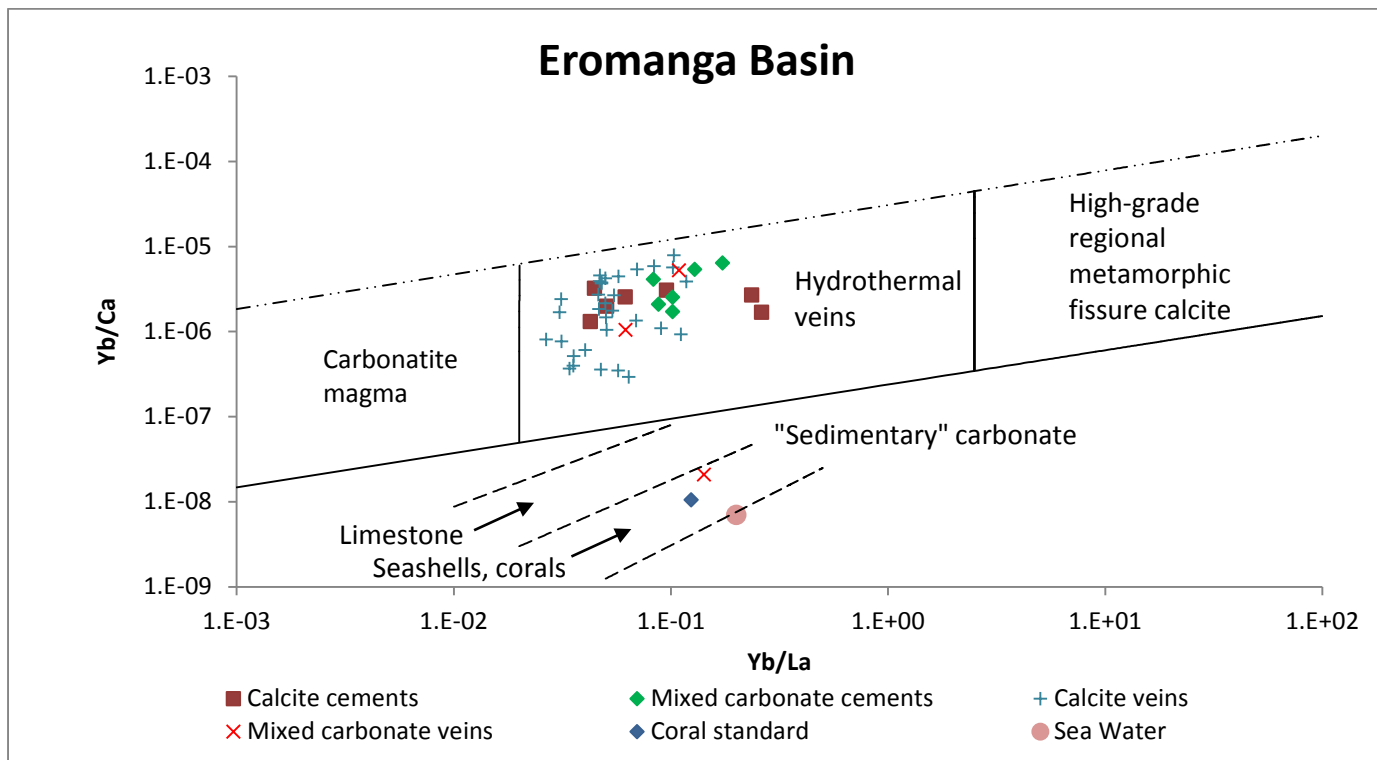
All except one sample have at least two orders of magnitude greater total REE than biogenic marine carbonate. The exception is calcite vein E98 (total REE 0.32 ppm), which was the only sample taken from the shell-rich marine Toolebuc Formation. This implies that all tested carbonate samples except one are not primary biogenic marine carbonate, irrespective of whether vein or cement or if the host formation has had any marine influence. Alternatively, if there was remobilisation of marine carbonate (e.g., dissolution of shells or limestone present at depth via acidic migrating fluid), the formerly marine trace element “signature” has been effectively replaced by the much greater concentration of REE in the migrating fluid.

The Y/Ho ratio is commonly used to determine whether or not sediment is of marine origin. The only carbonate cement sample with “marine” Y/Ho (>44) is siderite-calcite cement S87 (Y/Ho = 45.7) from the Bungil Formation, whereas the Y/Ho of vein E98 is 33.4 (Tables 19 and 20). Both magmatic and sedimentary Y/Ho values commonly range from 25-33 (Bau and Dulski, 1996). Aside from potentially being due to “marine influence”, high Y/Ho ratios such as that of S87 can be due to high fluorine concentrations within the REEY-bearing fluid prior to carbonate precipitation, as Y complexes quite strongly with F- (Bau and Dulski, 1996). There is a shallow marine unit near the top of this formation, so in spite of cement S87 containing relatively high total REE (130 ppm) a marine origin for its Y/Ho cannot be ruled out. Cement S87 probably represents a mix of marine and hydrothermal carbonate, given that its Yb/Ca vs Yb/La signature is hydrothermal, whereas E98 plots within the field of shells and corals (Figure 11).

High heat flux associated with basin extension during the Cretaceous break-up of Gondwana is a possible reason for the apparent hydrothermal signatures of the majority of cements and vein samples tested. Convecting groundwater in such a regime can obtain hydrothermal characteristics, and extension also opens multiple fluid-flow pathways (e.g., normal faults) from depth up into shallow formations. Some formations (e.g., Wallumbilla Formation) contain volcanic lithics and grains that were likely extruded during this time, but these are apparently the only direct evidence for local volcanism within the Eromanga Basin. Thick tuff layers containing large volcanic grains are known within some formations of the Surat Basin though. Widespread alkaline volcanism is generally a feature of continental break-up.

The two Surat cements that plot just inside the field of carbonatite magma, S70 and S86, are both also anomalous for other reasons. As previously mentioned, S86 has the highest Co/Ni of any tested sample (23.4) and S70 has one of the highest total REE concentrations (231 ppm). The samples with the highest total REE (veins S282 and S284) both plot close to the upper right corner of the carbonatite field in Figure 11b. Many of the quartz grains in sample S86 are “floating” within calcite and appear to have been partially dissolved and few other minerals are present. S70 meanwhile contains abundant Ca-bearing plagioclase grains as well as additional phases aside from calcite and quartz, such as micas, clays and minor dolomite.

A)



B)

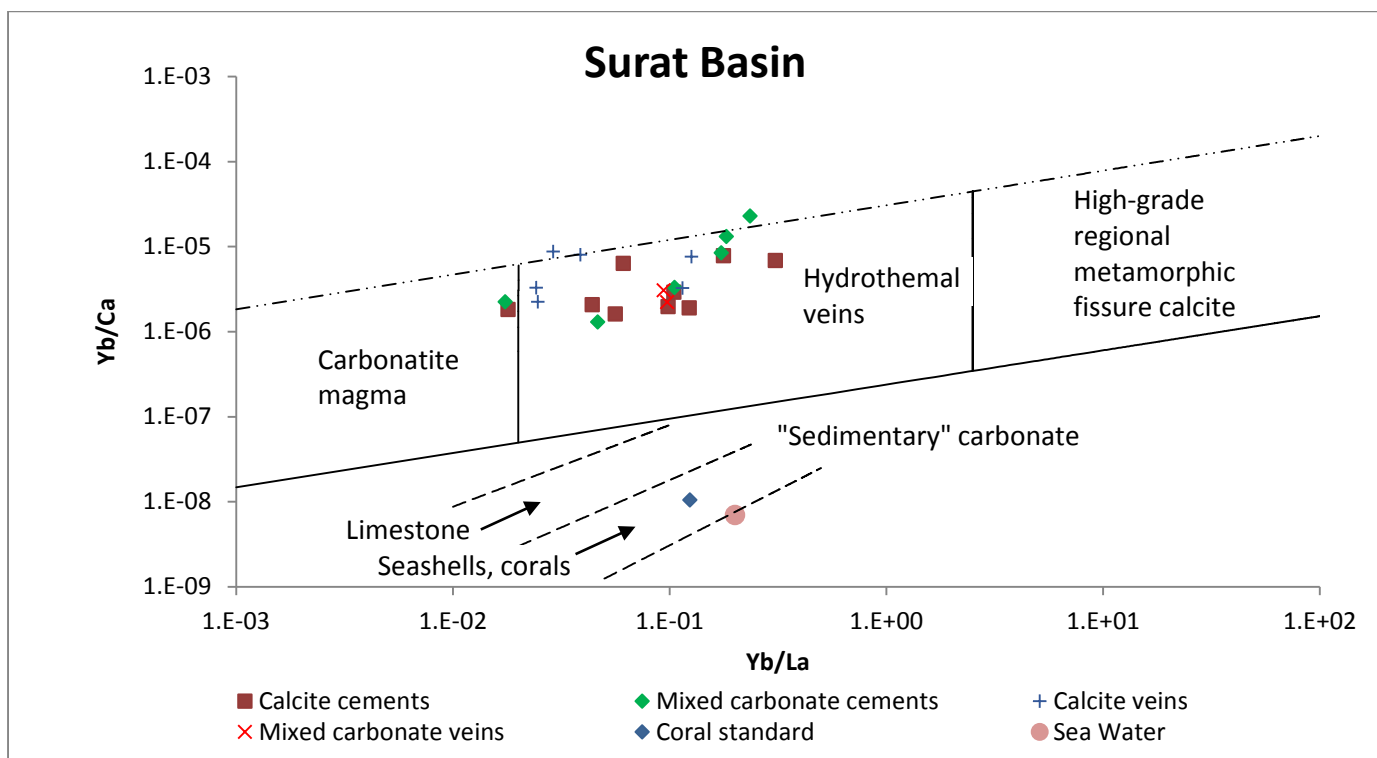


Figure 11: The different kinds of carbonate collected from A) the Eromanga Basin and B) the Surat Basin. Variation diagram modified after Möller (1983).

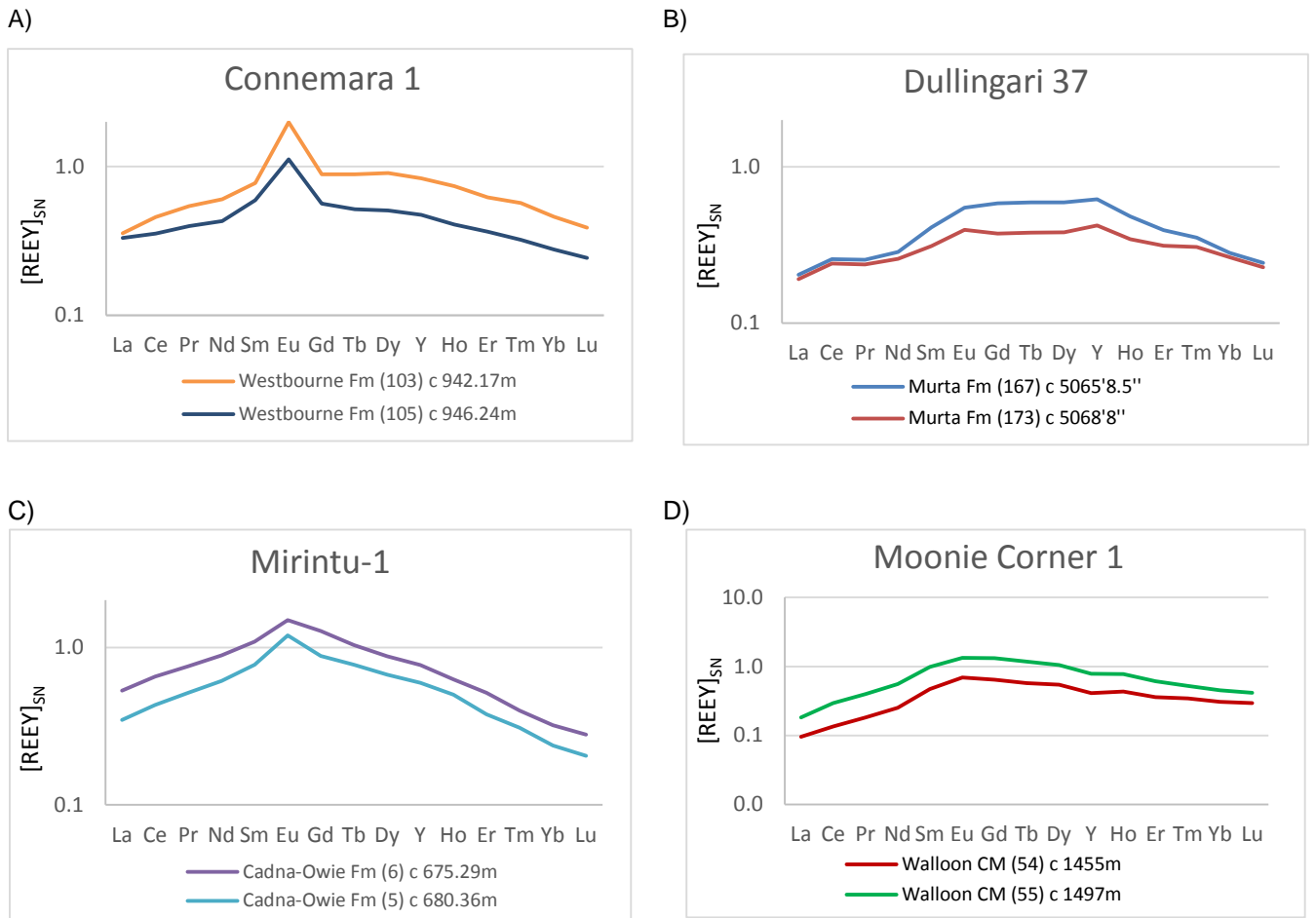


Figure 12: Similar normalised REE concentrations of two cements sampled up to 42m apart (vertically) within a given formation of four different wells: A) Westbourne Formation calcites from Connemara 1, Eromanga Basin, B) Murta Formation mixed carbonates from Dullingari 37, Eromanga Basin, C) Cadna-Owie Formation calcites from Mirintu 1, Eromanga Basin, and D) Walloon Coal Measures mixed carbonates from Moonie Corner 1, Surat Basin.

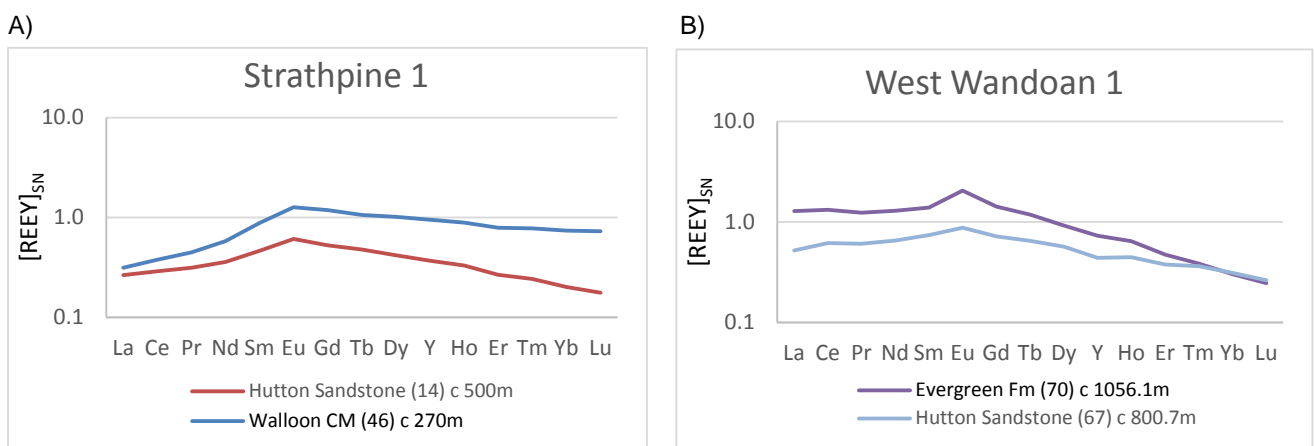


Figure 13: Two cement samples from different formations, one a calcite and the other mixed carbonate, displaying similar normalised REE concentrations to each other, in wells: A) Strathpine 1 - the REE concentrations progressively diverge from each other with increasing REE atomic number; B) West Wandoan 1 - the concentrations of Lu, Yb, and Tm are identical but then REE concentrations diverge with decreasing atomic number.

These calcite cements may well have precipitated from fluids associated with either carbonatites or alkaline magmatism. Carbonatites are often grouped with alkaline igneous rocks as they are associated with this type of volcanism and share some elemental similarities. The high total REE contents of some samples may be due to parent fluids associated with either alkaline pegmatites or carbonatites, as these magmatic fluids are both known to have high concentrations of REE's and ligands. The total REE content of S86, while relatively high compared with most samples is only 118.4 ppm, but that could be an artefact of dilution due to assimilation of low-REE material.

The shale (PAAS) normalised REEY values (Appendix Tables A4.1 and A4.3) of some samples show striking similarities to each other. It is convincing that in spite of the possibility of non-carbonate phases contributing to the REEY that was acid-leached from samples, a number of cement sample "pairs" taken up to 42 m apart from each other (vertically) in the same formations (and so reasonably may have different proportions of minerals) have quite similar REEY patterns. Examples of this from four different wells are given in Figure 12. For comparison, the 1.0 horizontal line in each plot represents the PAAS composition that the sample REE concentrations were "shale-normalised" to. Similarity in REEY patterns of cements from the same formations in individual wells shouldn't be that surprising, given that it is easy to imagine the cement within a single formation potentially precipitating at the same time and from the same fluid. However, similarity in the REEY patterns of calcite and mixed carbonate cements from different formations within the same wells has also been observed (e.g., Figure 13).

Cements S14 (Hutton Sandstone calcite) and S46 (Walloon Coal Measures mixed carbonate) have similar REEY patterns that diverge with increasing atomic number of the REE, with S46 also having greater Y and higher overall REE than S14 (Figure 13a). It is possible that this is an example of ligand REEY fractionation during a fluid migration event, though in the case of the HREE enrichment of S46 it could also be due to the fact that the Walloon Coal Measures contain more organic matter than the Hutton Sandstone. HREE bind more strongly to organic matter than LREE do. Alternatively, perhaps sample S46 was simply less diluted by low-REE content local groundwater, as could have been the cause for Hutton Sandstone sample S14. One of the "mixed" carbonate species in S46 may also have had higher affinity for REEY, particularly HREE, than plain calcite too.

Calcite cement S67 (Hutton Sandstone) and mixed carbonate cement S70 (Evergreen Formation) from West Wandoan 1 have near-identical Lu, Yb and Tm, and similar overall REEY patterns that diverge with decreasing REE atomic number from Er (Figure 13b). Similar to the comparison between S14 and S46, mixed carbonate S70 has more than twice as much total REE as calcite S67, has one of the highest REE contents of any tested sample, and also has a more positive Eu anomaly than S67. Both samples probably precipitated during the same fluid migration event, but S70 was likely closer to the REE-enriched fluid source. The LREE form less stable complexes than the HREE and are the first to drop out of solution as the pH becomes more alkaline, and so perhaps the fluid became more diluted and hence less acidic as it moved from the Evergreen Formation into the more permeable Hutton Sandstone, resulting in calcite precipitation that was less enriched in LREE at the point at which S67 formed, 150 m above S70. This is seemingly the opposite of the story outlined for the Strathpine 1 samples S14 and S46, but depending upon the position that the samples

precipitated in the fluid mixing front, and the amount and type of organic matter present, both scenarios could occur during the same event.

Veins, especially within faults, are the major conduits through which fluids can migrate from depth whilst retaining their trace element signatures. Some examples of veins from the same wells, with extraordinarily similar REEY patterns in spite of them occurring in different formations, are shown in Figure 14. Interestingly, similar veins E76 and E161 are both mixed carbonates with similar total REE concentrations (55.8 ppm and 60 ppm respectively), and in spite of having been sampled 420 m apart they basically look like the same sample. Similarity between REEY patterns of veins and cements has also been observed.

An example of a vein and a cement from different formations in the same well, but with similar REEY patterns, is given in Figure 15. The La concentrations of the two samples are almost the same, but the patterns diverge with increasing REE atomic number and the shallower vein has less total REE than the cement. This might be an example of REE fractionation via clay sorption and from a relatively ligand-pore fluid. In this scenario, the smaller HREE ions (with greater charge density) bind more effectively to mineral surfaces than the LREE do, which can result in the fluid becoming progressively HREE depleted with distances travelled through a sedimentary package. Alternatively, it could also simply be indicative of progressive REE precipitation due to more alkaline pH within the shallower unit up to the point at which vein 107 formed.

Four veins in particular, out of several collected from Blackall 2 core, show striking partial overlaps and similarities in their REE patterns (Figure 16). Notably, in terms of major elements they do have distinct differences (Tables 15-18). E92 is clean calcite, the mixed carbonate E95 has high Mg and S, calcite E91 has elevated Mn and P, and “calcite” E100 has the greatest manganese concentration of all tested samples (65,900 ppm, which is 14 %_{Ca+Mn}).

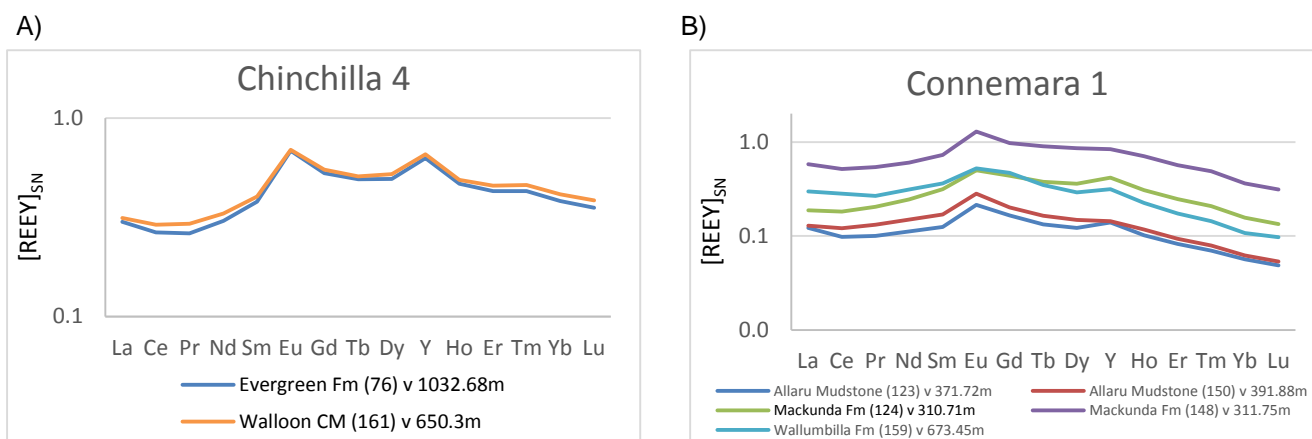


Figure 14: Veins from different formations with very similar normalised REE patterns: A) mixed carbonate veins of the Evergreen Formation and Walloon Coal Measures from Chinchilla 4, Surat Basin; B) calcite and mixed carbonate veins of the Allaru Mudstone, Mackunda Formation, and Wallumbilla Formation from Connemara 1, Eromanga Basin.

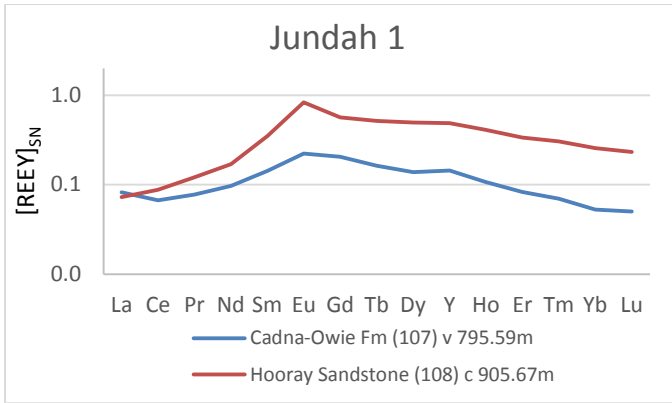


Figure 15: Two different calcite samples, one a vein and one a cement, from different formations of the same well and yet displaying similar PAAS-normalised REE patterns. The samples have similar La concentration, +ve Eu anomalies and are MREE-enriched, but the REE patterns diverge towards the HREE.

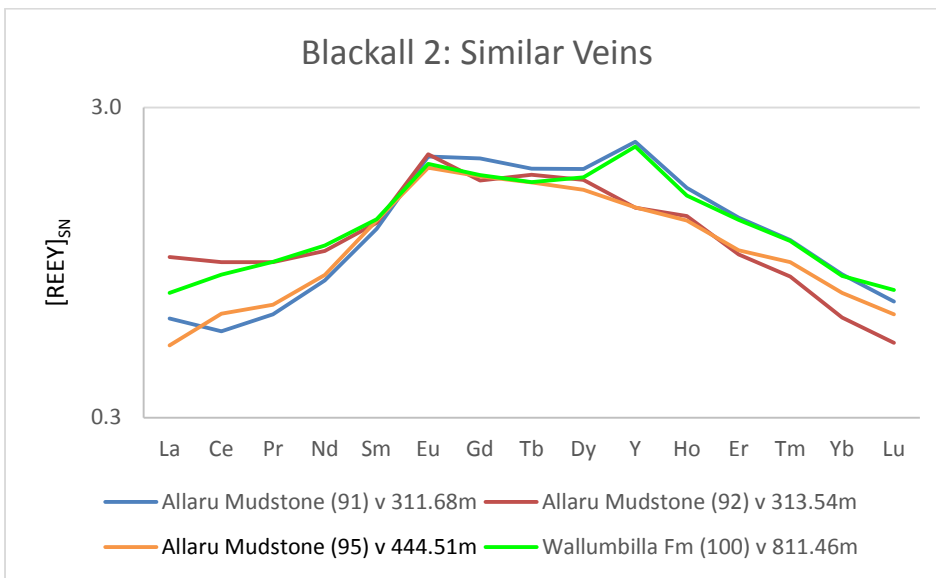


Figure 16: Normalised REE concentration patterns of calcite and mixed carbonate veins from Blackall 2 that show overlapping partial similarities to each other.

Veins E100 and E91 probably had the same parent fluid given that their concentrations of Sm, Y and the HREE's Ho, Er, Tm, and Tb are nearly identical and both have high Mn, in spite of these calcites having precipitated 500 m apart (vertically) and in different formations. Similarly, calcites E100 and E92 (just a few metres below E91) have identical Pr, Sm, and Dy. E92 and E91 have the same Sm and Eu. However, E91 has notably less La, Cr, Pr and Nd than both E92 and E100, but similar Nd and Sm to mixed carbonate E95 (130 m below) which has the same concentration of Sm as E92 and E100. Interestingly samples E91 and E95 have 138.9 ppm and 138.6 ppm total REE respectively, and E92 and E100 also have similar total REE concentrations to each other (188.6 ppm and 176.9 ppm respectively).

It is probable that each of these four veins formed from the same migrating parent fluid. The pattern variations are not likely to be due to mixing of two or more distinct REE-enriched fluids of different origins, given that each of the veins share identical concentrations of at least two REE's with at least one other vein. Therefore,

perhaps the differences in concentrations of some of the REE's are due to subtle variations in fractionation of sub-populations of the same fluid, and possibly also partial re-mixing of these.

Sometimes different samples from widely spaced localities are found to have similar normalised REEY concentration patterns. One of the most striking examples of this is given in Figure 17. In the case of biogenic marine carbonates, such similarity can simply be due to the samples having precipitated from the same parent sea water. In river sediments, it could be an indication of shared provenance. However, one of the samples is a cement and the other is a vein, and neither have a marine signature. The wells Merrimelia 32 and Mitchell 1 are roughly 750 km apart and in different states (Queensland and South Australia). There is also at least an eight million year time difference between the two formations. The fact that E277 is a vein within an older unit than the cement E162 means that it is possible that the two did form at the same or similar time, though of course the vein could also be considerably older/younger than the cement. Perhaps one way that two non-marine fluids, occurring spatially so far apart, could exhibit very similar REE profiles is if they were related to magmatism? It could also be a coincidence.

In addition to being able to graphically demonstrate similarities and differences between samples, normalised REE values can also provide information regarding the redox conditions, temperatures, sources and ligand saturation of mineralising fluids. Some of the shale and chondrite normalised REE ratios and anomalies (differences between the actual and the calculated normalised REE values) are collated in Appendix Tables A4.5-A4.8. Simplified interpretation of some of this information for the cements and veins tested is given in Tables 21 and 22.

Most samples appear to be the product of at least mild metasomatism. This could be an artefact of the positive MREE-anomaly that the samples exhibit especially when shale-normalised, which causes their $(La/Sm)_{SN}$ to be <1 thus giving the appearance of metasomatism. The MREE-anomaly itself could potentially have been caused by metasomatism though. Regardless, cement samples E7, E108, S54 and S55 have very low $(La/Sm)_N$ irrespective of whether normalised to shale or chondrite, and so probably are the products of strong metasomatism under relatively high temperature and high fluid-rock ratio conditions). Calcites E7 and E108 are also among the few to have both chondrite-normalised (CN) positive European anomalies and $(Tb/Yb)_{CN} >1$, together with cements E103, E105, S263, S272 and veins E127, S84, and S156. These factors suggest that the samples precipitated from what were originally hot and reduced acidic fluids, whereas the majority of samples with positive $(Eu)_{SN}$ anomalies coupled with $(Tb/Yb)_{SN} >1$ may be more indicative of lower temperature acidic decomposition of particularly plagioclase feldspars. Only a few samples do not have positive $(Eu)_{SN}$ anomalies, and these include samples E98 and S278 which both potentially have partially marine trace element signatures as mentioned earlier.

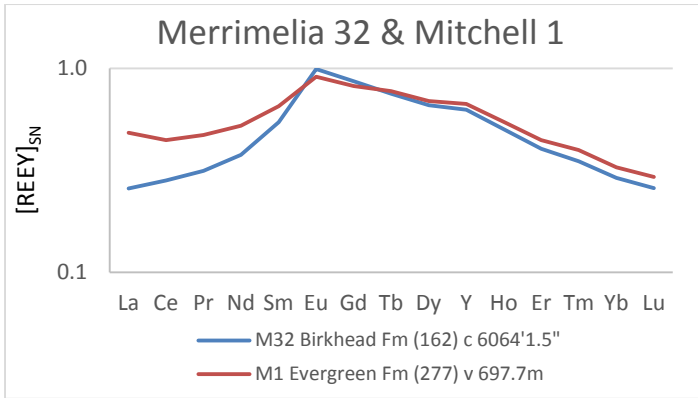


Figure 17: Calcite samples, one cement the other a vein, from different formations in wells separated by 750km, displaying similar normalised REEY concentration patterns.

Table 21: Interpretations of cement sample normalised REE ratio and anomaly data. The top row indicates the significance of the shaded sections*.

Basin	Sample #	Well	Formation	Depth (m unless marked ft)	Possibly metasomatic	Probably pH > 9.5 with CO ₃ ²⁻ forming pento- carbonato- Ce(VI) complexes	Possibly [HS] >> [SO ₄ ²⁻], or >250°C fluid, or inheritance of negative Eu anomaly from REE-parent minerals	Decomposition of plagioclase probably influenced fluid REE	Fluid possibly influenced by oxidising conditions
							Possibly [SO ₄ ²⁻] >> [HS-]		Strongly
N/A	JCp1	N/A	(International coral standard)	N/A					
Eromanga	5	Mirintu-1	Cadna-Owie Formation	680.36					
	6	Mirintu-1	Cadna-Owie Formation	675.29					
	7	Saltern Creek 1	Namur Sandstone	1651'2"					
	8	Winna-1	Murta Fm.	1008.08					
	79	Jackson South 2	Westbourne Formation	4279'5"					
	103	Connemara 1	Westbourne Formation	942.17					
	105	Connemara 1	Westbourne Formation	946.24					
	108	Jundah 1	Hooray (Namur) Sandstone	905.67					
	121	Thargomindah 3	Hooray (Namur) Sandstone	1171.58					
	162	Merrimelia 32	Birkhead Formation	6064'1.5"					
	167	Dullingari 037	Murta Formation	5065'8.5"					
	173	Dullingari 037	Murta Formation	5068'8"					
	201	Muteroo 1	Namur Sandstone	5290					
	202	Muteroo 1	Namur Sandstone	5350					
Surat	10	Chinchilla 4	Hutton Sandstone	799.385					
	14	Strathpine 1	Hutton Sandstone	500					
	46	Strathpine 1	Walloon Coal Measures	270					
	54	Moonie Corner 1	Walloon Coal Measures	1455					
	55	Moonie Corner 1	Walloon Coal Measures	1497					
	67	West Wandoan 1	Hutton Sandstone	800.70					
	70	West Wandoan 1	Evergreen Formation	1056.10					
	81	Yapunyah 1	Evergreen Formation	4993'8"					
	85	Cameron 1	Springbok Sandstone	147.91					
	86	Mitchell 2	Bungil Formation	69.43					
	87	Mitchell 2	Bungil Formation	85.91					
	263	Chinchilla 4	Walloon Coal Measures	580.73					
	272	Chinchilla 4	Evergreen Formation	1143					
	278	Mitchell 2	Bungil Formation	82.81					
280	Mitchell 2	Evergreen Formation	825.53						

Table 22: Interpretations of vein sample REE ratio and REE anomaly data.

Basin	Sample #	Well	Formation	Depth (m unless marked ft)	Possibly metasomatic	Probably pH > 9.5 with CO ₃ ²⁻ forming pentocarbonato-Ce(VI) complexes	Possibly [HS ⁻] >> [SO ₄ ²⁻], or >250°C fluid, or inheritance of negative Eu anomaly from REE-parent minerals	Decomposition of plagioclase probably influenced fluid REE	Fluid influenced by oxidising conditions
							Possibly [SO ₄ ²⁻] >> [HS ⁻]		Strongly
N/A	JCp1	N/A	(International coral standard)	N/A					
Eromanga	2	Mirintu-1	Cadna-Owie Formation	696					
	3	Mirintu-1	Cadna-Owie Formation	677.6					
	4	Mirintu-1	Cadna-Owie Formation	677.6					
	90	Blackall 1	Birkhead Formation	773.16					
	91	Blackall 2	Allaru Mudstone	311.68					
	92	Blackall 2	Allaru Mudstone	313.54					
	93	Blackall 2	Allaru Mudstone	314.6					
	94	Blackall 2	Allaru Mudstone	443.7					
	95	Blackall 2	Allaru Mudstone	444.51					
	96	Blackall 2	Allaru Mudstone	474.19					
	97	Blackall 2	Allaru Mudstone	475.88					
	98	Blackall 2	Toolebuc Formation	660.38					
	99	Blackall 2	Wallumbilla Formation	665.71					
	100	Blackall 2	Wallumbilla Formation	811.46					
	107	Jundah 1	Cadna-Owie Formation	795.59					
	115	Thargomindah 2	Allaru Mudstone	544.14					
	116	Thargomindah 2	Allaru Mudstone	556.31					
	117	Thargomindah 2	Allaru Mudstone	560.86					
	123	Connemara 1	Allaru Mudstone	371.72					
	124	Connemara 1	Mackunda Formation	310.71					
	125	Blackall 2	Allaru Mudstone	474.93					
	127	Blackall 1	Hooray (Namur) Sandstone	622.35					
	148	Connemara 1	Mackunda Formation	311.75					
	150	Connemara 1	Allaru Mudstone	391.88					
	151	Thargomindah 2	Allaru Mudstone	454					
	152	Thargomindah 1A	Adori Sandstone	966.86					
	153	Thargomindah 2	Mackunda Formation	409.66					
	154	Blackall 2	Allaru Mudstone	314.47					
	157	Thargomindah 2	Allaru Mudstone	576.18					
	159	Connemara 1	Wallumbilla Formation	673.45					
277	Mitchell 1	Evergreen Formation	697.7						
286	Blackall 2	Allaru Mudstone	606.855						
287	Blackall 2	Wallumbilla Formation	713.2						
295	Blackall 2	Wallumbilla Formation	798.805						
298	Blackall 2	Cadna-Owie Formation	833.725						
Surat	76	Chinchilla 4	Evergreen Formation	1032.68					
	84	Cameron 1	Walloon Coal Measures	230					
	156	Cameron 1	Walloon Coal Measures	230.7					
	161	Chinchilla 4	Walloon Coal Measures	650.3					
	279	Mitchell 2	Evergreen Formation	824.37					
	281	Mitchell 2	Evergreen Formation	828.25					
	282	Mitchell 2	Evergreen Formation	831.39					
284	Chinchilla 4	Evergreen Formation	1032.84						

The majority of cement and vein carbonates precipitated from anoxic fluids. At least nine cements and thirteen veins show evidence of mixing between probably hot and deeply sourced fluids with more oxygenated shallow/near-surface fluids. Three of those cements show strong evidence of oxygenated water (E7, E103, and S86), whereas the veins were only mildly oxidic. As previously mentioned S86 has the highest Co/Ni ratio of all the samples and was one of two to plot within the carbonatite field of the variation diagram in Figure 10b. It probably represents mixing between a metal-enriched sulfidic alkaline magmatism-related fluid and shallow oxygenated groundwater, and that mixing may have been responsible for rapid precipitation of the strong calcite cement (congruent twinning and extinction angle) within this quartzose sandstone (Figure 9).

3.4. Fluid inclusion studies

3.4.1. Fluid inclusion temperatures and salinity analyses

3.4.1.1. Introduction

This study examined 73 doubly polished sections from drill core from the Surat and Eromanga basins and 3 polished sections from drill cuttings for fluid inclusions in carbonate cements that would be suitable for fluid inclusion microthermometry. Although most samples contained abundant fluid inclusions in the quartz grains only 37 samples contained suitable inclusions in the carbonate cements. The majority of these samples are described in detail in Appendix 5 and a summary of the microthermometric data is given in Tables 23 and 24 (Eromanga and Surat basins, respectively).

The 3 doubly polished thin sections prepared from unconsolidated drill cuttings material from the South Australian region of the Eromanga Basin (samples 189, 197, 201) consist mainly of individual grains that are mostly quartz. A variety of fluid inclusions with varying liquid/vapour ratios were observed in the cores of the grains but were not examined as this study was focused on the later diagenetic fluids. Very little of the interstitial carbonate cement remained between the grains but was examined for fluid inclusions where possible. Unlike the rest of the samples, the majority of the fluid inclusion data were obtained from quartz overgrowths in these three samples in the hope that this could still yield useful palaeo-temperature and salinity data with the acknowledgement that the quartz overgrowths and carbonate cement may not be concurrent (Table 23).

No gases were detected visually in any of the fluid inclusions in carbonate, although many of the quartz grains contained abundant CO₂-rich fluid inclusions in the cores of the grains but not in the quartz overgrowths. Twelve samples have yielded fluid inclusion crusher results for CO₂ and five for C2-C5 wet gases. Although such inclusions were not directly observed in the calcite samples, it is possible that they may have been present either in minute amounts or else within inclusions in the quartz grains/overgrowths.

The study of fluid inclusions in diagenetic environments requires a great deal of caution. There are several problems commonly encountered in diagenetic environments that lead to post-entrapment modifications to the fluid inclusions and these are as follows.

Table 23: Eromanga Basin summary fluid inclusion data (temperature and salinity). Grey-shaded samples contain calcite veins.

Sample #	Source	Formation	Depth (m unless marked as ft)	Carb zone thickness	Notes	Homogenisation Temp (°C)	Salinity (Wt% NaCl eq)
127	Blackall 1	Hooray (Namur) Sandstone	622.35-622.6	20m (8m net)	Calcite vein in cemented zone	< 70	
90	Blackall 1	Birkhead Formation	773.16-773.24	Veins & sporadic fault associated cement	Calcite vein in cemented zone	< 70	
154	Blackall 2	Allaru Mudstone	314.47-314.48	Sporadic and frac associated	Possibly cone-in-cone and concretion calcite? Shells?	< 70	
93	Blackall 2	Allaru Mudstone	314.6-314.61	Sporadic and frac associated	Calcite vein	< 70	
98	Blackall 2	Toolebuc Formation	660.38-660.54	110m (98m net carbonate, 28m net sandstone laminations) and also frac associated (starting above this depth)	Calcite filled fractures, cone-in-cone, slickensides, concretions, pyritised fossils	60.7 - 88.5	0 - 1.7
124	Connemara 1	Mackunda Formation	310.71-311	Sporadic and frac associated	Calcite veining and cone-in-cone, rare shells	< 70 (or 79.5 – 230.0)	
103	Connemara 1	Westbourne Formation	942.17-942.37	40m (30m net)	Calcite cement	< 70	11.2 – 13.7
105	Connemara 1	Westbourne Formation	946.24-946.34	40m (30m net)	Calcite cement	< 70	
165	Dullingari 036	Murta Formation	4883'3" - 4883'4"	19m (13m net) (62 ft (43 ft net))	Oil, calcite cement, 350 feet below limestone	131.8 - 191.3	7.2
167b	Dullingari 037	Murta Formation	5065'8.5" - 5065'10.5"	65m (62m net) (214 ft (202 ft net))	Calcite cement	184.8	
173	Dullingari 037	Murta Formation	5068'8" - 5069	Sporadic	Calcite cement	85.1 – 114.6	13.8 – 14.7
171	Dullingari 039	Murta Formation	5024'9" - 5025'1.5"	Sporadic	Calcite cement and veins, 70 feet above limestone	< 70 (or 130.4 – 154.6)	
78	Jackson South 2	Westbourne Formation	4279'6.5"- 4279'9"	Sporadic	Oil stained, calcite cement, veins nearby, some siderite	< 70	
189	Gidgealpa 18	Namur Sandstone	5580' – 5590'	97.5m (73m net) (320 ft (240 ft net))	Quartz overgrowths	85.4 – 113.6	
77	Jackson South 2	Westbourne Formation	4279'9"-4280'2"	Sporadic and frac associated	Oil stained, siderite nodule, calcite cement, veins nearby	84.5 – 108.1	
166	Jena 2	Murta Formation	3882'9" - 3882'11"	136m (43m net) (445 ft (140 ft net))	Oil show, calcite cement and veins	72.4 - 93.8	Metastable
108	Jundah 1	Hooray (Namur) Sandstone	905.65	50m (34m net), fault-zone	Strong calcite cement, near calcite filled faults and other fractures. Also cone-in-cone calcite. Coalified plant fossils.	< 70 (or 86.3-116.2)	Metastable
111	Jundah 1	Hooray (Namur) Sandstone	940.48-940.58	50m (34m net), fault zone	Calcite cement, near 20cm fault zone at 953.69m	< 70	

Sample #	Source	Formation	Depth (m unless marked as ft)	Carb zone thickness	Notes	Homogenisation Temp (°C)	Salinity (Wt% NaCl eq)
163	Marabooka 004	Oodnadatta	3433' - 3433'6"	15m (9m net) (50 ft (30 ft net))	Calcite cement and veins, 100 feet above and 350 feet below limestone	70 - 71.4	
201	Muteroo 1	Namur Sandstone	5290' – 5300' Calcite cement	65.5m (58m net) (215 ft (190 ft net))	Calcite cement and quartz overgrowths	87.1 -122.7	0.0 – 0.5
172	Narcoonowie 004	Murta Formation	4382'5" - 4382'7"	131m (61m net) (430 ft (200 ft net))	6 feet below & 6 feet above oil, calcite cement	86.0 - 109.6	
164	Narcoonowie 004	Murta Formation	4395' - 4395'4"	131m (61m net) (430 ft (200 ft net))	5 feet below oil, calcite cement and veins	< 70 (or 112.6)	
197	Spencer West 1	Namur Sandstone	5000' – 5010'	129.5m (97.5m net) (425 ft (320 ft net))	Quartz overgrowths	87.3 – 101.5	
152	Thargomindah 1A	Adori Sandstone	966.86-967.12	10m (5m net)	Calcite cement and veins, micro-faults	82.1 - 144.0	0.0 - 0.5
118	Thargomindah 2	Cadna-Owie Formation	956.38-956.44	25m (16m net)	Calcite cement. Fault with offset of 1.3m filled with calcite at 997m	81.1 – 104.6	
168b	Ulandi 5	Cadna-Owie	3914'10" - 3915'1"	61m (24m net) (200 ft (80 ft net))	Oil show, calcite cement	< 70 (or 151.2 – 173.2)	5.8
8	Winna-1	Murta Formation	1008.08-1008.12	42m (11m net)	Good oil shows, moderate siliceous and strong calcite cement.	108.6 (or 108.6 – 163.0)	

Change in Shape (Necking Down): Necking down is the process where irregularly-shaped inclusions change their shape to minimize surface free energy. Fluid inclusions respond to this thermodynamic drive over time by changing shape to achieve more rounded or negative crystal shapes. The likelihood of necking down occurring in diagenetic systems is high, especially for inclusions trapped at maximum temperature or during cooling of the system. If only single-phase inclusions were present in the crystal before necking down then the inclusions will still be representative of the conditions that existed before necking down. However, if multiphase inclusions were initially present in the crystal, then the formation of multiple inclusions during necking down will prevent us from determining the conditions that existed prior to necking. In many diagenetic systems, necking down is not an insurmountable problem. While one sample may contain necked inclusions another sample from the same area may have primary inclusions that have not experienced significant necking down.

Nucleation Metastability: The most common example of this type of metastability is a one-phase, liquid fluid inclusion that is expected to have a vapour bubble but it has not yet nucleated that phase. Most inclusions that should homogenise below 70°C exist as all-liquid inclusions at room temperature because metastability has prevented nucleation of a vapour bubble. It is rare for aqueous, two-phase inclusions less than 20µm diameter to have homogenisation temperatures below about 60– 70°C (e.g., Tables 23 and 24). Therefore, the presence of a majority of all-liquid fluid inclusions in a fluid inclusion population is taken to indicate trapping at temperatures below 70°C.

Table 24: Surat Basin summary fluid inclusion data (temperature and salinity). Grey-shaded samples contain calcite veins.

Sample #	Source	Formation	Depth (m unless marked as ft)	Carb zone thickness	Notes	Homogenisation Temp (°C)	Salinity (Wt% NaCl eq)
82	Alton 3A	Either Evergreen or Precipice, unspecified.	6066'3"	Sporadic	Oil show, 100 feet above minor coal	< 70	
85	Cameron 1	Springbok Sandstone	147.91-148	5m (4.5m net)	Calcite cement with siderite nodules up to 1cm, 10m below and 15m above coal.	< 70 (or 119.5-273.5)	0.7 - 4.0
84	Cameron 1	Walloon Coal Measures	230-230.22	Sporadic calcite fracture fill and cement.	Calcite cement and veins, 2m below and 5m above coal.	< 70	
10	Chinchilla 4	Hutton Sandstone	799.6	Sporadic, probably fault related	Calcite cement	112.2-135.3	1.74
75	Chinchilla 4	Adori Sandstone	1101.11-1101.34	Sporadic calcite fracture fill and cement.	Fracture fill calcite and cement.	157.4-163.9	
86	Mitchell 2	Bungil Formation	69.43-69.52	Sporadic	Calcite cement, burrows filled with pyrite, plant fragments	< 70	
88	Mitchell 2	Gubberamunda Sandstone	292.68-292.78	Sporadic	"Mottled" calcite cement in minor finely laminated intervals. Abundant garnets 3m below this.	130.0 – 299.1	0
83	Moonie 38	Evergreen Formation	1727.65-1727.79	219m (91m net)	Oil show, calcite cement	74-126.9	
80	Yapunya 1	Evergreen Formation	4970'4"-4970'10"	283m (204m) 930 ft (670 ft net)	Calcite cement, 15 feet above oil show.	ND	
81	Yapunya 1	Evergreen Formation	4993'8"-4994'4"	283m (204m) 930 ft (670 ft net)	Calcite cement, 10 feet below and 50 feet above oil show	< 70	

Thermal Re-equilibration: When rocks are buried during diagenesis they are subjected to temperatures and pressures within the bounds of the hydrostatic and lithostatic gradients. However, inclusions trapped within these rocks may follow a completely different path. This is because the fluid inclusion P-T conditions are confined to a specific isochore that can lead to internal overpressuring of an inclusion. As a result of internal overpressuring, some inclusions may re-equilibrate readily and repeatedly while others may not re-equilibrate at all. The re-equilibration of fluid inclusions appears to be strongly correlated with the size of the inclusion. Experimental studies have shown that large fluid inclusions are more likely to re-equilibrate than small ones. Over a given size range some fluid inclusions appear resistant to thermal re-equilibration while others do not. The only way to determine if thermal re-equilibration has occurred is to identify those inclusions trapped at the same time as a fluid inclusion assemblage and evaluate if they provide variable or consistent data.

This study has taken into consideration the above mentioned possible post-entrapment changes to the fluid inclusions. Therefore, although a wide range of homogenisation temperatures may be reported for some samples, we have used the petrographic context to determine the most likely trapping temperatures of these inclusions. Often this is at the lower end of the reported homogenisation temperatures or below 70°C if the majority of fluid inclusions within the cement/veins are all-liquid single phase types. It is important to note that the temperatures obtained from fluid inclusions relate to the precipitation temperature, which is not necessarily the maximum temperature of the fluid prior to precipitation of minerals. For example, a hotter (deeper sourced) fluid could have mixed with a colder (shallower) fluid before (or during) precipitation.

3.4.1.2. Discussion of fluid inclusion analyses

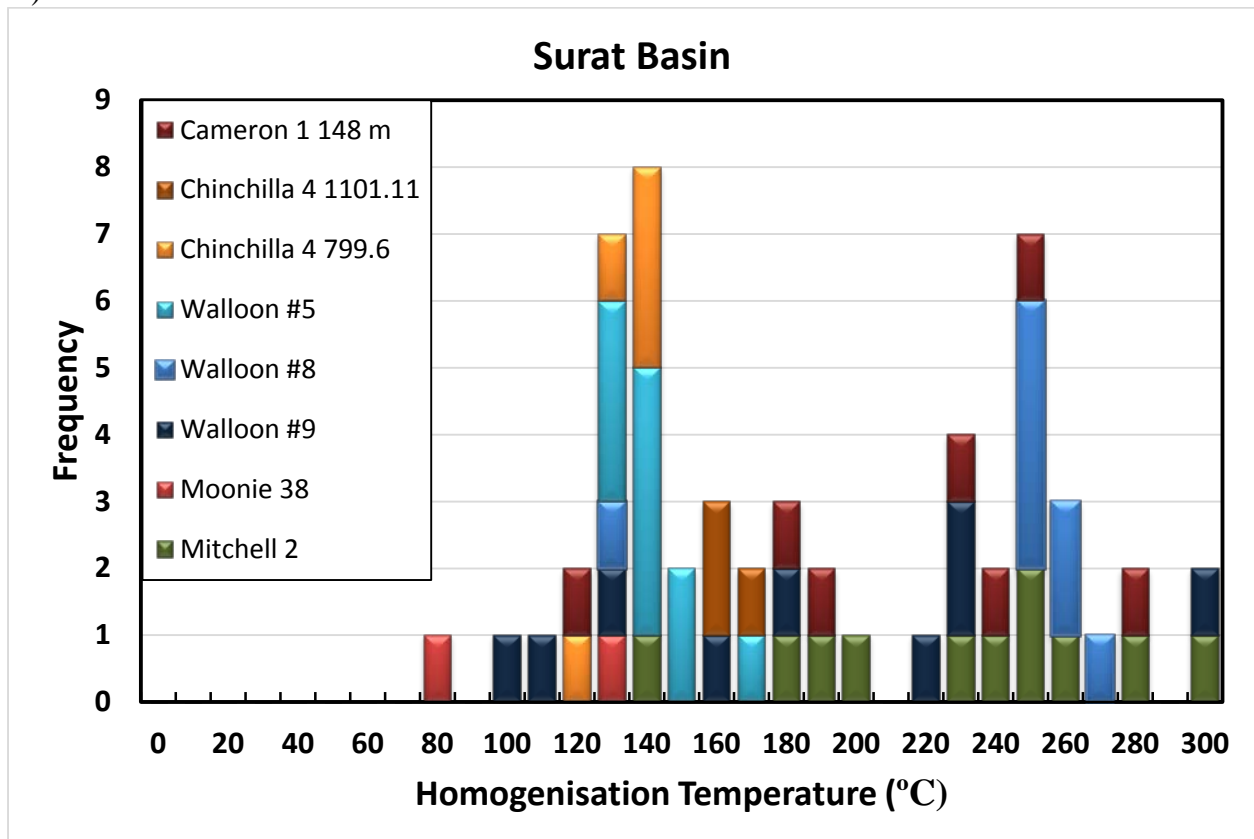
Tables 23 and 24 summarise the well samples suitable for fluid inclusion study and the resulting homogenisation or estimated trapping temperatures in °C and salinities in wt.% NaCl eq. Possible temperatures for minority two-phase inclusions in some samples are also included, in spite of the presence of all liquid inclusions indicating a likely precipitation temperature of less than 70°C. The Surat Basin data set shown in Figure 18 includes samples from near-surface coal measure deposits at a site of known significant carbonate vein mineralisation within the central Surat Basin (Kogan Creek mine). The latter analyses were funded by an internal UQ grant separate from this project, but the data are relevant to determining the range of conditions under which carbonates have precipitated in the Surat Basin.

Interestingly the two Surat data sets have very similar fluid inclusion homogenisation temperatures that are bimodal, with modes around 140 and 250 °C (Figure 18a). This may suggest that the homogenisation temperatures of the two-phase fluid inclusions in calcite cement samples that also contain all liquid inclusions (e.g., sample 85, Table 24) are primary temperatures indicative of mixing between higher and lower temperature fluid during precipitation, or pulses of fluid and carbonate precipitation have occurred at different temperatures. These elevated temperatures occur mainly in samples from wells located within the Moonie-Goondiwindi and Leichardt-Burunga fault corridor in the eastern Surat and are anomalously high relative to what is known of the regional thermal history (Raza *et al.*, 2009). Salinity could not be determined for the majority of Surat Basin samples due to metastable ice melting behaviour but ranged from 0 to 4 wt% NaCl equivalent (0 to 40,000 ppm) where it was determined (Tables 24 and 25). The Eromanga fluid inclusion homogenisation temperatures are also bimodal, with modes at 90 and 190 °C (Figure 18b); however, the higher temperature population is restricted to the Murta Formation in Dullingari 36 and 37 located on the Queensland-South Australia border. The Eromanga samples typically have much higher salinities than the Surat samples based on ice melting temperatures, which indicate salinities up to 14.7 wt% NaCl equivalent (147,000 ppm) (see Tables 23 and 25)

The fluid inclusion data provide evidence of relatively high temperatures of formation for a subset of samples in the eastern Surat and the Eromanga Basin in the vicinity of the Queensland-South Australia border. Figure 19 shows the distribution of Surat and Eromanga wells sampled relative to current thermal anomalies at 5 km depth. The red portions of the map indicate that heat is being trapped by a “blanket” of sediment. Dark blue regions by contrast indicate rapid heat flux often due to water-saturated faults that are presently acting as good conductors of heat from depth to the near-surface. The distribution of thermal anomalies has shifted over time as heat sources such as granites were emplaced, heat conduits opened or closed, and as regions were covered/denuded. In this context, work by Middleton *et al.* (2014a,b) on the Cooper-Warburton basins that underlie the Eromanga in western Queensland and northern South Australia provides evidence for three periods of fluid flow and elevated thermal regime associated with regional tectonism during the Carboniferous, Late Triassic and Cretaceous. Integrated analyses of authigenic illite from the Nappamerri Trough indicate an influx of evolved high-latitude meteoric waters under an extremely high geothermal gradient and high water/rock ratios (relatively high water flux). This hydrothermal system was interpreted to result from continent-wide transmission of tensional stress originating from episodic rifting of the eastern Australian

margin in the mid Cretaceous based on Sm–Nd, Rb–Sr and Ar–Ar dating and may well have affected the overlying Eromanga Basin strata.

A)



B)

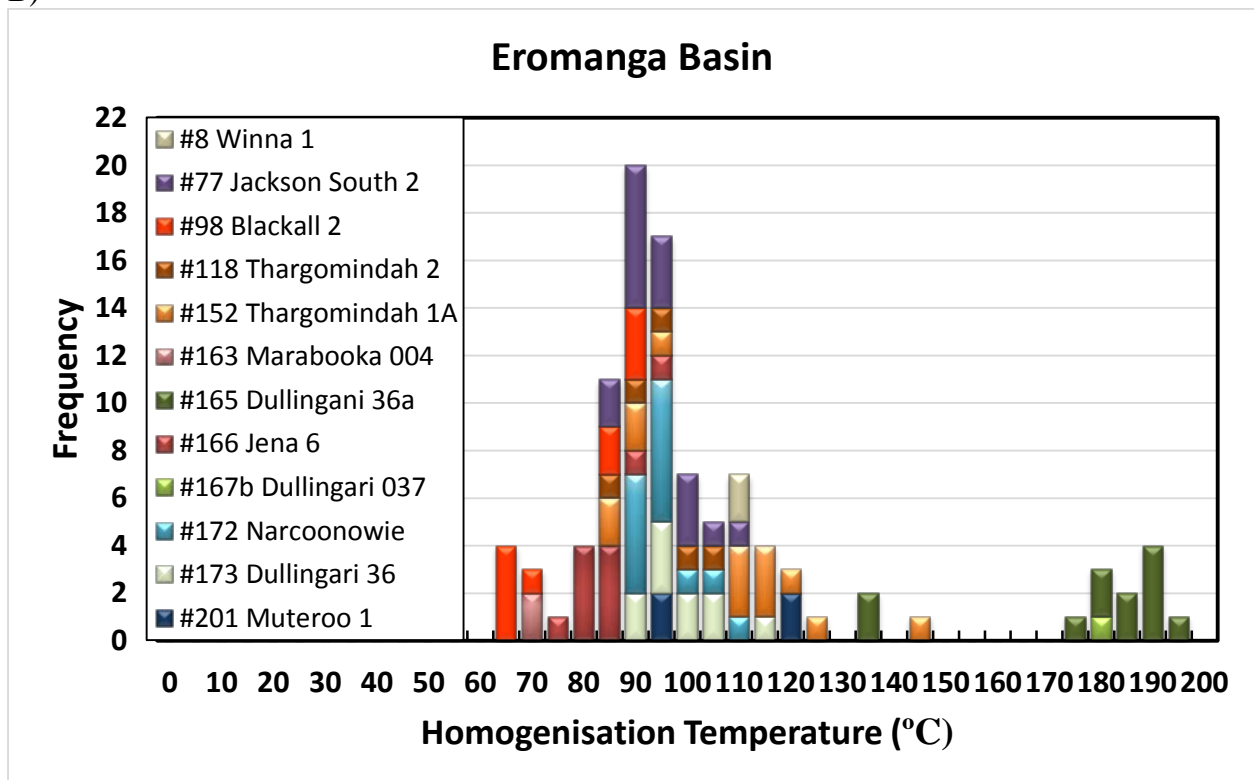


Figure 18: Fluid inclusion homogenisation temperatures for GAB carbonate cements and veins.

Table 25: Summary of carbonate fluid inclusion data for 35 drill core and chip samples of carbonate cements and veins¹.

	< 70°C		~ 70°C to < 120°C		~ 80°C – > 120°C	
	Number of samples	Salinity measurements (NaCl eq. wt %)	Number of samples	Salinity measurements (NaCl eq. wt %)	Number of samples	Salinity measurements (NaCl eq. wt %)
Eromanga	8	11.2 – 13.7	7 (+2)	0 – 1.7, 13.8 – 14.7	5 (+3)	0 – 0.5, (5.8), 7.2
Surat	4	N/A	1	N/A	3 (+1)	0, (0.7 – 4.0)

¹Values in brackets are for samples in which it is possible that the fluid inclusions may have either leaked or re-equilibrated and are therefore not necessarily indicative of the true precipitation temperatures/salinities.

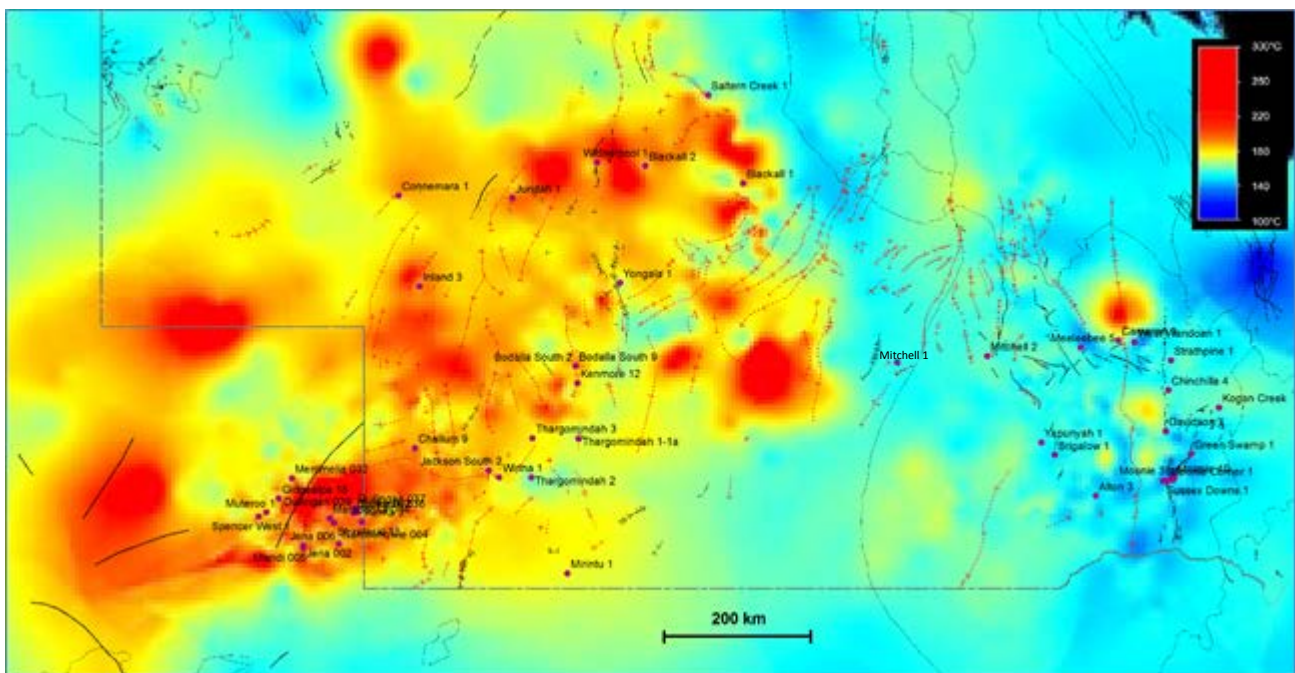


Figure 19: Locations of sample sites plotted on a map of thermal anomalies at 5 km depth; modified after Chopra and Holgate (2005).

3.4.2. Fluid inclusion gases

3.4.2.1. Samples and methods

Based on fluid inclusion characterisation presented in previous ANLEC Project 7-1011-0189 progress reports, 12 samples were selected for analysis of gases released during mechanical disintegration of the fluid inclusions. The samples generally show a wide range of fluid inclusion abundance and homogenisation temperatures (Table 26; 8, 98, 103, 113, 152, 162, 165, 166, 167b, 168b, 171, 172), and cover a wide geographical extent across the Eromanga Basin (Figure 20).

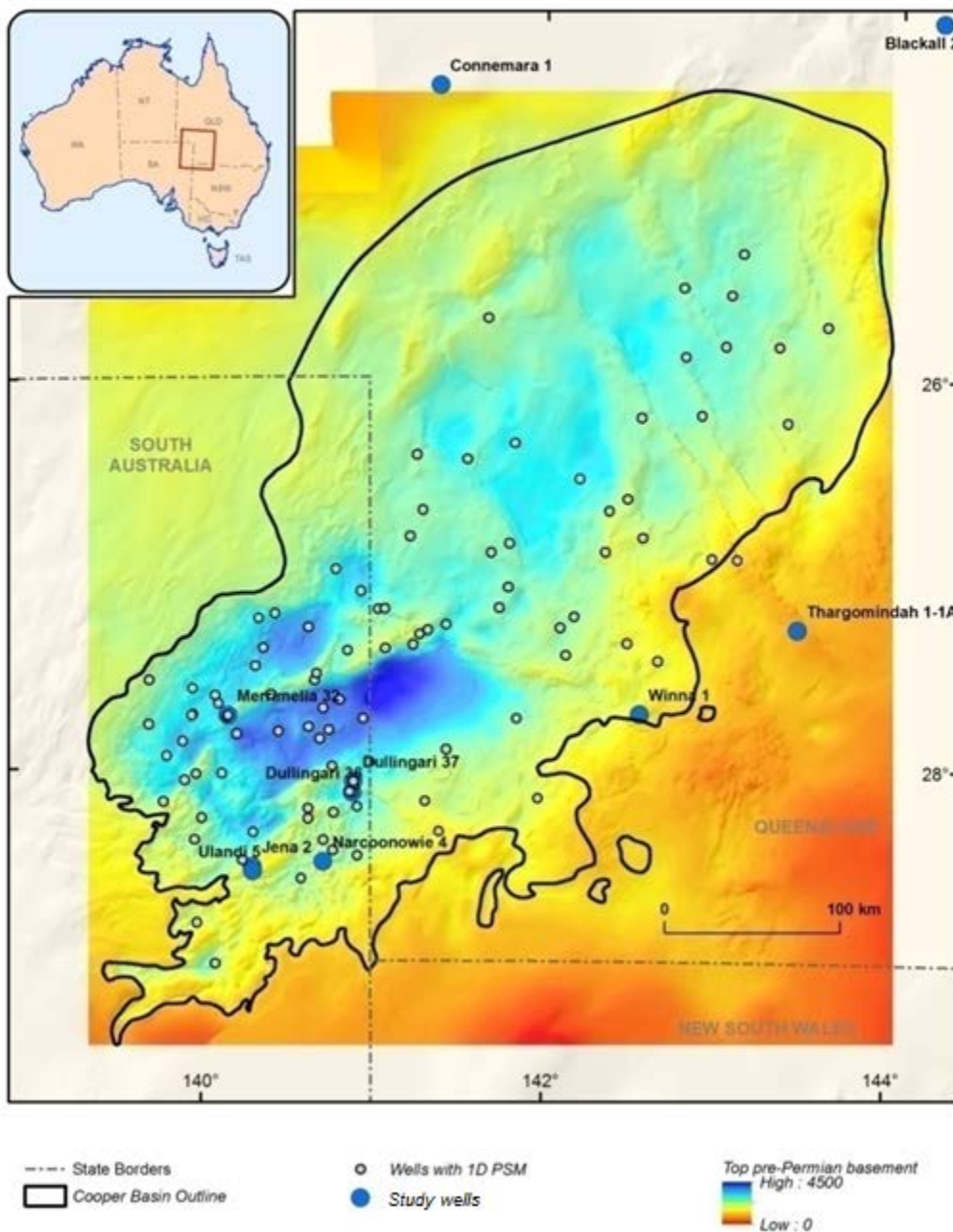


Figure 20: Location map showing the majority of the wells sampled for fluid inclusion gases in the Eromanga Basin. Note: open circles show wells used in 1D modelling; colour scale is depth in metres to base of Cooper Basin. Cooper Basin outline is from Stewart *et al.* (2013).

The samples were prepared and analysed for fluid inclusion gases according to Sohn *et al.* (2014). Pneumatic crushing of the sample is not selective towards the environment of the fluid inclusion. For example, the core from Merrimelia-32, Murta Formation had no observable fluid inclusions hosted in carbonate but still delivered abundant fluid inclusion gas on crushing, highlighting the indiscriminate nature of the analytical methodology, showing no distinctions between different FI-hosted minerals (for this sample the fluid inclusions are likely to reside within the quartz matrix).

3.4.2.2. Abundance and stable isotopes

Carbon dioxide

CO₂ was detected in all fluid inclusion gases (Table 26; note that the absolute gas concentrations were not quantified). CO₂ was dominant over the hydrocarbon gases (i.e., [CO₂]/[CO₂+C₁-C₅]>0.5), except for Merrimelia 32 (Birkhead Formation, Eromanga Basin) where [CO₂] was subordinate. Interestingly this sample contained only dolomite, whereas calcite was the dominant carbonate mineral in the other samples. The carbon isotopic composition of CO₂ is shown in Table 26 where δ¹³C-CO₂ ranges from -12.2 to -30.0‰.

Compared to these fluid inclusion gases from the Eromanga Basin, natural gases from the underlying Cooper Basin generally exhibit δ¹³C-CO₂ > -12 ‰, while the only example of a natural gas from the Eromanga Basin has δ¹³C-CO₂ = -20.5 ‰. Since CO₂ is likely to be derived from a combination of high maturity Cooper coals and deeper inorganic sources (Wycherley *et al.*, 1999) vertical migration with precipitation of carbonate should result in progressive depletion in ¹³C (becomes isotopically lighter) of the residual CO₂, as is found in the fluid inclusion gases and the strong depletion in ¹³C in the Eromanga Basin natural gas, derived from a Permian source (see below). The isotopic difference between carbonate and the fluid inclusion CO₂ (Δδ¹³C_{carb-gas}) is generally greater than 7 ‰ (Table 26). Except for Jena-2 (Murta Formation), this large isotopic fractionation is more than predicted if both current phases were in equilibrium at the time of fluid inclusion growth. Over the observed fluid inclusion homogenisation temperature range of 60.7 to 191.3 °C, the calculated Δδ¹³C_{carb-gas} would be 6.8 to 0 ‰, respectively (Ohmoto and Rye, 1979). For Jena-2 the observed Δδ¹³C_{carb-gas} of 5.43 ‰ (Table 26) is within the range of the calculated isotopic fractionation between 5.9 and 4.2‰ for fluid inclusion homogenisation temperatures of 72.4 to 93.8 °C (Table 26), suggesting the present carbonate was in equilibrium with the CO₂ at the time of fluid inclusion formation. For the majority of samples, however, CO₂ bound in fluid inclusions is not in equilibrium with the carbonate minerals, suggesting that carbonate continues to precipitate following fluid inclusion formation and further cooling.

Table 26: Carbon isotope composition of Eromanga fluid inclusion samples; * δ¹³C calcite - δ¹³C CO₂.

Sample	Well	Formation	CO ₂	Δδ ¹³ C*	C ₁	C ₂	C ₃	<i>i</i> -C ₄	<i>n</i> -C ₄	<i>i</i> -C ₅	<i>n</i> -C ₅	FI homogenisation	FI salinity
			‰	‰	‰	‰	‰	‰	‰	‰	‰	‰	°C
165	Dullingari 36	Murta	-12.57	8.65	-45.11	-26.57	-25.49	-25.97	-24.32	-25.93	-23.66	131.8 - 191.3	7.2
167b	Dullingari 37	Murta	-13.26	8.95								184.8	
171	Dullingari 39	Murta	-19.57	11.97								130.4 - 154.6	
98	GSQ Blackall 2	Toolebuc	-30.00	8.63								60.7 - 88.5	0 - 1.7
103	GSQ Connemara 1	Westbourne	-14.78	12.04								<70	11.2 - 13.7
152	GSQ Thargomindah 1A	Adori Sst	-18.39	8.97	-46.74							82.1 - 144	0 - 0.5
113	GSQ Thargomindah 1A	Adori Sst	-12.22	10.51									
166	Jena 2	Murta	-14.32	5.43								72.4 - 93.8	metastable
162	Merrimelia 32	Birkhead	-17.39		-35.11	-26.08	-25.46	-26.90	-24.96	-27.12	-24.59		
172	Narcoonowie 4	Murta	-13.57									86 - 109.6	
168b	Ulandi 5	Cadna-Owie	-13.38	7.77	-45.22							151.2 - 173.5	5.8
8	Winna 1	Murta	-13.92	9.71	-38.87	-25.51	-24.17	-23.73	-23.23	-25.99	-24.06	108.6 - 163	

Hydrocarbon gases

Gaseous hydrocarbons were detected in 5 of the 12 samples with wet gases (C₂-C₅) present in only 3 samples (Table 26; note that the absolute gas concentrations were not quantified). The carbon isotopic compositions of the C₁-C₅ FI hydrocarbon gases are shown in Table 26. For the natural gases, the similarity in the carbon isotopes of the C₁-C₅ hydrocarbons between the Eromanga and Cooper basins natural gases suggests that the source of the Eromanga gas is from the underlying Cooper Basin and the gas has migrated up into the Eromanga Basin to a stratigraphic level higher than any of the fluid inclusion samples. For the fluid inclusion hydrocarbon gases, the carbon isotopic composition of individual gas components generally increases from methane to *n*-pentane, typical of thermogenic gas (Chung *et al.*, 1988; James, 1983, 1990) (Figure 21). The fluid inclusion wet (C₂-C₅) gases fall within the range of the carbon isotopes for wet gases in natural gases from the Cooper and Eromanga basins (Figure 21). On the other hand, fluid inclusion methane is more depleted in ¹³C (lighter) than methane in natural gases in three (Dullingari-36, Thargomindah 1A, Ulandi 5) of the six fluid inclusion gases (Figure 21), suggesting an additional and variable input of biogenic methane to the former gases.

Cross plots of the carbon isotopes of ethane versus methane and ethane versus propane can be used for gas-gas correlation and gas maturity estimates (Figure 22). Using GORIsotopes software (www.geoisochem.com), the maturity (vitrinite reflectance) at the time of gas generation and expulsion from the source rock can be calculated (Table 27 lists the calculated vitrinite reflectance (R_{0gas} %)). The implications of this gas maturity data for the source of the mineralising fluids are discussed in Section 3.5.3.

The hydrogen isotopic composition of the C₁-C₂ hydrocarbon gases from fluid inclusion gas from Merrimelia-32, Birkhead Formation (the only fluid inclusion gas with adequate gas concentration) are plotted in Figure 23 ($\delta DC_1 = -234.5$ ‰; $\delta DC_2 = -174.0$ ‰). The fluid inclusion gas plots within the range of the natural gases from the Cooper and Eromanga basins, again supporting a similar Cooper Basin Permian origin for the gaseous hydrocarbons.

3.4.3. Bulk crush-leach analyses

Thirteen samples were chosen for trial bulk crush-leach analysis in view of the small size of fluid inclusions in the Surat and Eromanga carbonates that renders them unsuitable for in situ chemical analysis techniques. The basis for sample selection was a combination of fluid inclusion thermo-barometry/salinity results and visual “cleanliness” of cement/vein material. Bits of the samples which looked cleanest were coarsely broken into chips of a few millimetres diameter for washing and sonic cleaning. The cleaning consisted of: 1) flooding with tap water to remove the bulk of the loose colloidal material; 2) hand-rinsing with deionised water – agitating and decanting out of clean beakers until the water looked clear; 3) Milli-pore water soaks in clean beakers in a sonic bath, periodically changing the water as it became cloudy over the course of a few days. This was followed by a further three bouts of 15 mins in the sonic bath, changing Milli-pore water between each, after the solutions had first gone clear. The chips were then oven dried for a week, prior to crushing by hand using a clean agate mortar and pestle.

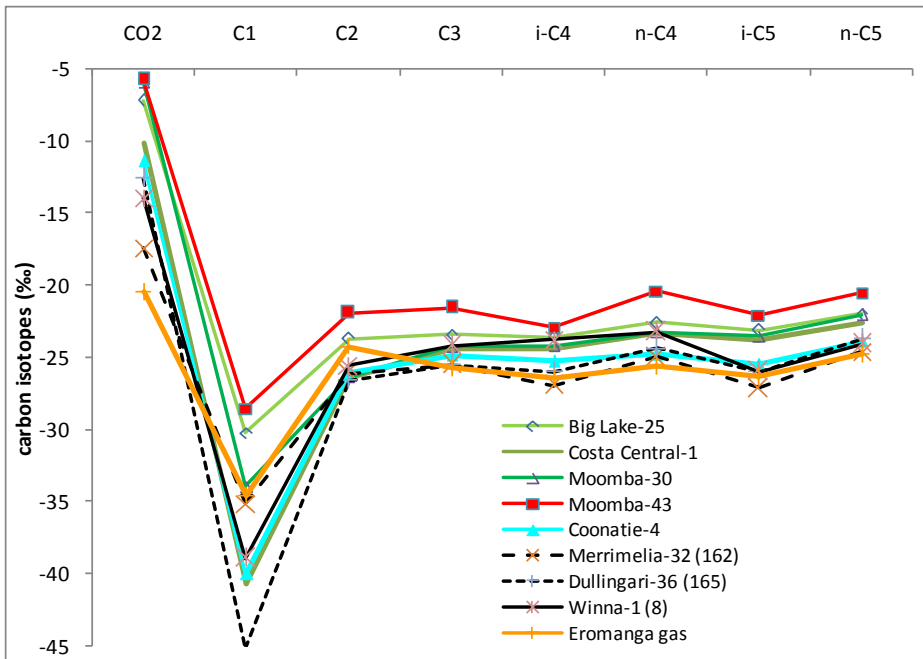


Figure 21: Carbon isotopes for CO₂ and C₁-C₅ for FI gases, together with representative natural gases from the Cooper Basin and a natural gas from the Eromanga Basin.

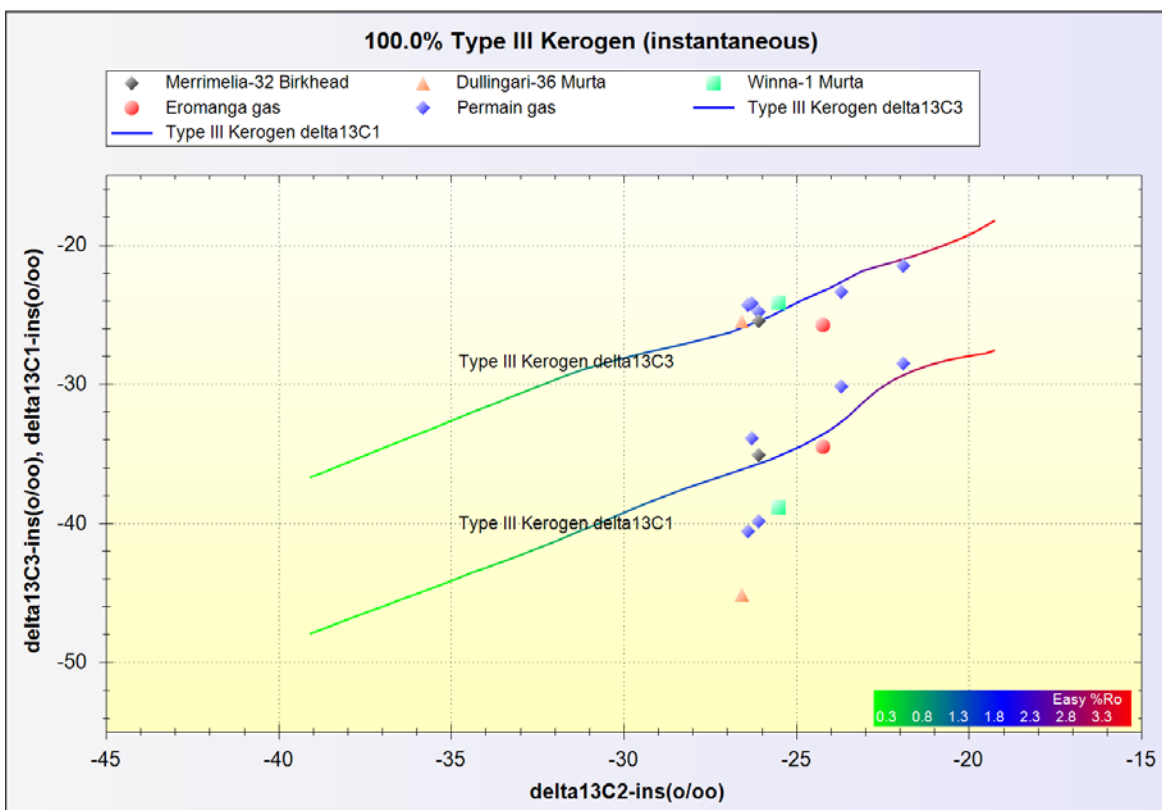


Figure 22: Plot of carbon isotopes of ethane versus methane (C₂-C₁ bottom curve) and ethane versus propane (C₂-C₃ top curve). The calculated curves are the modelled carbon isotopic composition of instantaneously generated natural gas from Type III kerogen typical of Cooper source rocks (Kuske *et al.*, 2015) at a modelled heating rate of 2°C per million years used as 'defaults' in the GORIsotopes2 version 2.4.9.0 software. Note: the samples plotting below the C₂-C₁ isotope curve most likely reflect an additional and variable input of isotopically light biogenic methane.

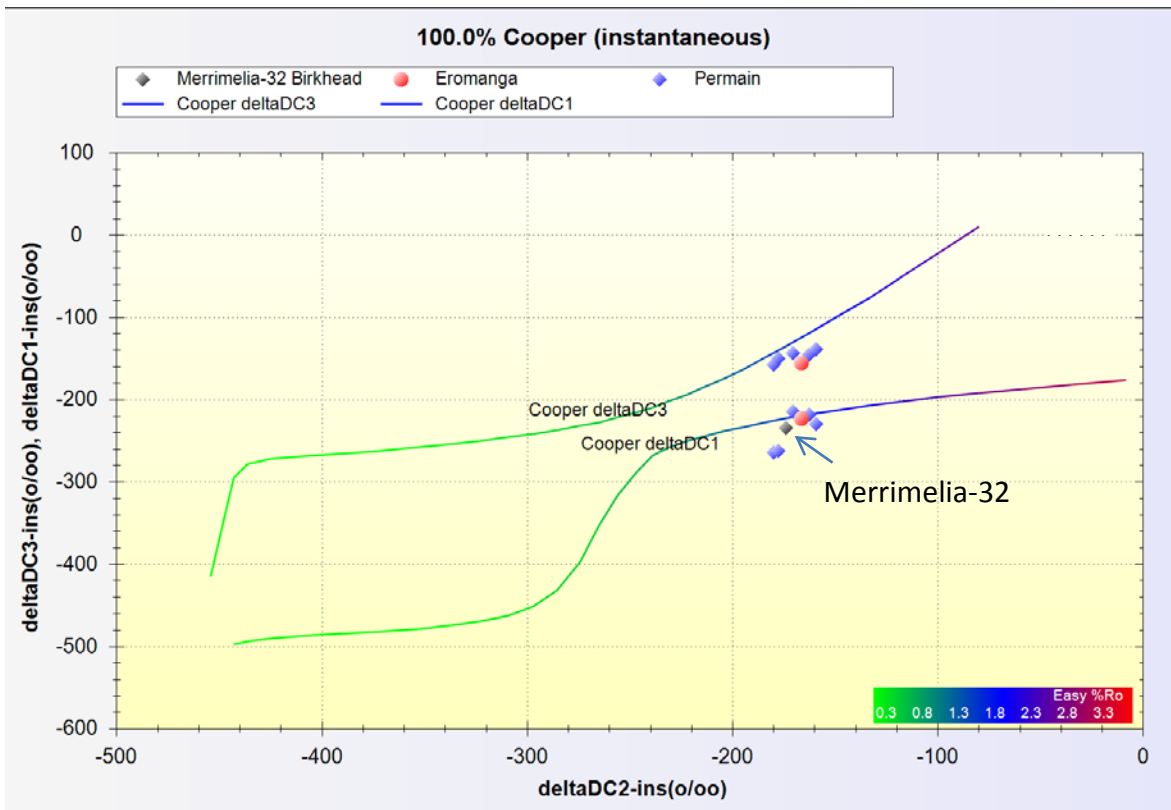


Figure 23: Plot of hydrogen isotopes of ethane versus methane (C2-C1 bottom curve) and ethane versus propane (C2-C3 top curve). The calculated curves are the modelled hydrogen isotopic composition of instantaneously generated natural gas at a modelled heating rate of 2°C per million years. GORIsotopes2 version 2.4.9.0 software defaults were used except for a user-defined hydrogen isotopic composition of precursors to methane, ethane and propane of -190 ‰, -190 ‰ and -180 ‰, respectively.

A quantity of each powder was then accurately weighed using an analytical balance (about 0.5 to 1.0 grams) and soaked in an accurately measured volume of Milli-pore water (~10 mL) within acid-cleaned containers. The sample powders were sonicated for a couple of hours followed by further soaking overnight and a final 15 mins of agitation and sonication the next morning. Samples were then centrifuged to settle the fines prior to solutions being transferred to acid-cleaned Teflon beakers via acid-cleaned pipette tips. Solutions were dried down and then re-dissolved in 2% double-distilled nitric acid for ICP-MS analysis. Results were normalised per gram of sample powder and per 10mL of water used for leaching.

Six of the trial bulk crush-leach experiments were clearly successful (Table 28). Samples S19, S84, E103, E110, E111, and E163 show linear trends of increased dissolved Na and K with greater dissolved Ca concentration when samples are grouped according to basin (Figure 24). The Na and K concentrations relative to Ca are greater for the Eromanga samples compared with the Surat, which agrees with the overall results of the thin section fluid inclusion salinity investigation. The trends of increasing Na and K with Ca also indicate that they are largely related to the carbonate cement as opposed to any clay within the sample powders. Samples S10 and E197, for which there are crush-leach concentration data, are not included in the plots as E197 had such a small sample weight following washing this is likely to have skewed the normalised results for it, and S10 only had detectable Ca and nothing else. For the five other tested samples, all elements were all below detection and so are excluded from the results table.

Table 27: Calculated maturity at base of selected formations and fluid inclusion gas maturity.

Sample	Well	Formation	Sample Top Depth m	FI homogenisation °C	Ro gas %	°C calc	Ro gas %	°C calc	Predicted temperatures (°C) from Trinity Project			
					C1inst	C1inst	C2inst	C2inst	Base Cooper 0 Ma	Base Cooper 90 Ma	Top Westbourne 0 Ma	Top Westbourne 90 Ma
165	Dullingari 36	Murta	1488.42	131.8 - 191.3	0.66	99	1.48	153	156	173	106	122
167b	Dullingari 37	Murta	1544.03	184.8					158	176	108	126
171	Dullingari 39	Murta	1531.55	130.4 - 154.6					152	169	105	124
98	GSQ Blackall 2	Toolebuc	660.38	60.7 - 88.5					N/A	N/A	n.d.	n.d.
103	GSQ Connemara 1	Westbourne	942.17	<70					N/A	N/A	n.d.	n.d.
152	GSQ Thargomindah 1A	Adori Sst	966.86	82.1 - 144	0.47	76			N/A	N/A	n.d.	n.d.
113	GSQ Thargomindah 1A	Adori Sst	970.18						N/A	N/A	n.d.	n.d.
166	Jena 2	Murta	1183.46	72.4 - 93.8					92	108	88	106
162	Merrimelia 32	Birkhead	1848.35		1.77	165	1.56	157	113	115	94	97
172	Narcoonowie 4	Murta	1335.76	86 - 109.6					109	128	94	115
168b	Ulandi 5	Cadna-Owie	1193.24	151.2 - 173.5	0.65	97			94	110	87	106
8	Winna 1	Murta	1008.08	108.6 - 163	1.30	144	1.67	161	100	131	85	118

N/A = location was beyond the lateral extent of the Cooper Basin. n.d. = not determined as the well is outside the constraints of the Trinity thermal model.

Table 28: Bulk crush-leach results (ppb) normalised per gram of powder for a 10 mL water-soak per sample.

Concentration range	Basin	Sample	Al	Ba	Ca	Cr	Cu	Fe	K	Li	Mg	Mn	Na	Ni	P	Rb	S	Sr	Ti	V	Zn	
>10ppb	Surat	10	<DF	<DF	21,959	<DF	<DF	<DF	<DF	<DF	<DF	<DF	<DF	<DF	<DF	<DF	<DF	<DF	<DF	<DF	<DF	<DF
		19	32	179	20,488	<DF	0	22	61	0	1,090	2	1,402	0.2	<DF	0.1	74	560	<DF	<DF	1	
		84	8,775	175	44,570	1	2	1,906	2,715	4	1,623	1,542	66,733	4.7	35	17	80	503	121	52	40	
	Eromanga	103	<DF	<DF	24,213	<DF	<DF	<DF	<DF	<DF	<DF	<DF	<DF	<DF	<DF	<DF	<DF	<DF	<DF	<DF	<DF	<DF
		110	6,434	77	16,524	19	5	3,699	4,297	6	1,783	40	5,283	17	<DF	10	96	343	118	19	35	
		111	7,551	126	19,982	17	5	1,452	6,403	9	1,653	46	12,593	11	<DF	12	96	502	154	18	46	
		163	10,888	21	23,385	10	17	12,719	7,269	14	2,841	200	18,810	<DF	214	17	70	389	200	45	25	
197	<i>2,318</i>	<i>448</i>	<i>163,290</i>	<DF	<DF	<i>1,197</i>	<i>2,180</i>	<DF	<i>5,976</i>	<i>56</i>	<i>20,894</i>	<DF	<DF	<DF	<i>600</i>	<i>578</i>	<DF	<DF	<DF			
Concentration range	Basin	Sample	As	Ce	Co	Ga	Gd	La	Mo	Nd	Pb	Sb	Sc	Sm	Y	Zr	Dy	Er	Eu	Pr		
<10ppb & at least one sample >1ppb	Surat	10	<DF	<DF	<DF	<DF	<DF	<DF	<DF	<DF	<DF	<DF	<DF	<DF	<DF	<DF	<DF	<DF	<DF	<DF	<DF	
		19	<DF	<DF	<DF	0.01	<DF	0.01	1	<DF	0.02	0.3	<DF	0.003	0.02	0.02	<DF	<DF	<DF	<DF		
		84	7	7	8	3	1	4	1	4	3	0.4	3	1	6	3	1	1	1	1		
	Eromanga	103	<DF	<DF	<DF	<DF	<DF	<DF	<DF	<DF	<DF	<DF	<DF	<DF	<DF	<DF	<DF	<DF	<DF	<DF	<DF	
		110	2	0.4	7	4	<DF	<DF	2	0.3	4	2	1	<DF	0.5	3	<DF	<DF	<DF	<DF		
		111	<DF	<DF	6	4	<DF	<DF	<DF	<DF	5	<DF	<DF	<DF	<DF	4	<DF	<DF	<DF	<DF		
		163	<DF	<DF	<DF	<DF	<DF	<DF	<DF	<DF	<DF	<DF	<DF	<DF	<DF	7	<DF	<DF	<DF	<DF		
197*	<DF	<DF	<DF	<DF	<DF	<DF	<DF	<DF	<DF	<DF	<DF	<DF	<DF	<DF	<DF	<DF	<DF	<DF	<DF			

*197 italicised to indicate small sample size following cleaning (5x below others), which has skewed the normalised concentration values

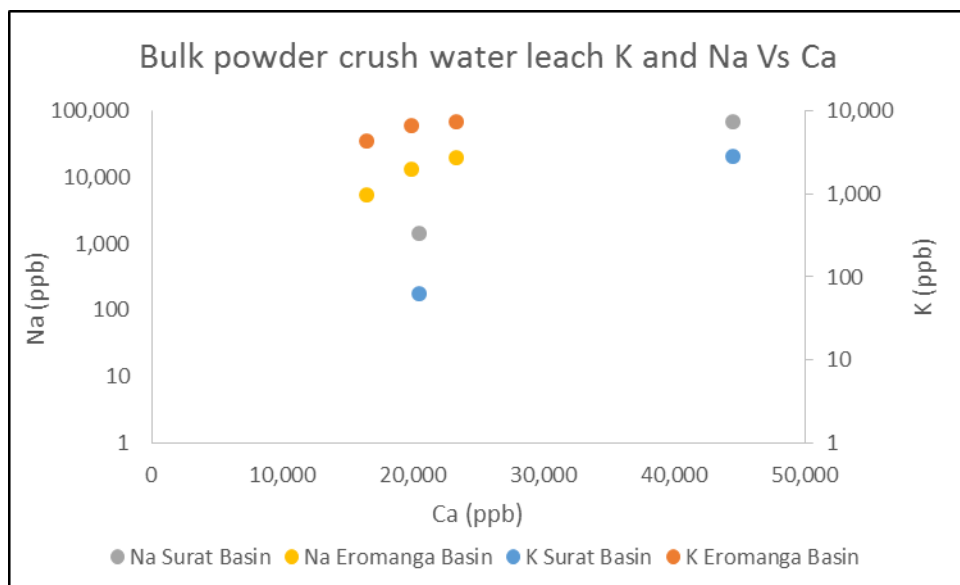


Figure 24: Successful bulk crush-leach results showing basin-dependent trends of increasing Na and K with dissolved Ca concentration.

3.5. Eromanga Basin burial history model

3.5.1. Geological model

An integrated 3D geological model for the Cooper-Eromanga-Lake Eyre basin succession was developed by Geoscience Australia as part of this ANLEC project to provide regional constraints on the geometry and stratigraphy of the basins. Formation ages, along with the timing of key tectonic events and regional erosion estimates, were included to capture the regional burial history for thermal maturity modelling. For the Eromanga and Lake Eyre basins the 3D model developed was modified from work completed for groundwater assessments (GA, 2013; Nelson *et al.*, 2012; Smerdon and Ransley, 2012; Smerdon *et al.*, 2012), whereas a new 3D model for the Cooper Basin was utilised (Hall *et al.*, 2015c). Table 29 lists the regional 3D model horizons with ages and associated reference sources.

The Pennsylvanian to Holocene structural and stratigraphic evolution of the study region has been divided into three main stages of basin formation (Draper, 2002; Gravestock and Jensen-Schmidt, 1998; McKellar, 2013; Moussavi-Harami, 1996a; Radke, 2009):

Stage I: Pennsylvanian to Triassic Cooper Basin;

Stage II: Jurassic to early Cretaceous Eromanga Basin; and

Stage III: Cenozoic Lake Eyre Basin.

Figures 25 and 26 show the revised Cooper and Eromanga basin stratigraphy, respectively.

3.5.2. Burial history and thermal maturity modelling

Petroleum systems modelling was conducted using the Trinity-Genesis-KinEx software suite (<http://www.zetaware.com>). Genesis-derived 1D burial history and maturity models were constructed for over 90 wells across the basin (Hall *et al.*, 2015a; Hall *et al.*, 2015b; Hall *et al.*, 2015d; Kuske *et al.*, 2015) and additional 1D models were developed for key wells with fluid inclusion gas data (Table 27, Figures 30 – 33). The purpose of this work was to investigate whether or not petroleum migration from depth (e.g., Cooper Basin) was associated at all with carbonate precipitation in shallower aquifers (e.g., Eromanga Basin).

The basic models were constructed using well header data from Geoscience Australia (GA, 2015) and formation tops sourced from the state survey databases (DNRM, 2015; DSD, 2015). Stratigraphic ages were assigned from a range of sources (see full listing in Table 29) according to the GTS 2012 Timescale (Gradstein *et al.*, 2012). Lithologies were assigned from variable sources depending on data availability (Table 30). Lithology mixes for the Toolachee, Epsilon, Daralingie and Patchawarra formations were determined from electrofacies maps, providing the proportion of sand, silt, shale and coal by well (Hall *et al.*, 2015c; Sun and Camac, 2004). All other formations were assigned a relative lithology percentage from published descriptions (Alexander *et al.*, 1998; Beardsmore, 2004; Gray *et al.*, 2002). The thermal conductivities were assigned to each lithology after (Beardsmore, 2004). The increase in coal content in the Cooper Basin succession, combined with the low thermal conductivities of these coals (0.2 W/mK), results in an increase in geothermal gradient from the base Eromanga Group to the top Permian in many of the wells (Beardsmore, 2004).

Table 29: Cooper–Eromanga–Lake Eyre regional 3D model horizons with associated ages. As lithostratigraphic units have been used, some horizons are time transgressive and as a result assigned ages are an approximate estimate only. In the 3D model, the Cuddapan Formation is included in the base Eromanga succession as it is not present over large parts of the study areas and only reaches a maximum thickness of ~ 50 m.

Province	Horizon Name	Description	Stratigraphic Age	Age (Ma)	Key References
Lake Eyre Basin	DEM/ Top Eyre Basin	Ground surface	Present day	0	(Whiteway, 2009)
Eromanga Basin	Top Winton	Top Winton formation at the base of the Tertiary (a-horizon)	Cenomanian	95	(DMITRE, 2001; Nelson <i>et al.</i> , 2012)
Eromanga Basin	Top Mackunda	Top Mackunda Fm	Albian	101	(Gray <i>et al.</i> , 2002; Radke <i>et al.</i> , 2012)
Eromanga Basin	Top Allaru	Top Allaru Mst	Albian	102	(Alexander <i>et al.</i> , 2006; Gray <i>et al.</i> , 2002; Nelson <i>et al.</i> , 2012; Radke <i>et al.</i> , 2012)
Eromanga Basin	Top Toolebuc	Top Toolebuc Fm or Oodnadatta Fm	Albian	104	(Gray <i>et al.</i> , 2002; Radke <i>et al.</i> , 2012)
Eromanga Basin	Top Cadna-owie	Top Cadna-owie Fm (c-horizon)	base Albian/ top Barremian	126	(DMITRE, 2009; Gray <i>et al.</i> , 2002; Nelson <i>et al.</i> , 2012; NGMA, 2001; Radke <i>et al.</i> , 2012)
Eromanga Basin	Top Murta	Top Murta Fm, Hooray Sst or AlgebuckinaSst	Valanginian	135	(Gray <i>et al.</i> , 2002; Radke <i>et al.</i> , 2012)
Eromanga Basin	Top Westbourne	Top Westbourne Fm	top Tithonian	145	(Gray <i>et al.</i> , 2002; Nelson <i>et al.</i> , 2012; Radke <i>et al.</i> , 2012)
Eromanga Basin	Top Adori	Top Adori Sst	Tithonian	150	(Alexander <i>et al.</i> , 2006; Gray <i>et al.</i> , 2002)
Eromanga Basin	Top Birkhead	Top Birkhead Fm	Callovian	166	(Gray <i>et al.</i> , 2002; Radke <i>et al.</i> , 2012)
Eromanga Basin	Top Hutton	Top Hutton Sst (h-horizon)	Base Bathonian	168	(DMITRE, 2001; Gray <i>et al.</i> , 2002; Radke <i>et al.</i> , 2012)
Cooper Basin	Top Nappamerri	Top Nappamerri Group (n-horizon)	Ladinian	238	(DMITRE, 2001; Hall <i>et al.</i> , 2015c; Nelson <i>et al.</i> , 2012)
Cooper Basin	Top Toolachee	Top, or near top, of Permian sediments (Toolachee F) (p-horizon)	top Chanhshingian	252	(DMITRE, 2009; Hall <i>et al.</i> , 2015c; NGMA, 2001)

Province	Horizon Name	Description	Stratigraphic Age	Age (Ma)	Key References
Cooper Basin	Top Daralingie	Top Daralingie Unconformity & correlative unconformities	Capitanian	263	(DMITRE, 2001; Hall <i>et al.</i> , 2015c)
Cooper Basin	Top Roseneath	Top Roseneath Shale	early Wordian	267	(Hall <i>et al.</i> , 2015c)
Cooper Basin	Top Epsilon	Top Epsilon Fm	Roadian	269	(Hall <i>et al.</i> , 2015c)
Cooper Basin	Top Murteree	Top Murteree Shale	Kungurian	274	(Hall <i>et al.</i> , 2015c)
Cooper Basin	Top Patchawarra	Top Patchawarra formation (v-horizon)	Kungurian	277	(DMITRE, 2001; Hall <i>et al.</i> , 2015c)
Cooper Basin	Top Glacial	Top glacial sediments including both the Tirrawarra Sandstone and Merrimelia Formation (wx-horizon)	Asselian	296	(DMITRE, 2001; Hall <i>et al.</i> , 2015c)
Pre--Permian basement	Top pre-Permian basement	Top pre-Permian units which include Proterozoic metamorphic rocks, Warburton Basin sedimentary rocks and volcanic rocks, sedimentary rocks equivalent in age to the Devonian Adavale Basin and the Big Lake Suite granodiorites (Boucher, 1997; Alexander <i>et al.</i> , 1998).	Pennsylvanian	304	(DMITRE, 2009; Hall <i>et al.</i> , 2015c; NGMA, 2001)

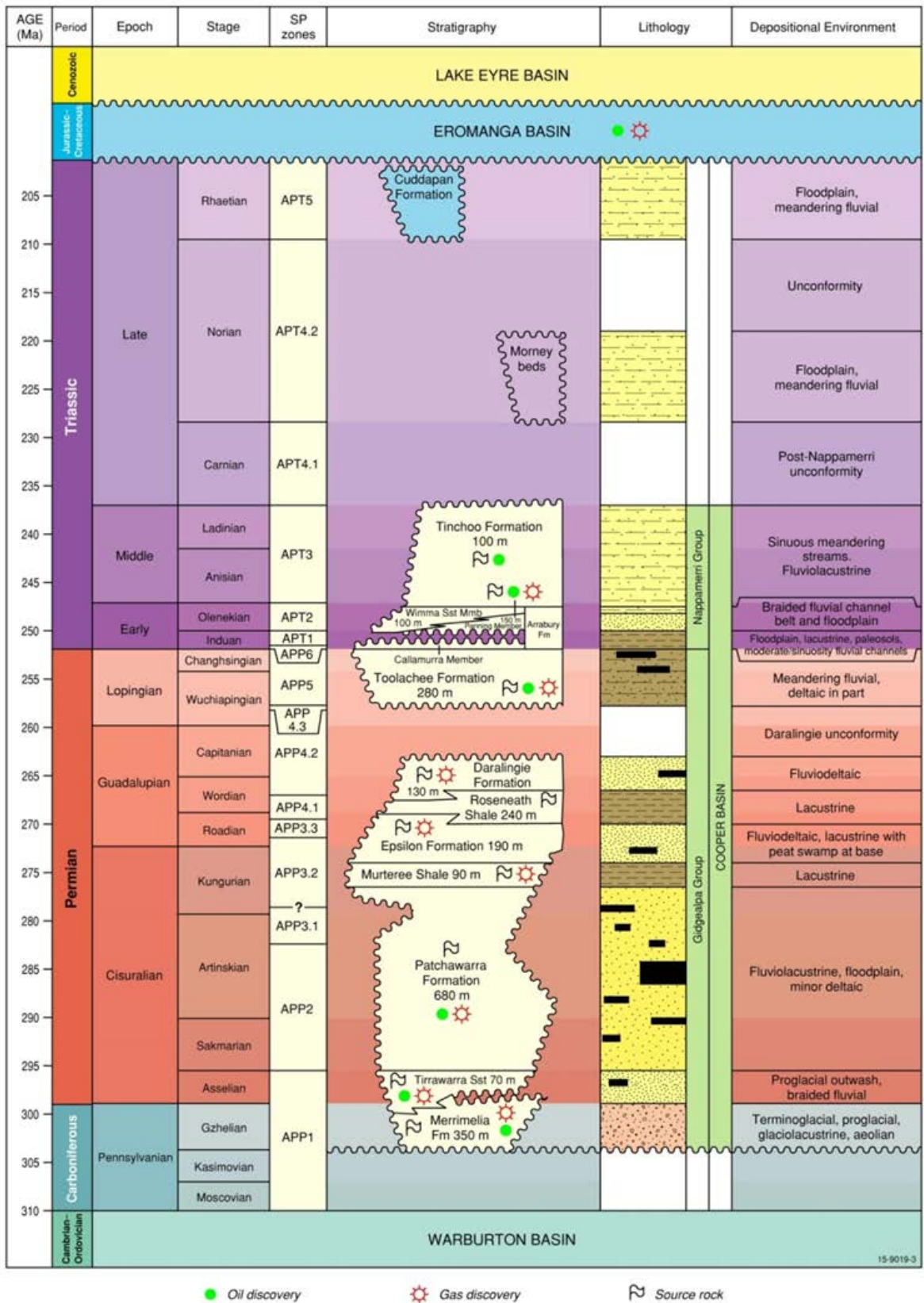


Figure 25: Stratigraphy of the Cooper Basin showing depositional facies, conventional petroleum occurrences and identified source rocks (modified after Carr *et al.*, 2016; Hall *et al.*, 2015c).

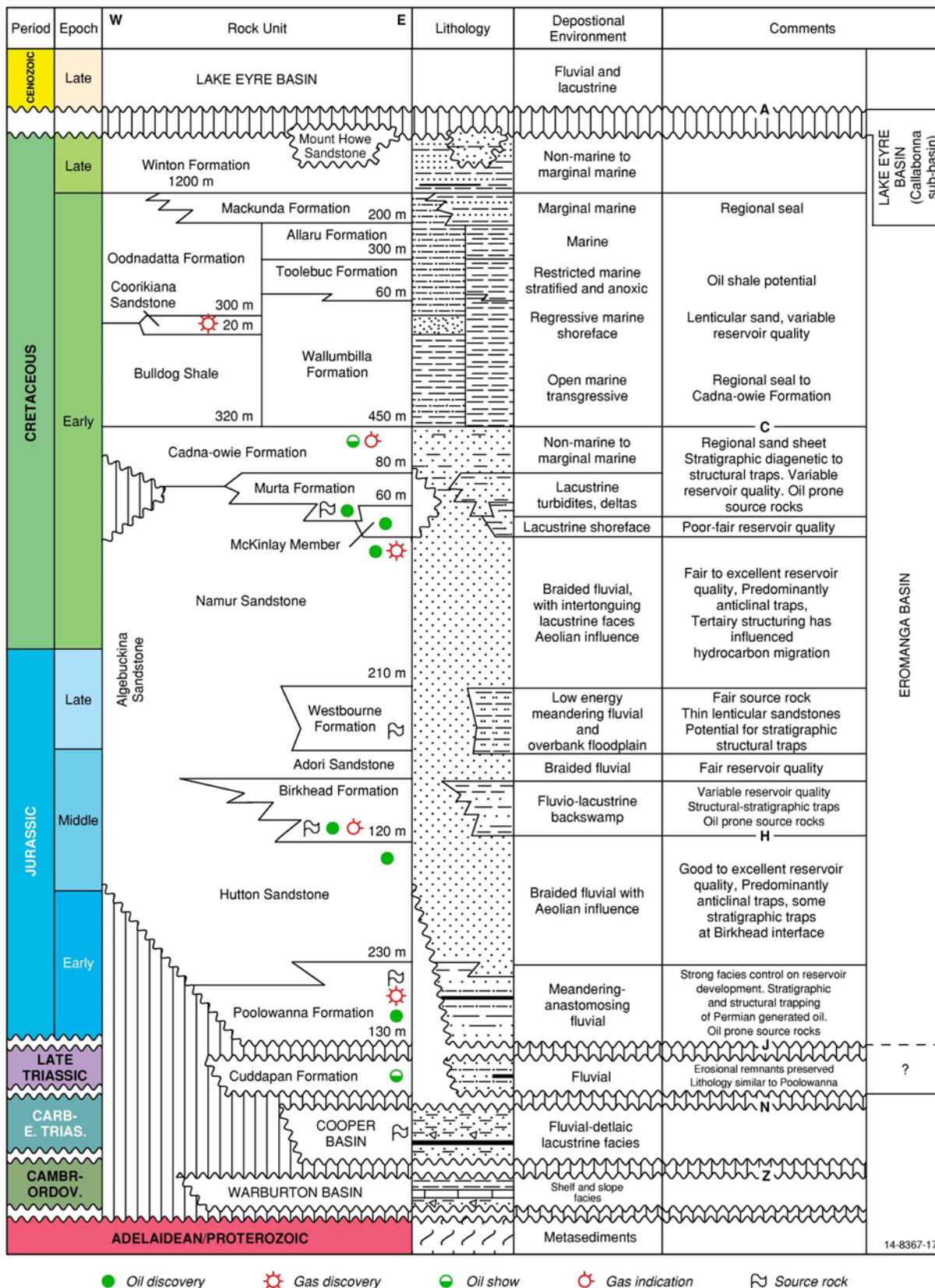


Figure 26: Eromanga Basin stratigraphy, depositional environment, thickness and petroleum occurrences (from DSD, 2015). Stratigraphy based upon Moussavi-Harami (1996b). Refer to DSD for further information on shows and indications.

Table 30: Cooper–Eromanga–Lake Eyre stratigraphy and associated lithologies. All formations are included in the 1D burial history models. However some simplifications have been made when grouping stratigraphic units in the Eromanga Basin in the 3D model that do not take into consideration the time transgressive nature of deposition. Lithology mixes also vary spatially.

Province	Top Horizon Name	Formations included in Layer Below	Lithology	Key References
Lake Eyre Basin	DEM	Lake Eyre Basin	Eyre Fm: sandstone, conglomerate. Namba Fm: fine to medium-grained sand, silt, clay, thin dolomite and limestone interbeds.	(Callen <i>et al.</i> , 1995; Radke <i>et al.</i> , 2012)
Eromanga Basin	Top Winton Fm	Winton Fm	Interbedded fine- to coarse-grained green-grey sandstone, carbonaceous shale, siltstone, coal seams.	(Cook <i>et al.</i> , 2013; Gray <i>et al.</i> , 2002; Radke <i>et al.</i> , 2012)
Eromanga Basin	Top Mackunda Fm	Mackunda Fm	Fine- to very fine-grained sandstone, siltstone, mudstone.	(Cook <i>et al.</i> , 2013; Gray <i>et al.</i> , 2002; Radke <i>et al.</i> , 2012)
Eromanga Basin	Top Allaru	Allaru Mst; Oodnadatta Fm	Allaru Fm: mudstone, interbedded calcareous siltstone, limestone, lesser fine-grained sandstone. Oodnadatta Fm: claystone, siltstone, fine-grained sandstone inter-beds.	(Cook <i>et al.</i> , 2013; Gray <i>et al.</i> , 2002; Radke <i>et al.</i> , 2012)
Eromanga Basin	Top Toolebuc	Toolebuc Fm; Wallumbilla Fm; Coorikiana Sst; Bulldog Shale	Toolebuc Fm: calcareous, carbonaceous mudstone. Wallumbilla Fm: mudstone, siltstone. Coorikiana Sst: fine-grained sandstone, minor conglomerate, siltstone, mudstone inter-beds. Bulldog Shale: mudstone, minor interbeds of siltstone and very fine-grained sandstone	(Cook <i>et al.</i> , 2013; Gray <i>et al.</i> , 2002; Radke <i>et al.</i> , 2012)
Eromanga Basin	Top Cadna-owie	Cadna-owie Fm	Siltstone, fine-grained sandstone inter-beds, minor carbonaceous claystone.	(Cook <i>et al.</i> , 2013; Gray <i>et al.</i> , 2002; Radke <i>et al.</i> , 2012)
Eromanga Basin	Top Murta	Murta Fm; upper Namur Sst; Hooray Sst; AlgeuckinaSst (upper)	Murta Fm: siltstone, shale, very fine- to fine-grained sandstone, minor medium- to coarse-grained sandstone. Namur Sst: sandstone, minor siltstone, mudstone. Algeuckina Sst: fine- to coarse-grained sandstone, conglomerate. Hooray Sst: sandstone, lesser siltstone and mudstone and minor coal	(Cook <i>et al.</i> , 2013; Gray <i>et al.</i> , 2002; Radke <i>et al.</i> , 2012)
Eromanga Basin	Top Westbourne	Westbourne Fm; AlgeuckinaSst (lower)	Westbourne Fm: interbedded dark grey shale and siltstone with minor sandstone.	(Cook <i>et al.</i> , 2013; Gray <i>et al.</i> , 2002; Radke <i>et al.</i> , 2012)
Eromanga Basin	Top Adori	Adori Sst; AlgeuckinaSst (base)	Adori Sst: Sandstone with minor siltstone and conglomerate	(Cook <i>et al.</i> , 2013; Gray <i>et al.</i> , 2002; Radke <i>et al.</i> , 2012)
Eromanga Basin	Top Birkhead	Birkhead Fm	Interbedded siltstone and fine-grained sandstone	(Cook <i>et al.</i> , 2013; Gray <i>et al.</i> , 2002; Radke <i>et al.</i> , 2012)

Province	Top Horizon Name	Formations included in Layer Below	Lithology	Key References
Eromanga Basin	Top Hutton	Hutton Sst; Poolowanna Fm	Hutton Sst: fine to coarse-grained quartzose sandstone, minor siltstone interbeds. Poolowanna Fm: carbonaceous siltstone, sandstone, rare coal seams.	(Cook <i>et al.</i> , 2013; Gray <i>et al.</i> , 2002; Radke <i>et al.</i> , 2012)
Cooper Basin	Nappamerri Gp	Tinchooo Fm; Arrabury Fm	Tinchoo Fm: interbedded siltstone and sandstones, minor coal seams, intraclast conglomerate beds. Arrabury Fm: mudstone, siltstone, thin fine to medium-grained sandstone interbeds	(Alexander <i>et al.</i> , 1998; Gray and McKellar, 2002; Sun and Camac, 2004)
Cooper Basin	Toolachee Fm	Toolachee Fm	Interbedded fine to coarse-grained quartzose sandstone, mudstone, carbonaceous shale, thin coal seams and minor conglomerates	(Alexander <i>et al.</i> , 1998; Hall <i>et al.</i> , 2015c; Sun and Camac, 2004)
Cooper Basin	Daralingie Fm	Daralingie Fm	Interbedded carbonaceous and micaceous siltstone, mudstone, coal with minor sandstone	(Alexander <i>et al.</i> , 1998; Hall <i>et al.</i> , 2015c; Sun and Camac, 2004)
Cooper Basin	Roseneath Shale	Roseneath Shale	Siltstone, mudstone, minor fine-grained sandstone	(Alexander <i>et al.</i> , 1998; Gray and McKellar, 2002; McKellar, 2013)
Cooper Basin	Epsilon Fm	Epsilon Fm	Fine to medium-grained sandstone carbonaceous siltstone and shale interbeds, occasional coals	(Alexander <i>et al.</i> , 1998; Hall <i>et al.</i> , 2015c; Sun and Camac, 2004)
Cooper Basin	Murteree Shale	Murteree Shale	Argillaceous siltstone, minor fine-grained sandstone	(Alexander <i>et al.</i> , 1998; Gray and McKellar, 2002; McKellar, 2013)
Cooper Basin	Patchawarra Fm	Patchawarra Fm	Interbedded sandstone, siltstone, shale, coal	(Alexander <i>et al.</i> , 1998; Hall <i>et al.</i> , 2015c; McKellar, 2013; Sun and Camac, 2004)
Cooper Basin	Top Glacial sediments	Tirrawarra Sandstone, Merrimelia Fm	Tirrawarra Sst: fine to coarse-grained sandstone, conglomerates, minor shale interbeds, rare thin coal seams. Merrimelia Fm: conglomerate, diamictite, sandstone, conglomeratic mudstone, siltstone, shale.	(Alexander <i>et al.</i> , 1998; Gray and McKellar, 2002)

The region has experienced multiple phases of burial, uplift and erosion since the onset of Cooper Basin sedimentation. The ages and erosion estimates associated with these key events are shown in Table 31. The Late Cretaceous uplift and erosion of the Winton Formation has the biggest impact on the burial and thermal history model of the basins and an erosion map for this event has been included in the 3D model (modified from Mavromatidis and Hillis, 2005). Maximum depth of burial of the Cooper-Eromanga succession and hence maximum paleo-temperature profiles were reached immediately prior to this event at around 90 Ma (Deighton *et al.*, 2003; Deighton and Hill, 1998; Duddy and Moore, 1999; Hoffmann, 1989; Moussavi-Harami, 1996a, b, c).

Table 31: Major unconformities with estimated age ranges and erosion amounts, included in the burial history modelling. Note the top Namba and Eyre unconformities are not included in the 3D model as the 1D modelling results show they have negligible impact on the burial and thermal histories.

Unconformity Name	Description	Erosion	Min Strat Age	Min Age (Ma)	Max Strat Age	Max Age (Ma)	Key References
Top Namba unconformity	Minor phase of contraction	< 50 m	Pliocene	2	Miocene	12	(Callen <i>et al.</i> , 1995; Moussavi-Harami, 1996c; Radke <i>et al.</i> , 2012)
Top Eyre unconformity	Minor phase of contraction	< 30 m	Eocene	24	Eocene	42	(Moussavi-Harami, 1996c; Radke <i>et al.</i> , 2012; Wopfner <i>et al.</i> , 1974)
Top Winton unconformity	Structural inversion of the region produced significant uplift and erosion of the Central Eromanga Basin.	100– 1200 m Dependant on location within the basin and depocentres	Late Cretaceous	62	Late Cretaceous	90	(Mavromatidis and Hillis, 2005; Moussavi-Harami, 1996c)
Cuddapan Fm unconformity	Hiatus in deposition; negligible erosion	< 10		199	Rhaetian	202	(Moussavi-Harami, 1996c)
Post-Nappamerri Group unconformity	Negligible effect in the troughs, but resulted in further erosion on the structural highs	<180 m (structural highs only)	Carnian	228	Ladinian	237	(Hall <i>et al.</i> , 2015c; Mavromatidis and Hillis, 2005; McKellar, 2013; Moussavi-Harami, 1996c)
Daralingie Formation unconformity		~65	Wuchiapingian	258	Capitanian	263	(Hall <i>et al.</i> , 2015c; Mavromatidis, 2006; Moussavi-Harami, 1996c)

Thermal boundary conditions were modelled as transient heat-flow from base lithosphere, which required addition of a lithospheric model. Moho thickness was estimated from the AusMoho model of Kennett *et al.* (2011) and a generic total lithospheric thickness of 120 km was assumed. Upper crustal, radiogenic heat production properties were used from published studies (e.g. Beardsmore, 2004; Meixner *et al.*, 2012). Carboniferous granodiorites of the Big Lake Suite in the Nappamerri Trough are associated with a present day elevated thermal anomaly (e.g. Beardsmore, 2004; McLaren and James Dunlap, 2006; Meixner *et al.*, 2009; Meixner *et al.*, 2012; Middleton, 1979). Measured concentrations of U, Th and K give a total volumetric heat production in the range of 7.2–10.1 μWm^{-3} , considerably higher than the basement heat production of average upper crustal rocks (Beardsmore and Cull, 2001; McLaren and James Dunlap, 2006; Meixner *et al.*, 2012; Middleton, 1979; Rudnick and Gao, 2003).

Present day surface temperatures were derived from average annual temperature measurements (BOM, 2015) and paleotemperatures were estimated from Wygrala (1989). Paleowater depth variation through time was based on Deighton *et al.* (2003).

The following model calibration steps were undertaken:

- Lithologies were calibrated using velocity, density and thermal conductivity data in key wells.
- All models were calibrated using present day corrected temperature (OZTemp database; Holgate and Gerner, 2010) and maturity indicators (Ro, Tmax; see also Hall *et al.*, 2015a).

Dullingari-36 well (fluid inclusion sample in Murta Member) will exemplify the workflow used to ultimately derive the interpretive temperature maps. Figure 27 presents the 1D burial history model for this well. However in order to access deeper undrilled stratigraphy the adjacent Dullingari-1 well was used to model the deeper Eromanga and Cooper Basin successions (Figures 28 and 29).

The Genesis-derived 1D thermal history models were integrated with the 3D geological model and source rock property data to create a Trinity-derived multi-1D petroleum systems model (Hall *et al.*, 2015a; Kuske *et al.*, 2015). Outputs relevant to this study from the multi-1D petroleum system model are the temperature maps for key stratigraphic intervals through time. Figures 30 and 31 are temperature maps of the base of Cooper Basin at present day and 90 Ma, while Figures 32 and 33 are corresponding maps for the top Westbourne Formation (most comprehensively mapped formation) in the Eromanga Basin at 0 and 90 Ma.

Although hydrocarbon generation began in the Permian within the Nappamerri Trough, peak oil and gas expulsion across most of the basin occurred during the Cretaceous.

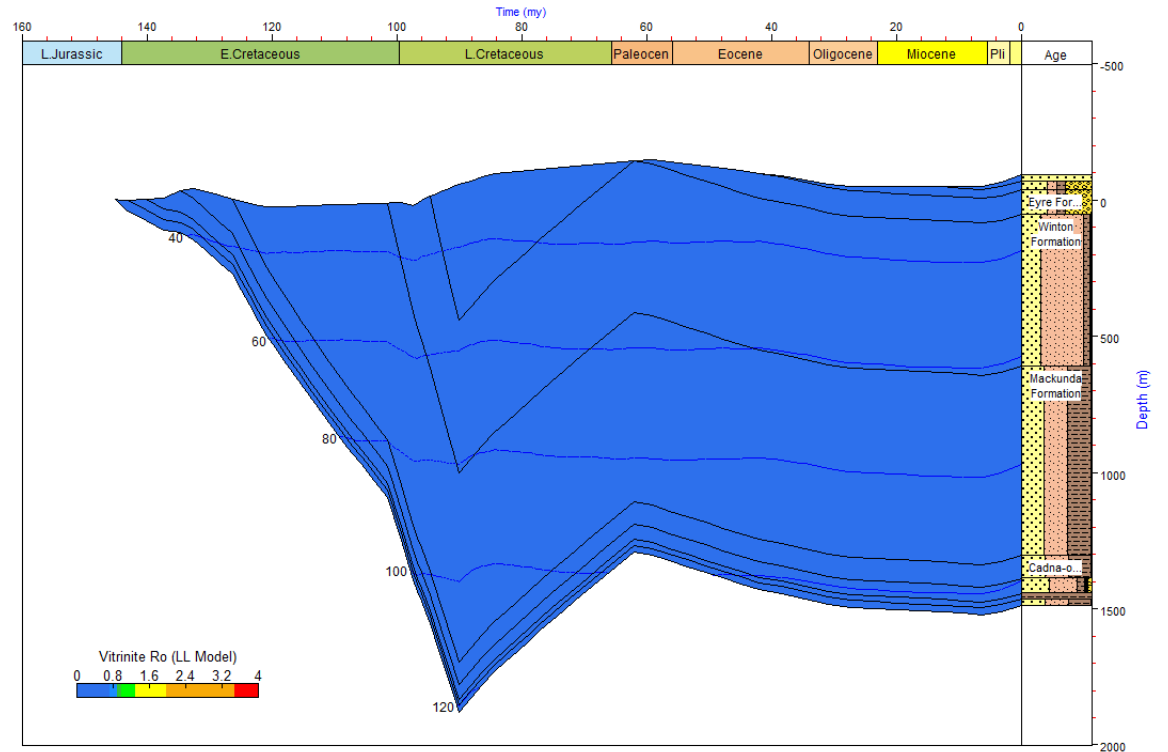
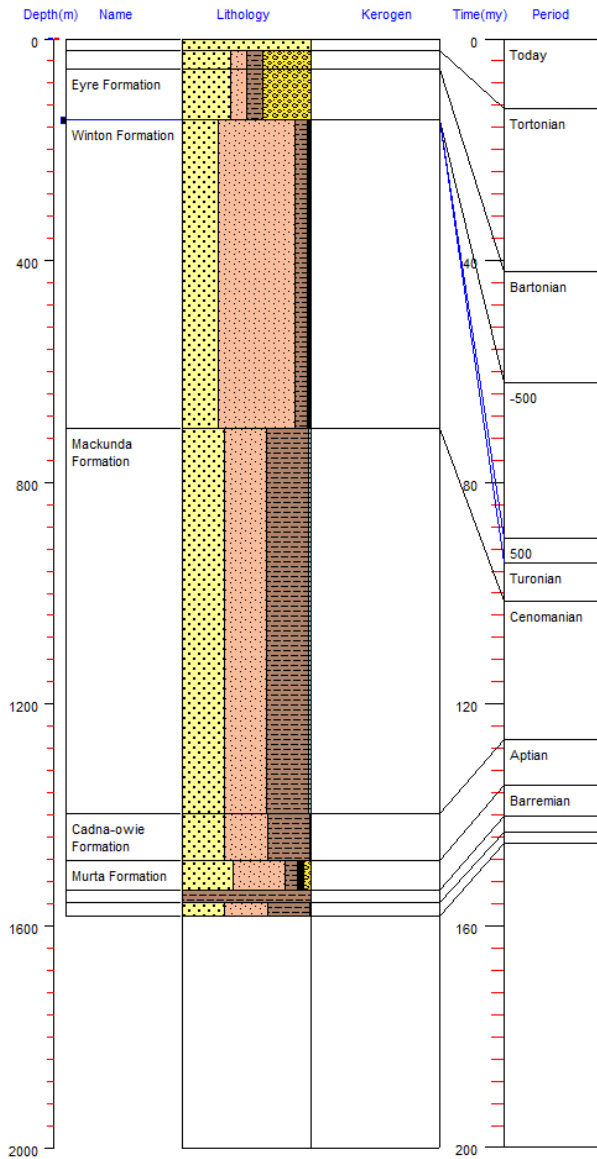


Figure 27: Stratigraphy and Genesis-derived 1D burial history model for Dullingari-36 showing low maturity for whole of well succession.

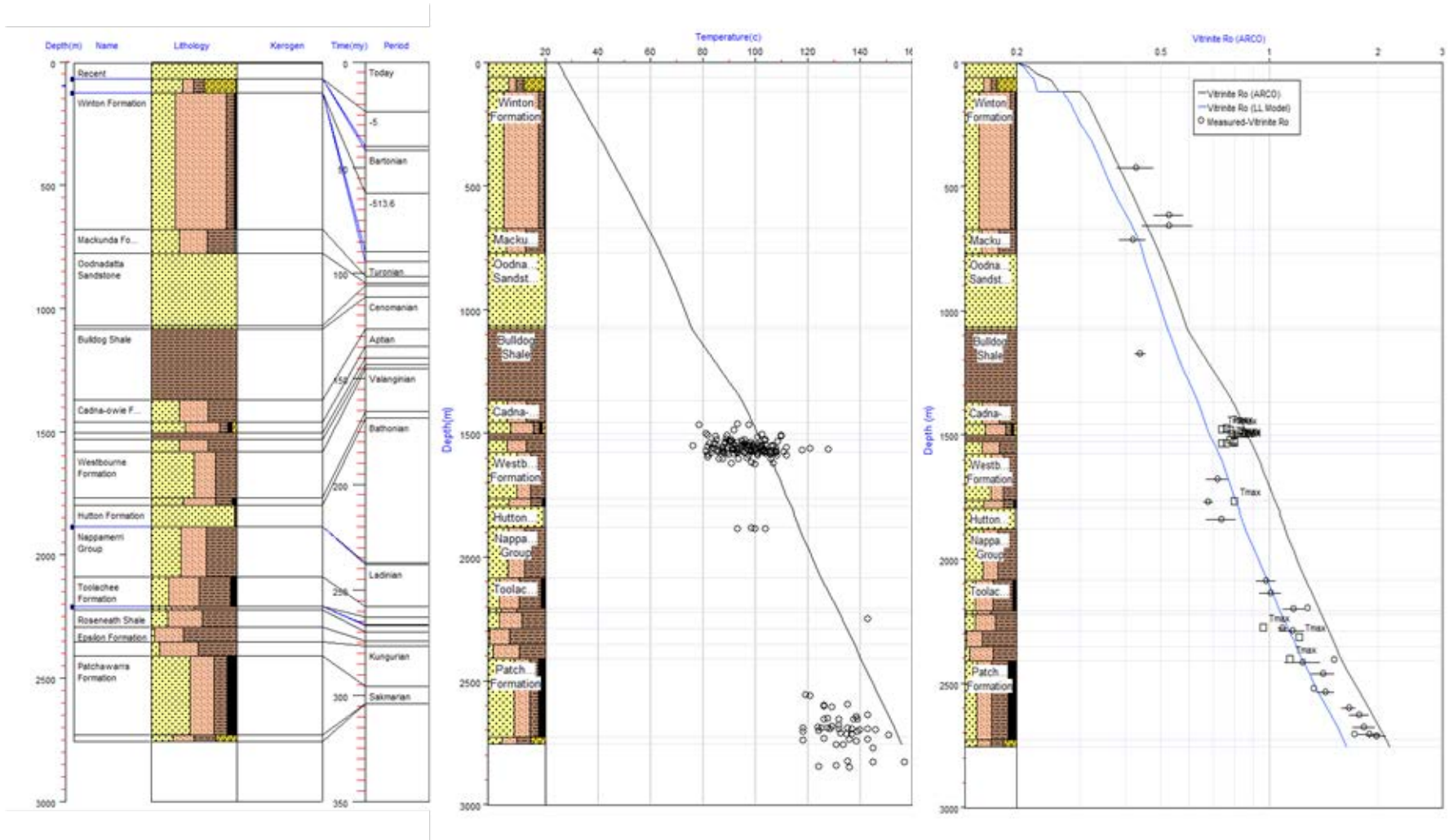


Figure 28: Eromanga and Cooper stratigraphy, temperature and vitrinite reflectance used to constrain the Genesis-derived 1D model for Dullangari-1. Note: modelled temperature is the black line (middle); modelled vitrinite reflectance (right) using the two default models; blue line is the kinetic model of LLNL and the black line is an ARCO empirical model. Note: Hall *et al.* (2015a,b,c,d) generally observed that the LLNL model gave a better fit between observed and calculated (modelled) vitrinite reflectance for $R_{o,calc} < 2-3\%$ while the ARCO model was used in wells at much higher maturities (also refer to Figure 33).

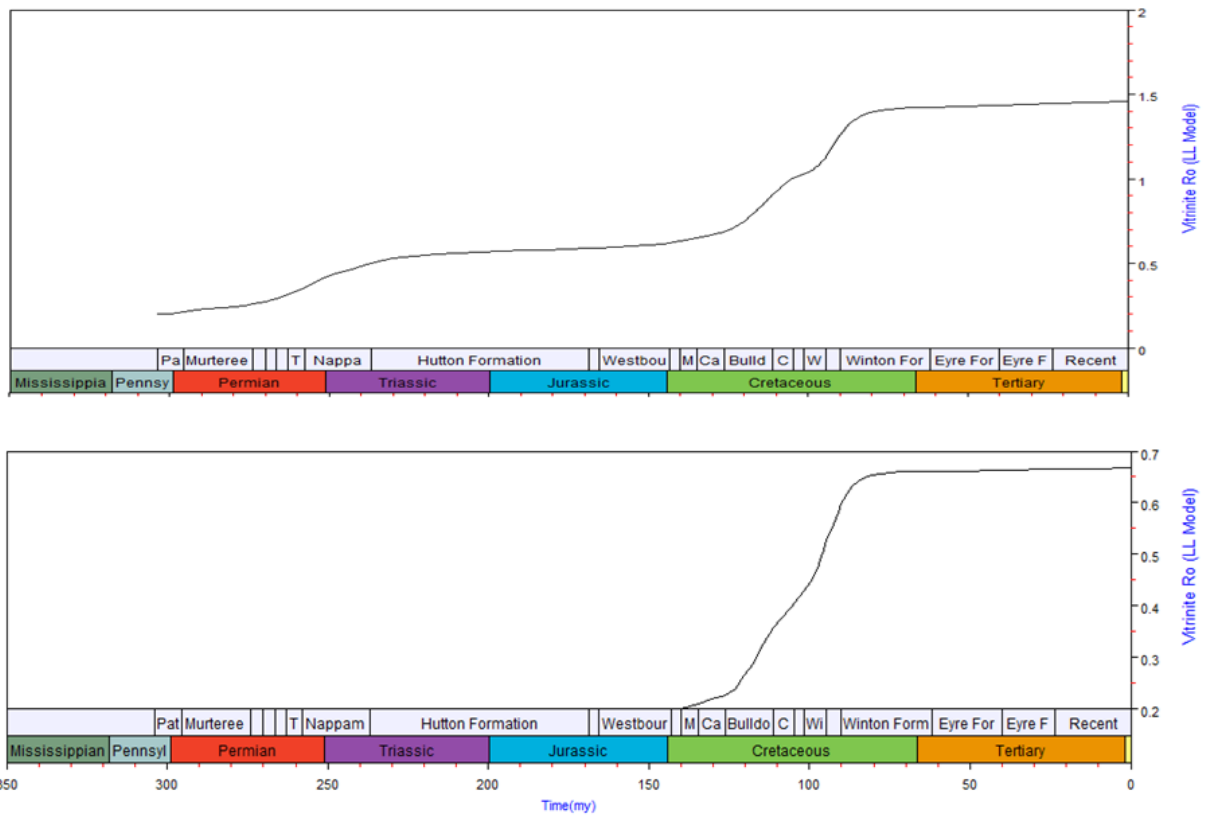


Figure 29: Modelled vitrinite reflectance through time for the base of Cooper Basin (top) and base of Murta Formation, Eromanga Basin (bottom) in Dullingari-1.

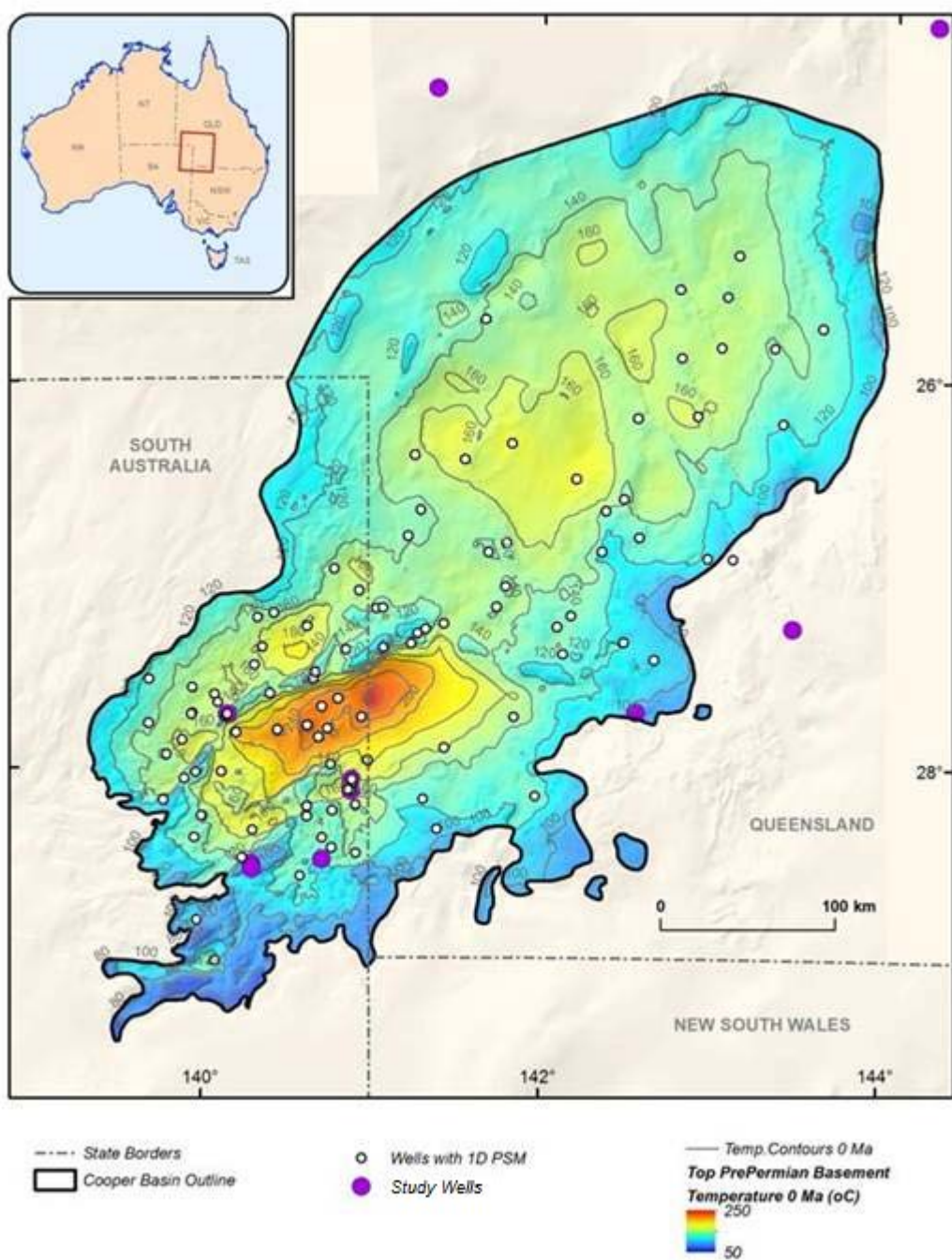


Figure 30: Temperature map at present day for base of Cooper Basin derived from the from multi-1D petroleum model.

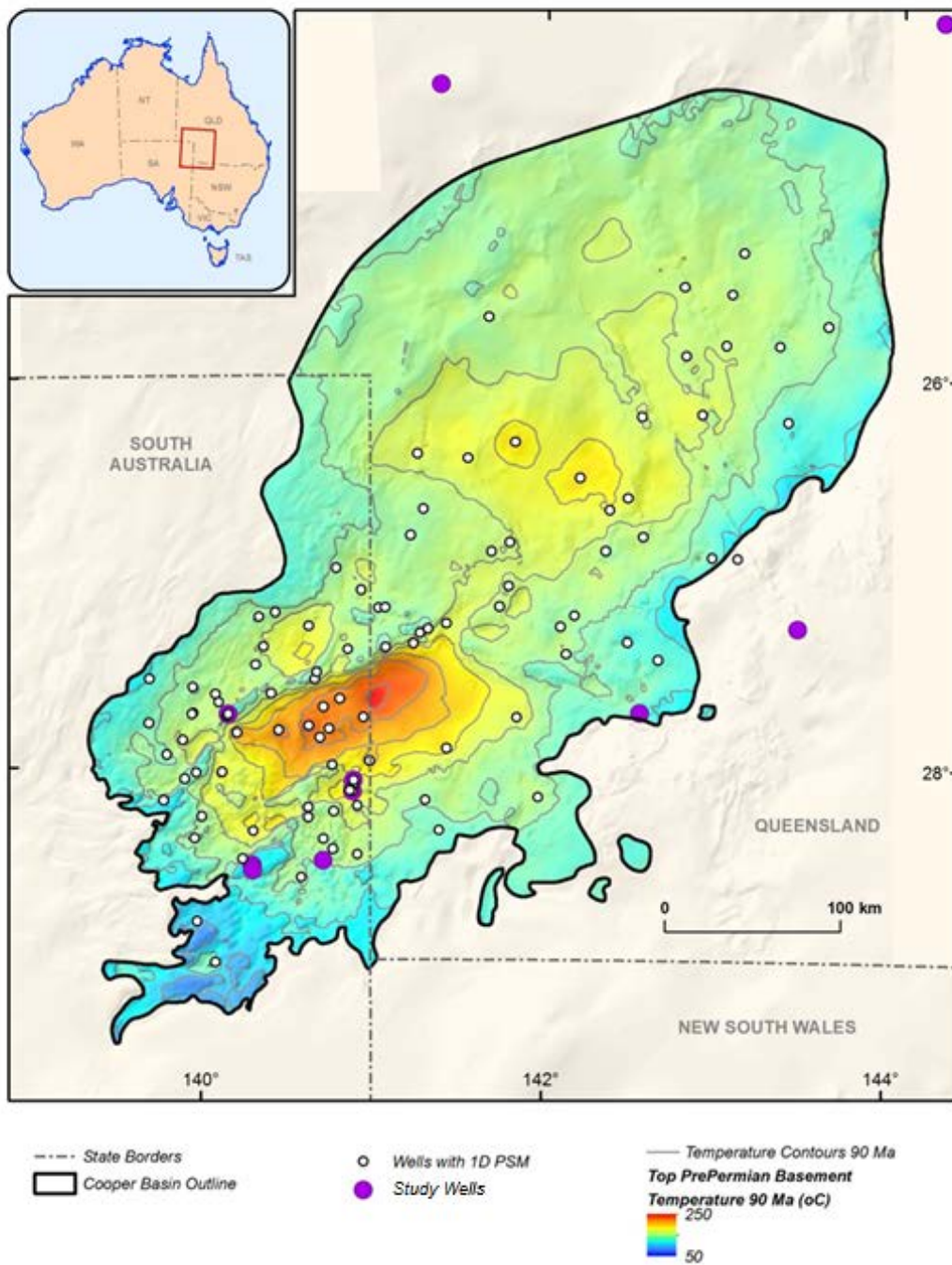


Figure 31: Temperature map at 90 Ma for base of Cooper Basin derived from the from multi-1D petroleum model.

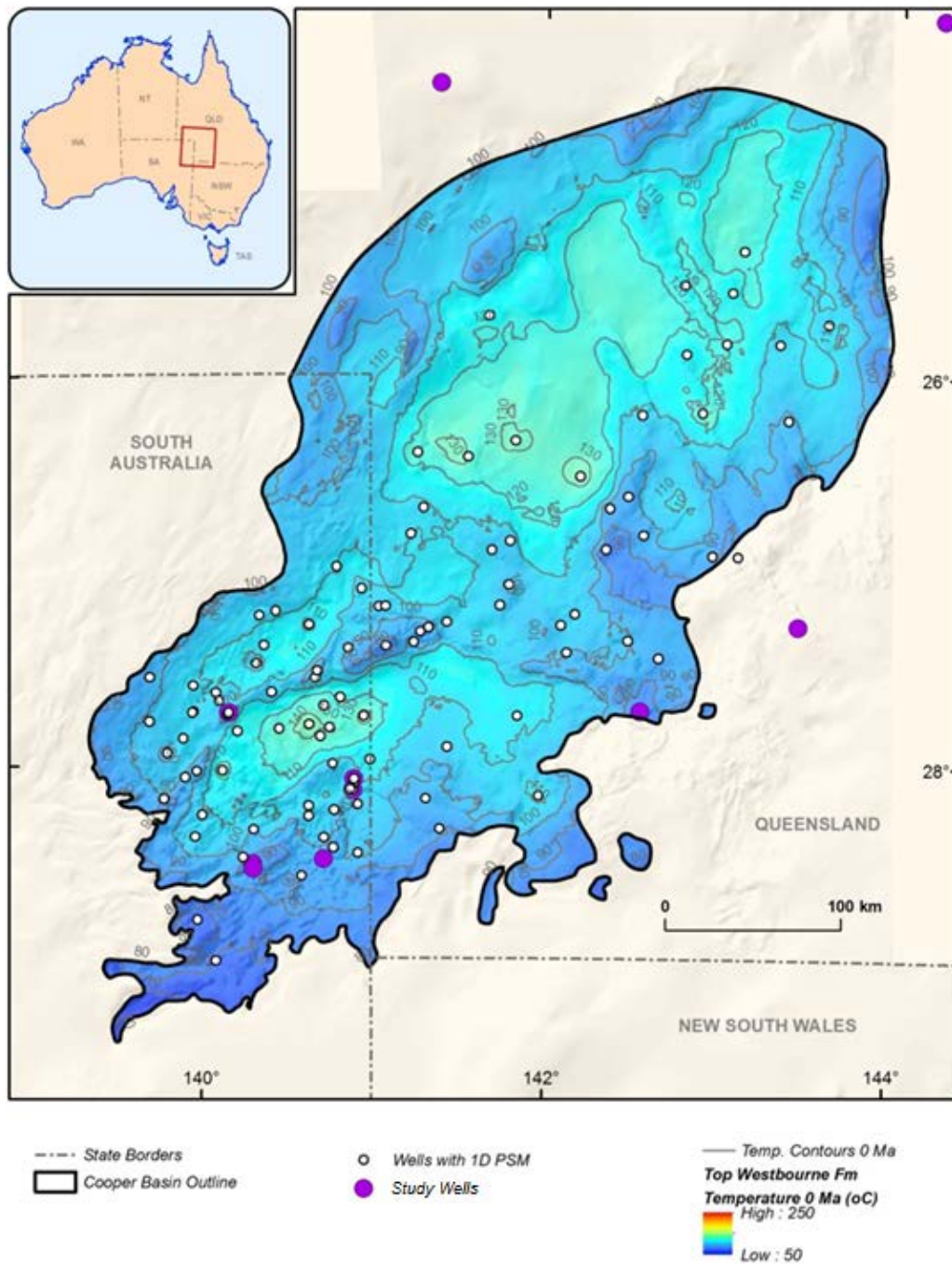


Figure 32: Temperature map at 0 Ma for Top Westbourne Formation derived from the from multi-1D petroleum model.

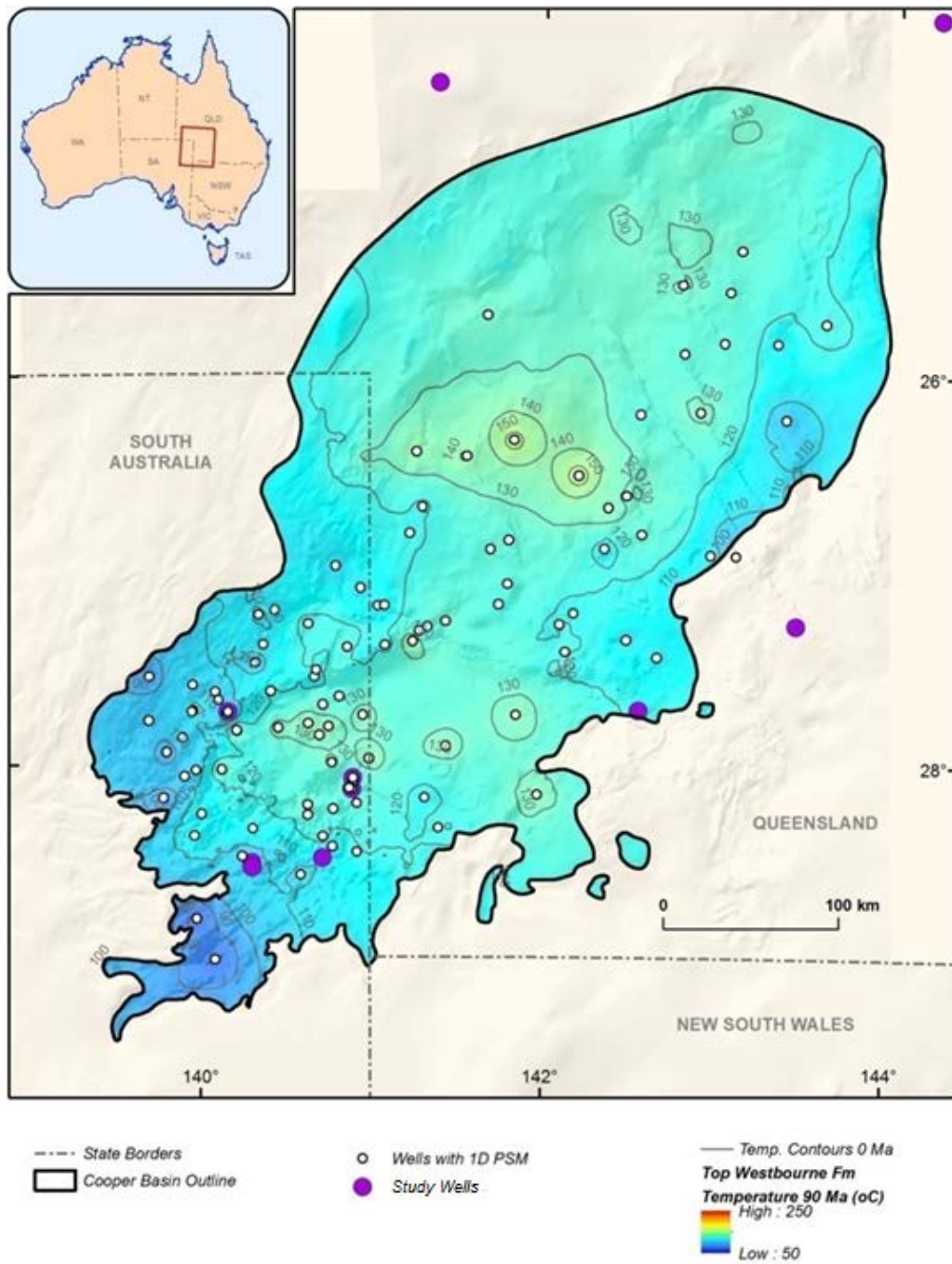


Figure 33: Temperature map at 90 Ma for Top Westbourne Formation derived from the from multi-1D petroleum model.

3.5.3. Fluid inclusion homogenisation temperatures and host rock maturity

The fluid inclusion sample from the Murta Member in Dullingari-36 has a measured homogenisation temperature range of 132 to 193 °C within the carbonate grains. The maximum modelled host rock maturity (base Murta Member) is at a vitrinite reflectance of $R_{o\text{calc}}\% = 0.67\%$ at present day (same as for Dullingari-1 in Figure 34). From the Trinity model the modelled maximum temperature reached for this sample at any time in the past is lower than the measured fluid inclusion homogenisation temperature. For the underlying Westbourne Formation the modelled maximum temperature of 122°C occurs at 90 Ma (Table 27). Hence deeper hotter fluids are involved. The deepest sedimentary section in the Dullingari field at the base of the Cooper Basin attains at maximum $R_{o\text{calc}}\%$ (present day) = 1.46 % and a modelled temperature of between 152 –158 °C at 0 Ma and 169 - 176 at 90 Ma for Dullingari field wells (Table 27). This modelled temperature lies within the middle of the temperature range for fluid inclusion homogenisation. From the hydrocarbon gases in the fluid inclusions, the modelled gas maturity is $R_{o\text{gas}} = 1.48\%$ using the $\delta^{13}\text{CC2} - \delta^{13}\text{CC3}$ relationship in Figure 22. However, a much lower maturity of $R_{o\text{gas}} = 0.66\%$ is derived from the $\delta^{13}\text{CC2} - \delta^{13}\text{CC1}$ relationship due to methane being more depleted in ^{13}C with the resulting greater isotopic difference between methane and ethane. Therefore an additional source of methane is required to mix with the thermogenic methane. An obvious candidate is isotopically light biogenic methane. However, given the likely high formation temperature of the higher hydrocarbons (>80°C; Table 27), this gas would need to have formed and been preserved when the Murta Formation was at a lower temperature. The good correspondence between the hydrocarbon gas maturity and the maturity around the base of the Cooper Basin in the Dullingari field implies a good gas-source correlation with the effective source rocks being the coals and carbonaceous shales of the Patchawarra Formation (Kuske *et al.*, 2015). For the Merrimelia 32 fluid inclusion gas the higher gas maturity compared to downhole maturities (Table 27) indicates a deeper Cooper source within the adjacent basinal trough.

Given the hydrocarbon gases and CO₂ are derived from the Cooper Basin, and that the temperatures for fluid inclusion homogenisation in the Dullingari field wells and also at Ulandi 5, Winna 1 and Narcoonowie 4 are similar or higher than maximum burial temperature (at 90 Ma) at the base of the Cooper Basin (Table 27) the involvement of hot pre-Cooper Basin fluids is likely. Mixing with Cooper Basin derived gaseous hydrocarbons (and CO₂) along the migration pathway has occurred up to the Eromanga host rock. Once in-place the fluid can further mix with biogenic methane (not present at Merrimelia 32 and Winna 1) within the host rock before being preserved in a fluid inclusion. Considering the minimum distance of ~1200 m (i.e. vertically from base of Cooper Basin to Murta Formation) in the Dullingari field, these mobile fluids would most likely have been initially at significantly higher temperatures and cool along the migration pathway through the country rocks. Using the above approach the modelled maturities for gaseous hydrocarbons in the other fluid inclusion samples are shown in Table 27. Jena 2 and those wells outside the limits of the Cooper Basin (GSQ Blackall 2, GSQ Connemara 1, GSQ Thargomindah 1A) generally have the lowest fluid inclusion homogenisation temperatures suggesting the parent fluids, if derived from basement fluids, may have a longer migration pathway resulting in cooler fluids entering the host rock. Fluid inclusion methane from the Adori Sandstone in GSQ Thargomindah 1A is the most depleted in ^{13}C , suggesting an increased input from biogenic methane.

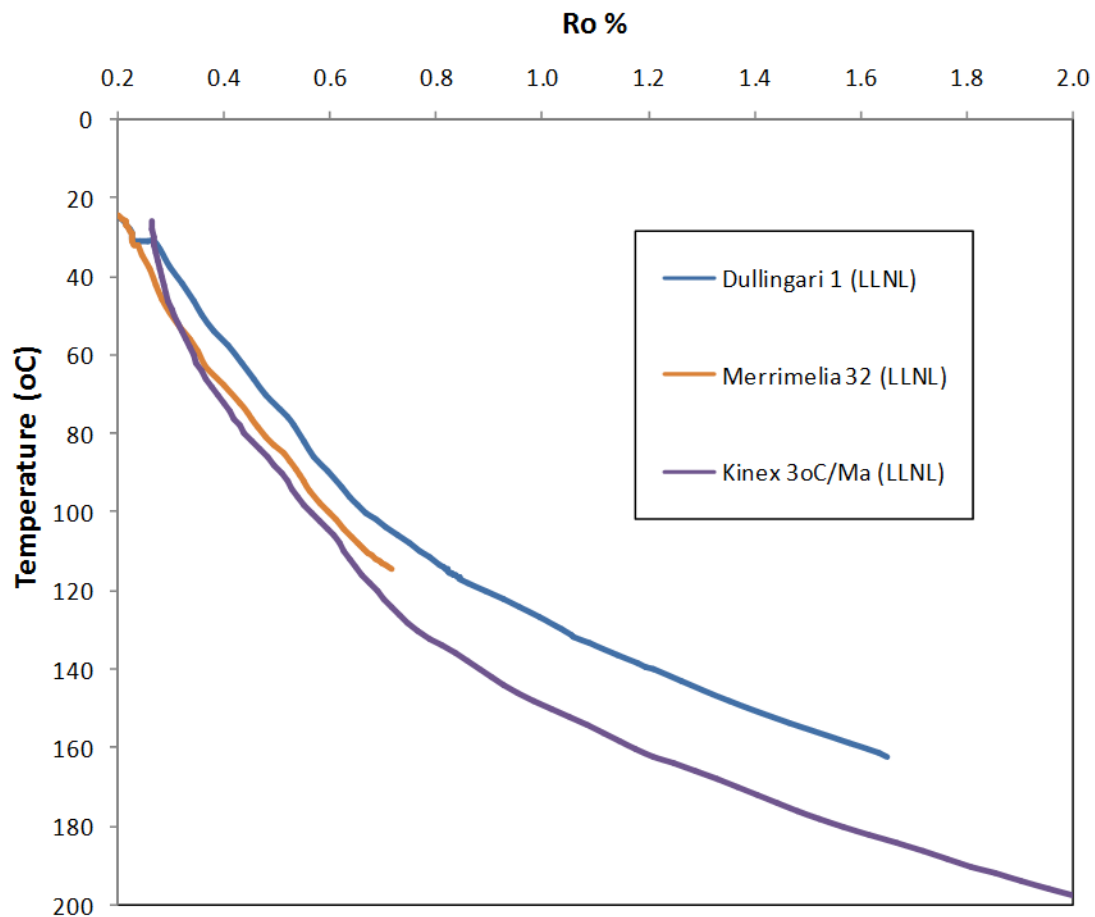


Figure 34: Modelled vitrinite reflectance versus temperature for Dullingari-1 and Merrimelia-32 using the Genesis-derived 1D burial history model and the calculated vitrinite reflectance. Note: Kinex-derived model for a simple burial history 3°C/Ma and the calculated vitrinite reflectance using the LLNL kinetic model.

3.6. Summary discussion

3.6.1. Discussion of results of natural analogues study

Calcite cement and vein-fill mineralisation was commonly found in much higher abundance than other carbonates in the samples assessed. In total, 116 samples taken were calcite cemented, whereas 43 contained siderite and only 30 had dolomite/ankerite according to the XRD analysis. In part, this may be due to sampling intervals having primarily been chosen on the basis of well log notes indicating the presence of calcite. Presence of calcite is easier to determine than presence of less acid-reactive carbonates such as dolomite and ankerite during well logging. Siderite, whilst not very reactive with cool dilute HCl, is fairly easy to recognize given its distinctive red colour on weathered core. So although well logs were also checked for mention of other carbonates and these intervals were sampled too, it is possible that loggers simply did not recognise some intervals that may have contained dolomite and/or ankerite. Even so, there may also be mineralogical reasons for the prevalence and abundance of calcite found.

Several of the unstable aluminosilicate minerals likely to alter during early diagenesis do contain calcium in addition to other ions such as iron and magnesium, hence the potential for ankerite, Ca-Mg-siderite and ferroan dolomites to form early on. Any amphiboles or pyroxenes that may have been present would be likely to have rapidly altered liberating dissolved ions (including iron) that would be available for precipitation of diagenetic minerals. In this context, halos and intergrowths of siderite and/or ankerite are commonly observed associated with degraded unstable minerals such as biotite and chlorite (Figures 3 and 35). Part of the explanation for the much higher abundance of calcite relative to ferroan carbonates could be the fact that minerals such as ankerite and siderite require a source of dissolved iron in order to form.

If any dissolved oxygen was present within the groundwater, oxides of iron are more likely to precipitate than iron-bearing carbonate minerals due to oxidation of dissolved iron (Fe^{2+}) to insoluble Fe^{3+} being a highly favourable reaction, especially under near-neutral pH conditions. Many aluminosilicate mineral sources of iron have a tendency to alter early on in the burial history of sediment, while close to the surface and hence are more likely to be exposed to dissolved oxygen. Other diagenetic alteration products such as smectites commonly contain iron and magnesium, and so formation of these minerals also lessens the potential for precipitation of carbonates with diverse cation chemistry.

A somewhat more stable mineral that is reactive with moderately acidic solutions is plagioclase. Given that plagioclase is likely to persist after other aluminosilicate minerals have reacted, alteration of this mineral is a possible source of calcium for calcite precipitation at multiple stages throughout geological time (e.g., Figure 36). Moreover, cleavage-fractured plagioclase framework grains, as is commonly the case in sandstones, have a relatively high surface area available for reaction with groundwater. Qualitatively, Ca-plagioclase appeared to be less common in significantly calcite cemented intervals in comparison to intervals containing less than 100 m net thickness of calcite cement (Table 8), but this could be statistically coincidental.

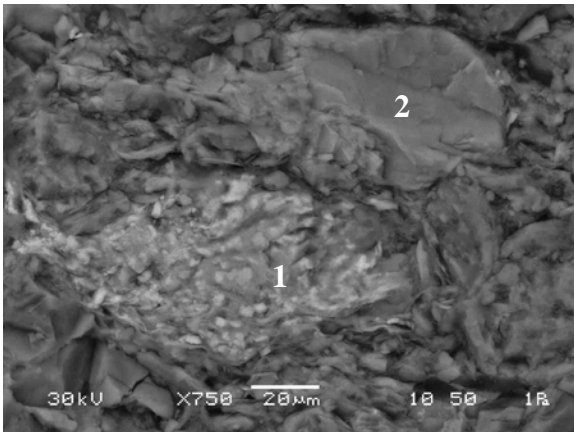


Figure 35: Chlorite and siderite alteration of probable biotite grain (1), adjacent to much less altered phlogopite grain (2) with a sample of the Evergreen Formation, 897 m, Chinchilla 4 core, Surat Basin. Modified after Dawson *et al.* (2014).

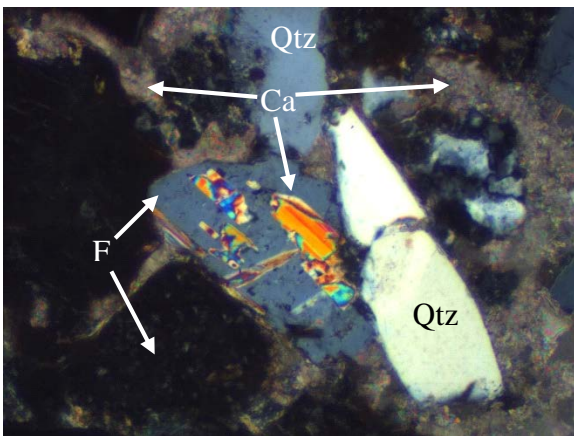


Figure 36: Upper Precipice Sandstone (1165 m), West Wandoan 1 core, Surat Basin. Plagioclase feldspar grains, bottom one almost completely altered to clay and centre grain undergoing replacement by calcite with congruent twinning (bright colours). Calcite is also present as cement between framework grains, precipitated amongst clay palettes. XPL x100 (Dawson *et al.*, 2014).

Other possible sources for post-burial calcite mineralisation are limestones and related shallow marine-estuarine biogenetic and early diagenetic calcium carbonate. Fault intersection of these units and hydrothermal fluid migration could have resulted in partial acid leaching of these units and mobilisation of the calcium to higher units where it precipitated as calcite cements and veins. The trace elements analyses of all but two vein samples indicate the involvement of hydrothermal fluids in the process of carbonate mineralisation.

Acidic pH may be buffered (acidity consumed by reactions) by the rock in the reservoir (natural alkalinity), especially where carbonates are already present. The modelled carbon isotope compositions of the majority of fluids from which the assessed carbonate cement and vein samples precipitated are either marine or mantle/magmatic, with the oxygen isotopes indicating mixing between meteoric waters and more evolved basinal fluids. The subset of samples that indicate hydrocarbon maturation-sourced CO₂ may indicate co-migration of deeper hydrocarbons and brine up into shallower intervals.

3.6.2. Model for carbonate authigenesis in the GAB

The styles of authigenic carbonate cements and veins sampled for this study fall into broad categories. Samples were taken from intervals dominated by sandstone, interbedded lithologies, or mudstone/siltstone, with or without accessory elements such as coal, oil, and thin limestone in some cases. Mineralisation was categorised as either extensive over a greater than ~ 30 m interval, restricted from 5 to 30 m or sporadic. Sometimes cementation was associated with veins and faults that were themselves mineralised with calcite. Within sandstone-dominated intervals, calcite cementation occurred across a variety of lithologies from quartzose arenites through lithic to argillaceous sandstones. Few samples picked from well completion report descriptions as containing diverse carbonate species actually did, so only a limited number of samples dominated by siderite and dolomite/ankerite were collected.

There appear to be three main lithological contexts for significant authigenic carbonate occurrences within the Great Artesian Basin; 1) obviously marine-influenced glauconitic sandstones and mudstone/siltstone proximal to limestone/dolomite and often also containing oolitic limestone and shell fragments, 2) lithic, feldspathic, micaceous and argillaceous sandstones with potentially reactive mineralogies and not obviously marine-influenced, and 3) calcite-cemented quartzose sandstones that are the least common of the three contexts but most relevant as a natural analogue of mineralisation trapping in CO₂ geosequestration.

Primary carbonate precipitates such as small pedogenic siderite nodules, shells and very thin limestone layers occurred during sedimentation in lacustrine to marine strata. Early cementation, related in part to near-surface weathering or perhaps early maturation of organic material, may have happened during initial lithification of the sediments. Continued burial diagenesis-related cementation could have been promoted by compaction-related fluid migration that may in part relate to some of the veining also observed, especially in marine-influenced strata. However, it is also likely that syndepositional tectonism was occurring, and that some faults and associated veins observed may have formed early in the history of carbonate cemented formations. Thus, even early cementation could have been induced by deeper fluids migrating into shallower units, with the process also potentially occurring up to several times from the Mesozoic to the present day in some places. Much of the evidence presented in this report suggests that fluid migration from depth played the dominant role in significant carbonate mineralisation observed.

Fluid inclusion data together with stable (C, O) and radiogenic (Sr) isotope compositions of carbonate precipitates provide information on the thermal and fluid flow history of sedimentary basins and the physicochemical conditions and timing of CO₂ trapping in sedimentary reservoirs (Middleton *et al.*, 2014a; Middleton *et al.*, 2014b; Uysal *et al.*, 2011; Uysal *et al.*, 2000; Uysal *et al.*, 2007). The fluid inclusion and stable isotope data for Eromanga and Surat basin carbonate cements and veins show these formed across a range of temperatures under very different fluid regimes. All but one of the carbonates with $\delta^{18}\text{O}$ values greater than 20 ‰ occur in marine-influenced strata of the Eromanga and Surat basins that suggest this mineralisation was related to marine pore waters and resulted at least in part from redistribution of biogenic carbonate in the host strata under relatively low temperature conditions ($\leq 80^\circ\text{C}$). The available fluid inclusion data support this conclusion.

The majority of calcite cements and veins in the Surat and Eromanga basins precipitated from Mesozoic groundwater and/or basinal brines in the temperature range of 80 to 120°C. The Surat carbonate cements with the least positive $\delta^{18}\text{O}$ values likely formed at temperatures $\geq 120^\circ\text{C}$ and occur in wells Chinchilla 4, Davidson 1, Green Swamp 1, Strathpine 1, Sussex Downs 1 and West Wandoan 1 that lie on or adjacent to the Moonie-Goondiwindi and Burunga-Leichhardt fault systems and subsidiary faults. Three other samples from Chinchilla 4 and Moonie 38 also formed at similarly elevated temperatures based on fluid inclusion homogenisation temperatures. Movement on these older faults is thought to have continued throughout deposition of the Surat Basin succession and would have provided pathways for hot fluid migration from the underlying Bowen Basin (Figure 37).

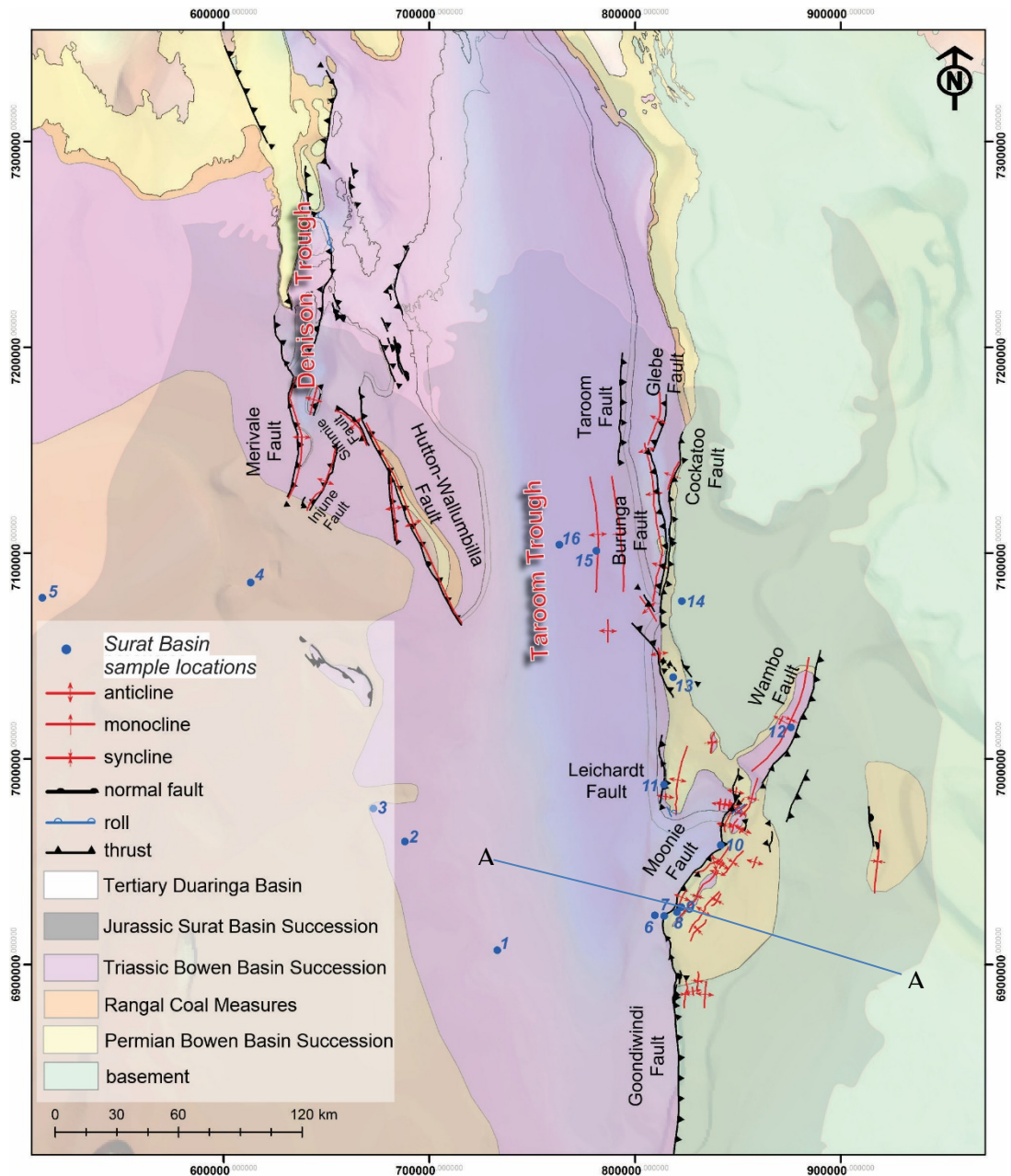
Only one Eromanga Basin carbonate has a highly ^{18}O -depleted isotopic composition; however, this sample and eight other carbonate samples from the south-western portion of the Eromanga Basin formed at temperatures $\geq 120^\circ\text{C}$ based on fluid inclusion homogenisation temperatures. Calculated oxygen isotope compositions are consistent with mixing between ground water of meteoric origin and high salinity basinal brines possibly sourced from the underlying Cooper Basin. Recent work by (Middleton *et al.*, 2014a; Middleton *et al.*, 2014b) on the Cooper-Warburton basins that underlie the Eromanga in western Queensland and northern South Australia indicate a mid-Cretaceous influx of evolved high-latitude meteoric waters under an extremely high geothermal gradient and high water/rock ratios (high fluid flux). This hydrothermal system was interpreted to result from continent-wide transmission of tensional stress originating from episodic rifting of the eastern Australian margin and may well have driven basinal brines out of the Cooper Basin.

Carbonate precipitation in veins is most likely the result of fluid-pressure cycling due to fault-valve behaviour as calcite solubility is directly proportional to $p\text{CO}_2$ and inversely proportional to temperature (Roberts *et al.*, 2004), whereas the drivers for precipitation of carbonate cements in the adjacent strata are more complex. The majority of formation waters and more evolved shallow groundwaters are near saturation with respect to calcite but may have very different physicochemical characteristics. The mixing of such carbonate waters may lead to supersaturated or undersaturated conditions for particular carbonate phases depending on the nature of the original fluids and whether the system is open or closed with respect to CO_2 gas (cf. Wigley and Plummer, 1976). Mixing of fluids saturated with calcium carbonate but with different temperatures may result in a solution that is undersaturated or oversaturated with respect to calcite depending on the chemistry of the end members (Corbella *et al.*, 2003; Wigley and Plummer, 1976). The temperature effect is relatively minor except where there is a significant temperature difference between the fluids such as occurs when a hot geothermal or deep basinal fluid mixes with shallow ground water. Mixing of two fluids saturated with calcite but with different Ca concentrations under closed system conditions typically produces a fluid that is supersaturated with calcite; the extent of supersaturation increases with difference in the cation chemistry and alkalinity, and is greatest when equal proportions of the two fluids mix (Corbella *et al.*, 2003; Wigley and Plummer, 1976).

Our findings support the original hypothesis of this research that significant carbonate cementation in shallow clastic aquifer systems may form where fluids migrating vertically from deeper levels or leaky hydrocarbon traps mix with local formation water. However, the carbon isotope evidence for mixed carbon sources in the majority of cases may indicate that calcite precipitation occurs in the more basic and dilute region of the

mixing zone where the migrating CO₂ is associated with hydrocarbons. This is supported by isotopic analysis of Eromanga fluid inclusion gases, which shows that the CO₂ is likely to be derived from a combination of Permian overmature coals and inorganic sources. Gaseous hydrocarbons found in fluid inclusions in a subset of Eromanga Basin samples are sourced from the underlying Cooper Basin. This thermogenic gas can occasionally be mixed with subordinate, local biogenic methane.

A)



- | | | | |
|---------------|--------------------|----------------------|--------------------|
| 1. Alton 3 | 5. Mitchell 1 | 9. Moonie 40 | 13. Chinchilla 4 |
| 2. Brigalow 1 | 6. Sussex Downs 1 | 10. Green Swamp 1 | 14. Strathpine 1 |
| 3. Yapunyah 1 | 7. Moonie Corner 1 | 11. Davidson 1 | 15. West Wandoan 1 |
| 4. Mitchell 2 | 8. Moonie 38 | 12. Kogon Creek Mine | 16. Cameron 1 |

B)

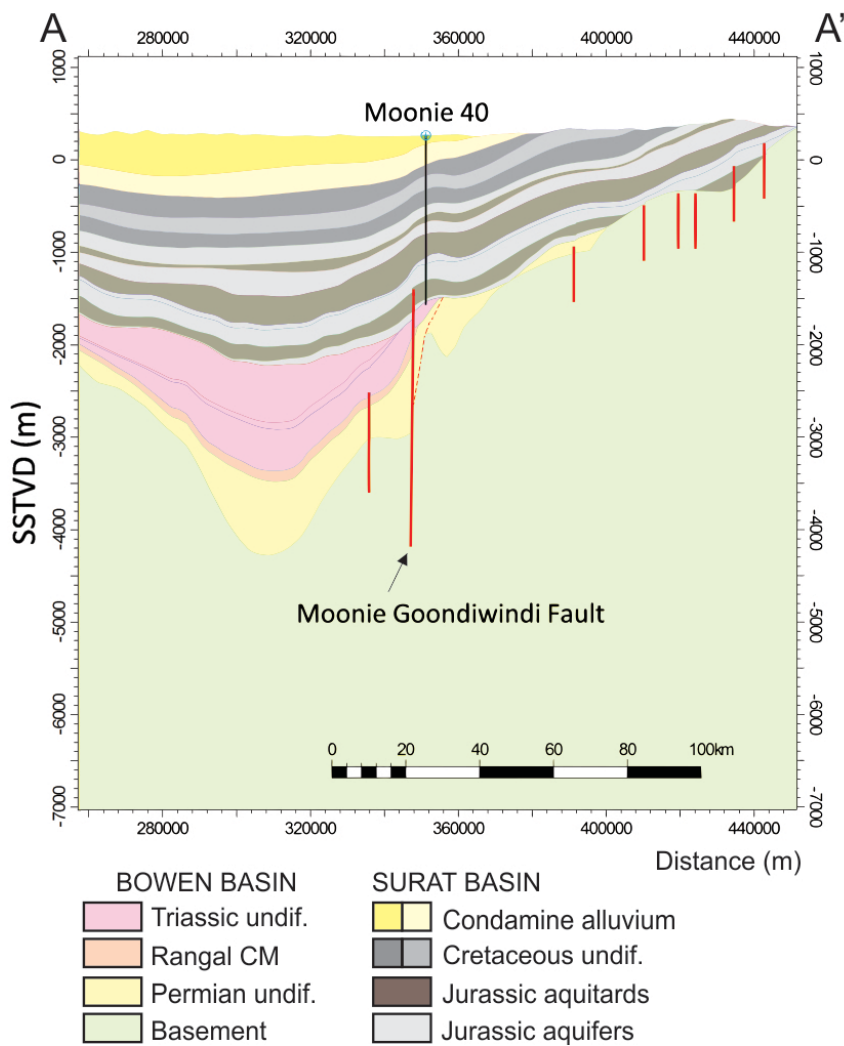


Figure 37: A) Structural elements map of the Surat Basin showing sample locations relative to major faults, subsurface solid geology of the Bowen Basin beneath the Surat Basin, and the location of conceptual cross-section A-A'. B) Conceptual cross-section A-A' of the Moonie area showing the proposed fault pathway for ascending brines. Structural elements map and basement faults (red lines) modified from Babaahmadi *et al.* (2015, 2016). Dashed red line=inferred fault. 25x vertical exaggeration. Modelled horizons are from Sliwa (2015).

Fluid inclusion homogenisation temperatures of Eromanga Basin samples are generally higher than maximum temperatures found in the rocks hosting the fluid inclusions and within the underlying sedimentary column, suggesting that the source of the fluids is deeper and hotter. This suggests that hydrothermal fluids from beneath the Cooper Basin pick-up Permian-sourced gaseous hydrocarbons and CO₂ along the migration pathway to the Eromanga Basin host formations. Fluid inclusion homogenisation temperatures within Eromanga Basin sediments are generally lower away from the Cooper Basin edge, suggesting longer fluid migration distances and more cooling. Higher temperature carbonate cements in the eastern Surat are largely restricted to the Precipice Sandstone, Evergreen Formation and Hutton Sandstone that suggests the Walloon Subgroup acted as a regional seal with hydrothermal fluids sourced from the underlying Bowen Basin focused into the more permeable sandstone-dominated units.

4. Laboratory corroboration of accelerated carbonate mineralisation

Some initial mineralisation experiments on Wandoan Project samples have been performed to evaluate the potential for engineered accelerated mineralisation trapping to maximise the use of storage porosity in the Precipice Sandstone or the Hutton Sandstone. The parameters of the experiments are based upon knowledge gained from analyses of carbonate cement and vein samples collected throughout the GAB (Dawson *et al.*, 2013; Golding *et al.*, 2014), as well as literature information (e.g., the desktop study by Golding *et al.*, 2013b) and information gained through complementary studies of fluid-rock interactions (Dawson *et al.*, 2015; Farquhar *et al.*, 2015; Pearce *et al.*, 2014; Pearce *et al.*, 2015c). Samples of Precipice Sandstone and Hutton Sandstone core, representing more and less reactive sandstone lithologies, have been reacted under simulated in-situ conditions.

Rock samples have been characterised pre- and post-reaction with SEM-EDS to identify precipitation of carbonates. Sub-plugs of selected core (containing a lithological boundary) have been characterised pre- and post-reaction additionally with QEMSCAN and micro CT to quantify identify spatial distributions of carbonate precipitation. Fluid analyses for major cations and anions that are markers of mineral precipitation were also performed.

A major obstacle to mineral trapping of CO₂ is the requirement for there to be a source of cations available to react with dissolved CO₂. The Precipice Sandstone is predominantly a quartzose high porosity aquifer; however, it does contain variable amounts of potentially reactive minerals such as carbonates, feldspars, clays and micas, especially towards the top of the formation. In some locations, there are also minor silty-muddy baffle units and even very thin coal seams. Therefore, depending upon which location and depth within the Precipice is chosen as a CO₂ injection point, there may be more or less reactive mineralogies for the CO₂ plume to come in contact with and produce divalent cations for potential mineral trapping of CO₂.

Natural analogue studies of high CO₂ reservoirs in Australia and New Zealand have shown that carbonate precipitation has occurred at the interface where lithology changes from clean and high porosity/permeability to dirty and low porosity/permeability (e.g., Higgs *et al.*, 2013; Higgs *et al.*, 2015; Watson *et al.*, 2004). In this region acidic fluids that have dissolved silicates and become enriched in divalent cations are impeded or baffled and interact with more alkaline fluids (Figure 38). At least one baffle unit is likely present within the middle of the high permeability portion of the Precipice Sandstone in the vicinity of West Wandoan 1, with more frequent baffle units occurring towards the top of the formation. This section of core was one of those selected for reaction.

Choosing to inject below baffle units within the primary reservoir will optimise potential for mineral trapping of CO₂ to occur in the medium to long term. The mixing front of CO₂ acidified water at the perimeter of the rising plume of injected CO₂ will interact with reactive minerals at the interface with baffle units, releasing cations for later precipitation.

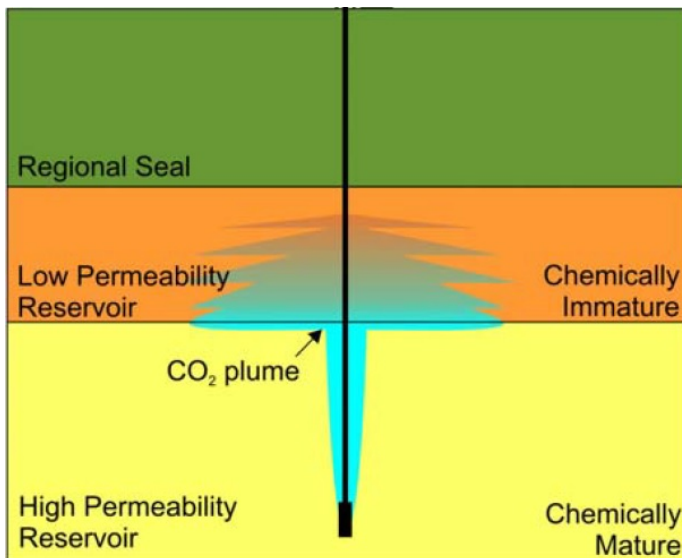


Figure 38: Schematic of an ideal reservoir system optimised for CO₂ storage, showing CO₂ rich fluid (blue) baffled in an area of low vertical permeability. Modified after Watson and Gibson-Pool (2005).

Nucleation sites may accelerate carbonate precipitation. These may take the form of high surface area clays (e.g., illite, chlorite, smectite, or kaolinite), which provide high porosities to trap/adsorb CO₂ and fluid along with a source of cations. Also, pre-existing carbonates provide seed nucleation sites. Calcite, siderite and ankerite have been observed in the upper Precipice Sandstone and throughout the Evergreen Formation often associated with clays such as kaolin, mica, and chlorite. The lower Evergreen sections of West Wandoan 1 core contain calcite cement associated with Ca-plagioclase and pore-filling clays. The Hutton Sandstone also contains calcite-cemented intervals, with calcite cementing kaolin. Therefore, units containing high surface area clays may be more likely to generate carbonate cementation in the short term as opposed to those devoid of clays.

Flue gas stream acid (i.e., sulphuric and carbonic acid) leaching and dissolution reactions have been performed on lithologically variable West Wandoan 1 core from the Precipice Sandstone and Hutton Sandstone to evaluate the release of divalent cations. A low concentration of SO₂ in CO₂ has been used. Additionally, another possibility is to consider the concept of adding a small amount of SO₂ at the well head, at concentrations higher than expected to be allowed in pipeline gas. This would negate the need to worry about pipeline issues with transporting impure CO₂, whilst providing the benefits of increased porosity/permeability in the near well-bore region via enhanced acidic reactions and increased potential for carbonate mineral precipitation in the far-field. The well would have to be designed with appropriate materials.

The natural analogues study detailed in this report has shown that dissolved SO₂ played a role in some of the carbonate precipitation events assessed. Natural ground-waters often contain dissolved SO₂ in the form of sulphate anions largely balanced by sodium and/or calcium. This is often either the end result of magmatic volatile fluid (e.g., water-CO₂-SO₂) interaction with rocks or else near-surface weathering alteration of sulphide minerals within the groundwater recharge areas. The artificial addition of a small quantity of SO₂ to a CO₂ sequestration reservoir (e.g., ≤ 0.1 vol%) could mimic these natural processes on a comparatively small-scale.

The use of a pH buffer and source of carbonate (e.g., sodium bicarbonate (NaHCO_3)) may also accelerate carbonate formation in laboratory experiments by somewhat replicating reservoir pH buffering (e.g. Peuble *et al.*, 2015). A potential source of NaHCO_3 -rich fluid is the reject brine concentrate from CSG desalination plants. Alternatively, pH could also be adjusted with a compound such as KOH to alkaline pH after initial silicate dissolution to accelerate laboratory results to reservoir time scales (Liu and Maroto-Valer, 2011; Summers *et al.*, 2004). Brine mixing experiments with a high calcium concentration saline brine replicating a possible CSG desalination system reject brine were also performed using a quartzose sample of the Precipice Sandstone.

4.1. Core characterisation

4.1.1. Fluid-rock interaction experiments

Two core sections from the West Wandoan 1 well were selected. The Precipice Sandstone at 1207.6m, a clay rich fine-grained interlaminated “baffle” section containing biotite/muscovite (Fe and Mg source), was selected for reaction with either pure CO_2 and brine (cube A1) or the SO_2 - CO_2 gas mixture and brine (cube A2). The Hutton Sandstone at 724 m containing reactive chlorite and plagioclase (Fe, Mg, Ca sources) was also selected for reaction with SO_2 - CO_2 -brine including pre and post micro-CT and QEMSCAN characterisation of a sub-plug by FEI as detailed in Appendix 6.

The Precipice 1207.6 m core interval contained major quartz (~ 53 %), muscovite/biotite (23 %) and kaolinite (23%) as determined by XRD. SEM-EDS of the surfaces additionally identified that the muscovite was Fe-rich with some occasional chloritisation. Organic matter (coal) was identified (Figure 39), along with trace (Ca)-phosphate (plus rare earth elements), K-feldspar, zircon, sphalerite and Ti-oxide.

The Hutton 724 m sample is a medium to coarse grained sandstone; XRD indicated major quartz (~ 79 %), and also K-feldspar (orthoclase 5%), plagioclase (labradorite 5 %), kaolinite (7 %), chlorite (3 %) and possible traces of carbonate. SEM-EDS of a block sample surface indicated that chlorite is Fe-Mg-rich. Zircon, Ti-oxide (rutile), coal, and Fe-Mg or Fe-Ti altered micas were also identified (Figure 40). Occasional Ca-phosphates (+/- rare earth elements) were present. An Fe-Mg silicate with traces of Ca signatures was observed that had the morphology of illite. Traces of ankerite were also observed, along with Ca and S signatures on clays indicating traces of gypsum/anhydrite.

A representative sub-plug of Hutton 724 m only was characterised by micro CT and QEMSCAN as detailed in Sommacal *et al.*, Appendix 6. The mineral components of the sub-plug slice pre-reaction are shown in Table 32 and Figure 41 and had good agreement with XRD and relatively high chlorite content. A resolvable porosity of 7% (voxel size 2.2 μm) was calculated for the sub-plug with 21.6 vol% high density clays (mainly chlorite). Kaolinite and chlorite were mainly pore filling and bridging. A high percentage of originally unclassified pixels were re-interpreted as framework grains containing a mixture of K-feldspar and chlorite (Appendix 6). These likely exist due to previous natural fluid-rock reaction processes.

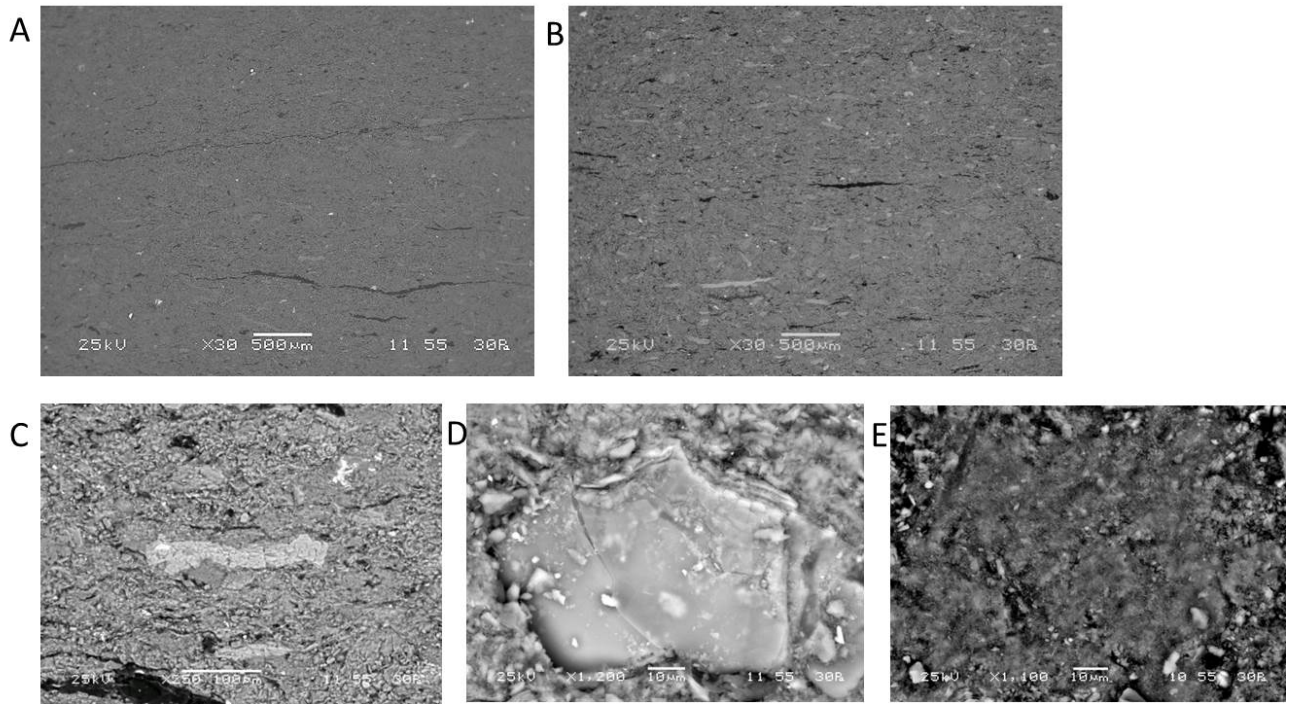


Figure 39: Selected SEM images of Precipice 1207.6 m. A) Surface view of cube A1, B) surface view of cube A2 both with dark organic matter and bright muscovite/biotite. C) Fe-rich muscovite/biotite and sphalerite (cube A1), D) Fe-rich muscovite and kaolinite (cube A1), E) fine grained kaolinite (cube A2).

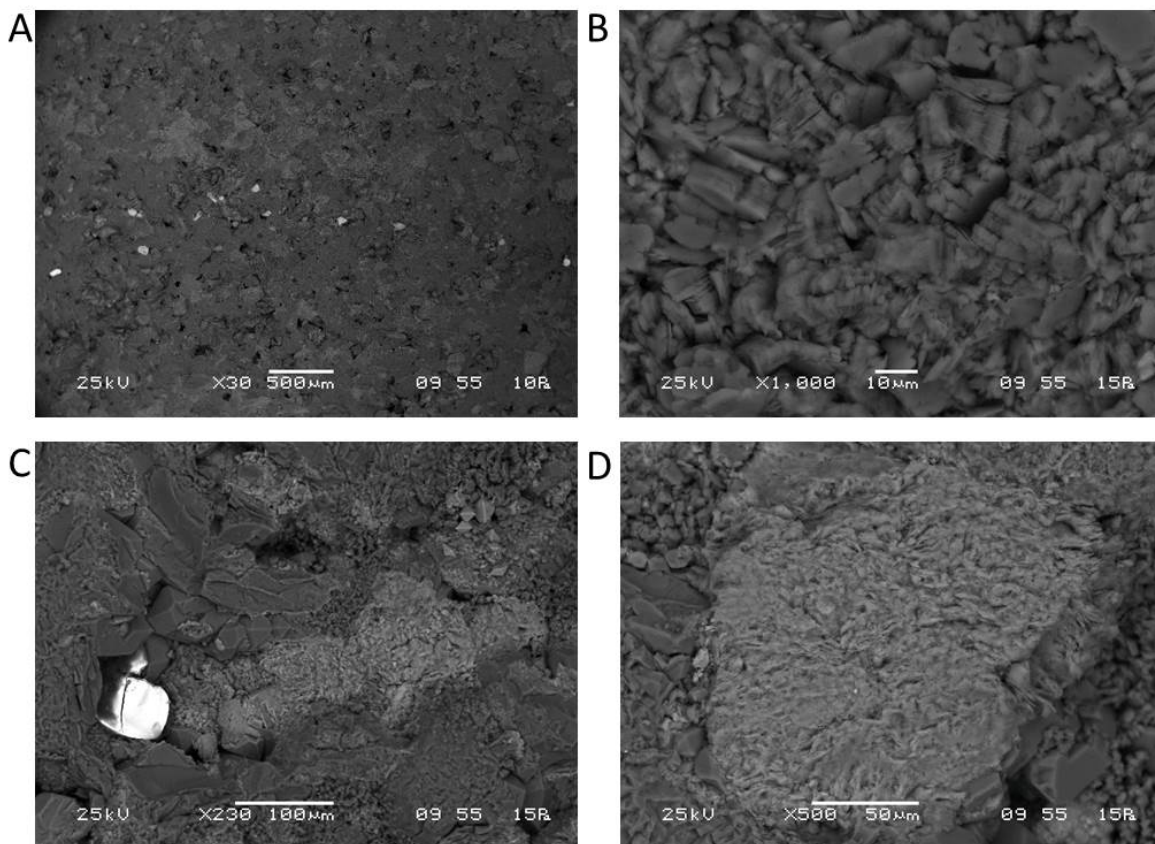
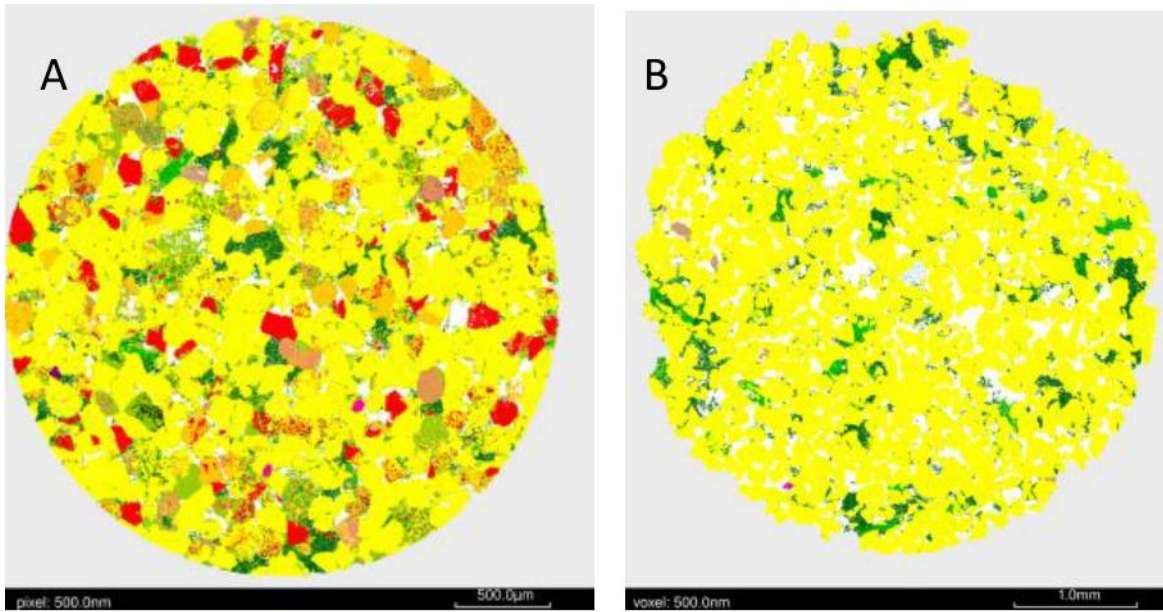


Figure 40: Selected SEM images of Hutton 724 m. A) Surface view with bright zircon and Ti-oxide (rutile) grains and some open porosity, B) kaolin, C) bright zircon and Fe-rich silicate, D) Fe-Mg chlorite.

Table 32: Mineral components of polished sub-plug slices by QEMSCAN (area %) pre and post reaction, modified from Silvano *et al.*, Appendix 6.

Mineral	Hutton 724m (pre)	Hutton 724m (Post)	Precipice 1212m (pre)	Precipice 1212m (post)
Quartz	62.7	64.8	89.2	89.9
Alkali Feldspar	7.2	8.2	-	-
K Feldspar– Chlorite mixture	3.5	2.2	-	-
Plagioclase	7.4	5.3	-	-
Muscovite/Illite	1.35	1.2	3.5	2.2
Kaolinite	4.4	5.75	6.5	6.8
Chlorite	11.8	11.5	-	<0.1
Calcite	-	-	-	0.3
Dolomite	-	-	-	0.1
Zircon	0.1	<0.1	-	<0.1
Rutile	0.8	0.4	0.7	0.5
Spinel	<0.1	-	-	-
Apatite	<0.1	<0.1	-	-
Unclassified and traces	0.65	0.5	0.1	0.2



Mineral	QEMSCAN Legend
Quartz	Yellow
Alkali Feldspar	Orange
K Feldspar–Chlorite mixture	Light Orange
Plagioclase	Red
Muscovite/illite	Green
Kaolinite	Dark Green
Chlorite	Light Green
Calcite	Cyan
Dolomite	Blue
Zircon	Magenta
Rutile	Brown
Spinel	Purple
Apatite	Grey
Unclassified + traces	Black
Total	

Figure 41: Pre reaction QEMSCAN images of A) Hutton 724 m, and B) Precipice 1212 m, and colour key. Modified from Appendix 6.

4.1.2. Brine mixing experiment

A section of the clean quartzose Precipice Sandstone was sampled from the West Wandoan 1 core at 1211.65 m depth (referred to as Precipice 1212 m) for reaction including pre and post micro-CT and QEMSCAN characterisation of a sub-plug by FEI (Appendix 6).

XRD of core off-cuts indicated major quartz, with traces of kaolinite, muscovite, orthoclase (K-feldspar), lazurite, and zircon. SEM-EDS additionally identified S signatures on clays along with KCl and Na sulphates. Some quartz grains had undergone previous alteration (Figure 42). The mineral components of the sub-plug

slice pre-reaction are shown in Table 32. A resolvable porosity of 11 % (voxel size 2.2 μm) was calculated for the sub-plug with 7.2 vol% high density clays (mainly illite and muscovite). Kaolin is mainly pore filling as shown in Figure 41 (and Appendix 6).

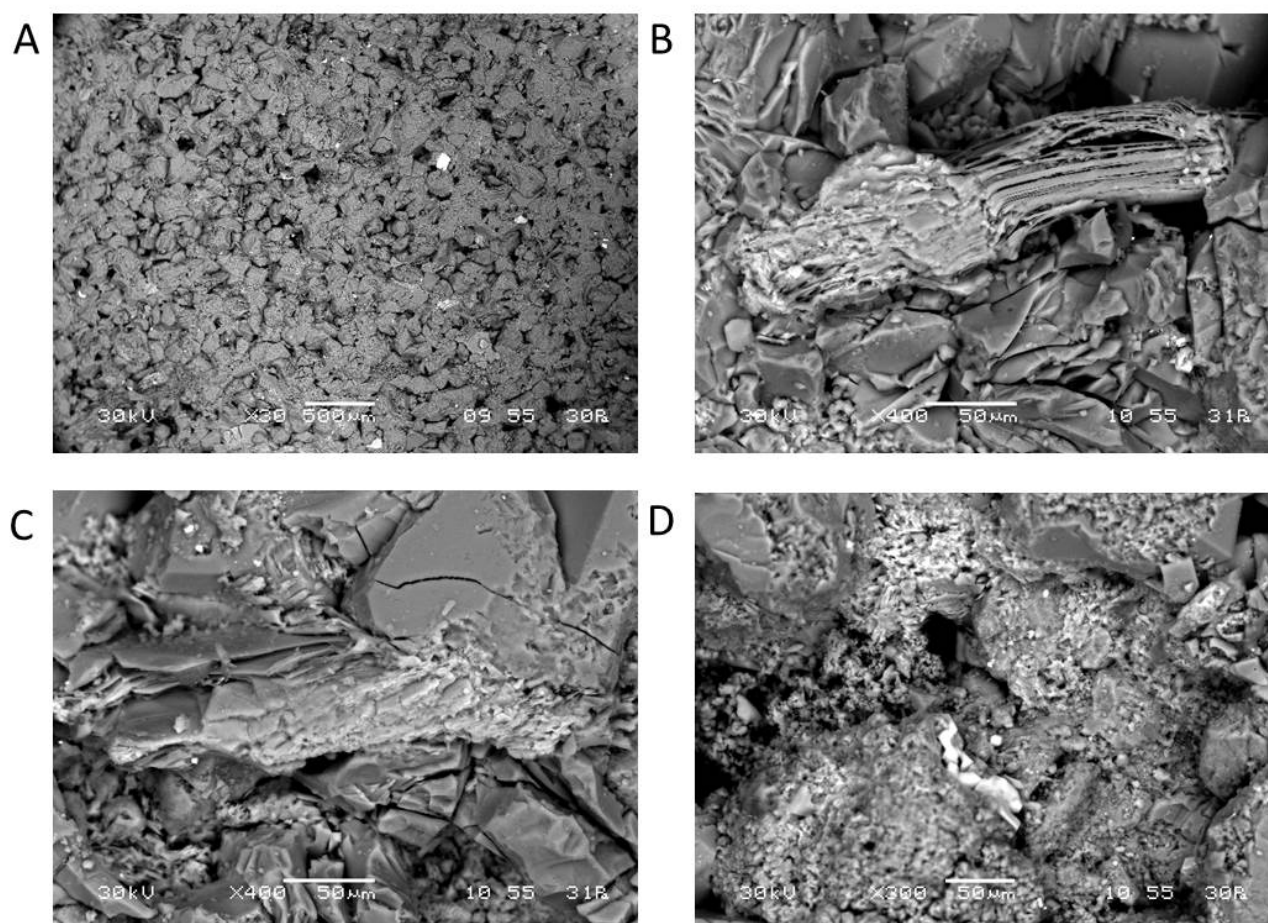


Figure 42: Selected SEM images of Precipice 1212 m. A) Surface view with quartz framework grains and open porosity (and bright zircon). B) Muscovite with traces of Fe and Mg signature. S, Na and Cl elemental signatures were also present. C) Muscovite and Ti-oxide. D) Amorphous silica/altered quartz and bright KCl.

4.2. Experimental methods

4.2.1. Fluid-rock interaction experiments

Experiments generally followed the methods and conditions used in previous projects (ANLEC 7-1110-0101, and ANLEC 7-0311-0128 SP5) for consistency with some modifications. Long term batch experiments were performed in Parr reactors at 120 bar and 60°C for approximately 10 weeks (Pearce *et al.*, 2015a). A low salinity brine (100ml of 1500 ppm NaCl) was added with the rock core sample (cube and offcut) at a brine/rock ratio of 7. Reactors were then purged with N₂ and pressurised for 5 days to provide a baseline brine-rock soak. After fluid sampling N₂ was depressurised and reactors filled with either pure CO₂ (block A1) or 160 ppm SO₂ (block A2) with a balance of CO₂. After another 18 days sodium bicarbonate was added (to 105 ppm) to approximate reservoir buffering (in line with average alkalinity ranges reported for Woleebee Creek and Reedy Creek Precipice groundwater, cross reference ANLEC 7-0314-0229). Fluid was sampled during

the experiments, with pH and electrical conductivity immediately measured. Aliquots were diluted 20 times and acidified to 2 % ultra-pure nitric acid for analysis of ions by ICP-OES or ICP-MS. Total inorganic and organic carbon, alkalinity, and sulphate were determined on selected unacidified samples (total organic carbon analyser and ion chromatography). A blank experiment without a core sample was also performed to check cations were not leached from the reactor.

4.2.2. Brine mixing experiment

Experiments were designed to replicate conditions from the static GWB modelling (Progress report 4, with further modelling in this report section 5). Core blocks of the Precipice 1212 m core and a sub-plug were submerged in 165 ml of a complex brine (Table 33) at 100 bar and 50°C. A low pressure CO₂ flush was performed to purge air followed by pressurisation with pure food grade CO₂. Minimal incremental sampling was performed so as to attempt to match the static GWB model on which the experiment was based with the experiment running for approximately 8 weeks. Fluid samples were diluted and preserved to 2 % nitric acid for analysis by ICP-OES.

Table 33: Initial brine composition for the groundwater mixing experiments (TDS was not measured).

Species	Concentration (mg/kg)
Ca ²⁺	12,501.60
Na ⁺	44,678.34
K ⁺	230.77
Mg ²⁺	688.64
Cl ⁻	40,864.02
HCO ₃ ⁻	111,174.40

4.3. Post-reaction core characterisation

4.3.1. Fluid-rock experiments

The Precipice 1207.6 m core samples after pure CO₂-brine reaction showed no significant changes (Figures 43 and 44a, b). In contrast the sample surfaces post SO₂-CO₂ reaction were visibly coated in red-brown precipitates mainly on the shale sections. SEM-EDS showed Fe-leaching from chloritized muscovite/biotite, and Ca signatures were removed by mineral dissolution. After SO₂-CO₂ reaction only, Fe-rich precipitates were visible on and in pre-existing clays with no S signatures (indicating no significant pyrite or FeS precipitation (Figure 44c, d).



Figure 43: Precipice 1207.6 m core block photos, left before reaction, centre post reaction with CO₂-brine (block A1), right post reaction with SO₂-CO₂-brine (block A2), note red-brown colouration.

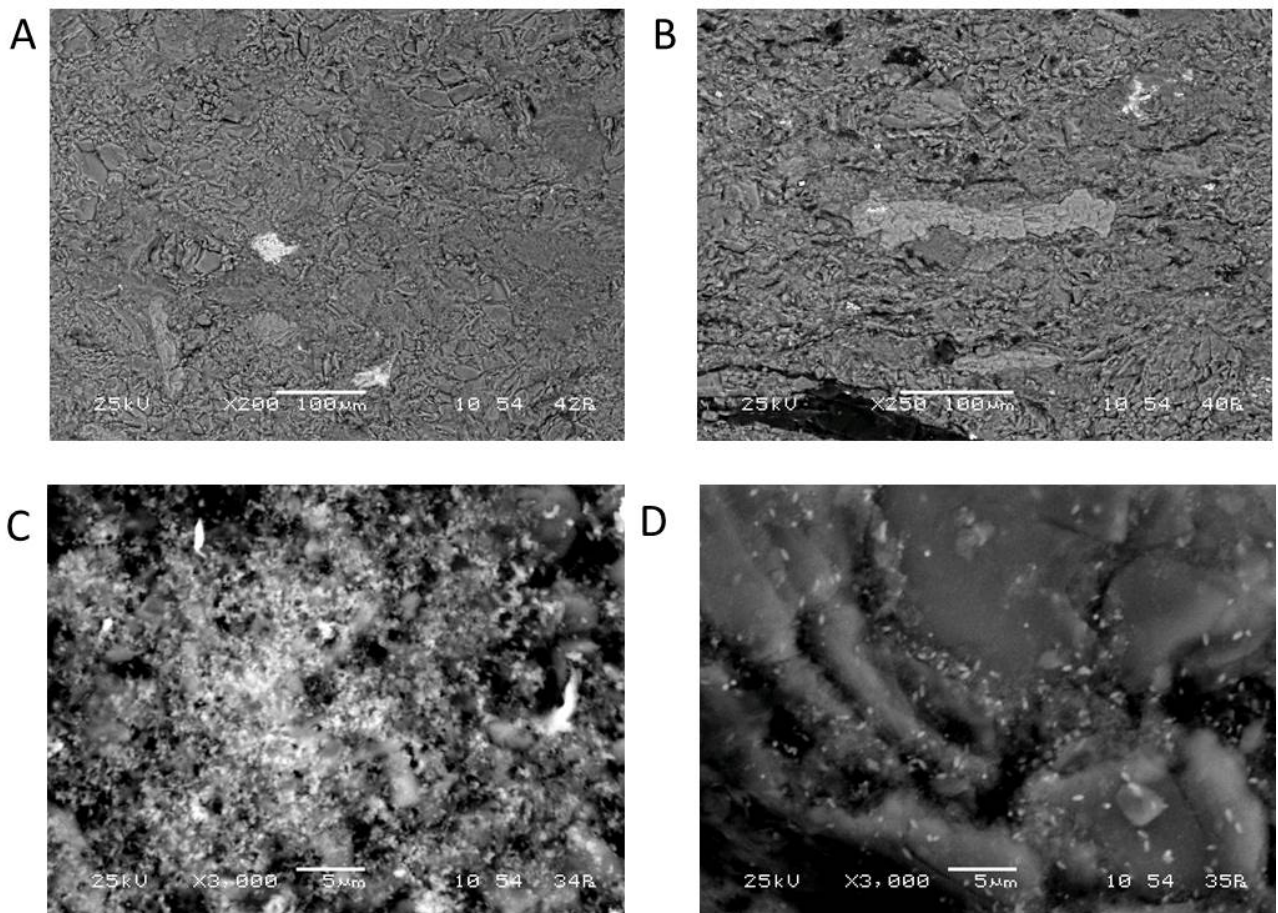


Figure 44: SEM images of Precipice 1207.6 m after reaction A-B) with CO₂-brine, and C-D) with SO₂-CO₂ brine. Note fine-grained bright Fe-rich precipitates on clays after reaction with SO₂-CO₂-brine in C-D.

The Hutton 724 m sandstone core block sample had a brown colouration post SO₂-CO₂ reaction (Figure 45), with generally less visible precipitation than on Precipice 1207.6 m after reaction. Quartz and zircon surfaces were not visibly altered post SO₂-CO₂ reaction (Figure 46a). Chlorite showed minor dissolution/alteration with reduced Fe signatures in EDS (Figure 46b). Fe-rich precipitates containing Ni and Cr signatures were mainly on pre-existing kaolin clays (Figure 46c, d).

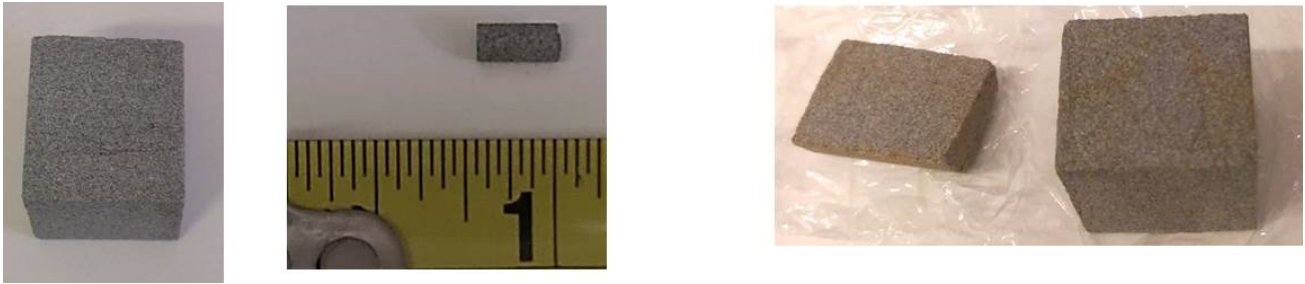


Figure 45: Hutton 724 m sample photos, left block and sub-plug before reaction, right offcut and block post reaction with SO₂-CO₂-brine, note brown colouration.

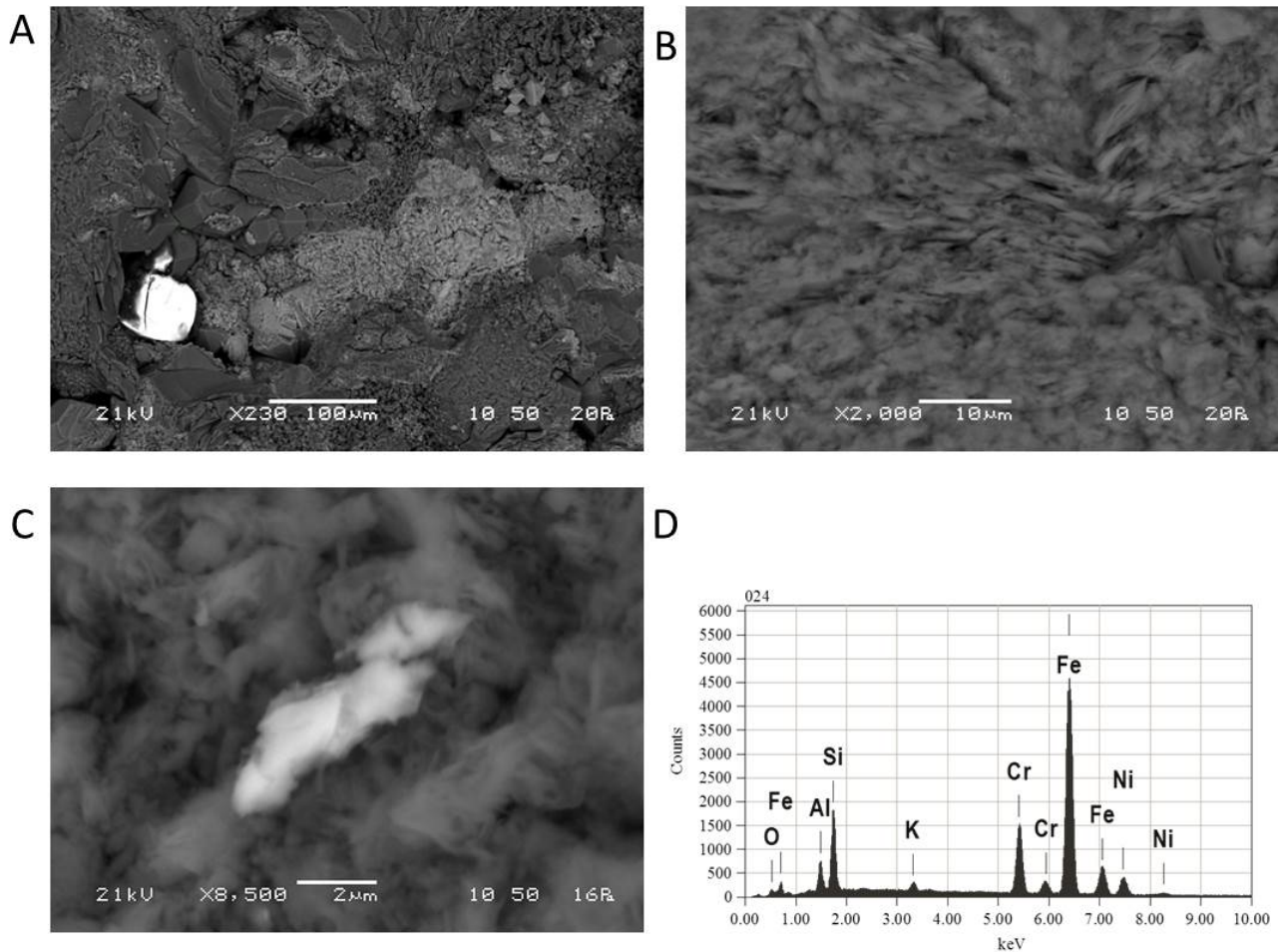


Figure 46: SEM-EDS of Hutton 724 m post reaction. A) Zircon, quartz and Fe-rich silicate surfaces. B) Fe-rich chlorite booklets appeared altered with a reduced Fe elemental signature. C) Fe-rich precipitates with Cr and Ni signatures on kaolinite and D) EDS spectrum of bright precipitate in C (note technical issues resulted in no carbon peak).

Micro CT and QEMSCAN images also showed Fe-leaching from chlorite, although the chlorite content determined by QEMSCAN did not change significantly (Appendix 6). Minor dissolution and precipitation of minerals in pore spaces (Appendix 6, Figure 68) and movement or fine material or clays were also observed. There was a small reduction in the amount of plagioclase, muscovite/illite and the component of K-feldspar-chlorite mixture determined by QEMSCAN; however, these could also be owing to heterogeneities in the sub-plug slices (Table 32 and Appendix 6). Precipitated minerals were likely in too low abundance or too fine

grained to be quantified by QEMSCAN. Very small traces of Fe-containing minerals were observed in the unclassified minerals; however, they could not be definitively assigned to the result of reaction rather than already being present pre-reaction. Figure 47 shows unclassified minerals in the K-feldspar-chlorite mixture.

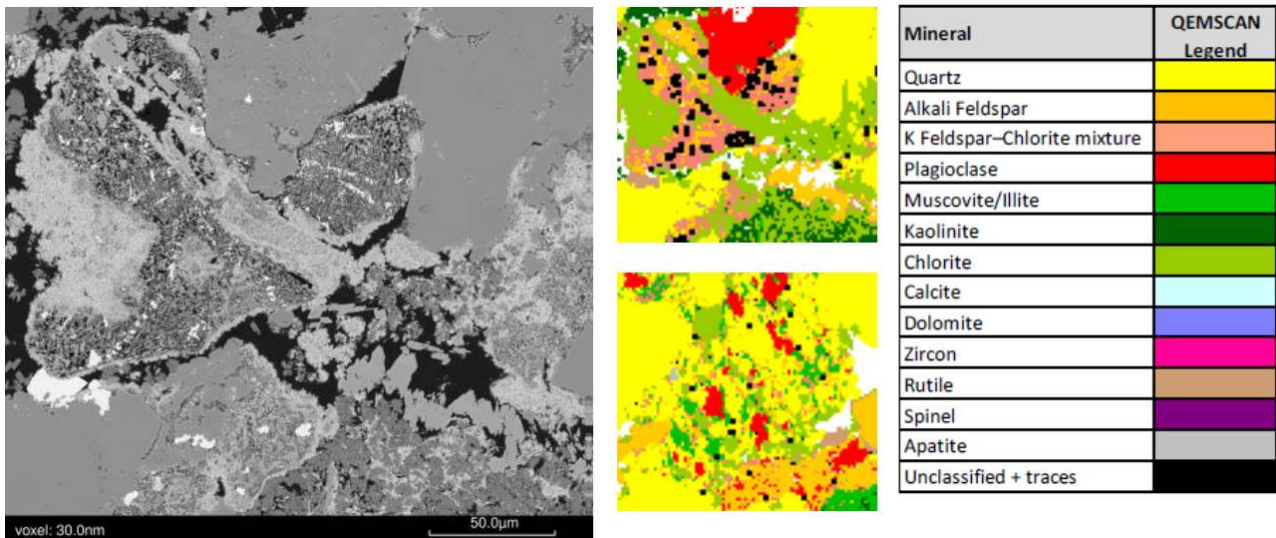


Figure 47: High resolution SEM image (left) and associated QEMSCAN mineral maps (center) at the same scale, with the colour legend (right). Hutton 724 m post reaction (modified from Appendix 6).

4.3.2. Brine mixing experiment

The quartzose sandstone Precipice 1212 m was selected for brine mixing experiments. Existing minerals in the Precipice 1212 m core samples post-reaction showed no alteration, corrosion or dissolution. Fine grained Ca-containing precipitates were observed in and around pre-existing muscovite booklets (Figure 48). Some fine-grained precipitates observed in SEM-EDS contained Ca and Mg (although it is possible this could be interaction of the EDS beam with underlying silicates). QEMSCAN of the sub-plug slice post-reaction did quantify 0.3 and 0.1 area% calcite and dolomite (Table 32). Figure 49 shows a high resolution SEM image and mineral map of calcite and dolomite precipitated in a pore space of Precipice 1212 m after CO₂ reaction in the brine. Movement of clays (kaolin) in pore space after reaction was also observed that has the potential to plug/unblock pore throats (Appendix 6).

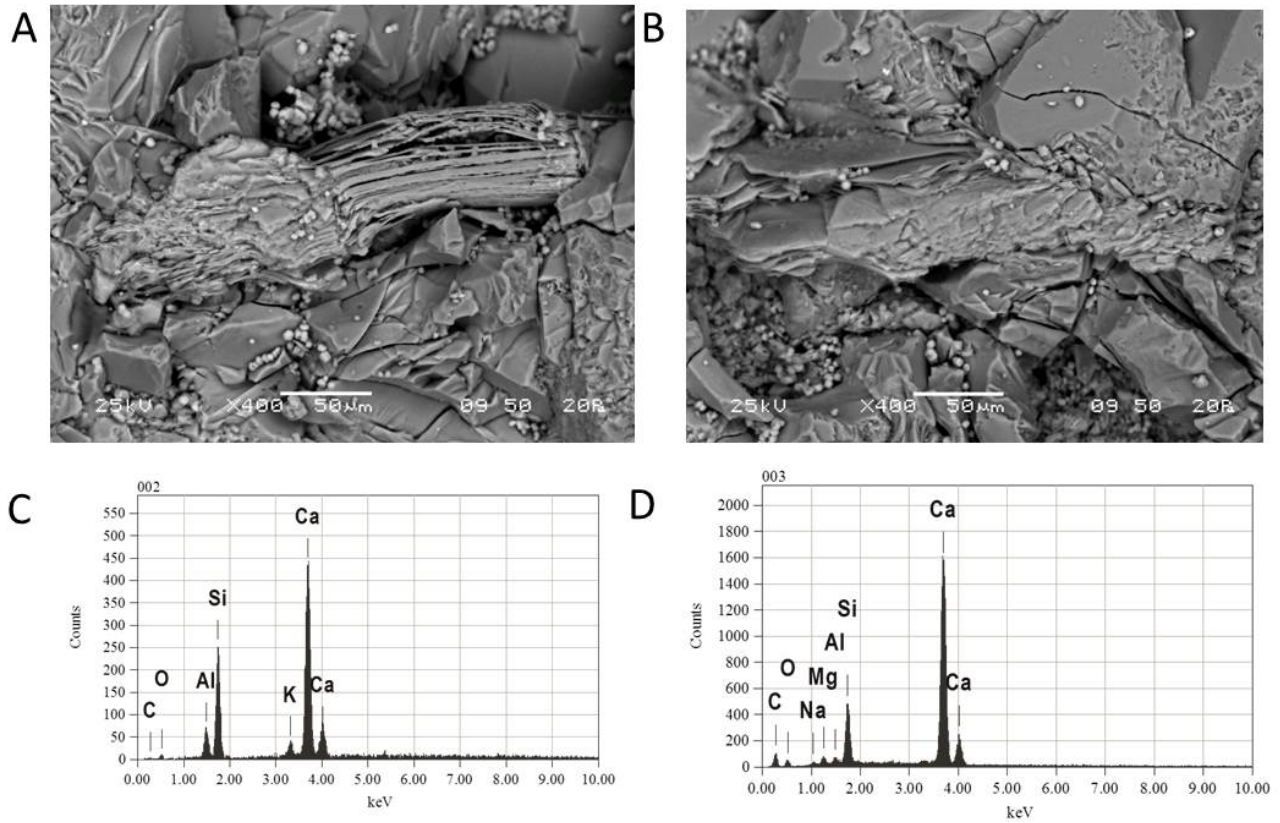


Figure 48: SEM-EDS of Precipice 1212 m post reaction. A) and B) muscovite with fine-grained bright precipitates. C) and D) EDS spectra of precipitates in A) and B) indicating Ca content (note C peak low intensity due to technical issues).

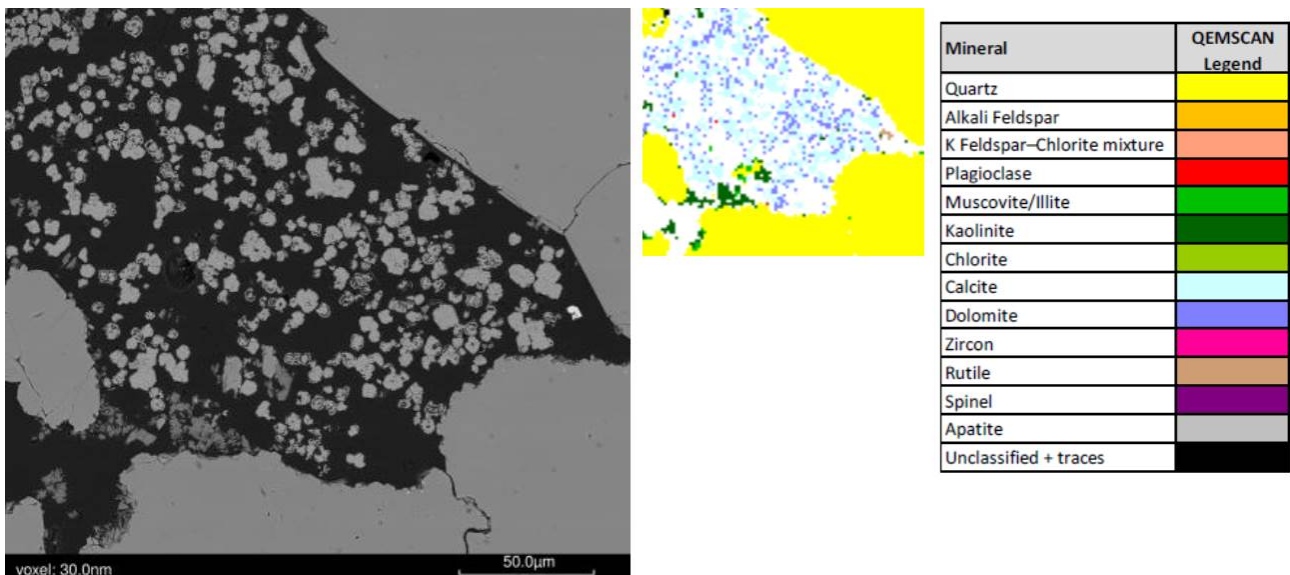


Figure 49: High resolution SEM image and QEMSCAN mineral map of Precipice 1212 m post reaction with calcite and dolomite in pore space (modified from Appendix 6).

4.4. Water chemistry

4.4.1. Fluid-rock interaction experiments

During reaction of Precipice 1207.6 m with SO₂-CO₂ and low salinity brine, solution pH was lower than on pure CO₂ reaction initially through the dissolution of SO₂ and generation of sulphuric acid (Figure 50). Small decreases in pH near the end of the SO₂-CO₂ experiment could indicate mineral precipitation of e.g., siderite during which acidity is generated. The concentration of dissolved inorganic carbon (IC) decreased at the end of the SO₂-CO₂ reaction (potentially indicating carbonate precipitation), whereas it continued to increase with pure CO₂. Total dissolved organic carbon (TOC) was present and of a similar concentration in both reactions. Alkalinity varied from 107 to 360 mg/kg at 192 h reaction then subsequently decreased during pure CO₂ reaction. Alkalinity reached a maximum of 991 mg/kg after 192 h of reaction with SO₂-CO₂ gas likely reflecting increased mineral dissolution, and then subsequently decreased.

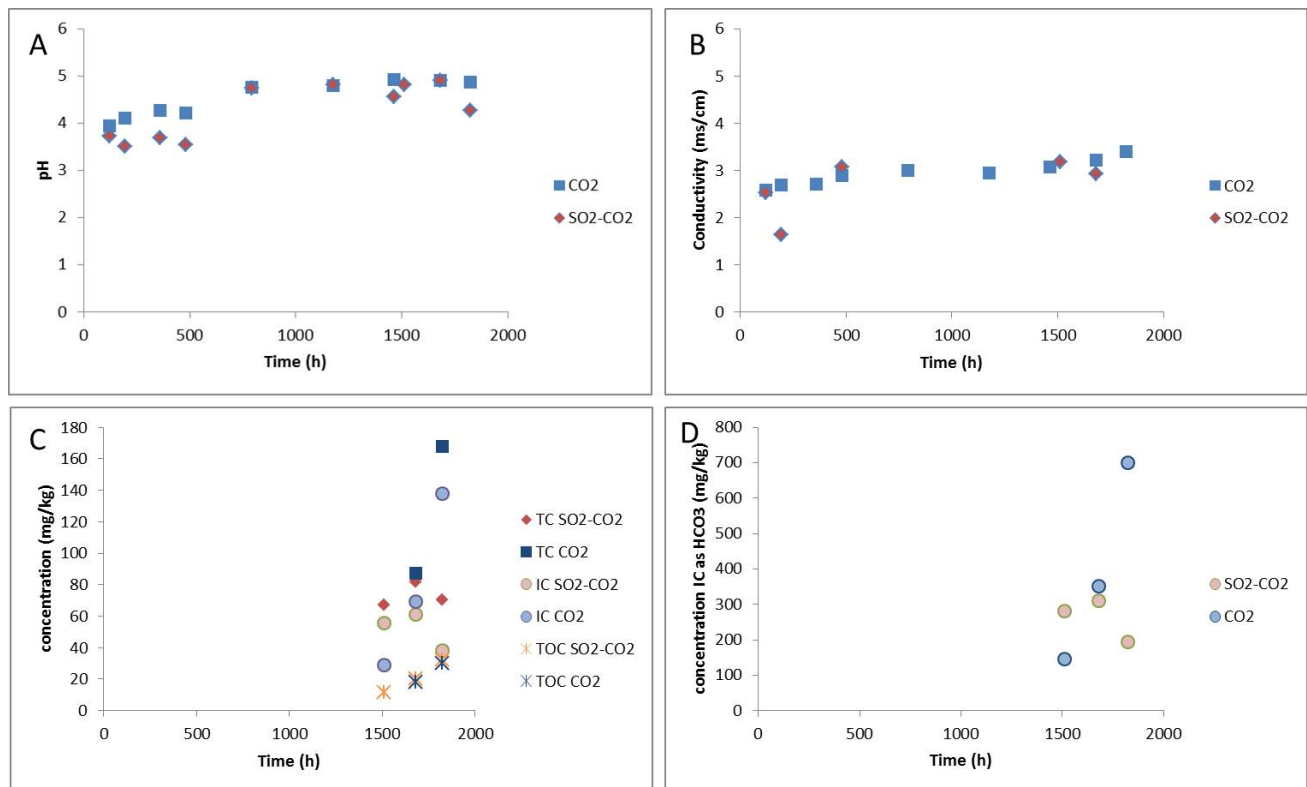


Figure 50: Water chemistry during CO₂-brine or SO₂-CO₂-brine reaction of Precipice 1207.6 m. A) Solution pH, B) solution electrical conductivity, C) dissolved concentrations of total carbon (TC), inorganic carbon (IC), and total organic carbon (TOC), D) dissolved inorganic carbon converted to bicarbonate concentration.

After gas injection, dissolved major element concentrations including Ca, Mg, Fe, Mn, Al increased (Figure 51) through mineral dissolution (or ion exchange) from Precipice 1207.6 m with either pure or impure CO₂. Dissolved Ca and Mg, and Ca and Sr were correlated (R² values above 0.9) with similar trends, in general subsequently decreasing in dissolved concentration in the presence of SO₂-CO₂ gas, indicating common sources and sinks. Dissolved Fe and Mn increased gradually with higher concentrations in the presence of SO₂-CO₂ gas, and subsequently decreased after ~ 1200 h indicating a common sink such as precipitation of an Fe-Mn carbonate, e.g., siderite. Traces of sphalerite were present in Precipice 1206.7 m pre-reaction; this also contributed to dissolved S in both reactions and may have possibly been the source of other dissolved elements including low concentrations of As and Pb (Figure 52) that subsequently decreased in concentration near the end of SO₂-CO₂ reaction likely incorporated into or adsorbed on precipitates. Other possible sources of As and Pb include desorption from trace Fe-oxides and other mineral surfaces.

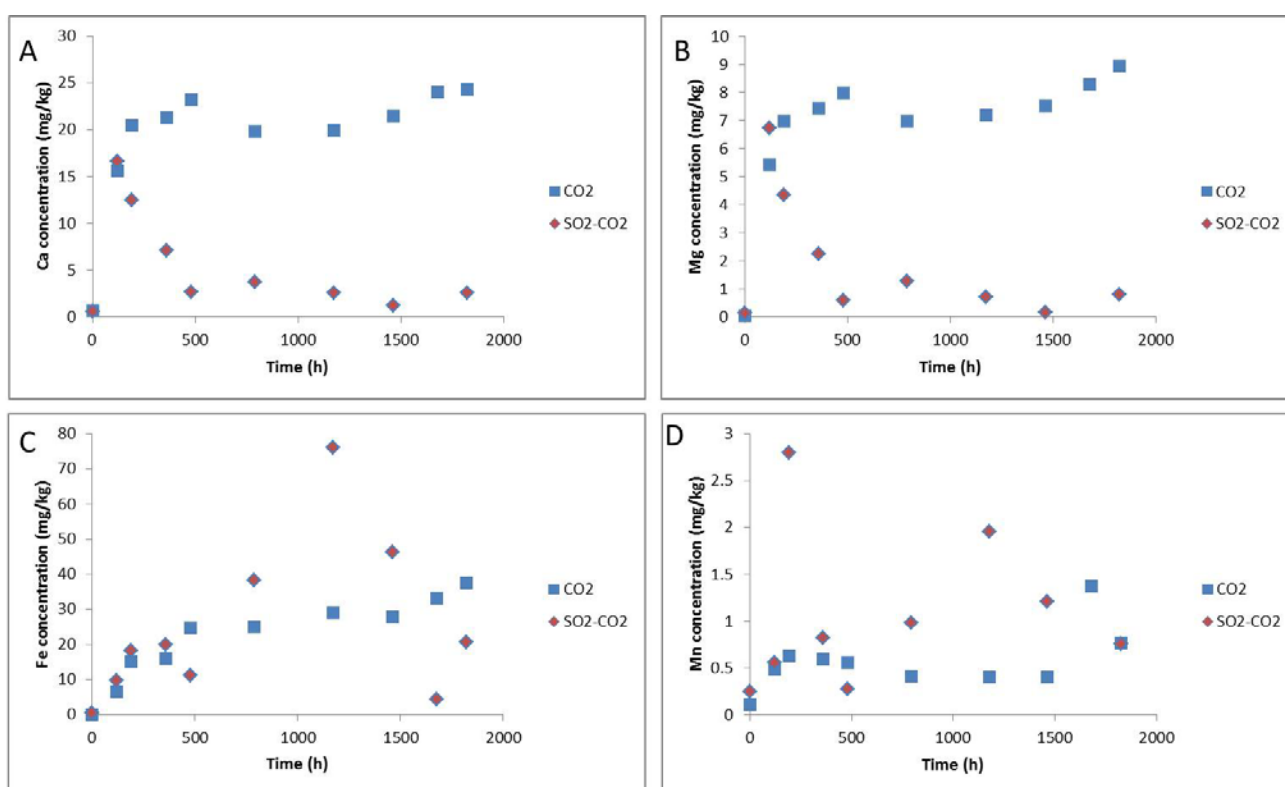


Figure 51: Water chemistry during CO₂-brine or SO₂-CO₂-brine reaction of Precipice 1207.6 m. A) Dissolved Ca concentration, B) dissolved Mg concentration, C) dissolved Fe concentration, D) dissolved Mn concentration.

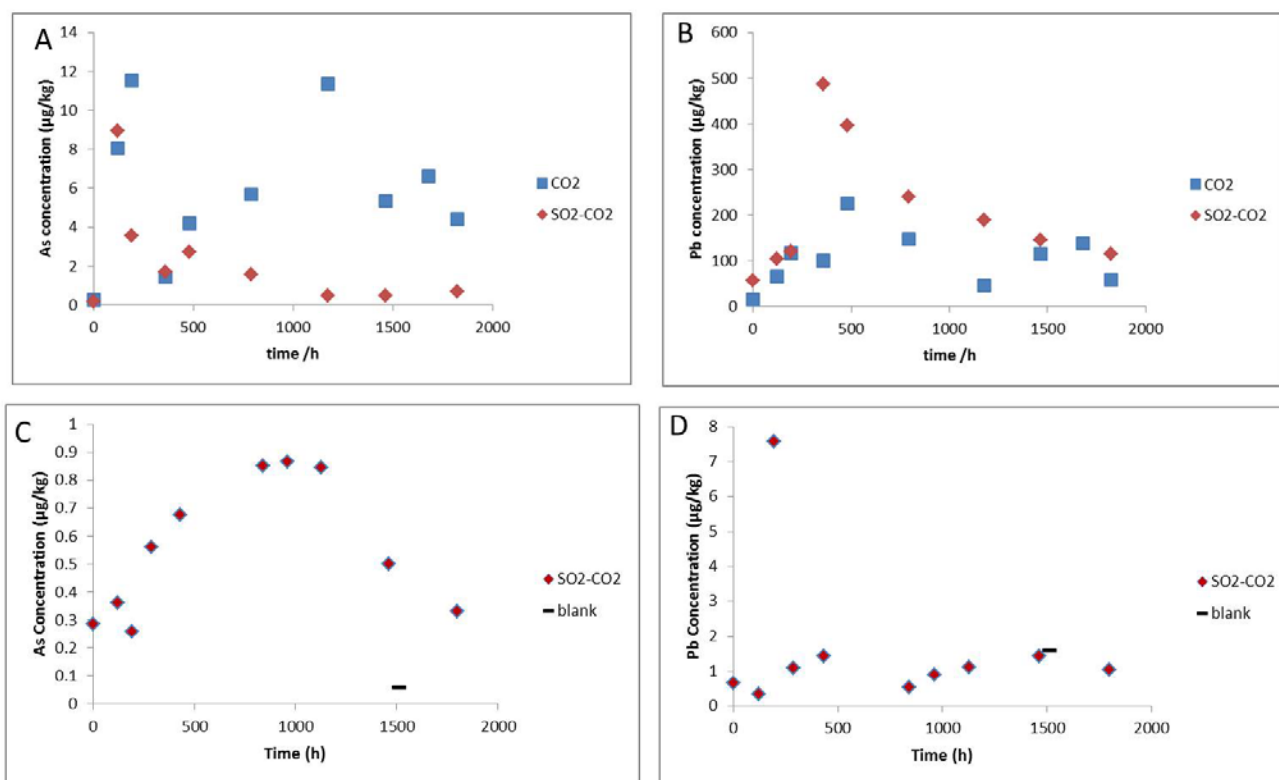


Figure 52: Concentrations of As and Pb during A-B) CO₂-brine or SO₂-CO₂-brine reaction of Precipice 1207.6 m, and C-D) SO₂-CO₂-brine reaction of Hutton 724 m and blank experiment, note the different scales on the y axis.

Geochemical models considering dissolution and precipitation (not desorption or ion exchange) were initially constructed using the determined mineral content in cores, and run at 60°C with a CO₂ fugacity of 0.73 experimental data to match water chemistry by varying reactive surface areas (Pearce *et al.*, 2015). SO₂ was added to match the concentration of sulphate observed in experiments. Models were then upscaled for a water volume of 1kg and porosities of 8% for P1207.6 m (given the similar lithology to characterised core samples) and 7 % for H724 m (Table 34). Surface areas were scaled according to the method of Frank and Kirste (e.g., framework grains including quartz reduced by a factor of 10, and clays reduced by 100) (Frank *et al.*, 2014; Pearce *et al.*, 2015). After 10 years reaction of P1207.6 m, 1.33 times more predicted ankerite volume was precipitated with SO₂ present, and 2.57 times more siderite volume precipitated compared to the pure CO₂ reaction (Figure 53). Kaolinite, pyrite and smectite (nontronite) precipitation were also predicted. The main mineral dissolving (contributing to the dissolved Fe) was muscovite/biotite (annite).

During the SO₂-CO₂ reaction of Hutton 724 m core block and sub-plug, a higher solution pH, increasing electrical conductivity, and increased Ca concentration indicate mineral dissolution and more pH buffering (Figures 54 and 55). Dissolved inorganic carbon was initially high and subsequently decreased after 500h of reaction, with TOC initially 24 mg/kg, subsequently variable up to 36 mg/kg (Figure 53). Dissolved concentrations of Ca, Mg, Fe and Mn increased on gas injection, with Ca subsequently decreasing after 500 h and Fe after 1200 h (Figure 55). This indicates a Ca-containing mineral precipitation followed by Fe-carbonate or oxide precipitation. Dissolved concentrations of As, Pb, Ni and Cr increased then subsequently decreased as they were likely incorporated or adsorbed on precipitates (Figure 56). With As and

Pb at much lower concentrations in Hutton 724 m reaction than during reaction of Precipice 1207.6 m likely reflecting the lower abundance of trace elements present in the Hutton 724 m sandstone core.

Table 34: Input mineral volume % and surface areas used in Geochemist Workbench (version 9) models.

Minerals	Vol %		Surface area (cm ² /g)
	Precipice 1207.6m	Hutton 724m	
Quartz (chalcedony)	51.92	64.28	10
K-Feldspar	0.00	7.65	10
Albite	0.40	7.68	10
Kaolinite	23.25	4.61	105
Illite	0.64	1.33	0.1
Muscovite	10.43	3.27	105
Biotite	10.43	0.94	105
Chlorite	0.41	10.15	105
Calcite	0.03	0.00	0.001
Ankerite	0.03	0.03	0.001
Siderite	0.03	0.03	0.001
Hematite	1.82	0.03	0.001
Dolomite	0.03	0.03	0.001

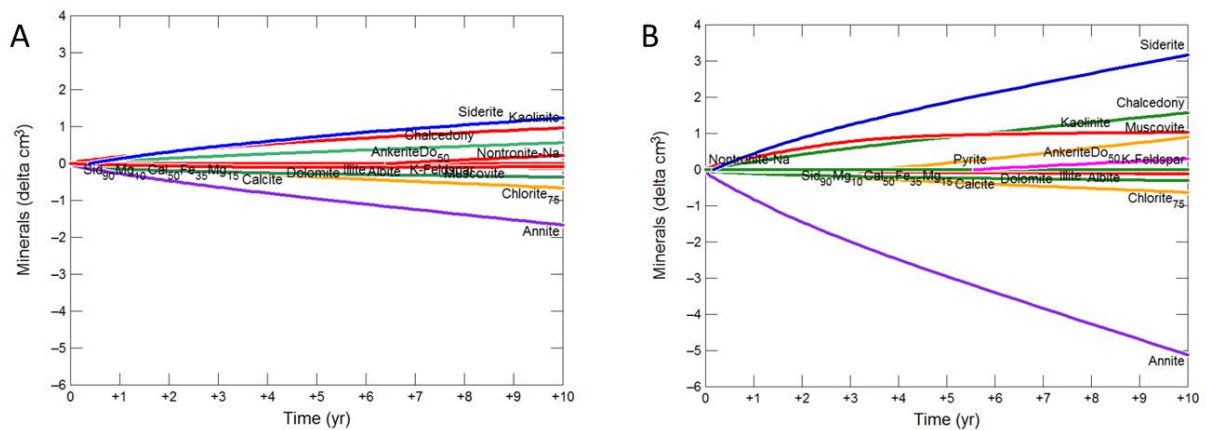


Figure 53: Modelled mineral volume change during reaction of Precipice 1207.6m with A) pure CO₂-brine, B) SO₂-CO₂-brine over 10 years.

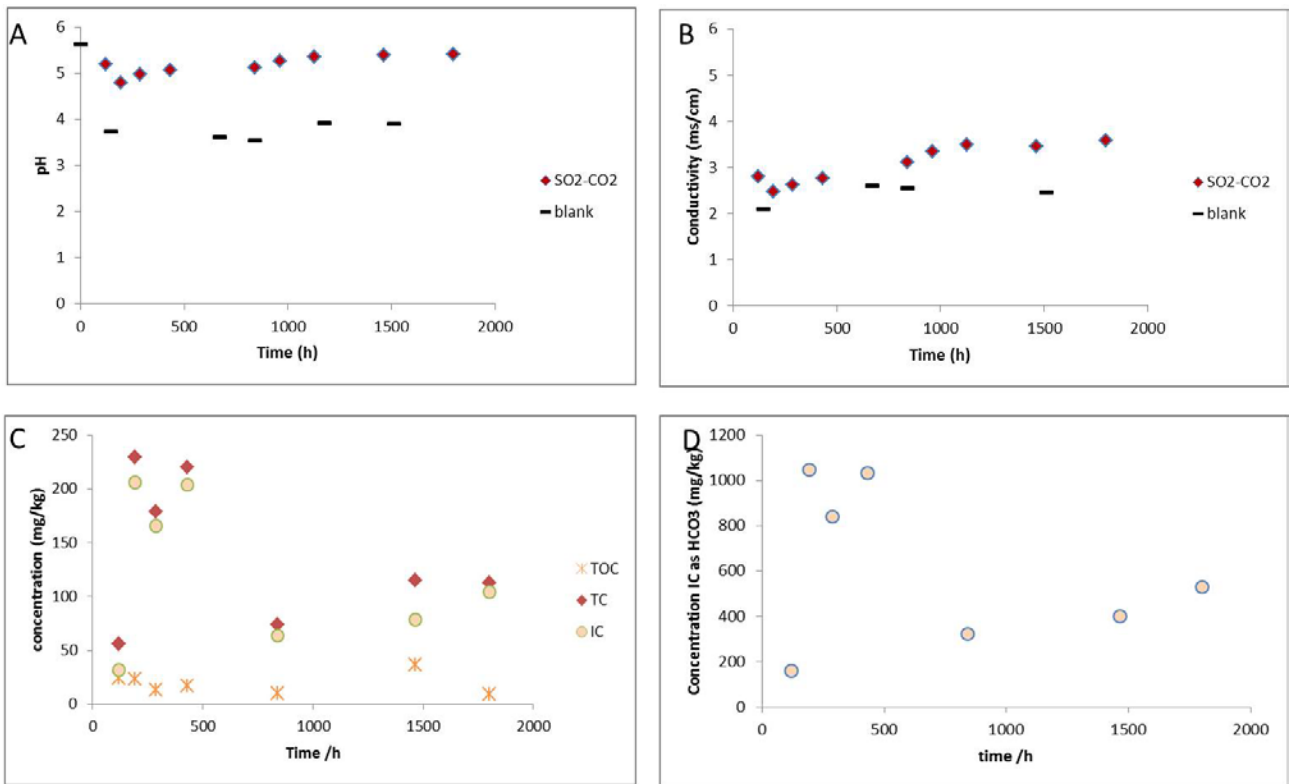


Figure 54: Water chemistry during SO₂-CO₂-brine reaction of Hutton 724 m and blank experiment. A) Solution pH, B) solution electrical conductivity, C) dissolved concentrations of total carbon (TC), inorganic carbon (IC), and total organic carbon (TOC), D) dissolved IC converted to bicarbonate concentration.

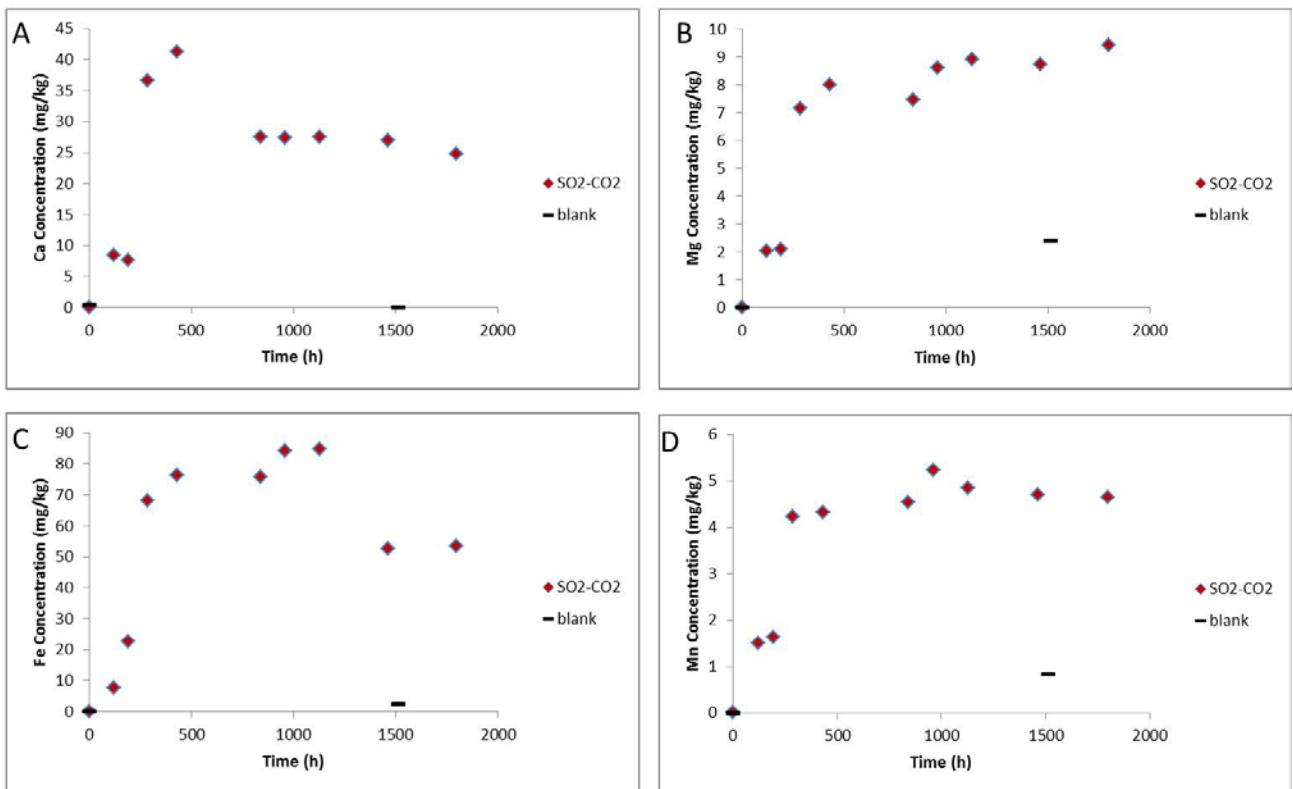


Figure 55: Water chemistry during SO₂-CO₂-brine reaction of Hutton 724 m, and blank experiment. A) Dissolved Ca concentration, B) dissolved Mg concentration, C) dissolved Fe concentration, D) dissolved Mn concentration.

When the fluids in the SO₂-CO₂ reaction of Hutton 724 m were cooled and depressurised at the end of the experiment, dissolved concentrations of Fe, Mn, and As decreased (Ca, Mg were not affected) suggesting if fluids moved to lower pressure and temperature areas (e.g., up faults) those metals could be deposited as mineral precipitates.

In geochemical modelling of reaction of Hutton 724 m after 10 years siderite, kaolinite, magnesite, ankerite and pyrite precipitation were predicted (with hematite a transitory precipitate) (Figure 56). The volume of precipitated siderite was over 4 times that predicted to be precipitated on reaction of Precipice 1207 m. The main mineral dissolving (contributing to the dissolved Fe) was chlorite. This assumes that chlorite continues to be available for reaction although precipitation of clay and carbonate coatings on reacting minerals may actually reduce available surface areas.

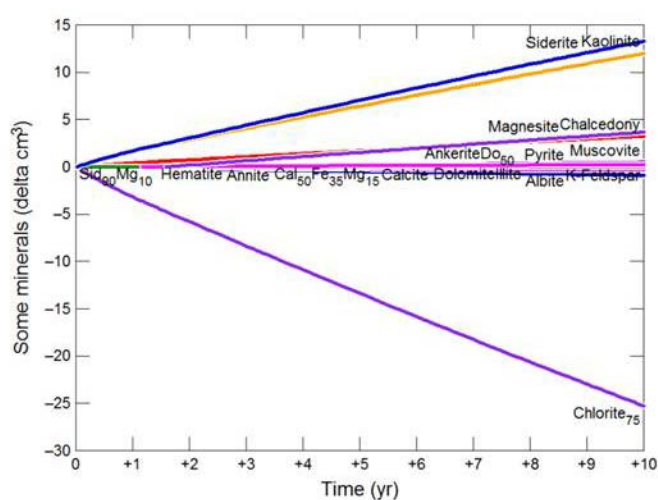


Figure 56: Modelled mineral volume change over 10 years reaction of Hutton 724 m core with SO₂-CO₂-brine.

4.4.2. Brine mixing experiment

The pH during reaction of Precipice 1212 m was fairly constant over 3 sampling measurements at pH 7.2, 7.12, and 7.1, lower than the initial brine (pH 8.3), with solution conductivity at 92.3, 82.8 and 91.5 ms/cm. Overall Ca, Mg, Sr, Cr concentrations decreased relative to the initial brine concentrations during reaction through carbonate precipitation (Figure 57), with Al increasing slightly. Fe and Cr increased slightly likely from minor muscovite/illite dissolution or calcium induced ion exchange of clays. When the fluids in the CO₂-brine reaction of Precipice 1212 m were cooled and depressurised at the end of the experiment, dissolved concentrations of Ca, Mg, Fe and Sr decreased suggesting further mineral precipitation occurred at this stage in experiments and could occur if fluids rapidly moved to lower pressure and temperature areas (e.g., up faults).

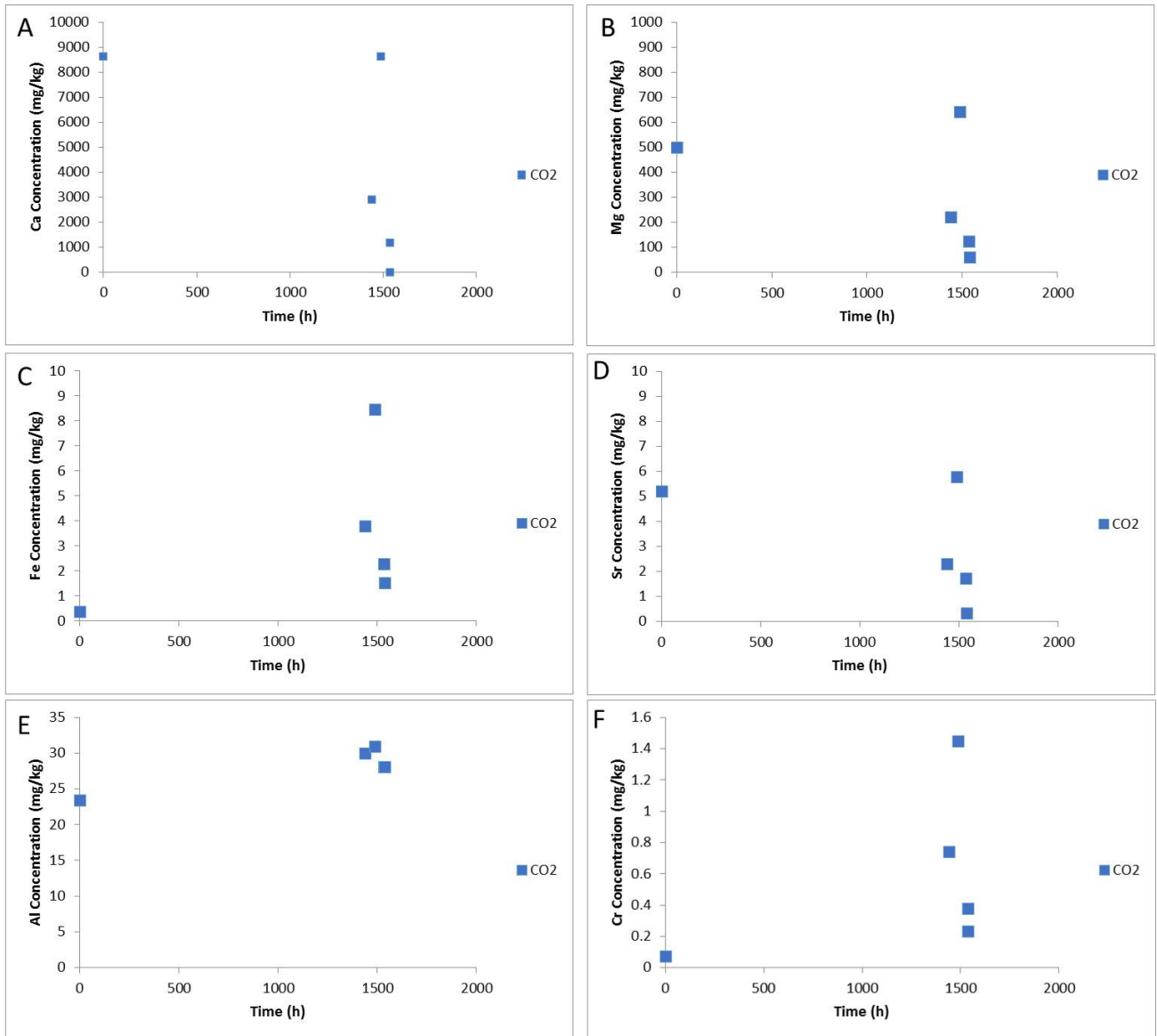


Figure 57: Water chemistry during CO₂-complex brine reaction of Precipice 1212 m core, and last point after depressurisation. A) Dissolved Ca concentration, B) dissolved Mg concentration, C) dissolved Fe concentration, D) dissolved Sr concentration, E) dissolved Al concentration, and F) dissolved Cr concentration.

4.5. Discussion

The alteration of chlorite and biotite/muscovite to mainly siderite, ankerite and kaolinite was observed on reaction of a Hutton Sandstone sample and a mudstone layer of the Precipice Sandstone. Greater dissolution of silicates and conversion of liberated Fe to Fe^{2+} by SO_2 resulted in higher predicted volumes of siderite precipitation in agreement with previous work on iron oxide-rich sediments (Palandri and Kharaka, 2005). Precipitates were observed mainly on clays in clay-rich shaley sections. The mudstone layers in the Precipice Sandstone may act as baffles resulting in horizontal migration of CO_2 and reaction with minerals in the base to form carbonates and clays. The low expected permeability of the mudstone would reduce rapid penetration of CO_2 or brine. It should be noted that the mudstone layers in the WW1 Precipice Sandstone around 1207 m are ~ 2 m thick with a further 2 m of interlaminated mudstone and sandstone (<1 m thick in the Chinchilla 4 core) compared to the majority of the Precipice Sandstone that is mainly quartzose with minor amounts of minerals such as muscovite.

Significant siderite cementation (max 50 %) has been observed elsewhere in the Surat Basin Westgrove Ironstone Member in core from the Chinchilla 4 well; siderite rims around chlorite have been linked to precipitation from previous CO_2 alteration of chlorite/biotite (Farquhar *et al.*, 2015). Small amounts of siderite (halos) and ankerite have also been observed in Evergreen Formation samples from the WW1 core associated with calcite cements (7-0311-0128 SP1). The precipitation of kaolinite and siderite around the lithological boundary of the reservoir-seal interface through CO_2 induced alteration of chlorite, biotite/muscovite, carbonates or feldspars has been observed in other sites with naturally high concentrations of CO_2 (Higgs *et al.*, 2013; Watson *et al.*, 2004). The study of natural analogues of CO_2 storage with SO_2 has, however, been very limited. Acid gas injection of CO_2 and H_2S mixtures has been in operation for many years by the oil and gas industry to dispose of the by-products of natural gas production, with also H_2S co-sequestration now in operation at the Hellisheidi geothermal power plant (Bachu *et al.*, 2005; Gislason *et al.*, 2010). A natural analogue of SO_2 co-injection has been reported with a geochemically different system, the Madison Limestone, in which H_2S (maximum 4.5 vol%) and dissolved sulphate and HS^- (dissolution products of SO_2) are naturally present along with supercritical CO_2 (65-95 vol%) (Kaszuba *et al.*, 2011). The sulphide and sulphate minerals pyrite and anhydrite formed in the Madison Limestone along with carbonates calcite and dolomite, and native sulphur. Recent modelling efforts in the sandstones of the North German Basin have shown that in that case low concentrations of SO_2 increase silicate dissolution and may increase or not effect carbonate mineral trapping; however, high concentrations of SO_2 resulted in more sulphate (gypsum/anhydrite) and sulphide (pyrite) mineral precipitation reducing mineral trapping of CO_2 as carbonates (Waldmann and Rütters, 2016). That work, however, focussed on lower reactivity rock reservoir sandstones rather than shale layers or clay rich cap-rock. Elsewhere, using mineralogies of Gulf Coast aquifers in the US, geochemical modelling of SO_2 co-injection predicted precipitation of the carbonates ankerite, dawsonite and siderite, with SO_2 sequestered as alunite and pyrite (Xu *et al.*, 2007). Mineral trapping by precipitation of sulphates is likely to be more rapid than precipitation of carbonates to reduce porosity as gypsum has a high molar volume and may prevent CO_2 migration. Gypsum formation for example from calcite cemented Hutton Sandstone has been observed within short experimental time scales (Pearce *et al.*, 2015a).

The use of a high concentration of dissolved Ca and bicarbonate in a saline brine replicating potential CSG waste brine co-injection with CO₂ resulted in calcite and dolomite precipitation in pore space of clean Precipice Sandstone. Geochemical modelling and more detailed discussion of this system are in the next section. Co-injecting existing components of gas streams is generally more likely to be accepted than waste disposal (Victorian Greenhouse Gas Aact). Waste water has, however, been co-injected from the Hellisheidi geothermal power plant with dissolved CO₂ (or CO₂-H₂S) storage into reactive basalt in the Carbfix and Sulfix projects to accelerate mineral trapping. Disposal of waste brines into the Precipice Sandstone would require consideration of factors such as water quality approvals, geochemical effects of dissolved oxygen in brine, and possible operational issues such as pump or injector scaling (observed during Carbfix) or loss of injectivity.

5. Model Scenarios of CO₂ Injection with Mineralisation Trapping

The analyses of the majority of carbonate veins and cements assessed have indicated that mixing between waters of different compositions took place either just prior to or else during precipitation. Seven of the samples containing suitable fluid inclusions for salinity determination held saline waters ranging from 17,000 up to 147,000 ppm NaCl equivalent. The brines themselves are likely to contain abundant ions aside from NaCl, such as Ca, Mg, Fe, Mn and K. For comparison, groundwater within the recharge zones of the northern and eastern Surat Basin generally has less than 1500 ppm NaCl (Habermehl, 2002) (and sometimes < 250 ppm (Radke et al., 2000)), whereas seawater has roughly 35,000 ppm NaCl.

To illustrate potential short-term mineral reactions that may take place within the Precipice during CO₂ sequestration, geochemical modelling was performed with the Geochemist's Workbench (GWB). The models were constrained to an area of 1 km², with good-sand thickness of 53 m (based upon downhole gamma log curve being less than 50 API). A reservoir porosity of 20 % and a constant reservoir temperature were assumed. The fugacity of CO₂ was set at 80 bar for the reservoir, and simulation time was 25 years. Script files and a modified version of the Thermo-database (developed by Dirk Kirste, Simon Fraser University), were used within the models to define the dissolution/precipitation behaviour of the base mineralogy during the simulations.

CO₂ sequestration was simulated either with groundwater (Figure 58), or with brine diluted in groundwater by about 1:12 (Figure 59). Two different reservoir mineralogies (with either K-feldspar or andesine plagioclase) were used giving a total of four models. The groundwater composition (Table 35) was based upon the average water chemistry of three samples produced from depths between 1050 and 1300 m (average temperature of 52.2°C) from two wells (Feitz *et al.*, 2014). The undiluted brine composition was broadly based upon CSG desalination brine concentrates (pers. comm. Dr Jim Undershultz, 2015). A simplification of the average XRD mineralogy of several intervals of the Precipice Sandstone in different wells, supplemented with SEM-EDS survey results, was used as the base reservoir mineralogy (Table 36).

The CO₂-sandstone-groundwater simulations produced an overall net increase in dissolved CO₂ relative to that originally injected, due to dissolution of minor calcite. There was precipitation of ankerite in each of the models (Figure 58), though not enough to off-set the loss of calcite. Ankerite is stable at relatively low pH compared with most other carbonates. Quartz and diaspore (aluminium hydroxide) were also predicted to precipitate under mildly acidic conditions in response to reaction of aluminosilicates including feldspar. Veins and nodules of ankerite and aluminium hydroxide have been observed together in sedimentary rocks, for example samples from the Prosper Haniel mine in Germany (Dawson *et al.*, 2012) that were not part of this study.

Both of the CO₂-sandstone-brine models resulted in calcite precipitation for the full 25 years of the simulations (Figure 59). Dissolution of aluminosilicate minerals occurred, as was also the case for the CO₂-sandstone-groundwater models. When andesine plagioclase was reacted in place of K-feldspar, five times more calcite and almost an order of magnitude more kaolinite was precipitated as a result of CO₂-water-rock reactions and

the alkalinity of the injected brine. The pH of the CO₂-sandstone-brine models was more alkaline than that of the groundwater models, and hence kaolinite (and less quartz) was precipitated in place of diaspore.

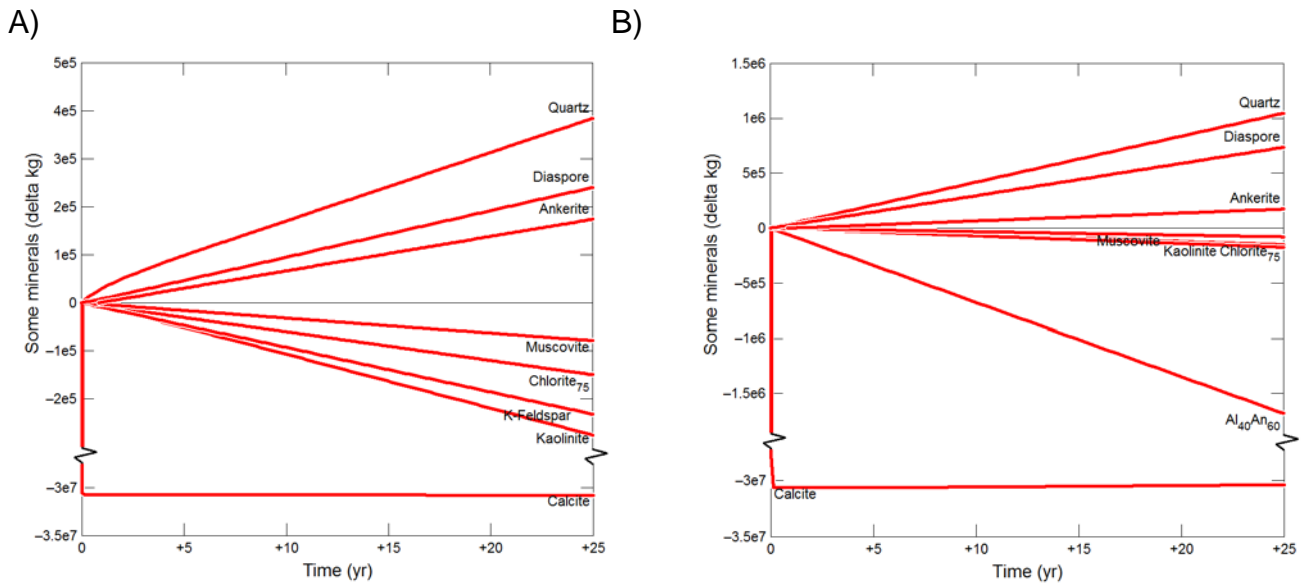


Figure 58: CO₂ reacted in groundwater with A) Precipice Sandstone model mineralogy and B) the same Precipice mineralogy in (A) with andesine plagioclase (labelled Al₄₀An₆₀) instead of K-feldspar. Vertical scale is truncated for clarity, and the y-axis scales are different to make the mineral components legible.

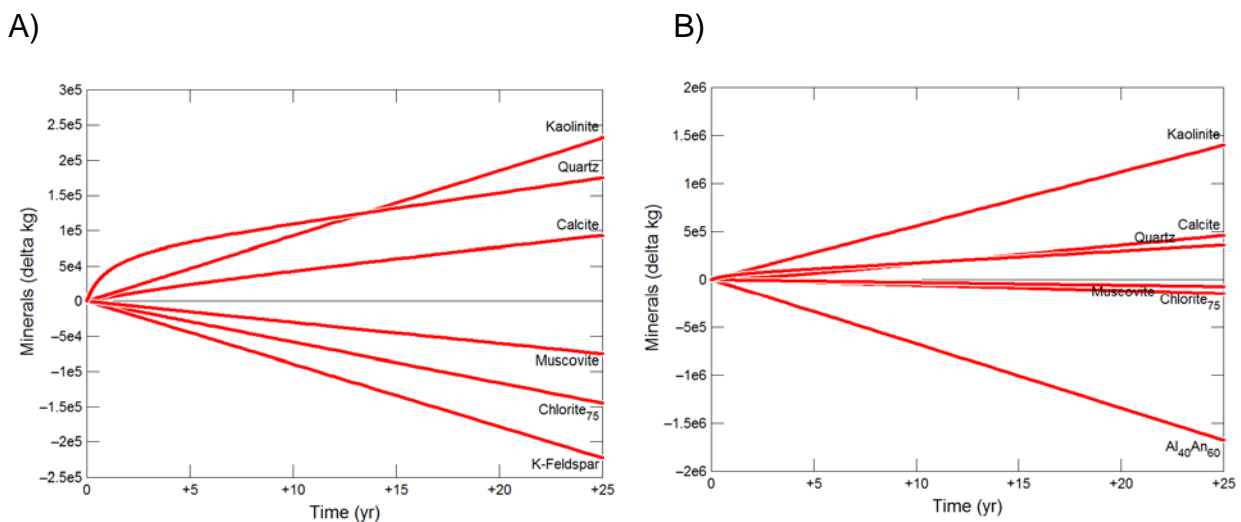


Figure 59: CO₂ reacted in a mixture of brine and groundwater with A) Precipice Sandstone model mineralogy with K-feldspar and B) the same Precipice mineralogy in (A) but with andesine plagioclase in place of K-feldspar. The y-axis scales are different to make the mineral components legible.

All model scenarios actually contained roughly the same quantity of dissolved CO₂ equivalent (a solution mixture mass-fraction of about 0.05) at the end of the modelled 25 year timeframe. Of this, up to 41MT or 43MT of CO₂ can be solubility trapped as bicarbonate anions, and up to 3.7KT or 4KT as carbonate anions, during the groundwater and brine scenarios, respectively. However, the brine scenarios contained nearly five times as much initially dissolved bicarbonate, and about forty-two times more initially dissolved divalent

cations than the groundwater scenarios. Even without any mineral reactions, if all of the dissolved divalent cations in each scenario eventually reacted with CO₂ to form carbonate minerals, the total CO₂ that could be mineral-trapped is about 13.2 MT in the brine scenario and 0.32 MT in the groundwater scenario; a roughly ten-fold difference. The net calcite precipitation observed in the brine scenarios, as opposed to net dissolution in the groundwater scenarios, was probably due to a combination of greater alkalinity and greater initial dissolved cation concentrations. The presence of reactive aluminosilicate minerals (e.g., plagioclase) also evidently enhances mineral trapping; if all plagioclase in the models actually reacted to form calcite, then up to 30.8 MT of CO₂ could ultimately be mineral trapped this way. However, in the modelled scenarios, if sufficient bicarbonate ions are not initially present then precipitation of carbonate minerals will not occur until sufficient mineral reactions have taken place to produce adequate bicarbonate ions in solution.

Table 35: Fluid parameters of the input groundwater and brine-groundwater mixtures used for GWB modelling, with the undiluted brine composition for comparison.

Aqueous components	Groundwater	Brine & groundwater mix	Brine (undiluted)	Units
H ₂ O	10,600	10,600	883	ML
CO ₂ (g)	80	80	N/A	fugacity (bar)
O ₂ (g) ↔ O ₂ (aq)	-40	-40	N/A	log fugacity
Al ³⁺	0.0001	0.0001	0	mg/Kg (ppm)
Br ⁻	0	0.3	4	
Ca ²⁺	22.4	1,041.7	12,232	
Cl ⁻	858.8	4,220	40,334	
F ⁻	0	1.1	13	
Fe ²⁺	0.053	0.11	1	
HCO ₃ ⁻	1,228.8	5,986.5	57,092	
K ⁺	23.2	23.2	265	
Mg ²⁺	2.88	56.3	676	
Mn ²⁺	0.0001	0.26	3	
Na ⁺	951	3,540.4	31,073	
SiO ₂ (aq)	24.6	24.6	295	
(SO ₄) ²⁻	0	0.33	4	
Sr ²⁺	0	0.034	0.4	

Table 36: Mineral parameters used in the GWB models.

Minerals	Mass (kg)	Mass (%)	Surface area (cm ² /g)	Initial rate constant (mol/cm ² sec)
Calcite	5.16e+08	0.46	25	5.012e-05
Chlorite	7.36e+06	0.01	70	1.622e-14
Kaolinite	3.11e+09	2.76	70	4.898e-16
Muscovite	4.84e+08	0.43	30	1.38e-16
Quartz	1.08e+11	95.79	10	3.98e-18
K-Feldspar (Precipice model)	3.17e+08	0.28	10	8.71e-15
Andesine (Models with plagioclase instead of K-feldspar)	3.17e+08	0.28	10	8.71e-15

Pore-filling kaolinite with calcite cement and quartz grain-overgrowths were common features among many samples of this study (as described elsewhere in this report), and the CO₂-sandstone-brine model results fit well with this observation. Furthermore, the precipitation of minerals observed in all modelled scenarios could also potentially serve as a mechanism for self-sealing in the event of CO₂-rich fluid migrating up into formations above the primary reservoir. Calcite, quartz and clays were observed filling faults that were sampled during this study.

6. Conclusions

The oxygen isotope values and fluid inclusion data for GAB cement and vein carbonates indicate that deeper hotter fluids mixed with shallower and fresher fluids during or just prior to carbonate precipitation in a number of cases. The migrating deeply-sourced fluids were mainly highly evolved meteoric water, though evolved basinal brines and/or fluids associated with Palaeozoic marine evaporite deposits were also implicated in the formation of some Eromanga carbonates. Most of the modelled fluid carbon isotope compositions are indicative of remobilised marine carbonate or mantle/magmatic CO₂, whereas a subset of samples had very negative modelled carbon isotopes consistent with an organic carbon source. Moreover, all but one vein and two cement samples analysed for trace elements plotted as hydrothermal carbonate on the variation diagram of Yb/Ca versus Yb/La, which was further supported by rare earth element (REE) ratios indicative of high fluid-rock ratios and the involvement of reducing acidic hydrothermal solutions. Fault-assisted fluid migration apparently played a major role in the carbonate authigenesis, and a subset of samples was associated with hydrocarbon migration.

Elevated fluid inclusion temperatures $\geq 120^{\circ}\text{C}$ in samples from wells located within the Moonie-Goondiwindi and Leichardt-Burunga fault corridor in the eastern Surat and Eromanga wells located on the Queensland-South Australia border are anomalously high relative to what is known about the regional thermal history. In this context, a reliable and reproducible analytical method was developed for the stable isotope analysis of gases trapped in fluid inclusions and applied to Eromanga Basin samples where burial history modelling was also feasible. The origin of the fluid inclusion CO₂ is likely to be a combination of Permian overmature coals and inorganic sources (e.g., mantle-derived CO₂). Carbon isotopic fractionation of the CO₂ (becomes depleted in ¹³C) has occurred most likely when carbonate minerals precipitate along the migration pathway before reaching the host rock. Gaseous hydrocarbons found in fluid inclusions in the Eromanga Basin samples are sourced from the underlying Cooper Basin. Eromanga fluid inclusion homogenisation temperatures are generally higher than maximum temperatures of the rocks hosting the fluid inclusions and within the underlying sedimentary column, suggesting that the sources of the fluids are deeper and hotter. Hydrothermal fluids from beneath the Cooper Basin pick-up Permian-sourced gaseous hydrocarbons and CO₂ along the migration pathway to the Eromanga Basin host formations. Fluid inclusion homogenisation temperatures within Eromanga Basin sediments are generally lower away from the Cooper Basin edge, suggesting longer fluid migration distances and more cooling.

The availability of cations for precipitation of dissolved CO₂ as carbonate minerals can be a rate limiting step in the process of CO₂ mineral trapping. Engineering injection to take advantage of CO₂ migration paths, e.g., injecting below baffle units and down-dip from a structural closure is one way to maximise carbonic acid dissolution of minerals encountered by the CO₂-water mixing front. Co-injecting a small quantity of SO₂ in order to form dilute sulphurous or sulphuric acid at specific depths, e.g., below baffle units, thus accelerating silicate mineral leaching within the CO₂-groundwater mixing front is another method of enhancing the dissolved cation content of the groundwater. This is similar to natural processes such as sulphate rich volcanic brine alteration. The role of SO₂ and potential mineral trapping is, however, not well understood as there are a lack of natural analogue studies targeted to volcanic processes or acid gas injection sites.

Experiments and modelling work reported here indicate the reaction of muscovite/biotite from the clay-rich mudstone baffle in the Precipice Sandstone would provide Fe and Mg for mineral trapping of CO₂ as siderite and ankerite (with precipitation of kaolinite). The co-injection of low concentrations of SO₂ with CO₂ enhanced silicate dissolution and subsequent carbonate mineral precipitation (with additionally precipitation of pyrite sequestering SO₂). In a chlorite rich section of the Hutton Sandstone, co-injection of SO₂ with CO₂ resulted in mainly alteration of chlorite with precipitation of siderite, ankerite, magnesite/dolomite and kaolinite. Dissolved metals released including Ni, Cr and Pb were subsequently sequestered in precipitated minerals in experiments. This agrees well with the observation of siderite, ankerite, kaolinite (and pyrite) precipitation from previous CO₂ alteration of minerals including chlorite, muscovite, biotite and feldspars in the vicinity of the CTSCo injection site (e.g., Chinchilla 4 and West Wandoan 1 wells).

Alternatively, direct addition of dissolved ions, for example, in the form of CSG desalination waste brine concentrate (or co-injecting CO₂ dissolved in brine or other waste water), would both increase the available cations for precipitation and potentially buffer the pH to near-neutral or even alkaline conditions if the brine was of sufficient bicarbonate content. Experiments reacting quartzose Precipice Sandstone core with CO₂ and a Ca-bicarbonate rich saline brine resulted in mineral trapping as calcite and dolomite precipitation in the pore space. Calcite, dolomite, siderite and ankerite cements have been observed from deep brine mixing processes in the GAB. Both brine mixing and SO₂ co-injection experiments indicate mineral precipitation would be enhanced if fluids moved rapidly to lower temperature and pressure regions (e.g., up faults).

7. Recommendations for Future Work

This ANLEC project has shown that the process of mineral trapping of CO₂ as carbonates has occurred naturally in sandstone reservoirs in the GAB in response to fluid mixing and fluid-rock interaction processes; however, a rate limiting step in the latter case is often the dissolution of silicates to provide the necessary divalent cations. Under conditions of high fluid flux even relatively low concentration solutions can provide sufficient cations for rapid carbonate precipitation provided that a source of carbonate anions is available. The transformation of dissolved CO₂ from carbonic acid to carbonate anions is locally accelerated by fluid-rock interactions that drive the system towards a sufficiently pH-buffered solution for carbonate formation. Mineralisation experiments on Precipice and Hutton sandstone samples representing less and more reactive lithologies in the current project indicate there is considerable potential for engineered accelerated mineralisation trapping. Avenues for further investigation include the direct addition of dissolved ions in the form of CSG waste water or desalination brine to accelerate carbonate formation, the impact of lithological variation in variably baffled reservoirs and the effects of gas compositions with low levels of impurities.

Specific recommendations for future work relevant to the Surat Demonstration Project follow:

- A more comprehensive experimental and geochemical modelling project further assessing the potential for an increase in mineral trapping by precipitation of carbonates and concurrent precipitation of clays through dissolved CO₂-water or CO₂-brine co-injection (including effects on porosity/permeability). Only a limited number of experiments and geochemical models formed part of the agreed project scope, with the bulk of the existing work having focused upon study of rocks containing historically-formed carbonate cements and veins.
- Water quality impact assessment from brine injection (including footprint of the brine from static modelling), and reactions/ reaction transport modelling to assess interaction of brine/ water with minerals such as clays resulting in ion exchange to release metals, e.g., Fe, or clay fines migration.
- An assessment of the potential for brine co-injection to induce salt precipitation reducing permeability hence injectivity in a range of core mineralogies for the site.
- Scenarios with pure CO₂ that makes outputs more generalised and easier to link to static models as well as more realistic PCC gas injection compositions (CTSCo) for experiments.

8. References

- Adamson, M., Dorsch, C., 1988. A-P 244P, SOC Deep Crossing 1, Final Well Report (#19919). QDEX - Queensland Digital Exploration Reports, Department of Natural Resources and Mines, The State of Queensland, Brisbane, Australia.
- Alexander, E.M., A., S., T.B., C., 2006. Chapter 5: Lithostratigraphy and environments of deposition., in: Cotton, T.B., Scardigno, M.F., Hibburt, J.E. (Eds.), *The Petroleum Geology of South Australia, Volume 2: Eromanga Basin.*, 2nd ed. South Australia Department of Primary Industries and Resources, Adelaide, Australia.
- Alexander, E.M., Gravestock, D.I., Cubitt, C., Chaney, A., 1998. Chapter 6: Lithostratigraphy and environments of deposition, in: Gravestock, D.I., Hibburt, J.E., Drexel, J.F. (Eds.), *The Petroleum Geology of South Australia, Volume 4: Cooper Basin.* South Australia Department of Primary Industries and Resources, Adelaide, Australia, pp. 69–115.
- Anon., 1964. Well Completion Report, LOL Saltern Creek No. 1 (# 1469), Longreach Oil Ltd, A-P 87p, QLD. QDEX - Queensland Digital Exploration Reports, Department of Natural Resources and Mines, The State of Queensland, Brisbane, Australia.
- Anon., 1982. IOL Moonie 37, Well Completion Report (#10806). QDEX - Queensland Digital Exploration Reports, Department of Natural Resources and Mines, The State of Queensland, Brisbane, Australia.
- Anon., 1984. Mirintu No. 1, Well Completion Report (# 13581), A-P 275p, QLD. QDEX - Queensland Digital Exploration Reports, Department of Natural Resources and Mines, The State of Queensland, Brisbane, Australia.
- Anon., 1991. A-P 267P, CDP Gibba 1, Well Completion Report (#23362). QDEX - Queensland Digital Exploration Reports, Department of Natural Resources and Mines, The State of Queensland, Brisbane, Australia.
- Anon., 1994. EPP 522, IOD Moonie Corner 1, Well Completion Report (#27720). QDEX - Queensland Digital Exploration Reports, Department of Natural Resources and Mines, The State of Queensland, Brisbane, Australia.
- Anon., 2001. A-P 676P, QGC Wyalla 1, Well Completion Report (#32867). QDEX - Queensland Digital Exploration Reports, Department of Natural Resources and Mines, The State of Queensland, Brisbane, Australia.
- Babaahmadi, A., Sliwa, R., Esterle, J., 2015. Understanding faults in the Surat Basin, from interpretation of seismic lines, aeromagnetic and gravity data. Report for Centre for Coal Seam Gas, The University of Queensland, Brisbane, unpublished.
- Babaahmadi, A., Sliwa, R., Esterle, J., 2016. Mapping fault lineaments in the basement of the Surat Basin from potential field data. Report for Centre for Coal Seam Gas, The University of Queensland, Brisbane, unpublished.
- Bachu, S., Haug, K., Michael, K., Buschkuehle, B., Adams, J., 2005. Deep injection of acid gas in Western Canada. *Developments in Water Science* 52, 623-635.
- Baily, T.A., 1996. A-P 548P, IOR Inland 3, Well Completion Report (#28852). QDEX - Queensland Digital Exploration Reports, Department of Natural Resources and Mines, The State of Queensland, Brisbane, Australia.

- Baker, J.C., Bai, G.P., Hamilton, P.J., Golding, S.D., Keene, J.B., 1995. Continental-scale magmatic carbon dioxide seepage recorded by dawsonite in the Bowen-Gunnedah-Sydney Basin system, eastern Australia. *Journal of Sedimentary Research* 65, 522-530.
- Balashov, Y.A., Girin, Y.P., 1969. On reserve of mobile rare earth elements in sedimentary rocks. *Geochemistry International USSR* 6.
- Balashov, Y.A., Ronov, A., Migdisov, A., Turanska, N.V., 1964. Effect of climate and facies environment on fractionation of rare earths during sedimentation. *Geochemistry International USSR*.
- Battrick, M.A., Ulmer, B., Slater, D.J., 1985. A-P 269P, HOA Bodalla South 1, Well Completion Report (#13872). QDEX - Queensland Digital Exploration Reports, Department of Natural Resources and Mines, The State of Queensland, Brisbane, Australia.
- Bau, M., Dulski, P., 1996. Distribution of yttrium and rare-earth elements in the Penge and Kuruman iron-formations, Transvaal Supergroup, South Africa. *Precambrian Research* 79, 37-55.
- Bau, M., Möller, P., 1992. Rare earth element fractionation in metamorphogenic hydrothermal calcite, magnesite and siderite. *Mineralogy and Petrology* 45, 231-246.
- Beardsmore, G., 2004. The influence of basement on surface heat flow in the Cooper Basin. *Exploration Geophysics* 35, 223-235.
- Beardsmore, G.R., Cull, J.P., 2001. *Crustal heat flow: a guide to measurement and modelling*. Cambridge University Press.
- Bhalgat, M.K., Diwu, Z., Haugland, R.P., Patton, W.F., 2006. Luminescent protein stains containing transition metal complexes. Google Patents.
- Boetius, A., Ravensschlag, K., Schubert, C.J., Rickert, D., Widdel, F., Gieseke, A., Amann, R., Jorgensen, B.B., Witte, U., Pfannkuche, O., 2000. A marine microbial consortium apparently mediating anaerobic oxidation of methane. *Nature* 407, 623-626.
- Boreham, C., Hope, J., Hartung-Kagi, B., 2001. Understanding source, distribution and preservation of Australian natural gas: A geochemical perspective. *APPEA Journal* 41, 523-547.
- Brown, N.C., 1984. Kerna 3 Well Completion Report (# 5573). PEPS - SA, Energy Resources Division, Department for Manufacturing, Innovation, Trade, Resources and Energy (DMITRE), State Government of South Australia, Adelaide, Australia.
- Burnett, P.J., Darling, R.A., 1986. A-P 267P, Eromanga Basin, PPL Winna 1, Well Completion Report (#15916). QDEX - Queensland Digital Exploration Reports, Department of Natural Resources and Mines, The State of Queensland, Brisbane, Australia.
- Callen, R.A., N.F., A., D.R., G., 1995. Lake Eyre Basin, in: Drexel, J.F., Preiss, W.V. (Eds.), *The Geology of South Australia, Volume 2, The Phanerozoic*. South Australia Geological Survey Bulletin, Adelaide, South Australia.
- Carothers, W.W., Adami, L.H., Rosenbauer, R.J., 1988. Experimental oxygen isotope fractionation between siderite-water and phosphoric acid liberated CO₂-siderite. *Geochimica et Cosmochimica Acta* 52, 2445-2450.
- Carr, L.K., Korsch, R.J., Palu, T.J., Reese, B., 2016. *Onshore Basin Inventory: the McArthur, South Nicholson, Georgina, Amadeus, Warburton, Wise, Galilee and Cooper basins*. Geoscience Australia, Canberra.

- Chaudhuri, S., Cullers, R.L., 1979. The distribution of rare-earth elements in deeply buried Gulf Coast sediments. *Chemical Geology* 24, 327-338.
- Chong, T.H., Sheikholeslami, R., 2001. Thermodynamics and kinetics for mixed calcium carbonate and calcium sulfate precipitation. *Chemical Engineering Science* 56, 5391-5400.
- Chopra, P., Holgate, F., 2005. A GIS analysis of temperature in the Australian Crust, Proceedings World Geothermal Congress, Antalya, Turkey.
- Chung, H.M., Gormly, J.R., Squires, R.M., 1988. Origins of Methane in the Earth Origin of gaseous hydrocarbons in subsurface environments: Theoretical considerations of carbon isotope distribution. *Chemical Geology* 71, 97-104.
- Clark, A.M., 1984. Chapter 2 - Mineralogy of the Rare Earth Elements, in: Henderson, P. (Ed.), *Developments in Geochemistry*. Elsevier, pp. 33-61.
- Class, H., Ebigo, A., Helmig, R., Dahle, H., Nordbotten, J., Celia, M., Audigane, P., Darcis, M., Ennis-King, J., Fan, Y., Flemisch, B., Gasda, S., Jin, M., Krug, S., Labregere, D., Naderi Beni, A., Pawar, R., Sbai, A., Thomas, S., Trenty, L., Wei, L., 2009. A benchmark study on problems related to CO₂ storage in geologic formations. *Comput Geosci* 13, 409-434.
- Clauer, N., Chaudhuri, S., 1995. *Clays in crustal environments: isotope dating and tracing*. Springer-Verlag.
- Clayton, R.N., Friedman, I., Graf, D.L., Mayeda, T.K., Meents, W.F., Shimp, N.F., 1966. The origin of saline formation waters 1. Isotopic composition. *Journal of Geophysical Research* 71, 3869-3882.
- Cohen, B., Vasconcelos, P., Knesel, K., 2007. 40Ar/39Ar constraints on the timing of Oligocene intraplate volcanism in southeast Queensland*. *Australian Journal of Earth Sciences* 54, 105-125.
- Cook, A.G., Bryan, S.E., Draper, J.J., 2013. Post-orogenic Mesozoic basins and magmatism, in: Jell, P.A. (Ed.), *Geology of Queensland*. Geological Survey of Queensland, Brisbane, Australia, pp. 515-575.
- Corbella, M., Ayora, C., Cardellach, E., 2003. Dissolution of deep carbonate rocks by fluid mixing: A discussion based on reactive transport modeling. *Journal of Geochemical Exploration* 78-79, 211-214.
- Dabney, L.R., 1965. A-P 57P, Union Oil Development Corp., Preliminary Final Report Ukaog Weringa No. 1 (# 1520). QDEX - Queensland Digital Exploration Reports, Department of Natural Resources and Mines, The State of Queensland, Brisbane, Australia.
- Dawe, R.A., Zhang, Y., 1997. Kinetics of calcium carbonate scaling using observations from glass micromodels. *Journal of Petroleum Science and Engineering* 18, 179-187.
- Dawson, G.K.W., 2012. Carbon dioxide sequestration in coal: The relationships between coal structure, texture, and mineralogy, and the role of mineral reactivity with carbonic acid, School of Earth Sciences. The University of Queensland, Brisbane, p. 235.
- Dawson, G.K.W., Biddle, D., Farquhar, S.M., Gao, J.-F., Golding, S.D., Jiang, X., Keck, R., Khan, C., Law, A.C.K., Li, Q., Pearce, J.K., Rudolph, V., Watson, A., Xing, H., 2014. ANLEC Project 7-1110-0101: Achieving Risk and Cost Reductions in CO₂ Geosequestration through 4D Characterisation of Host Formations. Final Report. ANLEC R&D, Manuka, ACT, Australia, p. 140.
- Dawson, G.K.W., Golding, S.D., Boreham, C.J., Mernagh, T., 2013. ANLEC Project 7-1011-0189: Authigenic carbonates as natural analogues of mineralisation trapping in CO₂ sequestration – Progress Report and Preliminary Results. The University of Queensland and Geoscience Australia, for ANLEC R&D and CO2CRC, Canberra, ACT, Australia, p. 68.

- Dawson, G.K.W., Golding, S.D., Esterle, J.S., Massarotto, P., 2012. Occurrence of minerals within fractures and matrix of selected Bowen and Ruhr Basin coals. *International Journal of Coal Geology* 94, 150-166.
- Dawson, G.K.W., Pearce, J.K., Biddle, D., Golding, S.D., 2015. Experimental mineral dissolution in Berea Sandstone reacted with CO₂ or SO₂-CO₂ in NaCl brine under CO₂ sequestration conditions. *Chemical Geology* 399, 87-97.
- Deighton, I., Draper, J.J., Hill, A.J., Boreham, C.J., 2003. A hydrocarbon generation model for the Cooper and Eromanga Basins. *APPEA Journal* 43, 433-451.
- Deighton, I., Hill, A., 1998. Thermal and burial history. *The Petroleum Geology of South Australia, Cooper Basin* 4, 143-155.
- Dekov, V.M., Egueh, N.M., Kamenov, G.D., Bayon, G., Lalonde, S.V., Schmidt, M., Liebetrau, V., Munnik, F., Fouquet, Y., Tanimizu, M., Awaleh, M.O., Guirreh, I., Le Gall, B., 2014. Hydrothermal carbonate chimneys from a continental rift (Afar Rift): Mineralogy, geochemistry, and mode of formation. *Chemical Geology* 387, 87-100.
- DMITRE, 2001. Seismic Mapping Data Sets over the Cooper Basin Sector, South Australia, in: Department for Manufacturing, I., Trade, Resources and Energy (DMITRE), South Australian Government (Ed.), Adelaide, Australia.
- DMITRE, 2009. Seismic Mapping Data Sets over the Cooper Basin Sector, South Australia, in: Department for Manufacturing, I., Trade, Resources and Energy (DMITRE), South Australian Government (Ed.), Adelaide, Australia.
- DNRM, 2015. Queensland Petroleum Exploration Data (QPED). Department of Natural Resources & Mines, Queensland Government, Brisbane, Australia.
- Domingo, C., Loste, E., Gómez-Morales, J., García-Carmona, J., Fraile, J., 2006. Calcite precipitation by a high-pressure CO₂ carbonation route. *The Journal of Supercritical Fluids* 36, 202-215.
- Draper, J.J., 2002. Geology of the Cooper and Eromanga Basins, Queensland, Queensland Mineral and Energy Review Series. Queensland Government, Natural Resources and Mines, Brisbane, Australia.
- Dromgoole, E.L., Walter, L.M., 1990. Iron and manganese incorporation into calcite: Effects of growth kinetics, temperature and solution chemistry. *Chemical Geology* 81, 311-336.
- DSD, 2015. PEPS-SA (Petroleum and Geothermal Attribute Database). Department of State Development, South Australia, Adelaide, Australia.
- Duan, Z., Li, D., 2008. Coupled phase and aqueous species equilibrium of the H₂O-CO₂-NaCl-CaCO₃ system from 0 to 250°C, 1 to 1000 bar with NaCl concentrations up to saturation of halite. *Geochimica et Cosmochimica Acta* 72, 5128-5145.
- Duan, Z., Sun, R., Zhu, C., Chou, I.M., 2006. An improved model for the calculation of CO₂ solubility in aqueous solutions containing Na⁺, K⁺, Ca²⁺, Mg²⁺, Cl⁻, and SO₄²⁻. *Marine Chemistry* 98, 131-139.
- Duddy, I.R., Moore, M.E., 1999. Thermal history reconstruction in Cooper-Eromanga Basin wells using Apatite and Zircon Fission Track analysis and vitrinite reflectance. Geotrack Report #668. Department of Primary Industries and Resources South Australia, Open File Envelope 8426., Adelaide, Australia.
- Dupraz, C., Reid, R.P., Braissant, O., Decho, A.W., Norman, R.S., Visscher, P.T., 2009. Processes of carbonate precipitation in modern microbial mats. *Earth-Science Reviews* 96, 141-162.

- Espiritu, E., James, A., 1999. A-P 610P, EAE Strathpine 3, Well Completion Report (#30941). QDEX - Queensland Digital Exploration Reports, Department of Natural Resources and Mines, The State of Queensland, Brisbane, Australia.
- Estensen, A., Longley, I., Griffiths, P., Knuckley, E., Batt, E., 1986. A-P 269P (1), LEA Kenmore 5, Well Completion Report (#15553). QDEX - Queensland Digital Exploration Reports, Department of Natural Resources and Mines, The State of Queensland, Brisbane, Australia.
- Etheridge, M., McQueen, H., Lambeck, K., 1991. The role of intraplate stress in tertiary (and mesozoic) deformation of the Australian continent and its margins: A key factor in petroleum trap formation. *Exploration Geophysics* 22, 123-128.
- Farquhar, S.M., 2015. CO₂-water-rock interactions in low-salinity reservoir systems, School of Earth Sciences PhD thesis. The University of Queensland, Brisbane, Australia, p. 187.
- Farquhar, S.M., Pearce, J.K., Dawson, G.K.W., Golab, A., Sommacal, S., Kirste, D., Biddle, D., Golding, S.D., 2015. A fresh approach to investigating CO₂ storage: Experimental CO₂-water-rock interactions in a low-salinity reservoir system. *Chemical Geology* 399, 98-122.
- Feitz, A., Ransley, T.R., Dunsmore, R., Kuske, T., Hodgkinson, J., Preda, M., 2014. Geoscience Australia and Geological Survey of Queensland Surat and Bowen Basins Groundwater Surveys Hydrochemistry Dataset (2009-2011), GeoCat # 78549, Canberra, ACT, Australia.
- Fergusson, C.L., 1991. Thin-skinned thrusting in the northern New England Orogen, central Queensland, Australia. *Tectonics* 10, 797-806.
- Finlayson, D.M., 1993. Crustal architecture across Phanerozoic Australia along the Eromanga-Brisbane Geoscience Transect: evolution and analogues. *Tectonophysics* 219, 191-211.
- Flaathen, T.K., Gislason, S.R., Oelkers, E.H., 2010. The effect of aqueous sulphate on basaltic glass dissolution rates. *Chemical Geology* 277, 345-354.
- Fleet, A.J., 1984. Chapter 10 - Aqueous and Sedimentary Geochemistry of the Rare Earth Elements, in: Henderson, P. (Ed.), *Developments in Geochemistry*. Elsevier, pp. 343-373.
- Foster, D.A., Murphy, J.M., Gleadow, A.J.W., 1994. Middle tertiary hydrothermal activity and uplift of the northern flinders ranges, South Australia: Insights from apatite fission-track thermochronology. *Australian Journal of Earth Sciences* 41, 11-17.
- Franks, P.C., 1969. Nature, origin, and significance of cone-in-cone structures in the Kiowa Formation (Early Cretaceous), north-central Kansas. *Journal of Sedimentary Research* 39, 1438-1454.
- Freeman, R.N., 1967. A-P 117P, Area 1, OOC Maryvale 1, Final Report (#2068). QDEX - Queensland Digital Exploration Reports, Department of Natural Resources and Mines, The State of Queensland, Brisbane, Australia.
- French, J.V., 1989. BUO Denbigh Downs 1, Well Completion Report (#17999). QDEX - Queensland Digital Exploration Reports, Department of Natural Resources and Mines, The State of Queensland, Brisbane, Australia.
- GA, 2013. Three-dimensional visualisation of the Great Artesian Basin. Geoscience Australia, Canberra.
- GA, 2015. National Petroleum Wells Database, viewed 27/04/2015, in: Australia, G. (Ed.), Canberra, Australia.

- Gislason, S.R., Wolff-Boenisch, D., Stefansson, A., Oelkers, E.H., Gunnlaugsson, E., Sigurdardottir, H., Sigfusson, B., Broecker, W.S., Matter, J.M., Stute, M., Axelsson, G., Fridriksson, T., 2010. Mineral sequestration of carbon dioxide in basalt: A pre-injection overview of the CarbFix project. *International Journal of Greenhouse Gas Control* 4, 537-545.
- Golding, S.D., Boreham, C.J., Esterle, J.S., 2013a. Stable isotope geochemistry of coal bed and shale gas and related production waters: A review. *International Journal of Coal Geology* 120, 24-40.
- Golding, S.D., Collerson, K.D., Uysal, I.T., Glikson, M., Baublys, K.A., Zhao, J.-X., 2000. Nature and source of carbonate mineralization in Bowen Basin coals, eastern Australia., in: Glikson, M., Mastalerz, M. (Eds.), *Organic Matter and Mineralisation: Thermal Alteration, Hydrocarbon Generation and Role in Metallogenesis*. Kluwer Academic Publishers, London, pp. 296-313.
- Golding, S.D., Dawson, G.K.W., Boreham, C.J., Mernagh, T., 2013b. ANLEC Project 7-1011-0189: Authigenic carbonates as natural analogues of mineralisation trapping in CO₂ sequestration – A desktop study. UQ, GA, ANLEC R&D and CO2CRC, Manuka, ACT, Australia, p. 47.
- Golding, S.D., Dawson, G.K.W., Mernagh, T., Boreham, C.J., 2014. ANLEC Project 7-1011-0189: Authigenic carbonates as natural analogues of mineralisation trapping in CO₂ sequestration - Progress Report 3. The University of Queensland and Geoscience Australia, for ANLEC R&D and CO2CRC, Canberra, ACT, Australia, p. 118.
- Golding, S.D., Uysal, I.T., Bolhar, R., Boreham, C.J., Dawson, G.K.W., Baublys, K.A., Esterle, J.S., 2013c. Carbon dioxide-rich coals of the Oaky Creek area, central Bowen Basin: a natural analogue for carbon sequestration in coal systems. *Australian Journal of Earth Sciences*, 1-16.
- Gradstein, F.M., Ogg, J.G., Schmitz, M.D., Ogg, G.M., 2012. *The Geologic Time Scale, Volumes 1 & 2*. Elsevier BV, p. 1144.
- Graf, J.L., 1977. Rare earth elements as hydrothermal tracers during the formation of massive sulfide deposits in volcanic rocks. *Economic Geology* 72, 527-548.
- Gravestock, D.I., Griffiths, M., Hill, A., 1983. The Hutton Sandstone – Two separate reservoirs in the Eromanga Basin – South Australia. *APPEA Journal* 23, 109-119.
- Gravestock, D.I., Jensen-Schmidt, B., 1998. Chapter 5: Structural setting, in: Gravestock, D.I., Hibburt, J.E., Drexel, J.F. (Eds.), *The Petroleum Geology of South Australia, Volume 4: Cooper Basin*. South Australia Department of Primary Industries and Resources, Adelaide, Australia, pp. 47–67.
- Gray, A.R.G., McKellar, J.L., 2002. Cooper Basin stratigraphy, *Geology of the Cooper and Eromanga Basins, Queensland*. Queensland Minerals and Energy Review Series. Department of Natural Resources and Mines, Queensland Government, Brisbane, Australia, pp. 9–26.
- Gray, A.R.G., McKillop, M., McKellar, J.L., 2002. Eromanga Basin Stratigraphy, in: Draper, J.J. (Ed.), *Geology of the Cooper and Eromanga Basins, Queensland*. Queensland Department of Natural Resources and Mines, Queensland Minerals and Energy Review Series, Brisbane, Australia, pp. 30–56.
- Green, D.C., 1963. Phillips Sunray QLD American, Kogan South 1, Well Completion Report (#1026). QDEX - Queensland Digital Exploration Reports, Department of Natural Resources and Mines, The State of Queensland, Brisbane, Australia.

- Haak, K.J., 1999. PI 59, SSL Challum 9, well completion report (# 31449). QDEX - Queensland Digital Exploration Reports, Department of Natural Resources and Mines, The State of Queensland, Brisbane, Australia.
- Habermehl, M., 2002. Hydrogeology, hydrochemistry and isotope hydrology of the Great Artesian Basin. GAB Fest.
- Hall, L.S., Boreham, C.J., Edwards, D.S., Palu, T.J., Buckler, T., Hill, A., Troup, A., 2015a. Cooper Basin Source Rock Geochemistry: Regional Hydrocarbon Prospectivity of the Cooper Basin, Part 2. Record 2015/xx. Geoscience Australia, Canberra.
- Hall, L.S., Hill, A.J., Palu, T., Boreham, C., Edwards, D., Troup, A., Wang, L., 2015b. Petroleum Systems Modelling for Petroleum Prospectivity Analysis in the Cooper Basin, Australia, AAPG/SEG International Conference & Exhibition, Melbourne, Australia.
- Hall, L.S., Hill, A.J., Troup, A., Korsch, R., Radke, B., Nicoll, R.S., Palu, T., Wang, L., Stacey, A., 2015c. Cooper Basin Architecture and Lithofacies: Regional Hydrocarbon Prospectivity of the Cooper Basin, Part 1. Record 2015/xx. Geoscience Australia, Canberra.
- Hall, L.S., Hill, A.J., Wang, L., Edwards, D., Kuske, T., Troup, A., Boreham, C., 2015d. Petroleum Systems Modelling for Unconventional Play Analysis in the Cooper Basin., AAPG/SEG International Conference & Exhibition, Melbourne, Australia.
- Hall, R., Gagen, S., 1989. AMX Widnerpool 1, Well Completion Report (#20102). QDEX - Queensland Digital Exploration Reports, Department of Natural Resources and Mines, The State of Queensland, Brisbane, Australia.
- Harrison, J., Higginbotham, G.T., 1964. Gidgealpa 1 Well Completion Report (# 363). PEPS - SA, Energy Resources Division, Department for Manufacturing, Innovation, Trade, Resources and Energy (DMITRE), State Government of South Australia, Adelaide, Australia.
- Henderson, P., 1984. Chapter 1 - General Geochemical Properties and Abundances of the Rare Earth Elements, in: Henderson, P. (Ed.), *Developments in Geochemistry*. Elsevier, pp. 1-32.
- Herrmann, A.G., 1978. Yttrium and lanthanides, in: Wedepohl, K.W. (Ed.), *Handbook of Geochemistry*. Springer-Verlag, Berlin, Germany, pp. 57-71-A to 57-71-O.
- Higgs, K.E., Funnell, R.H., Reyes, A.G., 2013. Changes in reservoir heterogeneity and quality as a response to high partial pressures of CO₂ in a gas reservoir, New Zealand. *Marine and Petroleum Geology* 48, 293-322.
- Higgs, K.E., Haese, R.R., Golding, S.D., Schacht, U., Watson, M.N., 2015. The Pretty Hill Formation as a natural analogue for CO₂ storage: An investigation of mineralogical and isotopic changes associated with sandstones exposed to low, intermediate and high CO₂ concentrations over geological time. *Chemical Geology* 399, 36-64.
- Hoefs, J., 1987. *Stable Isotope Geochemistry*. Springer-Verlag, Berlin.
- Hoffmann, K.L., 1989. The influence of pre-Jurassic tectonic regimes on the structural development of the southern Eromanga Basin, Queensland., in: O'Neil, B.J. (Ed.), *The Cooper and Eromanga Basins, Australia*. . Proceedings of the Petroleum Exploration Society of Australia. Society of Petroleum Engineers, Australian Society of Exploration Geophysicists (SA Branches), Adelaide, Australia., pp. 315–328.

- Holgate, F.L., Gerner, E.J., 2010. OzTemp Well Temperature Data, in: Australia, G. (Ed.), Canberra.
- Humphris, S.E., 1984. Chapter 9 - The Mobility of the Rare Earth Elements in the Crust, in: Henderson, P. (Ed.), *Developments in Geochemistry*. Elsevier, pp. 317-342.
- IPCC, 2005. Special report on carbon dioxide capture and storage. Technical report, intergovernmental Panel on Climate Change (IPCC), prepared by Working Group III.
- James, A.T., 1983. Correlation of natural gas by use of carbon isotopic distribution between hydrocarbon components. *AAPG bulletin* 67, 1176-1191.
- James, A.T., 1990. Correlation of Reservoired Gases Using the Carbon Isotopic Compositions of Wet Gas Components (1). *AAPG bulletin* 74, 1441-1458.
- Jenkins, C.C., 1984. DIO Yanda 1, Well Completion Report, A-P 259P (#13483). QDEX - Queensland Digital Exploration Reports, Department of Natural Resources and Mines, The State of Queensland, Brisbane, Australia.
- Jimenez-Lopez, C., Romanek, C.S., 2004. Precipitation kinetics and carbon isotope partitioning of inorganic siderite at 25°C and 1 atm. *Geochimica et Cosmochimica Acta* 68, 557-571.
- Kampman, N., Bickle, M., Wigley, M., Dubacq, B., 2014. Fluid flow and CO₂-fluid-mineral interactions during CO₂-storage in sedimentary basins. *Chemical Geology* 369, 22-50.
- Kaszuba, J.P., Navarre-Sitchler, A., Thyne, G., Chopping, C., Meuzelaar, T., 2011. Supercritical carbon dioxide and sulfur in the Madison Limestone: A natural analog in southwest Wyoming for geologic carbon-sulfur co-sequestration. *Earth and Planetary Science Letters* 309, 131-140.
- Kennett, B., Salmon, M., Saygin, E., AusMoho_Working_Group, 2011. AusMoho: the variation of Moho depth in Australia. *Geophysical Journal International* 187, 946-958.
- Kharaka, Y.K., Cole, D.R., Hovorka, S.D., Gunter, W.D., Knauss, K.G., Freifeld, B.M., 2006. Gas-water-rock interactions in Frio Formation following CO₂ injection: Implications for the storage of greenhouse gases in sedimentary basins. *Geology* 34, 577-580.
- Knauer, K., Delbaere, M., 1992. A-P 374P Block A, Surat Basin, PSA Strathpine 1, Well Completion Report (#24344). QDEX - Queensland Digital Exploration Reports, Department of Natural Resources and Mines, The State of Queensland, Brisbane, Australia.
- Knesel, K.M., Cohen, B.E., Vasconcelos, P.M., Thiede, D.S., 2008. Rapid change in drift of the Australian plate records collision with Ontong Java plateau. *Nature* 454, 754-757.
- Kuske, T., Hall, L., Hill, T., Troup, A., Edwards, D., Boreham, C., Buckler, T., 2015. Source Rocks of the Cooper Basin., AAPG/SEG International Conference & Exhibition, Melbourne, Australia.
- Kyranis, N., 1963. A-P 71P, Kogan 1, Well Completion Report (#1006). QDEX - Queensland Digital Exploration Reports, Department of Natural Resources and Mines, The State of Queensland, Brisbane, Australia.
- Laing, A.C.M., 1966. A-P 98P, QLD, AOD Yongala 1, Well Completion Report (#2017). QDEX - Queensland Digital Exploration Reports, Department of Natural Resources and Mines, The State of Queensland, Brisbane, Australia.
- Laing, A.C.M., 1967. A-P 98P, AOD Yongala 2, Well Completion Report (#2257). QDEX - Queensland Digital Exploration Reports, Department of Natural Resources and Mines, The State of Queensland, Brisbane, Australia.

- Large, R.R., Bull, S.W., Winefield, P.R., 2001. Carbon and Oxygen Isotope Halo in Carbonates Related to the McArthur River (HYC) Zn-Pb-Ag Deposit, North Australia: Implications for Sedimentation, Ore Genesis, and Mineral Exploration. *Economic Geology* 96, 1567-1593.
- Lawrence, M., Greig, A., Collerson, K., Kamber, B., 2006. Rare Earth Element and Yttrium Variability in South East Queensland Waterways. *Aquat Geochem* 12, 39-72.
- Liu, Q., Maroto-Valer, M.M., 2011. Parameters affecting mineral trapping of CO₂ sequestration in brines. *Greenhouse Gases: Science and Technology* 1, 211-222.
- Longley, I.M., Batt, E., 1985a. A-P 269P, HOA Bodalla South 2, Well Completion Report (#14142). QDEX - Queensland Digital Exploration Reports, Department of Natural Resources and Mines, The State of Queensland, Brisbane, Australia.
- Longley, I.M., Batt, E., 1985b. A-P 269P, HOA Mount Bellalie 1, Well Completion Report (#14566). QDEX - Queensland Digital Exploration Reports, Department of Natural Resources and Mines, The State of Queensland, Brisbane, Australia.
- Lowman, R., 2003a. PL 1, SSL Moonie 40, Well Completion Report (#35693). QDEX - Queensland Digital Exploration Reports, Department of Natural Resources and Mines, The State of Queensland, Brisbane, Australia.
- Lowman, R., 2003b. PL 1, SSL Moonie 41, Well Completion Report (# 35552). QDEX - Queensland Digital Exploration Reports, Department of Natural Resources and Mines, The State of Queensland, Brisbane, Australia.
- Lumsden, D.N., Shipe, L.G., Lloyd, R.V., 1989. Mineralogy and Mn geochemistry of laboratory-synthesized dolomite. *Geochimica et Cosmochimica Acta* 53, 2325-2329.
- Mackenzie, F.T., Lerman, A., Mackenzie, F., 2006. Mineralogy, chemistry, and reaction kinetics of the major carbonate phases, *Carbon in the geobiosphere — Earth's outer shell —*. Springer Netherlands, pp. 89-121.
- Mathur, S.P., 1983. Deep crustal reflection results from the central Eromanga Basin, Australia. *Tectonophysics* 100, 163-173.
- Mavromatidis, A., 2006. Burial/exhumation histories for the Cooper–Eromanga Basins and implications for hydrocarbon exploration, Eastern Australia. *Basin Research* 18, 351-373.
- Mavromatidis, A., Hillis, R., 2005. Quantification of exhumation in the Eromanga Basin and its implications for hydrocarbon exploration. *Petroleum Geoscience* 11, 79-92.
- McCrea, J.M., 1950. On the isotopic chemistry of carbonates and a paleotemperature scale. *The Journal of Chemical Physics* 18, 849-857.
- McKellar, J.L., 2013. The Cooper Basin, in: Jell, P.A. (Ed.), *Geology of Queensland*. Geological Survey of Queensland, Brisbane, Australia, pp. 204–212.
- McLaren, S., James Dunlap, W., 2006. Use of ⁴⁰Ar/³⁹Ar K-feldspar thermochronology in basin thermal history reconstruction: an example from the Big Lake Suite granites, Warburton Basin, South Australia. *Basin Research* 18, 189-203.
- Meixner, A., Holgate, F., Australia, G., 2009. *The Cooper Basin Region 3D Map Version 1: A Search for Hot Buried Granites*. Geoscience Australia.

- Meixner, A.J., Kirkby, A.L., Lescinsky, D.T., Horspool, N., 2012. The Cooper Basin 3D Map Version 2: Thermal Modelling and Temperature Uncertainty. Record 2012/60. Geoscience Australia, Canberra.
- Middleton, A., Uysal, I.T., Golding, S., Förster, H.-J., Allen, C., Feng, Y., Rhede, D., Marshall, V., van Zyl, J., 2014a. Geochronological (U–Pb, U–Th–total Pb, Sm–Nd) and geochemical (REE, $^{87}\text{Sr}/^{86}\text{Sr}$, $\delta^{18}\text{O}$, $\delta^{13}\text{C}$) tracing of intraplate tectonism and associated fluid flow in the Warburton Basin, Australia. *Contributions to Mineralogy and Petrology* 168, 1-22.
- Middleton, A.W., Uysal, I.T., Golding, S.D., 2014b. Chemical and mineralogical characterisation of illite–smectite: Implications for episodic tectonism and associated fluid flow, central Australia. *Geochimica et Cosmochimica Acta*.
- Middleton, M.F., 1979. Heat flow in the Moomba, Big lake and Toolachee gas fields of the Cooper Basin and implications for hydrocarbon maturation. *Exploration Geophysics* 10, 149-155.
- Mineyev, D., 1963. Geochemical differentiation of the rare earths. *Geochemistry* 12, 1129-1149.
- Mitchell, A.C., Dideriksen, K., Spangler, L.H., Cunningham, A.B., Gerlach, R., 2010. Microbially enhanced carbon capture and storage by mineral-trapping and solubility-trapping. *Environmental Science & Technology* 44, 5270-5276.
- Möller, P., 1983. Lanthanoids as a Geochemical Probe and Problems in Lanthanoid Geochemistry Distribution and Behaviour of Lanthanoids in Non-Magmatic-Phases, Systematics and the properties of the Lanthanides. Springer, pp. 561-616.
- Möller, P., Bau, M., 1993. Rare-earth patterns with positive cerium anomaly in alkaline waters from Lake Van, Turkey. *Earth and Planetary Science Letters* 117, 671-676.
- Moore, P.S., 1981. DIO Morney 1, Well Completion Report (#9551). QDEX - Queensland Digital Exploration Reports, Department of Natural Resources and Mines, The State of Queensland, Brisbane, Australia.
- Moussavi-Harami, R., 1996a. Burial history, in: Alexander, E.M., Hibbert, J.E. (Eds.), *Petroleum Geology of South Australia. Volume 2: Eromanga Basin*. South Australia Department of Mines and Energy, pp. 125–140.
- Moussavi-Harami, R., 1996b. Burial history of the Cooper Basin region in South Australia. *PESA Journal* 24, 57–76.
- Moussavi-Harami, R., 1996c. Burial history of the Cooper, Eromanga and Lake Eyre Basins in northeast South Australia. South Australia Department of Mines and Energy, Open file Envelope 9024.
- Mucci, A., 1988. Manganese uptake during calcite precipitation from seawater: Conditions leading to the formation of a pseudokutnahorite. *Geochimica et Cosmochimica Acta* 52, 1859-1868.
- Nance, W.B., Taylor, S.R., 1976. Rare earth element patterns and crustal evolution—I. Australian post-Archean sedimentary rocks. *Geochimica et Cosmochimica Acta* 40, 1539-1551.
- Nelson, G.C., Carey, H., Radke, B.M., Ransley, T.R., 2012. The three-dimensional visualisation of the Great Artesian Basin. A report to the Australian Government from the CSIRO Great Artesian Basin Water Resource Assessment. CSIRO Water for a Healthy Country Flagship, Australia.
- NGMA, 2001. National Geoscience Mapping Accord (NGMA) in: Cooper and Eromanga Basins, A., seismic mapping data sets. Custodian – Department for Manufacturing, Innovation, Trade, Resources and Energy (DMITRE) on behalf of the NGMA (Ed.). South Australian Government, Adelaide, Australia.

- Nguyen, D.L., Carmody, J.G., Gurney, E.H., 1996. EPP 565, ANU Green Swamp 1, Well Completion Report (#27926). QDEX - Queensland Digital Exploration Reports, Department of Natural Resources and Mines, The State of Queensland, Brisbane, Australia
- O'Brien, G.W., Lisk, M., Duddy, I.R., Hamilton, J., Woods, P., Cowley, R., 1999. Plate convergence, foreland development and fault reactivation: Primary controls on brine migration, thermal histories and trap breach in the Timor Sea, Australia. *Marine and Petroleum Geology* 16, 533-560.
- O'Neil, J.R., Clayton, R.N., Mayeda, T.K., 1969. Oxygen isotope fractionation in divalent metal carbonates. *Journal of Chemical Physics* 51, 5547-5559.
- O'Neill, G.J., 1985. Muteroo 1 Well Completion Report (# 6291). PEPS - SA, Energy Resources Division, Department for Manufacturing, Innovation, Trade, Resources and Energy (DMITRE), State Government of South Australia, Adelaide, Australia.
- Ohmoto, H., Rye, R.O., 1979. Isotopes of sulfur and carbon, in: Barnes, H.L. (Ed.), *Geochemistry of Hydrothermal Ore Deposits*, 2nd ed. John Wiley & Sons, New York, pp. 509-567.
- Ostler, S., 1989. Spencer West 1 Well Completion Report (# 7223/6). PEPS - SA, Energy Resources Division, Department for Manufacturing, Innovation, Trade, Resources and Energy (DMITRE), State Government of South Australia, Adelaide, Australia.
- Palandri, J.L., Kharaka, Y.K., 2004. A compilation of rate parameters of water-mineral interaction kinetics for application to geochemical modelling. US Geological Survey Open File Report 2004-1068, pp. 1-64.
- Palandri, J.L., Kharaka, Y.K., 2005. Ferric iron-bearing sediments as a mineral trap for CO₂ sequestration: Iron reduction using sulfur-bearing waste gas. *Chemical Geology* 217, 351-364.
- Parker, A., Rae, J.E., 1998. *Environmental Interactions of Clays: Clays and the Environment*. Springer Science & Business Media.
- Pearce, J.K., Farquhar, S.M., Dawson, G.K.W., Golding, S.D., 2014. Final Report: Geochemical reactivity and dissolution trapping capacity using supercritical CO₂. Prepared for FEI Lithicon Australia.
- Pearce, J.K., Farquhar, S.M., Dawson, G.K.W., Golding, S.D., 2015a. Final Report – Geochemical Reactivity and Dissolution Trapping Capacity using Supercritical CO₂, Uniquist report for FEI-Lithicon and ANLEC R&D.
- Pearce, J.K., Golding, S.D., Frank, A., Kirste, D., 2013a. SO_x and O₂ Co-contaminant impacts in geological carbon storage. CO₂CRC Report, RPT13-4173.
- Pearce, J.K., Golding, S.D., Frank, A.B., Kirste, D., 2013b. SO_x, O₂ and NO_x Co-contaminant Impacts on Geological Carbon Storage (CO₂CRC Report # RPT13-4173). CO₂CRC (Canberra, Australia), The University of Queensland (Brisbane, Australia), and Simon Fraser University (Burnaby, Canada).
- Pearce, J.K., Kirste, D., Dawson, G.K.W., Golding, S.D., Farquhar, S.M., 2015b. Project 1.5.3 Geochemical Impacts of SO₂ and O₂ Co-contaminants (impurities) in CO₂ storage, CO₂CRC report, p. 42.
- Pearce, J.K., Kirste, D.M., Dawson, G.K.W., Farquhar, S.M., Biddle, D., Golding, S.D., Rudolph, V., 2015c. SO₂ impurity impacts on experimental and simulated CO₂-water-reservoir rock reactions at carbon storage conditions. *Chemical Geology* 399, 65-86.
- Peuble, S., Godard, M., Luquot, L., Andreani, M., Martinez, I., Gouze, P., 2015. CO₂ geological storage in olivine rich basaltic aquifers: New insights from reactive-percolation experiments. *Applied Geochemistry* 52, 174-190.

- Pyle, D.E., 1965a. A-P 57P, QLD, Union - Kern - AOG Bennett 1, Well Completion Report (#1828). QDEX - Queensland Digital Exploration Reports, Department of Natural Resources and Mines, The State of Queensland, Brisbane, Australia.
- Pyle, D.E., 1965b. A-P 57P, QLD, Union - Kern - AOG Davidson 1, Well Completion Report (#1700). QDEX - Queensland Digital Exploration Reports, Department of Natural Resources and Mines, The State of Queensland, Brisbane, Australia.
- Pyle, D.E., 1966a. A-P 57P, QLD, Union - Kern - AOG Bennett 2, Well Completion Report (#1836). QDEX - Queensland Digital Exploration Reports, Department of Natural Resources and Mines, The State of Queensland, Brisbane, Australia.
- Pyle, D.E., 1966b. A-P 57P, QLD, Union - Kern - AOG Sussex Downs 1, Well Completion Report (#2018). QDEX - Queensland Digital Exploration Reports, Department of Natural Resources and Mines, The State of Queensland, Brisbane, Australia
- Pyle, D.E., Carey, A.R., Jack Jr., J.E., 1963. A-P 57P, QLD, Union - Kern - AOG Southwood 1, Well Completion Report (#1113). QDEX - Queensland Digital Exploration Reports, Department of Natural Resources and Mines, The State of Queensland, Brisbane, Australia.
- Pyle, D.E., Dabney, L.R., 1963. A-P 57P, UOD Moonie 13, Well Completion Report (#1106). QDEX - Queensland Digital Exploration Reports, Department of Natural Resources and Mines, The State of Queensland, Brisbane, Australia.
- Radke, B., 2009. Hydrocarbon and Geothermal Prospectivity of Sedimentary Basins in Central Australia Warburton, Cooper, Pedirka, Galilee, Simpson and Eromanga Basins. Geoscience Australia, Canberra, Australia.
- Radke, B.M., Ferguson, J., Cresswell, R.G., Ransley, T.R., Habermehl, M.A., 2000. Hydrochemistry and implied hydrodynamics of the Cadna-owie – Hooray Aquifer, Great Artesian Basin, Australia, in: Sciences, B.o.R. (Ed.), Canberra, ACT, p. 229.
- Radke, B.M., Kellett, J.R., Ransley, T.R., J.G., B., 2012. Lexicon of the lithostratigraphic and hydrogeological units of the Great Artesian Basin and its Cenozoic cover. A technical report to the Australian Government from the CSIRO Great Artesian Basin Water Resource Assessment. CSIRO Water for a Healthy Country Flagship, Australia.
- Raza, A., Hill, K.C., Korsch, R.J., 2009. Mid-Cretaceous uplift and denudation of the Bowen and Surat Basins, eastern Australia: Relationship to Tasman Sea rifting from apatite fission-track and vitrinite-reflectance data. *Australian Journal of Earth Sciences* 56, 501-531.
- Rigby, D., Smith, J., 1981. An isotopic study of gases and hydrocarbons in the Cooper Basin. *Australian Petroleum Exploration Association Journal* 21, 222-229.
- Roldalset, E., Rosenqvist, I.T., 1971. Rare earth elements in vivianite from Lake Åstrum. *Lithos* 4, 417-421.
- Robbie, S.M., Mitchell, J.A., 1996. PL 31, OCA Bodalla South 9, Well Completion Report (#28847). QDEX - Queensland Digital Exploration Reports, Department of Natural Resources and Mines, The State of Queensland, Brisbane, Australia.
- Roberts, J.A., Bennett, P.C., González, L.A., Macpherson, G., Milliken, K.L., 2004. Microbial precipitation of dolomite in methanogenic groundwater. *Geology* 32, 277-280.

- Rollet, N., Logan, G., Kennard, J., O'Brien, P., Jones, A., Sexton, M., 2006. Characterisation and correlation of active hydrocarbon seepage using geophysical data sets: An example from the tropical, carbonate Yampi Shelf, Northwest Australia. *Marine and Petroleum Geology* 23, 145-164.
- Rosenbaum, J., Sheppard, S.M.F., 1986. An isotopic study of siderites, dolomites and ankerites at high temperatures. *Geochimica et Cosmochimica Acta* 50, 1147-1150.
- Rudnick, R., Gao, S., 2003. Composition of the continental crust. *Treatise on geochemistry* 3, 1-64.
- Salomon, J.A., Short, D.A., Singley, W., 1990. PL 32, LEA Kenmore 12, Well Completion Report (#22042). QDEX - Queensland Digital Exploration Reports, Department of Natural Resources and Mines, The State of Queensland, Brisbane, Australia.
- Saunders, A.D., 1984. Chapter 6 - The Rare Earth Element Characteristics of Igneous Rocks from the Ocean Basins, in: Henderson, P. (Ed.), *Developments in Geochemistry*. Elsevier, pp. 205-236.
- Schulz-Rojahn, J., 1993. Calcite-cemented zones in the Eromanga Basin: Clues to petroleum migration and entrapment? *APEA Journal* 33, 63-63.
- Sharma, T., Clayton, R.N., 1965. Measurement of O 18 O 16 ratios of total oxygen of carbonates. *Geochimica et Cosmochimica Acta* 29, 1347-1353.
- Shaw, R.D., 1991. Tertiary structuring in southwest Queensland: implications for petroleum exploration. *Exploration Geophysics* 22, 339-344.
- Sheppard, S., Schwarcz, H., 1970. Fractionation of carbon and oxygen isotopes and magnesium between coexisting metamorphic calcite and dolomite. *Contributions to Mineralogy and Petrology* 26, 161-198.
- Shulgin, L., Kozmin, Y.A., 1963. Kinetics of the oxidation reduction reaction-Europium (III)-Europium (II). *Mezhdunarodnaya Kniga* 39 Eimitrova UL., 113095 Moscow, Russia, pp. 1857-1859.
- Slijderink, P., 1998. A-P 259P, SSL Ghina 1, Well Completion Report (#30876). QDEX - Queensland Digital Exploration Reports, Department of Natural Resources and Mines, The State of Queensland, Brisbane, Australia.
- Sliwa, R., 2015. Surat Cumulative Management Area Hydrostratigraphic Model. Report for OGISA, unpublished.
- Smerdon, B.D., Ransley, T.R., 2012. Water resource assessment for the Central Eromanga region. A report to the Australian Government from the CSIRO Great Artesian Basin Water Resource Assessment. CSIRO Water for a Healthy Country Flagship, Australia, Australia.
- Smerdon, B.D., Ransley, T.R., Radke, B.M., Kellett, J.R., 2012. Water resource assessment for the Great Artesian Basin. A report to the Australian Government from the CSIRO Great Artesian Basin Water Resource Assessment. CSIRO Water for a Healthy Country Flagship, Australia.
- Sohn, J.H., Boreham, C.J., Chen, J.H., Wintle, C., Mernagh, T., Dawson, G.K.W., Golding, S.D., 2014. On-line analyses of isotopic composition of fluid inclusion gases., AOGC2014: the 18th Australian Organic Geochemistry Conference: Life, Environments and Resources, Adelaide, Australia, p. 2pp.
- Spycher, N., Pruess, K., 2005. CO₂-H₂O mixtures in the geological sequestration of CO₂. 2 Partitioning in chloride brines at 12 to 100°C and up to 600 bar. *Geochimica et Cosmochimica Acta* 69, 3309-3320.
- Spycher, N., Pruess, K., Ennis-King, J., 2003. CO₂-H₂O mixtures in the geological sequestration of CO₂. 1 Assessment and calculation of mutual solubilities from 12 - 100°C and up to 600 bar. *Geochimica et Cosmochimica Acta* 67, 3015-3031.

- Stewart, A.J., Raymond, O.L., Totterdell, J.M., Zhang, W., Gallagher, R., 2013. Australian Geological Provinces, 2013.01 ed. Geoscience Australia, Canberra, Australia.
- Stumm, W., Morgan, J., 1970. Aquatic chemistry, New York, USA.
- Summers, C.A., Dahlin, D.C., Ochs, T.L., 2004. The effect of SO₂ on mineral carbonation in batch tests, 29th International Technical Conference on Coal Utilization & Fuel Systems, April 18-22, 2004. Coal Technology Association, Gaithersburg, MD, USA, Clearwater, Florida.
- Sun, X., Camac, B., 2004. Cooper Basin Electrofacies Mapping. SA Department of State Development, Resources and Energy.
- Surka, E., Rouse, K.R., 1984. HEP Tintaburra No. 1, A-P 299P (A), QLD, Well Completion Report (#13029). QDEX - Queensland Digital Exploration Reports, Department of Natural Resources and Mines, The State of Queensland, Brisbane, Australia.
- Taylor, B.W., 1985. Gidgealpa 18 Well Completion Report (# 5856). PEPS - SA, Energy Resources Division, Department for Manufacturing, Innovation, Trade, Resources and Energy (DMITRE), State Government of South Australia, Adelaide, Australia.
- Taylor, S.R., McClellan, S.M., 1985. The Continental Crust: Its Composition and Evolution. Blackwell Scientific Publications.
- Thornton, D.A., 1984. A-P 259P, QLD, DIO Challum 1 Well Completion Report (#13528). QDEX - Queensland Digital Exploration Reports, Department of Natural Resources and Mines, The State of Queensland, Brisbane, Australia.
- Thornton, D.A., Elliott, P., 1982. A-P 259P, DIO Tartulla 1, Well Completion Report (# 10810). QDEX - Queensland Digital Exploration Reports, Department of Natural Resources and Mines, The State of Queensland, Brisbane, Australia.
- Titheridge, D., 2010. A-P 788P, PAN Duke S3, Well Completion Report (#63747). QDEX - Queensland Digital Exploration Reports, Department of Natural Resources and Mines, The State of Queensland, Brisbane, Australia.
- Tolliday, R.G., How, T., 1986. HPP Brigalow 1, Well Completion Report (#12502). QDEX - Queensland Digital Exploration Reports, Department of Natural Resources and Mines, The State of Queensland, Brisbane, Australia.
- Toupin, D., Eadington, P.J., Person, M., Morin, P., Wieck, J.M., Warner, D., 1997. Petroleum hydrogeology of the Cooper and Eromanga basins, Australia; some insights from mathematical modeling and fluid inclusion data. AAPG Bulletin 81, 577-603.
- Turner, D.R., Whitfield, M., 1979. Control of seawater composition. Nature 281, 468-469.
- Uysal, I.T., Golding, S.D., Bolhar, R., Zhao, J.-x., Feng, Y.-x., Baublys, K.A., Greig, A., 2011. CO₂ degassing and trapping during hydrothermal cycles related to Gondwana rifting in eastern Australia. Geochimica et Cosmochimica Acta 75, 5444-5466.
- Uysal, I.T., Golding, S.D., Glikson, M., 2000. Petrographic and isotope constraints on the origin of authigenic carbonate minerals and the associated fluid evolution in Late Permian coal measures, Bowen Basin (Queensland), Australia. Sedimentary Geology 136, 189-206.

- Uysal, I.T., Zhao, J.-X., Golding, S.D., Lawrence, M.G., Glikson, M., Collerson, K.D., 2007. Sm-Nd dating and rare-earth element tracing of calcite: Implications for fluid-flow events in the Bowen Basin, Australia. *Chemical Geology* 238, 63-71.
- Van Lith, Y., Warthmann, R., Vasconcelos, C., McKenzie, J.A., 2003. Sulphate-reducing bacteria induce low-temperature Ca-dolomite and high Mg-calcite formation. *Geobiology* 1, 71-79.
- Vasconcelos, C., McKenzie, J.A., Bernasconi, S., Grujic, D., Tiens, A.J., 1995. Microbial mediation as a possible mechanism for natural dolomite formation at low temperatures. *Nature* 377, 220-222.
- Veevers, J.J., Conaghan, P.J., 1984. Phanerozoic earth history of Australia. Oxford University Press, USA.
- Vincent, P., Mortimore, I., McKirdy, D., 1985. Hydrocarbon generation, migration and entrapment in the Jackson–Naccowlah area, ATP 259P, southwestern Queensland. *Australian Petroleum Exploration Association Journal* 25, 62-84.
- Wajon, J.E., Ho, G.-E., Murphy, P.J., 1985. Rate of precipitation of ferrous iron and formation of mixed iron-calcium carbonates by naturally occurring carbonate materials. *Water Research* 19, 831-837.
- Waldmann, S., Rütters, H., 2016. Geochemical effects of SO₂ during CO₂ storage in deep saline reservoir sandstones of Permian age (Rotliegend) – A modeling approach. *International Journal of Greenhouse Gas Control* 46, 116-135.
- Wall, V.J., 1987. Hydrocarbon reservoir quality in the Cooper/Eromanga Basins. Final report, NERDDC Project No. 808 (ref 84/4067). Department of Earth Sciences, Monash University (unpublished).
- Watson, M.N., Gibson-Pool, C.M., 2005. Reservoir Selection for Optimised Geological Injection and Storage of Carbon Dioxide: A Combined Geochemical and Stratigraphic Perspective, Proceedings of the Forth Annual Conference on Carbon Capture and Sequestration, Alexandria, Virginia.
- Watson, M.N., Zwingmann, N., Lemon, N.M., 2004. The Ladbroke Grove–Katnook carbon dioxide natural laboratory: A recent CO₂ accumulation in a lithic sandstone reservoir. *Energy* 29, 1457-1466.
- Whiteway, T., 2009. Australian Bathymetry and Topography Grid, June 2009. Geoscience Australia, Canberra.
- Wigley, T.M.L., Plummer, L.N., 1976. Mixing of carbonate waters. *Geochimica et Cosmochimica Acta* 40, 989-995.
- Wildeman, T.E., Condie, K.C., 1973. Rare earths in Archean graywackes from Wyoming and from the Fig Tree Group, South Africa. *Geochimica et Cosmochimica Acta* 37, 439-453.
- Wildeman, T.R., Haskin, L.A., 1973. Rare earths in Precambrian sediments. *Geochimica et Cosmochimica Acta* 37, 419-438.
- Wopfner, H., Callen, R., Harris, W.K., 1974. The lower tertiary Eyre Formation of the Southwestern great Artesian basin. *Journal of the Geological Society of Australia* 21, 17-51.
- Wright, D.T., 1999. The role of sulphate-reducing bacteria and cyanobacteria in dolomite formation in distal ephemeral lakes of the Coorong region, South Australia. *Sedimentary Geology* 126, 147-157.
- Wright, D.T., Wacey, D., 2005. Precipitation of dolomite using sulphate-reducing bacteria from the Coorong Region, South Australia: Significance and implications. *Sedimentology* 52, 987-1008.
- Wycherley, H., Fleet, A., Shaw, H., 1999. Some observations on the origins of large volumes of carbon dioxide accumulations in sedimentary basins. *Marine and Petroleum Geology* 16, 489-494.

Wygrala, B., 1989. Integrated study of an oil field in the southern Po basin, northern Italy. Publikationen vor 2000.

Xu, T., Apps, J.A., Pruess, K., Yamamoto, H., 2007. Numerical modeling of injection and mineral trapping of CO₂ with H₂S and SO₂ in a sandstone formation. *Chemical Geology* 242, 319-346.

Zuddas, P., Mucci, A., 1998. Kinetics of calcite precipitation from seawater: II. The influence of the ionic strength. *Geochimica et Cosmochimica Acta* 62, 757-766.

Zuddas, P., Pachana, K., Faivre, D., 2003. The influence of dissolved humic acids on the kinetics of calcite precipitation from seawater solutions. *Chemical Geology* 201, 91-101.

Appendix 1: Samples collected

The samples are sorted into table according to basin, well, and depth, and are given a broad lithology code for the purpose of helping to distinguish between different contexts of carbonate mineralisation: S is sandstone, I is interbedded sandstone/siltstone/mudstone, M is mudstone/siltstone with possibly minor sandstone laminations in part, and C is coal seams. Codes with an additional letter hyphenated after them are intervals which include additional lithologies of note, namely L for thin limestone layers picked in well logs (incidentally only observed for cuttings samples) and C for the presence of coal chips/layers. The thickness of carbonate cemented intervals, or context of vein mineralisation, is also provided. The most significant cemented intervals (greater than 300 feet net calcite-cemented sandstone) are highlighted in yellow.

Table A1.1: Queensland Eromanga Basin brief sample descriptions.

Sample #	Well	Depth (m unless specified)	Formation	Lithology ^a	Brief notes	Carbonate cemented zone thickness (m) [*]	Sample Type
285	Blackall 1	195.52-196.6	Allaru Mudstone	I	Roughly layer aligned calcite vein swarm.	Veins & sporadic fault associated cement	Core
127	Blackall 1	622.35-622.6	Hooray (Namur) Sandstone	S	Calcite vein/s within subvertical fractures in calcite cemented zone, coalified plant fossils.	20 m (8 m net)	Core
89	Blackall 1	622.79-622.89	Hooray (Namur) Sandstone	S	Subvertical fractures in calcite cemented zone, coalified plant fossils.	20 m (8 m net)	Core
90	Blackall 1	773.16-773.24	Birkhead Formation	S	Calcite vein/fault fill.	Veins & sporadic fault associated cement	Core
91	Blackall 2	311.68-311.94	Allaru Mudstone	I	4 cm thick calcite fault infill. Interval has cone-in-cone(?), calcite frags, shells.	Sporadic and frac associated	Core
92	Blackall 2	313.54-313.61	Allaru Mudstone	I	Calcite vein and cement.	Sporadic and frac associated	Core
154	Blackall 2	314.47-314.48	Allaru Mudstone	I	Calcite veins/fault?	Sporadic and frac associated	Core
93	Blackall 2	314.6-314.61	Allaru Mudstone	I	Calcite vein 5 mm, near horizontal.	Sporadic and frac associated	Core
95	Blackall 2	444.51-444.565	Allaru Mudstone	M	Contorted "fibrous" calcite veins, also veining in frags. Shells present in interval.	Sporadic and frac associated	Core
94	Blackall 2	443.7-443.77	Allaru Mudstone	M	Calcite faults/veins.	Sporadic and frac associated	Core
96	Blackall 2	474.19-474.36	Allaru Mudstone	M	1.5 cm thick fault calcite with radiating veins. Interval has concretions and possibly cone-in-cone.	Sporadic and frac associated	Core
125	Blackall 2	474.93-475.08	Allaru Mudstone	M	Large calcite fault/veins.	Sporadic and frac associated	Core
97	Blackall 2	475.88-476.02	Allaru Mudstone	I	Calcite fault fill, veins, other mineralised fractures with minor offsets, possibly cone-in-cone and concretion calcite? Maybe ammonite shells in interval, mainly pyritised.	Sporadic and frac associated	Core
286	Blackall 2	606.855 - 606.91	Allaru Mudstone	I	5 mm thick horizontal calcite vein.	65 m, shells present, but also frac associated cement.	Core
98	Blackall 2	660.38-660.54	Toolebuc Formation	I	Large veins with shiny black minerals (phosphates etc.) and calcite. Shells in interval mostly pyritised. Some fish spines, pyritised worm burrows, pyrite nodules.	110 m (98 m net carbonate presence, 28 m net sandstone laminations) and also frac associated	Core

Sample #	Well	Depth (m unless specified)	Formation	Lithology ^a	Brief notes	Carbonate cemented zone thickness (m) [*]	Sample Type
99	Blackall 2	665.71-665.73	Wallumbilla Formation	M	Large calcite veins.	Sporadic and frac associated	Core
287	Blackall 2	713.2-713.24	Wallumbilla Formation	M	Horizontally sheared thick layer parallel calcite veins (up to 1.5 cm)	Sporadic and frac associated	Core
295	Blackall 2	798.805-798.92	Wallumbilla Formation	I	Fault with radiating calcite veins, most carrot shaped and oriented with thickest part up towards fault, which seems to be sealing against a more impermeable rock e.g., black carb mud.		Core
155	Blackall 2	809.5-809.56	Wallumbilla Formation	M	Fault calcite cement/veins?	Sporadic calcite fracture fill and cement.	Core
100	Blackall 2	811.46-811.47	Wallumbilla Formation	M	Calcite vein horizontal? Near fault/small intrusion?	Sporadic and frac associated	Core
300	Blackall 2	812.9-813	Wallumbilla Formation	M	Faulted green-grey clastic(?) dyke with very thin calcite veins potentially associated with horizontal veining (about 1 cm thick) which appears to have been partially infiltrated by dyke material.	Sporadic and frac associated	Core
298	Blackall 2	833.725-833.84	Cadna-Owie Formation	S	Fault (multisurface) with crack-seal calcite veins, at least one thick (5 mm), and associated cement in sandstone.	Sporadic and frac associated	Core
63	Bodalla South 2	150'	Winton Formation	I	Very abundant calcite.	64 m (30.5 m net) (210 ft (100 ft net))	Cuttings
51	Bodalla South 9	1596	Hutton Sandstone	S-C	Common brown calcite cement.	73 m (59.5 m net)	Cuttings
52	Bodalla South 9	1617	Hutton Sandstone	S	Common brown calcite cement.	73 m (59.5 m net)	Cuttings
248	Challum 9	6208'1.5"- 6208'5"	Hutton Sandstone	S	Minor calcite cement	Sporadic	Core
249	Challum 9	6208'11"- 6209'3.5"	Hutton Sandstone	S	Minor calcite cement	Sporadic	Core
102	Connemara 1	119.76-119.87	Winton Formation	S	Calcite cement & sporadic mud rip-up clasts, minor coal at 130 m.	Sporadic	Core
124	Connemara 1	310.71-311	Mackunda Formation	S	Calcite veins	Sporadic and frac associated	Core
148	Connemara 1	311.75-311.82	Mackunda Formation	S	Calcite veins	Sporadic and frac associated	Core
123	Connemara 1	371.72-371.83	Allaru Mudstone	I	Calcite veining and cone-in-cone, cement, shells	Sporadic and frac associated	Core
149	Connemara 1	390-390.18	Allaru Mudstone	S	Calcite veins, microfaults?	Sporadic and frac associated	Core
150	Connemara 1	391.88-392	Allaru Mudstone	I	Calcite veins	Sporadic and frac associated	Core
126	Connemara 1	395.4-395.5	Allaru Mudstone	S	Calcite veins, cement, microfaults?	Sporadic and frac associated	Core
158	Connemara 1	448.83-448.87	Allaru Mudstone	I	Calcite veins and cement	Sporadic and frac associated	Core
101	Connemara 1	450.2-450.21	Allaru Mudstone	I	Vein calcite (actually also ~ 50% aragonite) and cement near faults with clay infill	Sporadic and frac associated	Core
159	Connemara 1	673.45-673.48	Wallumbilla Formation	M	Calcite infill? Cone-in-cone	Sporadic and frac associated	Core
103	Connemara 1	942.17-942.37	Westbourne Formation	S	Calcite cement, mud rip-up clasts.	40 m (30 m net)	Core
106	Connemara 1	944.6-944.7	Westbourne Formation	S	Calcite cement	40 m (30 m net)	Core
104	Connemara 1	945.04-945.16	Westbourne Formation	S	Calcite cement	40 m (30 m net)	Core
105	Connemara 1	946.24-946.34	Westbourne Formation	S	Calcite cement	40 m (30 m net)	Core
1	Inland 3	4430'-4440'	Birkhead Formation	I	Calcite & apparently siderite cement, some siliceous	19 m (13 m net) (62 ft (43 ft net))	Cuttings
64	Inland 3	5570'-5580'	Hutton Sandstone	S	Siderite and calcite cement, siliceous in part	65 m (61.5 m net) (214 ft (202 ft net))	Cuttings

Sample #	Well	Depth (m unless specified)	Formation	Lithology ^a	Brief notes	Carbonate cemented zone thickness (m)	Sample Type
79	Jackson South 2	4279'5"-4280'2"	Westbourne Formation	I	Oil stained, calcite cement, veins, some siderite	Sporadic	Core
78	Jackson South 2	4279'6.5"-4279'9"	Westbourne Formation	I	Oil stained, siderite layer, calcite cement, veins	Sporadic	Core
77	Jackson South 2	4279'9"-4280'2"	Westbourne Formation	I	Oil stained, calcite cement, veins, some siderite	Sporadic	Core
107	Jundah 1	795.59-795.75	Cadna-Owie Formation	I	Calcite veins	Sporadic and frac associated	Core
108	Jundah 1	905.67-905.673	Hooray (Namur) Sandstone	S	Strong calcite cement associated with calcite filled faults and other fractures. Also cone-in-cone calcite. Coalified plant fossils.	50 m (34 m net), fault-zone	Core
109	Jundah 1	906.46-906.58	Hooray (Namur) Sandstone	S	Strong calcite cement associated with calcite filled faults and other fractures. Also cone-in-cone calcite. Coalified plant fossils.	50 m (34 m net), fault-zone	Core
110	Jundah 1	939.62-939.68	Hooray (Namur) Sandstone	S	Calcite cement. Interval has 20 cm fault zone at 953.69 m	50 m (34 m net), fault zone	Core
111	Jundah 1	940.48-940.58	Hooray (Namur) Sandstone	S	Calcite cement. Interval has 20 cm fault zone at 953.69 m	50 m (34 m net), fault zone	Core
112	Jundah 1	941.52-941.7	Hooray (Namur) Sandstone	S	Calcite veins, cement	50 m (34 m net), fault zone	Core
65	Kenmore 12	510	Mackunda Formation	S-L	Strong calcite cement, but apparently frequent limestone layers too	410 m (60 m net)	Cuttings
66	Kenmore 12	920	Wallumbilla Formation	I	Strong calcite cement, some siliceous, glauconite	30 m (8 m net)	Cuttings
56	Kenmore 12	1075	Cadna-Owie	I	Strong calcite cement, apparently dolomite frags	90 m (55 m net)	Cuttings
57	Kenmore 12	1350	Birkhead	I	Strong calcite cement below minor limestone, minor siliceous	195 m (135 m net)	Cuttings
3	Mirintu-1	677.6 (A1)	Cadna-Owie Formation	S	Lower of two layers of calcite fault-fill	30 m (15 m net), with veins and faults	Core
4	Mirintu-1	677.6 (A2)	Cadna-Owie Formation	S	Upper of two layers of calcite fault-fill	30 m (15 m net), with veins and faults	Core
2	Mirintu-1	696	Cadna-Owie Formation	S	Faults filled with calcite, sometimes two or possibly more layers	30 m (15 m net), with veins and faults	Core
6	Mirintu-1	675.29-675.33	Cadna-Owie Formation	S	Calcareous cement probably associated with faults	30 m (15 m net), with veins and faults	Core
5	Mirintu-1	680.36-680.395	Cadna-Owie Formation	S	Calcite fault fill, veins, and associated calcite cemented sandstone	30 m (15 m net), with veins and faults	Core
277	Mitchell 1	697.7-697.77	Evergreen Formation	I	45 degree fault with 5 mm thick calcite.	Sporadic and frac associated	Core
7	Saltern Creek 1	1651'2"-4"	Namur Sandstone	S	Calcite cement	Sporadic	Core
152	Thargomindah 1A	966.86-967.12	Adori Sandstone	S	Calcite veins/faults? cement	10 m (5 m net)	Core
113	Thargomindah 1A	970.18-970.28	Adori Sandstone	S	Calcite cement cut by calcite mineralised subvertical veins, also heavy mineral concentrations present along bedding laminations	10 m (5 m net)	Core
114	Thargomindah 2	409.02-409.12	Mackunda Formation	S	Some cone-in-cone nearby	Sporadic calcite fracture fill and cement.	Core
153	Thargomindah 2	409.66-409.73	Mackunda Formation	S	Calcite veins	Sporadic calcite fracture fill and cement.	Core
151	Thargomindah 2	454-454.03	Allaru Mudstone	I	Calcite veins	Sporadic calcite fracture fill and cement.	Core
115	Thargomindah 2	544.14-544.26	Allaru Mudstone	M	Brecciated zones, calcite cemented sandstone and fractures and cone-in-cone, shells. Calcite mixed with grey mud. Pyrite present.	Sporadic calcite fracture fill and cement.	Core
116	Thargomindah 2	556.31-556.37	Allaru Mudstone	M	Cone-in-cone? Calcite faults and veins in frags, concretions, shells. Calcite mixed with grey mud.	Sporadic calcite fracture fill and cement.	Core

Sample #	Well	Depth (m unless specified)	Formation	Lithology ^a	Brief notes	Carbonate cemented zone thickness (m)*	Sample Type
117	Thargomindah 2	560.86-560.96	Allaru Mudstone	I	Clay fault fill? Calcite veins.	Sporadic calcite fracture fill and cement.	Core
157	Thargomindah 2	576.18-576.29	Allaru Mudstone	I	Calcite veins	Sporadic and frac associated	Core
118	Thargomindah 2	956.38-956.44	Cadna-Owie Formation	S	Calcite cement.	25 m (16 m net)	Core
119	Thargomindah 2	998.44-998.52	Cadna-Owie Formation	S	Calcite cement sporadic and/or frac associated, bounded by faults over 1.3 m at 997 m	Sporadic calcite fracture fill and cement.	Core
120	Thargomindah 3	1115.47-1115.53	Hooray (Namur) Sandstone	S	Calcite cement associated with slicks and microfaults	15 m (7 m net)	Core
160	Thargomindah 3	1119.4-1119.45	Hooray (Namur) Sandstone	I	Fault gouge (non-carbonate)	Sporadic and frac associated	Core
121	Thargomindah 3	1171.58-1171.74	Hooray (Namur) Sandstone	I	Calcite cement associated with slicks and faults	10 m (5 m net)	Core
58	Widnerpool 1	559-562	Wallumbilla Formation	I-L	Calcite cement, near thin limestone	Sporadic	Cuttings
59	Widnerpool 1	862-865	Westbourne Formation	S	Calcite cement	75 m (60 m net)	Cuttings
8	Winna-1	1008.08-1008.12	Murta Fm.	S-C	Good oil shows, moderate siliceous and strong calcite cement, <1 mm coal wisps	42 m (11 m net)	Core
9	Yongala 1	2500'-2510'	Mackunda Formation	S	Calcite cement	128 m (82 m net) (420 ft (270 ft net))	Cuttings

*S = sandstone, I = interbedded sandstone/siltstone/mudstone, M = mudstone/siltstone sometimes with minor thin sandstone layers in part, C = coal, L = potential thin limestone layer/s within interval.

Table A1.2: South Australia Eromanga Basin brief sample descriptions.

Sample #	Well	Depth (m unless specified)	Formation	Lithology ^a	Brief notes	Carbonate cemented zone thickness (m)	Sample Type
169	Burke 002	5063'7"	Murta	S	Oil show, calcite cement, microfaulting	131 m (52 m net) (430 ft (170 ft net))	Core
165	Dullingari 036	4883'3"	Murta	I	Oil, calcite cement, 350 feet below limestone	21 m (6 m net) (70 ft (20 ft net))	Core
167	Dullingari 037	5065'8.5"	Murta	I	Calcite cement	91 m (61 m net) (300 ft (200 ft net))	Core
173	Dullingari 037	5068'8"	Murta	I	Calcite cement and siderite	91 m (61 m net) (300 ft (200 ft net))	Core
171	Dullingari 039	5024'9"	Murta	S	Calcite cement, 20 ft below oil show, 70 ft above limestone	76 m (42.5 m net) (250 ft (140 ft net))	Core
215	Gidgealpa 18	5000'	Namur Sandstone	S-C	Uncemented, minor coal frags	N/A	Cuttings
216	Gidgealpa 18	5300'	Namur Sandstone	S-C	Poor oil show, uncemented, minor coal frags	N/A	Cuttings
187	Gidgealpa 18	5510'	Namur Sandstone	S-C	Calcite cement, coal frags	Sporadic	Cuttings
188	Gidgealpa 18	5540'	Namur Sandstone	S-C	Calcite cement, minor coal frags	Sporadic	Cuttings
189	Gidgealpa 18	5580'	Namur Sandstone	S-C	Calcite cement, coal frags	97.5 m (73 m net) (320 ft (240 ft net))	Cuttings
190	Gidgealpa 18	5620'	Namur Sandstone	S-C	Calcite cement	97.5 m (73 m net) (320 ft (240 ft net))	Cuttings
192	Gidgealpa 18	5650'	Namur Sandstone	S	Calcite cement	97.5 m (73 m net) (320 ft (240 ft net))	Cuttings
191	Gidgealpa 18	5700'	Birkhead Formation	S-C	Minor coal frags	97.5 m (73 m net) (320 ft (240 ft net))	Cuttings
217	Gidgealpa 18	5900'	Hutton Sandstone	S-C	10 ft below oil show, uncemented, coal frags	N/A	Cuttings
218	Gidgealpa 18	6100'	Hutton Sandstone	S-C	Minor coal frags and calcite	Sporadic	Cuttings
166	Jena 2	3882'9"	Murta	I	Oil show, calcite cement & veins	135.5 m (42.5 m net) 445 ft (140 ft net)	Core
170	Jena 6	3934'1"	Murta	I	Oil show, calcite cement and siderite	99 m (33.5 m net) 325 ft (110 ft net)	Core
186	Kerna 3	5220'	Namur Sandstone	S-C	Calcite cement & coal frags	67 m (39.5 m net) (220 ft (130 ft net))	Cuttings
210	Kerna 3	5350'	Namur Sandstone	S	Calcite cement & some coal frags	Sporadic	Cuttings
211	Kerna 3	5410'	Namur Sandstone	S-C	Uncemented, coal frags	N/A	Cuttings
212	Kerna 3	5480'	Namur Sandstone	S-C	Apparently calcite cement (was dolomite in XRD) & some coal frags	Sporadic	Cuttings
181	Kerna 3	5500'	Namur Sandstone	S-C	Apparently calcite cement (dolomite in XRD) & coal frags	67 m (220 ft)	Cuttings
182	Kerna 3	5640'	Namur Sandstone	S	Calcite cement	67 m (220 ft)	Cuttings
183	Kerna 3	5700'	Namur Sandstone	S-C	Calcite cement & coal frags	67 m (220 ft)	Cuttings
184	Kerna 3	5750'	Namur Sandstone	S-C	Calcite cement & coal frags	Sporadic	Cuttings
185	Kerna 3	5880'	Namur Sandstone	S	Calcite cement	32 m (30.5 m net) (105 ft (100 ft net))	Cuttings
213	Kerna 3	6150'	Hutton Sandstone	S-C	Uncemented, coal frags	N/A	Cuttings
214	Kerna 3	6230'	Hutton Sandstone	S-C	Uncemented, coal frags	N/A	Cuttings
163	Marabooka 004	3433'	Oodnadatta	S	Calcite cement and veins, 100 feet above and 350 feet below limestone	15 m (9 m net) (50 ft (30 ft net))	Core
162	Merrimelia 32	6064'1.5" - 6064'5"	Birkhead Formation	S	Oil, calcite and siderite cement	30.5 m (15 m net) (100 ft (50 ft net))	Core

Sample #	Well	Depth (m unless specified)	Formation	Lithology ^a	Brief notes	Carbonate cemented zone thickness (m)	Sample Type
233	Merrimelia 32	6038'3"-6038'4"	Birkhead Formation	C	Conjugate faulted coal	Sporadic	Core
225	Muteroo 1	4820'	Namur Sandstone	S-C	Siderite apparently (not in XRD)	N/A	Cuttings
226	Muteroo 1	4930'	Namur Sandstone	S-C	Uncemented, minor coal frags	N/A	Cuttings
227	Muteroo 1	5120'	Namur Sandstone	S	Siderite	Sporadic	Cuttings
200	Muteroo 1	5150'	Namur Sandstone	S	Calcite cement & siderite	15 m (12 m net) (50 ft (40 ft net))	Cuttings
203	Muteroo 1	5240'	Namur Sandstone	S	Calcite cement & apparently siderite (not in XRD), coal frags	65.5 m (58 m net) (215 ft (190 ft net))	Cuttings
201	Muteroo 1	5290'	Namur Sandstone	S	Calcite cement & apparently siderite (not in XRD)	65.5 m (58 m net) (215 ft (190 ft net))	Cuttings
202	Muteroo 1	5350'	Namur Sandstone	S	Calcite cement & apparently siderite (not in XRD)	65.5 m (58 m net) (215 ft (190 ft net))	Cuttings
228	Muteroo 1	5400'	Namur Sandstone	I-C	Calcite cement, coal & apparently siderite (not in XRD)	65.5 m (58 m net) (215 ft (190 ft net))	Cuttings
229	Muteroo 1	5700'	Hutton Sandstone	S-C	Siderite apparently (not in XRD) & minor coal	N/A	Cuttings
230	Muteroo 1	5760'	Hutton Sandstone	S-C	Siderite apparently (not in XRD) & minor coal	N/A	Cuttings
231	Muteroo 1	6000'	Hutton Sandstone	S	Siderite apparently (not in XRD) & minor coal	Sporadic	Cuttings
232	Muteroo 1	6170'	Hutton Sandstone	S	Oil show, dolomite, siderite and rare coal frags	Sporadic	Cuttings
172	Narcoonowie 004	4382'5"	Murta	I	Minor calcite cement near oil shows	131 m (61 m net) (430 ft (200 ft net))	Core
164	Narcoonowie 004	4395'	Murta	S	5 feet below oil, calcite cement and veins	131 m (61 m net) (430 ft (200 ft net))	Core
199	Spencer West 1	4500'	Namur Sandstone	I	Calcite cement & siderite	131 m (61 m net) (430 ft (200 ft net))	Cuttings
219	Spencer West 1	4630'	Namur Sandstone	S-C	Uncemented, rare coal frags	N/A	Cuttings
193	Spencer West 1	4820'	Namur Sandstone	S	Calcite cement	129.5 m (97.5 m net) (425 ft (320 ft net))	Cuttings
194	Spencer West 1	4870'	Namur Sandstone	I	Calcite cement	129.5 m (97.5 m net) (425 ft (320 ft net))	Cuttings
195	Spencer West 1	4910'	Namur Sandstone	S	Calcite cement	129.5 m (97.5 m net) (425 ft (320 ft net))	Cuttings
196	Spencer West 1	4950'	Namur Sandstone	S	Calcite cement	129.5 m (97.5 m net) (425 ft (320 ft net))	Cuttings
197	Spencer West 1	5000'	Namur Sandstone	S	Calcite cement	129.5 m (97.5 m net) (425 ft (320 ft net))	Cuttings
198	Spencer West 1	5050'	Namur Sandstone	S	Calcite cement	129.5 m (97.5 m net) (425 ft (320 ft net))	Cuttings
220	Spencer West 1	5130'	Namur Sandstone	S	Minor calcite cement	Sporadic	Cuttings
221	Spencer West 1	5400'	Hutton Sandstone	S-C	Uncemented, rare coal frags	N/A	Cuttings
222	Spencer West 1	5500'	Hutton Sandstone	S-C	Uncemented, coal frags	N/A	Cuttings
223	Spencer West 1	5600'	Hutton Sandstone	S-C	Uncemented, rare coal frags	N/A	Cuttings
224	Spencer West 1	5700'	Hutton Sandstone	S-C	Uncemented, rare coal frags	N/A	Cuttings
174	Strzelecki 015	4750'	Namur Sandstone	I	Trace oil show, minor calcite	79 m (42 m net) (260 ft (138 ft net))	Cuttings
205	Strzelecki 015	4950'	Namur Sandstone	S-C	Uncemented, coal frags	N/A	Cuttings
175	Strzelecki 015	5050'	Namur Sandstone	S	Trace oil show, minor calcite	134 m (128 m net) (440 ft (420 ft net))	Cuttings
176	Strzelecki 015	5120'	Namur Sandstone	S-C	Trace oil show, minor calcite and coal frags	134 m (128 m net) (440 ft (420 ft net))	Cuttings
177	Strzelecki 015	5210'	Namur Sandstone	S-C	Trace oil show, minor calcite and coal frags	134 m (128 m net)	Cuttings

Sample #	Well	Depth (m unless specified)	Formation	Lithology ^a	Brief notes	Carbonate cemented zone thickness (m)	Sample Type
						(440 ft (420 ft net))	
178	Strzelecki 015	5300'	Namur Sandstone	S	Calcite cement, near trace oil show	134 m (128 m net) (440 ft (420 ft net))	Cuttings
179	Strzelecki 015	5380'	Namur Sandstone	S	Calcite cement	134 m (128 m net) (440 ft (420 ft net))	Cuttings
180	Strzelecki 015	5430'	Namur Sandstone	S-C	Calcite cement & coal frags	134 m (128 m net) (440 ft (420 ft net))	Cuttings
206	Strzelecki 015	5500'	Birkhead Formation	I-C	Oil, coal chips and minor calcite	Sporadic	Cuttings
207	Strzelecki 015	5600'	Hutton Sandstone	S-C	Trace oil show, uncemented, coal frags	N/A	Cuttings
208	Strzelecki 015	5750'	Hutton Sandstone	S-C	Uncemented, coal frags	N/A	Cuttings
209	Strzelecki 015	5850'	Hutton Sandstone	I-C	Uncemented, coal frags	N/A	Cuttings
204	Strzelecki 015	6275'7.5"	Toolachee	C	Coal (for vRo)	N/A	Core
168	Ulandi 5	3914'10"	Cadna-Owie	I	Oil show, calcite cement and siderite	61 m (24 m) (200 ft (80 ft net))	Core

^aS = sandstone, I = interbedded sandstone/siltstone/mudstone, M = mudstone/siltstone sometimes with minor thin sandstone layers in part, C = coal, L = potential thin limestone layer/s within interval.

Table A1.3: Queensland Surat Basin brief sample descriptions.







Sample #	Well	Depth (m unless specified)	Formation	Lithology ^a	Brief notes	Carbonate cemented zone thickness (m)	Sample Type
82	Alton 3	6066'-6066'6"	Evergreen Formation	S	Calcite cement, oil show, 100 feet above minor coal	Sporadic	Core
35	Brigalow 1	890	Rolling Downs Group	I	Calcite and glauconite cement	73 m (23.5 m net) (240 ft (77 ft net))	Cuttings
74	Cameron 1	120.27	Springbok Sandstone	S-C	Sandstone with calcite cement and siderite containing minor coal seam.	Sporadic	Core
85	Cameron 1	147.91-148	Springbok Sandstone	S	Calcite cement. Interval has siderite nodules up to 1 cm (not this sample), 10 m below and 15 m above coal.	5 m (4.5 m net)	Core
156	Cameron 1	230.7-230.92	Walloon Coal Measures	I	Calcite veins	Sporadic and frac associated	Core
84	Cameron 1	230-230.22	Walloon Coal Measures	M	Calcite cement and veins. Lots of solid calcite and reactive clays present.	Sporadic calcite fracture fill and cement.	Core
161	Chinchilla 4	650.45 m	Winton Formation	I	Interval has calcite, siderite, micro-faults, veins, cone-in-cone, coal cleat.	Sporadic calcite fracture fill and cement, siderite.	Core
10	Chinchilla 4	799.6	Hutton Sandstone	S	Calcite cement, 10 m above micro-faulted veined interval.	Sporadic, probably fault related	Core
76	Chinchilla 4	1032.68-1032.73	Evergreen Formation	I	Calcite cement and in fault plane, siderite also	Sporadic calcite fracture fill and cement.	Core
75	Chinchilla 4	1101.11-1101.34	Adori Sandstone	I	Calcite veins in sandstone near fault in siltstone	Sporadic calcite fracture fill and cement.	Core
36	Davidson 1	5440'-5450'	Hutton Sandstone	I-C	Strong calcite cement, some coal	23.5 m (20 m net) (240 ft (66 ft net))	Cuttings
11	Davidson 1	5840'-5850'	Precipice Sandstone	I-C	Strong calcite cement	55 m (21.5 m net) (180 ft (71 ft net))	Cuttings
12	Davidson 1	6010'-6020'	Precipice Sandstone	I-C	Extreme calcite cement	49 m (18 m net) (160 ft (60 ft net))	Cuttings
37	Green Swamp 1	1000	Green Swamp 1	I-C	Abundant calcite cement, apparently dolomite, abundant coal, some tuff	670 m (342 m net)	Cuttings
13	Green Swamp 1	1500	Hutton Sandstone	S-C	Abundant strong calcite cement, siliceous cement	347 m (276.5 m net)	Cuttings
38	Green Swamp 1	1620	Green Swamp 1	I	Abundant calcite in aggregates, also siliceous cement, apparently oolites too	347 m (276.5 m net)	Cuttings
86	Mitchell 2	69.43-69.52	Bungil Formation	S	Calcite cement, burrows filled with pyrite, plant frags though	Sporadic	Core
278	Mitchell 2	82.81-82.90	Bungil Formation	I	Contact between siderite and sandstone.	Sporadic	Core
87	Mitchell 2	85.91-85.97	Bungil Formation	S	Siderite cement/nodule	Sporadic	Core
88	Mitchell 2	292.68-292.78	Gubberamunda Sandstone	S	"Mottled" calcite cement in minor finely laminated intervals. Abundant garnets 3 m below this.	Sporadic	Core
279	Mitchell 2	824.37-824.47	Evergreen Formation	I	45 degree fault with 5 mm thick calcite.	Sporadic and frac associated	Core
280	Mitchell 2	825.53-825.64	Evergreen Formation	I	Possibly horizontally sheared intrusion.	Sporadic and frac associated	Core
281	Mitchell 2	828.25-828.26	Evergreen Formation	M	6 mm thick horizontal calcite	Sporadic and frac associated	Core
282	Mitchell 2	831.39-831.425	Evergreen Formation	M	40 degree calcite vein in shear	Sporadic and frac associated	Core
283	Mitchell 2	833.3-833.355	Evergreen Formation	M	Concave convex 45 degree calcite cemented shear (with the calcite itself also sheared).	Sporadic and frac associated	Core







Sample #	Well	Depth (m unless specified)	Formation	Lithology ^a	Brief notes	Carbonate cemented zone thickness (m)	Sample Type
83	Moonie 38	1727.65-1727.79	Evergreen Formation	S-C	Calcite cemented conglomeritic sandstone, discontinuous calcite mineralised cleated coal. Oil shows.	219 m (91 m net)	Core
53	Moonie 40	4830'	Hutton Sandstone	I	Common patchy hard calcite cement	271 m (152 m net) (890 ft (500 ft net))	Core
39	Moonie 40	1000'	Blythesdale Group	I-C	Common strong calcite cement, some coal	296 m (73 m net) (970 ft (240 ft net))	Cuttings
40	Moonie Corner 1	1270	Walloon Coal Measures	I-C	Strong calcite in aggregates, siliceous cement, some coal	390 m (240 m net)	Cuttings
41	Moonie Corner 1	1371	Walloon Coal Measures	I-C	Common abundant calcite, siliceous cement, and carbonaceous lithics (coal)	390 m (240 m net)	Cuttings
42	Moonie Corner 1	1437	Walloon Coal Measures	I-C	Strong calcite cement, siliceous cement, some coal	390 m (240 m net)	Cuttings
54	Moonie Corner 1	1455	Walloon Coal Measures	I-C	Strong calcite cement, some dolomite	390 m (240 m net)	Cuttings
55	Moonie Corner 1	1497	Walloon Coal Measures	I-C	Strong calcite cement, some dolomite	390 m (240 m net)	Cuttings
43	Moonie Corner 1	1818	Evergreen Formation	I-C	Strong calcite cement, siliceous cement, some coal, rare limestone	150 m (95 m net)	Cuttings
44	Moonie Corner 1	1905	Precipice Sandstone	S	Strong calcite and siliceous cement	60 m (47 m net)	Cuttings
45	Moonie Corner 1	1923	Precipice Sandstone	I	Calcite and siliceous cement	60 m (47 m net)	Cuttings
46	Strathpine 1	270	Walloon Coal Measures	I-C	Abundant calcite cement, some coal	Sporadic	Cuttings
47	Strathpine 1	390	Hutton Sandstone	I-C	Abundant calcite cement, some siliceous cement, coal	195 m (135 m net)	Cuttings
14	Strathpine 1	500	Hutton Sandstone	I-C	Abundant calcite cement	195 m (135 m net)	Cuttings
48	Strathpine 1	618	Evergreen Formation	I	Abundant calcite cement, some siliceous cement, coal	Sporadic	Cuttings
49	Strathpine 1	633	Evergreen Formation	M-C	Abundant calcite cement, some siliceous cement	Sporadic	Cuttings
62	Strathpine 1	678	Evergreen Formation	M	Abundant calcite cement	171 m (52 m net)	Cuttings
61	Strathpine 1	753	Precipice Sandstone	M	Abundant calcite cement, above oil	171 m (52 m net)	Cuttings
50	Strathpine 1	801	Precipice Sandstone	I	Abundant calcite cement, oil	171 m (52 m net)	Cuttings
15	Sussex Downs 1	6800'-6810'	Precipice Sandstone	I-C	Abundant white calcite and clay cement	Sporadic	Cuttings
60	West Wandoan 1	756-756.15	Hutton Sandstone	S	Uncemented	Sporadic	Core
67	West Wandoan 1	800.70-800.85	Hutton Sandstone	S	WC15 calcite cement	Sporadic	Core
73	West Wandoan 1	821.55-821.67	Hutton Sandstone	S	Uncemented	Sporadic	Core
68	West Wandoan 1	981.24-981.31	Evergreen Formation	I	Minor calcite cement	Sporadic	Core
69	West Wandoan 1	1043.70-1043.77	Evergreen Formation	S	Minor calcite cement	Sporadic	Core
70	West Wandoan 1	1056.10-1056.19	Evergreen Formation	S	Calcite cement	Sporadic	Core
71	West Wandoan 1	1165.44-1165.52	Precipice Sandstone	S	Quartzose sandstone with minor clays and calcite	Sporadic	Core
80	Yapunyah 1	4970'4"-4970'10"	Evergreen Formation	S-C	Calcite cement, 15 feet above oil show. Minor coals. Core sample from base of calcite zone (rest was chipped).	283.5 m (930 ft) spanning Hutton and Evergreen, 204 m net (670 ft net)	Core
81	Yapunyah 1	4993'8"-4994'4"	Evergreen Formation	S-C	Calcite cement, minor coal, 10 feet above fault, 10 feet below and 50 feet above oil shows. Core sample from base of calcite zone (rest was chipped).	283.5 m (930 ft) spanning Hutton and Evergreen, 204 m net (670 ft net)	Core





^aS = sandstone, I = interbedded sandstone/siltstone/mudstone, M = mudstone/siltstone sometimes with minor thin sandstone layers in part, C = coal, L = potential thin limestone layer/s within interval

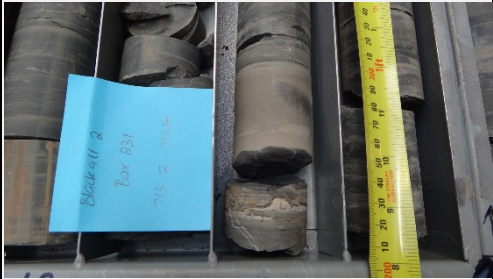

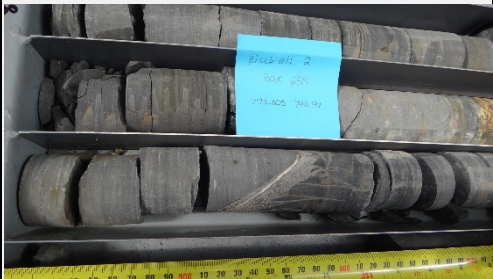



Appendix 2: Core sample photographs

Table A2.1: Eromanga Basin Core Sample Info (veins shaded, samples sorted by Well and Depth).







UQ Sample #	Well	Depth (m unless shown as ft.)	Formation	Sample photographs	UQ Sample #	Well	Depth (m unless shown as ft.)	Formation	Sample photographs
285	Blackall 1	195.52-196.6	Allaru Mudstone		89	Blackall 1	622.85	Hooray (Namur) Sandstone	
127	Blackall 1	622.35-622.6	Hooray (Namur) Sandstone		91	Blackall 2	311.68-311.94	Allaru Mudstone	
92	Blackall 2	313.54-313.61	Allaru Mudstone		94	Blackall 2	443.7-443.77	Allaru Mudstone	







UQ Sample #	Well	Depth (m unless shown as ft.)	Formation	Sample photographs	UQ Sample #	Well	Depth (m unless shown as ft.)	Formation	Sample photographs
154	Blackall 2	314.47-314.48	Allaru Mudstone		95	Blackall 2	444.1-444.56	Allaru Mudstone	
93	Blackall 2	314.6-314.61	Allaru Mudstone		96	Blackall 2	474.19-474.36	Allaru Mudstone	
125	Blackall 2	474.93-475.08	Allaru Mudstone		286	Blackall 2	606.855 - 606.91	Allaru Mudstone	


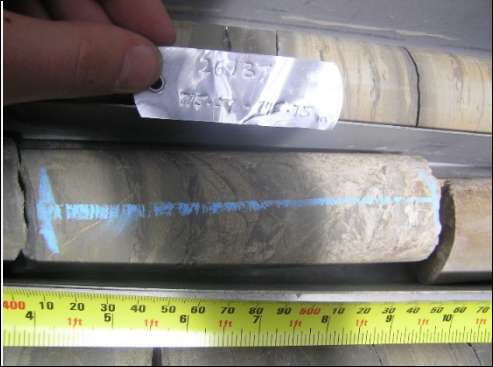




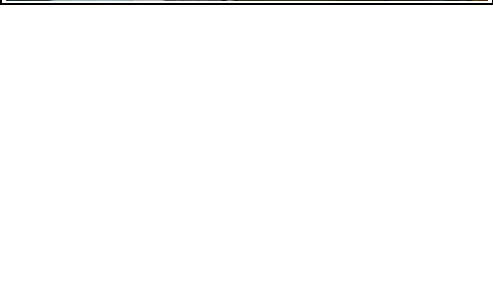
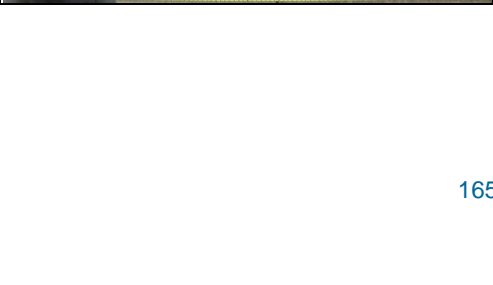
UQ Sample #	Well	Depth (m unless shown as ft.)	Formation	Sample photographs	UQ Sample #	Well	Depth (m unless shown as ft.)	Formation	Sample photographs
97	Blackall 2	475.88-476.02	Allaru Mudstone		99	Blackall 2	665.71-665.73	Wallumbilla Formation	
98s	Blackall 2	660.38-660.54	Toolebuc Formation		155	Blackall 2	809.50-809.56		







UQ Sample #	Well	Depth (m unless shown as ft.)	Formation	Sample photographs	UQ Sample #	Well	Depth (m unless shown as ft.)	Formation	Sample photographs
287	Blackall 2	713.2-713.24	Wallumbilla Formation		100	Blackall 2	811.46-811.47	Wallumbilla Formation	
295	Blackall 2	798.805-798.92	Wallumbilla Formation		300	Blackall 2	812.9-813	Wallumbilla Formation	
298	Blackall 2	833.725-833.84	Cadna-Owie Formation		124	Connemara 1	310.71-311	Mackunda Formation	


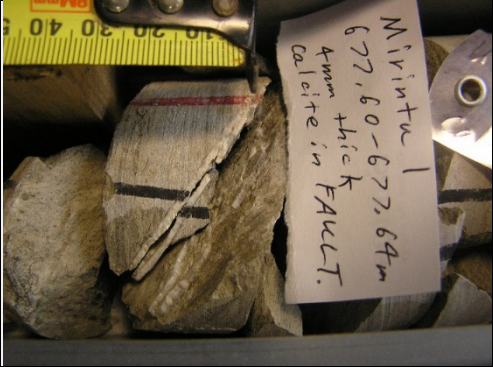
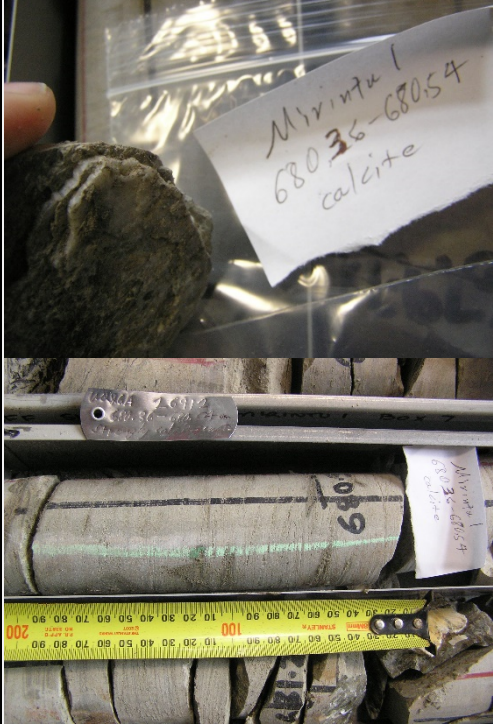

UQ Sample #	Well	Depth (m unless shown as ft.)	Formation	Sample photographs	UQ Sample #	Well	Depth (m unless shown as ft.)	Formation	Sample photographs
169	Burke 002	5063'7" - 5063'11"	Murta Formation		148	Connemara 1	311.75-311.82	Mackunda Formation	
102	Connemara 1	119.76-119.87	Winton Formation		123	Connemara 1	371.72-371.83	Allaru Mudstone	
149	Connemara 1	390-390.18	Allaru Mudstone		158	Connemara 1	448.83-448.87	Allaru Mudstone	

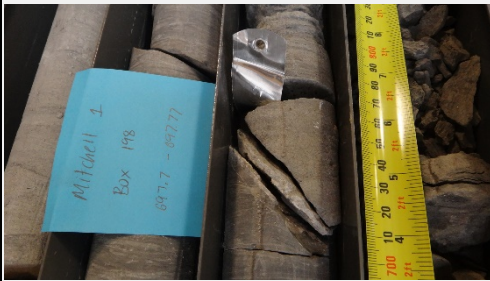

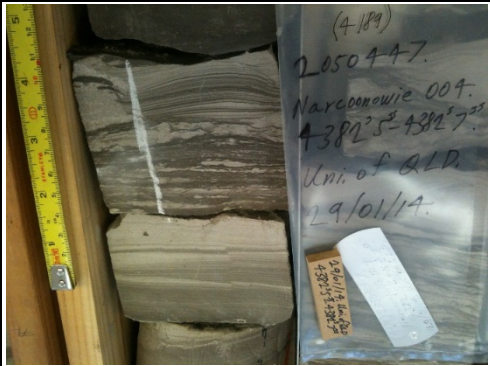



UQ Sample #	Well	Depth (m unless shown as ft.)	Formation	Sample photographs	UQ Sample #	Well	Depth (m unless shown as ft.)	Formation	Sample photographs
150	Connemara 1	391.88-392	Allaru Mudstone		101	Connemara 1	450.2-450.21	Allaru Mudstone	
126	Connemara 1	395.40-395.50	Allaru Mudstone		159	Connemara 1	673.45-673.48	Wallumbilla Formation	
104	Connemara 1	945.04-945.16	Westbourne Formation		105	Connemara 1	946.24-946.34	Westbourne Formation	

UQ Sample #	Well	Depth (m unless shown as ft.)	Formation	Sample photographs	UQ Sample #	Well	Depth (m unless shown as ft.)	Formation	Sample photographs
103	Connemara 1	942.17-942.37	Westbourne Formation		167	Dullingari 037	5065'8.5" - 5065'10.5"	Murta Formation	
106	Connemara 1	944.6-944.7	Westbourne Formation		173	Dullingari 037	5068'8" - 5069	Murta Formation	
165	Dullingari 036	4883'3" - 4883'4"	Murta Formation		171	Dullingari 039	5024'9" - 5025'1.5"	Murta Formation	
79	Jackson South 2	4279'5" - 4279'6.5"	Westbourne Formation		107	Jundah 1	795.59-795.75	Cadna-Owie Formation	

UQ Sample #	Well	Depth (m unless shown as ft.)	Formation	Sample photographs	UQ Sample #	Well	Depth (m unless shown as ft.)	Formation	Sample photographs
78	Jackson South 2	4279'6.5" - 4279'9"							
77	Jackson South 2	4279'9" - 4280'2"							
166	Jena 2	3882'9" - 3882'11"	Murta Formation		108	Jundah 1	905.67-905.73	Hooray (Namur) Sandstone	
170	Jena 6	3934'1" - 3934'4"	Murta Formation		109	Jundah 1	906.46-906.58	Hooray (Namur) Sandstone	





UQ Sample #	Well	Depth (m unless shown as ft.)	Formation	Sample photographs	UQ Sample #	Well	Depth (m unless shown as ft.)	Formation	Sample photographs
110	Jundah 1	939.62-939.68	Hooray (Namur) Sandstone		163	Marabooka 004	3433' - 3433'6"	Oodnadatta Formation	
111	Jundah 1	940.48-940.58	Hooray (Namur) Sandstone		74 (taken for vitrinite reflectance)	Merrimelia 32	6038'3" - 4"	Birkhead Formation	
112	Jundah 1	941.52-941.70	Hooray (Namur) Sandstone		162	Merrimelia 32	6064'1.5" - 6064'5"	Birkhead Formation	

UQ Sample #	Well	Depth (m unless shown as ft.)	Formation	Sample photographs	UQ Sample #	Well	Depth (m unless shown as ft.)	Formation	Sample photographs
6	Mirintu 1	675.29-675.33	Cadna-Owie Formation		3 (lower layer) & 4 (upper layer)	Mirintu 1	677.6	Cadna-Owie Formation	
5	Mirintu 1	680.36-680.54	Cadna-Owie Formation		2	Mirintu 1	695.89-695.5	Cadna-Owie Formation	

UQ Sample #	Well	Depth (m unless shown as ft.)	Formation	Sample photographs	UQ Sample #	Well	Depth (m unless shown as ft.)	Formation	Sample photographs
277	Mitchell 1	697.7-697.77	Evergreen Formation		204	Strzelecki 015	6275'7.5"-9"	Gidgealpa Formation (Permian coal taken for vitrinite reflectance)	
172	Narcooowie 004	4382'5" - 4382'7"	Murta Formation		113	Thargomindah 1A	970.18-970.28	Adori Sandstone	
164	Narcooowie 004	4395' - 4395'4"	Murta Formation		152	Thargomindah 1A	966.86-967.12	Adori Sandstone	

UQ Sample #	Well	Depth (m unless shown as ft.)	Formation	Sample photographs	UQ Sample #	Well	Depth (m unless shown as ft.)	Formation	Sample photographs
114	Thargomindah 2	409.02-409.12	Mackunda Formation		153	Thargomindah 2	409.66-409.73	Mackunda Formation	
151	Thargomindah 2	454-454.03	Allaru Mudstone		116	Thargomindah 2	556.31	Allaru Mudstone	
115	Thargomindah 2	544.14-544.26	Allaru Mudstone		117	Thargomindah 2	560.86-560.96	Allaru Mudstone	

UQ Sample #	Well	Depth (m unless shown as ft.)	Formation	Sample photographs	UQ Sample #	Well	Depth (m unless shown as ft.)	Formation	Sample photographs
					157	Thargomindah 2	576.18-576.29	Allaru Mudstone	
118	Thargomindah 2	956.38-956.44	Cadna-Owie Formation		168	Ulandi 5	3914'10" - 3915'1"	Cadna-Owie	

UQ Sample #	Well	Depth (m unless shown as ft.)	Formation	Sample photographs	UQ Sample #	Well	Depth (m unless shown as ft.)	Formation	Sample photographs
119	Thargomindah 2	998.44-998.52	Cadna-Owie Formation						
120	Thargomindah 3	1115.47-1115.53	Hooray (Namur) Sandstone		160	Thargomindah 3	1119.40-1119.45	Hooray (Namur) Sandstone	


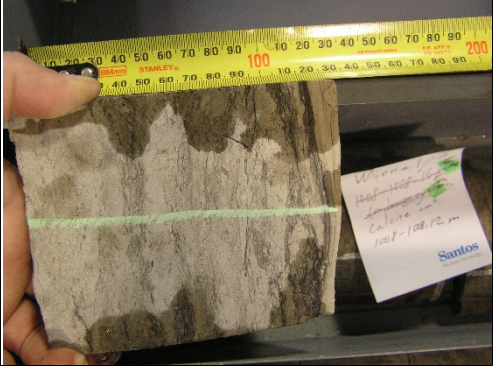

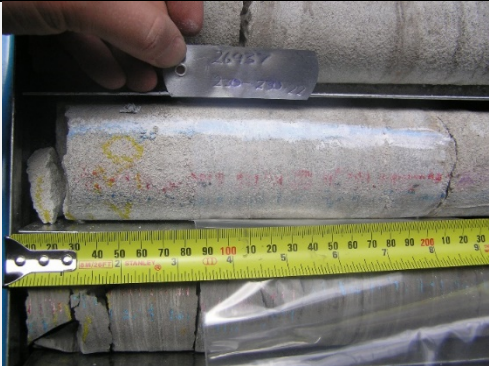


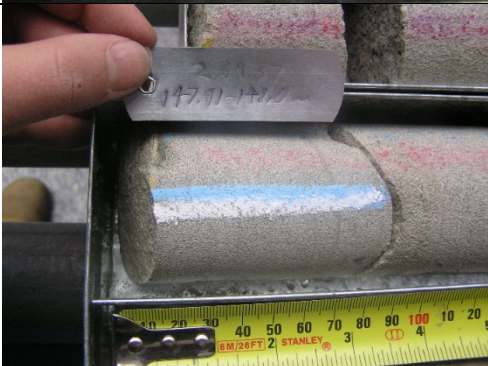





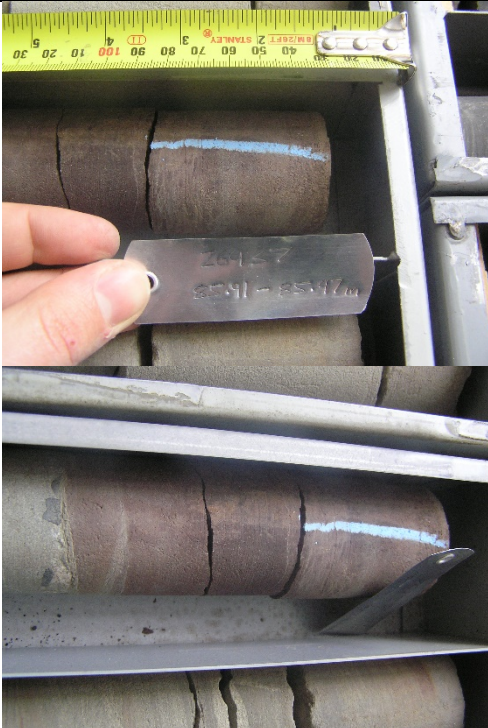



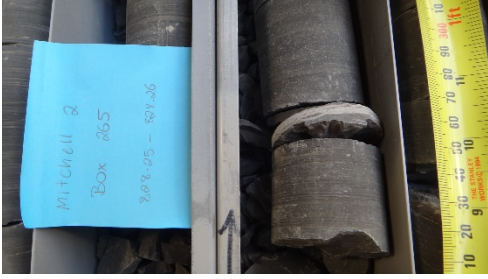

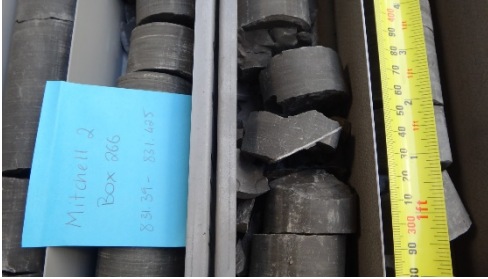

UQ Sample #	Well	Depth (m unless shown as ft.)	Formation	Sample photographs	UQ Sample #	Well	Depth (m unless shown as ft.)	Formation	Sample photographs
121	Thargomindah 3	1171.58-1171.74	Hooray (Namur) Sandstone		8	Winna-1	1008.08-1008.12	Murta Formation	

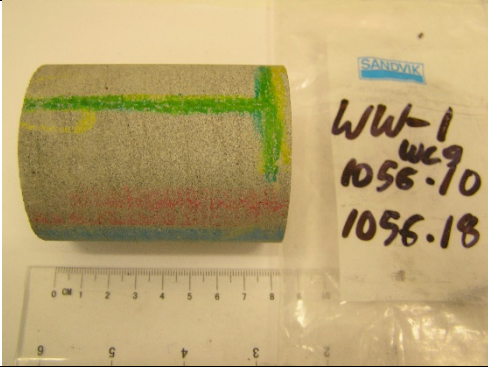

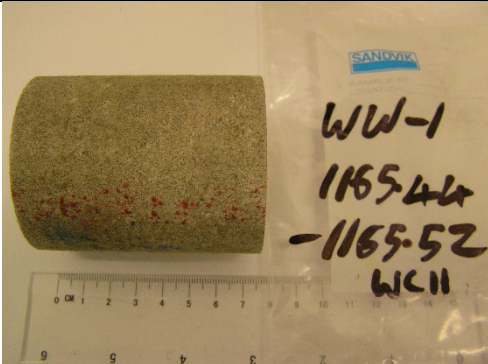

Table A2.2: Surat Basin Core Sample Info (veins shaded).

UQ Sample #	Well/mine location	Depth (m unless shown as ft.)	Formation	Sample photographs	UQ Sample #	Well/mine location	Depth (m unless shown as ft.)	Formation	Sample photographs
82	Alton 3A	6066'-6066'6"	Either Evergreen Formation or Precipice Sandstone (unspecified)		84	Cameron 1	230-230.22	Walloon Coal Measures	
248 (taken for vitrinite reflectance)	Cameron 1	Small piece from 120.27	Springbok Sandstone		156	Cameron 1	230.7-230.92	Walloon Coal Measures	
85	Cameron 1	147.91-148	Springbok Sandstone		10	Chinchilla 4	799.6	Hutton Sandstone	

UQ Sample #	Well/mine location	Depth (m unless shown as ft.)	Formation	Sample photographs	UQ Sample #	Well/mine location	Depth (m unless shown as ft.)	Formation	Sample photographs
161s ("calcite/siderite") & 161r (non-calcite black vein minerals)	Chinchilla 4	650.45	Tangalooma Sandstone, Taroom Coal Measures		75	Chinchilla 4	1101.11-1011.34	Evergreen Formation	
					76	Chinchilla 4	1032.68-1032.73	Evergreen Formation	
					86	Mitchell 2	69.43-69.52	Bungil Formation	

UQ Sample #	Well/mine location	Depth (m unless shown as ft.)	Formation	Sample photographs	UQ Sample #	Well/mine location	Depth (m unless shown as ft.)	Formation	Sample photographs
278	Mitchell 2	82.81-82.90	Bungil Formation		88	Mitchell 2	292.68-292.78	Gubberamunda Sandstone	
87	Mitchell 2	85.91-85.97	Bungil Formation		280	Mitchell 2	825.53-825.64	Evergreen Formation	

UQ Sample #	Well/mine location	Depth (m unless shown as ft.)	Formation	Sample photographs	UQ Sample #	Well/mine location	Depth (m unless shown as ft.)	Formation	Sample photographs
279	Mitchell 2	824.37-824.47	Evergreen Formation		283	Mitchell 2	833.3-833.355	Evergreen Formation	
281	Mitchell 2	828.25-828.26	Evergreen Formation		83	Moonie 38	1727.65-1727.79	Precipice Sandstone	
282	Mitchell 2	831.39-831.425	Evergreen Formation		67	West Wandoan 1	800.70-800.85	Hutton Sandstone	

UQ Sample #	Well/mine location	Depth (m unless shown as ft.)	Formation	Sample photographs	UQ Sample #	Well/mine location	Depth (m unless shown as ft.)	Formation	Sample photographs
70	West Wandoan 1	1056.10-1056.19	Evergreen Formation		80	Yapunya 1	4970'7"	Evergreen Formation	
71	West Wandoan 1	1165.44-1165.52	Precipice Sandstone		81	Yapunya 1	4993'8"-4994'4"	Evergreen Formation	

Appendix 3: XRD mineralogy

Table A3.1. Semi-quantitative XRD of QLD Eromanga Basin samples (% composition).

Sample #	Well	Depth (m unless specified ft)	Quartz	CARBONATES						PHYLOSILICATES			FELDSPARS				U-Apatite	Pyrite	
				Calcite	Dolomite	Ankerite / Fe-dolomite	Siderite	Rhodchrosite	Aragonite	Kaolin	Chlorite / Smectite	Illite / Muscovite	Orthoclase	Sanidine	Albite	Ca-Na Plagioclase			Na-Ca Plagioclase
127a	Blackall 1	622.35-622.6	46.98	14.22							3.97						34.83		
127b	Blackall 1	622.35-622.6	45.03	18.69							4.25						32.03		
89	Blackall 1	622.79-622.89	31.67	21							12.39				5.06				29.88
90	Blackall 1	773.16-773.24	35.63	17.81							1.62	8.83		14.56		21.55			
91	Blackall 2	311.68-611.94	15.08	45.57							1.35	9.02	18.52			10.47			
92a	Blackall 2	313.54-313.61	3.54	93.5												2.97			
92b	Blackall 2	313.54-313.61	7.12	92.88															
154	Blackall 2	314.47-314.48																	
93	Blackall 2	314.6-314.61	14.38	36.86							7.98		9.18			31.6			
94	Blackall 2	443.7-443.77	3.54	96.46															
95	Blackall 2	444.51-444.565	5.88	82.96	1							0.82	6.69			2.65			
96	Blackall 2	474.19-474.36	17.16	64.35							4.8		13.68						
125	Blackall 2	474.93-475.08	13.63	72.22							7.24					6.91			
97	Blackall 2	475.88-476.02	5.3	94.7															
98	Blackall 2	660.38-660.54	7.04	61.64				5.72										20.71	4.9
99	Blackall 2	665.71-665.73	23.15	52.11							5.02		19.72						
155	Blackall 2	809.5-809.56	21.23	53.71							4		21.06						
100	Blackall 2	811.46-811.47	0.72	99.28															
63	Bodalla South 2	150	27.3	2.9							6.5	3.1	24.1			17.3			18.8
51a	Bodalla South 9	1596	59.8	2.2							9.5			10		5.9			13.1
51b	Bodalla South 9	1596	58.8								10			10.9		9.4			9.1
52	Bodalla South 9	1617	86.3	4.2				1.8			2.8								
161	Chinchilla 4	650.45	11.5	78.44				5.14			4.92								
102	Connemara 1	119.76-119.87	24.06	27.47							3.87	5.13	12.71	6.52		20.25			
124	Connemara 1	310.71-311	24.63	42.59				0.83			2.66	3.34	6.92	4.15		14.87			
148	Connemara 1	311.75-311.82	28.44	20.89							3.95	5.44	12.99	6.48		21.8			
123	Connemara 1	371.72-371.83	24.59	43.2							2.48		8.67			21.07			
149	Connemara 1	390-390.18	16.73	37.46							4.46	3.77	25.23			12.35			
150	Connemara 1	391.88-392	10.02	64.43							3.25	2.83	14.35			5.13			
126a	Connemara 1	395.4-395.5	33.75	32.23							4.01		5.9	5.74		18.37			
126b	Connemara 1	395.4-395.5	34.87	33.49							3.66		7.15			20.84			
158	Connemara 1	448.83-448.87	32.58	17.68							9.25	4.67	17.57			18.25			
101	Connemara 1	450.2-450.21	2.6	39.98					57.43										
159	Connemara 1	673.45-673.48	17.09	50.3							5.72		17.66			9.24			
103	Connemara 1	942.17-942.37	44.9	24.86							4.53			2.26		23.44			
106	Connemara 1	944.6-944.7	75.34	1.9							4.34			4.52		13.9			
104	Connemara 1	945.04-945.16	31.4	44.66							7.1			2.99		13.85			
105	Connemara 1	946.24-946.34	84.03	3.82												12.15			
1	Inland 3	4430'-4440'	68.4	11.8		0.2	1.5				4.7	1.3	3.7	3.2		5.2			
64	Inland 3	5570'-5580'	79.3	4.8			2.7				4.7			8.4					
79	Jackson South 2	4279'5"-4280'2"	59.28	7.28		3.21	3.75				3.89		16.69	5.9					
78	Jackson South 2	4279'6.5"-4279'9"	49.36	8.76		2.17	21.1				6.74			7.53	4.33				
77	Jackson South 2	4279'9"-4280'2"	80.11	8.36	1.45		1.41							8.66					
107	Jundah 1	795.59-795.75	14.84	69.64							5.79					9.73			
108	Jundah 1	905.67-905.673	83.4	8.11							3.33					5.14			
109	Jundah 1	906.46-906.58	56.13	25.49								6.81				11.57			
110	Jundah 1	939.62-939.68	55.36	15.06							3.3			6.81		19.47			
111	Jundah 1	940.48-940.58	59.88	16.47							4.19					19.46			
112	Jundah 1	941.52-941.7	49.87	12.45							12.31			6.99		18.38			
65	Kenmore 12	510	13.1	8.3							3.7	14.1	12.5					22.3	
66	Kenmore 12	920	28.6	3.4							8.9	3.3	17.4			19.6			18.9
56	Kenmore 12	1075	33.3	2.5							7.8	5.4	19.4			13.8			16.8
57	Kenmore 12	1350	24.1	1.7							8.1	8.1	10.8	11.5		17			17.9
3	Mirintu-1	677.6																	
4	Mirintu-1	677.6																	
6	Mirintu-1	675.29-675.33	34.43	8.17							5.05	4.63	12.54			35.18			

5a	Mirintu-1	680.36-680.395	19.55	12.68					7.27	3.93	13.65	6.13			36.79				
5b	Mirintu-1	680.36-680.395																	
2	Mirintu-1	696																	
7	Saltern Creek 1	1651'2"-4'	53.05	4.77					8.5			3.4		30.28					
152	Thargomindah 1A	966.86-967.12	36.37	43.43					4.33			6.7			9.17				
113	Thargomindah 1A	970.18-970.28	62.61	23.21					3.67			6.01		4.51					
114	Thargomindah 2	409.02-409.12	30.43	22.28					4.92	25.52					36.84				
153	Thargomindah 2	409.66-409.73	21.7	35.53					1.86	3.19	11.45				26.26				
151	Thargomindah 2	454-454.03	16.14	47.69					4.9	3.33	14.67			13.27					
115	Thargomindah 2	544.14-544.26	12.16	72.14					6.94							8.76			
116	Thargomindah 2	556.31-556.37	28.66	29.67					7.2		20.27			14.2					
117	Thargomindah 2	560.86-560.96	20.5	37.6					7.84	6.15	10.33			17.57					
157	Thargomindah 2	576.18-576.29	12.88	48.11					3.98	3.67	16.37				14.99				
118	Thargomindah 2	956.38-956.44	37.13	17.99					4.9					39.98					
119	Thargomindah 2	998.44-998.52	46.81	6.79					3.82			11.37		31.2					
120	Thargomindah 3	1115.47-1115.53	94.27	5.73															
160-fault	Thargomindah 3	1119.4-1119.45	72.83						20.5		2.83	1.54	2.31						
160-sandstone	Thargomindah 3	1119.4-1119.45	49.08						15.83	1.35	16.24	6.5		11					
121	Thargomindah 3	1171.58-1171.74	45.12	33.37					5.87		5.81	4.27		5.56					
58	Widnerpool 1	559-562	50.05	1.64						6.61	13.95			27.75					
58	Widnerpool 1	559-562	38	3.6					8.2	3.2	12.4	8.6		16.7				11.3	
59	Widnerpool 1	862-865	52.7						13.1	5.7	24.8								
8	Winna-1	1008.08-1008.12	54.91	8.79	0.88				3.69		2.58	4.43	24.73						
9	Yongala 1	2500'-2510'	27.8	14.27					2.46	1.88	5.76	4.83						43	

Table A3.2. Semi-quantitative XRD of SA Eromanga Basin samples (% composition).

Sample #	Well	Depth (feet)	Quartz	CARBONATES				PHYLLOSILICATES					FELDSPARS					PHOSPHATES			Wulfenite
				Calcite	Dolomite	Ankerite / Fe-dolomite	Siderite	Kaolin	Chlorite / Smectite	Illite / Muscovite	Paragonite	Phlogopite	Orthoclase	Microcline	Albite	Ca-Na Plagioclase	Na-Ca Plagioclase	Andesine	Sr-Apatite	U-Apatite	
169	Burke 002	5063.7"	61.66	12.81			1.89	3.95		5.86				4.26		9.56					
165	Dullingari 036	4883.3"	92.47	3.88				3.65													
171	Dullingari 039	5024.9"	47.01	22.67			0.71	7.17		10.28				4.24			7.93				
167a	Dullingari 037	5065.8.5"	71.65	0.32			0.22	4.79	2.97	6.03			4.07	5.38		4.57					
167b	Dullingari 037	5065.8.5"	90.04	4.07				3.16					2.73								
167c	Dullingari 037	5065.8.5"	68.79					5.67		6.92			7.77	5.74	5.11						
173	Dullingari 037	5068.8"	29.94	25.94			8.6	8.36		15.2			5.24				6.72				
187	Gidgealpa 18	5510'	81.36	5.02			0.47						13.15								
188	Gidgealpa 18	5540'	81.53	7.56	0.66		1.26	1.8		2.17			5.02								
189	Gidgealpa 18	5580'	90.04	9.55		0.41															
190	Gidgealpa 18	5620'	98.11	1.24		0.65															
192	Gidgealpa 18	5650'	88.01	0.39			0.96	2.17		3.8			3.77						0.9		
191	Gidgealpa 18	5700'	90.75	0.34				2.59		4.84			1.48								
215	Gidgealpa 18	5000'	100																		
216	Gidgealpa 18	5300'	99.4				0.6														
217	Gidgealpa 18	5900'	100																		
218	Gidgealpa 18	6100'	98.43	0.57		1															
166	Jena 2 not 6	3882.9"	24.05	33.81		5.07	1.83	9.37		25.87											
170	Jena 6	3934.1"	51.67	15.14	1		9.97	7.88		9.01			5.32								
181	Kerna 3	5500'	94.49			2.43		0.32		2.75											
182	Kerna 3	5640'	82.87	8.75			1.02						7.36								
183	Kerna 3	5700'	86.27	7.28			0.93				1.55		3.96								
184	Kerna 3	5750'	99.04			0.96															
185	Kerna 3	5880'	91.28	1.73		1.39							5.6								
186	Kerna 3	5220'	95.2										4.8								
210	Kerna 3	5350'	95.04										4.96								
211	Kerna 3	5410'	100																		
212	Kerna 3	5480'	89.54			3.58							6.88								
213	Kerna 3	6150'	100																		
214	Kerna 3	6230'	99.54				0.46														
163	Marabooka 004	3433'	16.05	26.78				3.9		5.3			2.9				8.3				
162	Merrimelia 32	6064.1.5"	63.33		14.89			13.36		4.1					36.77						
233	Merrimelia 32	6038.3"													4.32						
200	Muteroo 1	5150'	83.98	2.37		4.27	0.94						8.45								
201	Muteroo 1	5290'	84.9	4.98 (& 10.12 Mg-calcite)																	
202	Muteroo 1	5350'	89.27	10.73																	
203	Muteroo 1	5240'	89.94	5.89															4.18		
225	Muteroo 1	4820'	92.38					1.21					6.41								
226	Muteroo 1	4930'	100																		
227	Muteroo 1	5120'	80.38			1.71	0.48	1.17		5.48			3.46						6.82		0.5
228	Muteroo 1	5400'	89	5.32									3.35						1.71	0.62	
229	Muteroo 1	5700'	96.82										2.33						0.84		
230	Muteroo 1	5760'	97.14										2.86								
231	Muteroo 1	6000'	98.63																		
232	Muteroo 1	6170'	93.13		2.88								3.48						1.37		
164	Narcooowie 004	4395'	54.46	17.22				7.23		10.34			8.43			2.33					
172	Narcooowie 004	4382.5"	67.46	0.85			1.33	8.76	1.28	20.32											
193	Spencer West 1	4820'	88.2	4.17		1.1	0.88						5.66								
194	Spencer West 1	4870'	46.7	4.84				7.42	4.66	15.62			7.21		13.56						
195	Spencer West 1	4910'	65.53	7.67			2.66	3.83		8.95			4.84						6.53		
196	Spencer West 1	4950'	94.38	3.56			2.06														
197	Spencer West 1	5000'	65.8	10.93				4.19		6.49			6.01			6.58					
198	Spencer West 1	5050'	74.72	6.84				2.41		8.52			2.6			4.92					
199	Spencer West 1	4500'	76.49	1.02			0.44	3.92		9.63			3.01		5.48						
219	Spencer West 1	4630'	97.95										2.05								
220	Spencer West 1	5130'	92.68	0.63			0.43						1.92						4.33		
221	Spencer West 1	5400'	86.19			0.34	0.62	2.96		3.96			5.92								
222	Spencer West 1	5500'	91.19					3.06					5.75								
223	Spencer West 1	5600'	100																		
224	Spencer West 1	5700'	100																		
175	Strzelecki 015	5050'	100																		
176	Strzelecki 015	5120'	90.06	1.75		1.72								6.47							
177	Strzelecki 015	5210'	97.98	1.27		0.75															
178	Strzelecki 015	5300'	92.9	7.1																	
179	Strzelecki 015	5380'	84.49	5.9		0.59		1.92		5.64						1.47					
180	Strzelecki 015	5430'	90.25	0.32	0.43		0.21	1.34					0.93		6.53						

Sample #	Well	Depth (feet)	Quartz	CARBONATES				PHYLLOSILICATES					FELDSPARS					PHOSPHATES				Wulfenite
				Calcite	Dolomite	Ankerite / Fe-dolomite	Siderite	Kaolin	Chlorite / Smectite	Illite / Muscovite	Paragonite	Phlogopite	Orthoclase	Microcline	Albite	Ca-Na Plagioclase	Na-Ca Plagioclase	Andesine	Sr-Apatite	U-Apatite	Monazite	
204	Strzelecki 015	6275'7.5"																				
205	Strzelecki 015	4950'	97.5					2.5														
206	Strzelecki 015	5500'	76.79	1.73		1.05	0.97	5.1						5.89								
207	Strzelecki 015	5600'	97.81					2.19														
208	Strzelecki 015	5750'	100																			
209	Strzelecki 015	5850'	100																			
174a	Strzelecki 015	4750'	65.7	0.68			0.31	4.57					4.54		6.55	5.05						
174b	Strzelecki 015	4750'	64.71	0.8			0.44	6.35						9.19								
168	Ulandi 5	3914'10"	47.47	25.34	1.84		6.66	8.58														

Table A3.3. Semi-quantitative XRD of Surat Basin samples (% composition).

Sample #	Well	Depth (m unless specified ft)	Quartz	CARBONATES				PHYLLOSILICATES				FELDSPARS						
				Calcite	Dolomite	Ankerite / Fe-dolomite	Siderite	Kaolin	Chlorite / Smectite	Illite / Muscovite	Biotite	Orthoclase	Sanidine	Albite	Ca-Na Plagioclase	Na-Ca Plagioclase	Anorthite	
22b	(Kogan Creek)	Open pit mine	9.22				90.78											
82	Alton 3	6066'-6066'6"	64.97	18.78				5.08					3.12					8.05
35	Brigalow 1	890'	21	4.5					4.6	14.9					33.4			21.6
84	Cameron 1	230-230.22	15.29	38.07				4.8	6.67	7.69								27.47
85	Cameron 1	147.91-148	50.96	16.14				2.03	1.18								29.68	
156	Cameron 1	230.7-230.92	4.17	78.48				3.78	5.87	7.7								
10	Chinchilla 4	799.6	86.95	5.89				1.9	0.48									
74	Chinchilla 4	120.27	26.22	40.79			7.72					6.92				18.34		
75	Chinchilla 4	1101.11-1101.34	59.1	2.3	0.7			1.7				9.3					26.9	
76	Chinchilla 4	1032.68-1032.73	31.8	14.81			4.11	6.47	3.45	17.82		6.97				14.57		
11	Davidson 1	5840'-5850'	41.71	2.99				5.55	14.47	14.1		8.38				12.78		
12	Davidson 1	6010'-6020'	56.49	4.04			1.16	9.14	2.33	10.71		12.48			3.64			
36	Davidson 1	5440'-5450'	63	0.7				5.7	1.6	11.5		6.7		4				6.9
13	Green Swamp 1	1500	58.54	4.91				3.85		5.65		8.05			19.04			
37	Green Swamp 1	1000	38.9	1.5			1	4.6	5.5	14.4		7.8		14				12.3
38	Green Swamp 1	1620	40.7	1.9			1.6	5.8	8	14.1		12.3		15.4				
86	Mitchell 2	69.43-69.52	95.36	4.64														
87	Mitchell 2	85.91-85.97	12.65	34.48			27.71	9.48	6.67	9								
88	Mitchell 2	292.68-292.78	48.57	22.79				4.4						13.73		10.52		
83	Moonie 38	1727.65-1727.79	78.23	3.92				2.16					13.75		1.94			
39	Moonie 40	1000'	23.5					8.5		22				20.4				21
40	Moonie Corner 1	1270	19.9	3.4				5.7	9	12.6		9.3		17.3				19.2
41	Moonie Corner 1	1371	29.1	3			2.6	7.4	5.8	12.5		10.6		14.1				16.9
42	Moonie Corner 1	1437	30.3	4.6			3.2	10.3	3.6	22.5				12.9				14.9
44	Moonie Corner 1	1905	89.7					5.1										
45	Moonie Corner 1	1923 m	57.13	0.54	0.56		0.56	8.22		11.75		7.47	6.18		3.91		3.69	
53	Moonie Corner 1	4830	84.1	3			1.4	9.9										
54	Moonie Corner 1	1455	58.8		1		0.9	10				10.9		9.4				9.1
55	Moonie Corner 1	1497	30.9	1.5			2.1	11.4	1.7	17.5		8.7		11.7				13.7
43a	Moonie Corner 1	1818	22	1.6				18.1	5.4	10				17.5				19.2
43b	Moonie Corner 1	1818	36.5					5.7	5.6	12.4		11.8		13				13.3
14	Strathpine 1	500	68.66	5.49				4.31	1.59	4.19		11.8		3.96				
46	Strathpine 1	270	49.3	9.92			7.26	9.8		10.3		9.7		9.1				7.8
47	Strathpine 1	390	108.03					9.78	9.76	10.9		8.97		9.83				9.44
48	Strathpine 1	618	69.7	2.2				7				10.5		7				4.9
49	Strathpine 1	633	32.6	1.9			1.6	5.8	5.4	15.5		11.3		12.1				15.1
50	Strathpine 1	801	22.3	1.8				7.7	13.2	20.8		9.4		10.3				12.8
61	Strathpine 1	753	69.5	1.3	0.8			5.6		5.9		6.7						9.1
62	Strathpine 1	678	41.6	1.5	0.9			5.3	2.1	18		8		11				11.8
15	Sussex Downs 1	6800'-6810'	55.81	2.21			1.09	5.73		16.98		8.84		9.34				
60	West Wandoan 1	756-756.15	81.58					3.87				6.74		7.8				
67	West Wandoan 1	800.70-800.85	30.1	21.3				7.2		9.9	2.2	3.9		13.8			11.6	
67	West Wandoan 1	800.70-800.85	30.1	21.3				7.2		9.9	2.2	3.9		13.8				11.6
70	West Wandoan 1	1056.10-1056.19	27.29	16.27	0.52			2.1	0.89	19.28		6.07			12.85		14.73	
80	Yapunyah 1	4970'4"-4970'10"	72.34	10.22				11.11				6.33						
81	Yapunyah 1	4993'8"-4994'4"	82.52	9.39				2.9				5.19						

Table A4.7. Surat Basin chondrite-normalised REE anomaly and ratio data*

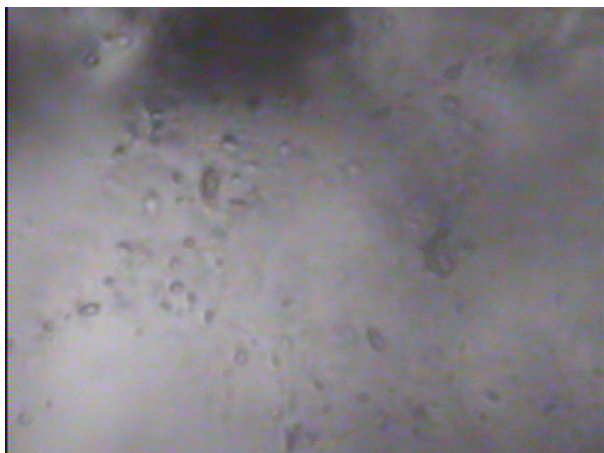
Type	Sample #	Well	Formation	Depth (m unless marked ft)	La _{CN} /La _{CN} *	Ce _{CN} /Ce _{CN} *	Eu _{CN} /Eu _{CN} *	(La/Sm) _{CN}	(Tb/Yb) _{CN}	(Eu/Sm) _{CN}	(Pr/Yb) _{CN}	(Pr/Tb) _{CN}	(Tb/Yb) _{CN}
N/A	JCp1	N/A	(International coral standard)	N/A	1.55	0.69	0.76	3.84	1.12	0.70	2.48	2.22	1.12
Cement	10	Chinchilla 4	Hutton Sandstone	799.385	0.71	1.07	0.91	1.01	1.95	0.87	2.59	1.33	1.95
	14	Strathpine 1	Hutton Sandstone	500	0.88	0.98	0.81	2.43	2.93	0.68	9.09	3.10	2.93
	46	Strathpine 1	Walloon Coal Measures	270	0.96	1.03	0.85	1.52	1.77	0.74	3.51	1.98	1.77
	54	Moonie Corner 1	Walloon Coal Measures	1455	0.83	0.97	0.87	0.87	2.32	0.76	3.45	1.49	2.32
	55	Moonie Corner 1	Walloon Coal Measures	1497	0.74	0.98	0.80	0.79	3.20	0.69	5.09	1.59	3.20
	67	West Wandoan 1	Hutton Sandstone	800.70	0.80	1.02	0.78	3.01	2.57	0.61	11.36	4.41	2.57
	70	West Wandoan 1	Evergreen Formation	1056.10	0.91	1.04	0.98	3.93	4.81	0.76	23.74	4.94	4.81
	81	Yapunyah 1	Evergreen Formation	4993'8"	0.74	0.94	0.98	1.57	2.35	0.85	5.24	2.23	2.35
	85	Cameron 1	Springbok Sandstone	147.91	0.80	0.94	0.66	1.93	1.29	0.57	3.44	2.67	1.29
	86	Mitchell 2	Bungil Formation	69.43	0.94	0.85	0.74	7.57	2.55	0.58	17.40	6.83	2.55
	87	Mitchell 2	Bungil Formation	85.91	1.63	1.10	0.94	4.38	1.33	0.91	2.70	2.03	1.33
	263	Chinchilla 4	Walloon Coal Measures	580.73	0.95	0.95	1.14	3.93	2.12	0.94	8.79	4.14	2.12
	272	Chinchilla 4	Evergreen Formation	1143	0.85	0.93	1.23	2.36	2.98	1.05	8.49	2.85	2.98
	278	Mitchell 2	Bungil Formation	82.81	1.27	1.02	0.91	4.18	1.10	0.81	3.17	2.89	1.10
280	Mitchell 2	Evergreen Formation	825.53	1.50	1.07	0.67	1.58	2.40	0.55	4.70	1.95	2.40	
Vein	76	Chinchilla 4	Evergreen Formation	1032.68	1.25	1.10	1.04	3.37	1.58	0.93	3.98	2.51	1.58
	84	Cameron 1	Walloon Coal Measures	230	1.17	0.99	1.74	2.38	1.48	1.50	3.69	2.49	1.48
	156	Cameron 1	Walloon Coal Measures	230.7	1.41	1.01	2.07	3.44	1.22	1.83	3.08	2.53	1.22
	161	Chinchilla 4	Walloon Coal Measures	650.3	1.10	1.05	1.00	3.31	1.51	0.89	4.11	2.72	1.51
	279	Mitchell 2	Evergreen Formation	824.37	1.02	0.97	0.67	2.63	5.84	0.54	19.04	3.26	5.84
	281	Mitchell 2	Evergreen Formation	828.25	1.15	1.12	0.75	2.83	4.87	0.59	17.10	3.51	4.87
	282	Mitchell 2	Evergreen Formation	831.39	1.23	1.23	0.69	2.90	5.66	0.61	13.68	2.42	5.66
	284	Chinchilla 4	Evergreen Formation	1032.84	0.89	1.10	0.73	2.27	4.48	0.60	13.75	3.07	4.48
*Cell colour legend: green fill >1.1, green writing 1.1-1.05, red writing 0.95-0.9, red fill <0.9					> 1 (CN) could indicate pH > 9.5 with CO ₃ ²⁻ forming pentacarbonato-Ce(VI) complexes (Dekov <i>et al.</i> , 2014; Möller and Bau, 1993). <1 can mean relatively oxidised fluid	> 1 could indicate [SO ₄ ²⁻] >> [HS] and/or decomposition of plagioclase (Möller, 1983). < 1 can be due to [HS] >> [SO ₄ ²⁻], Eu reduction at >250°C in hydrothermal fluid (Möller and Bau, 1993) or inheritance of anomaly from parent minerals	<1 may be indicative of metasomatism (Bau and Möller, 1992)	>1 may be indicative of sorptive fractionation processes during REE mobilisation (Bau and Möller, 1992)	High ratio (>1) coupled with slightly elevated (Tb/Yb) _{CN} could indicate hot reducing acidic hydrothermal solution (Bau & Möller 1992)	>1 LREE & <1 HREE positive anomalies. Neither Pr nor Yb behave anomalously (Lawrence <i>et al.</i> , 2006)	MREE positive anomaly if both (Pr/Tb) _{CN} <1 (red) and (Tb/Yb) _{CN} >1 (green), assuming no Tb anomaly (Lawrence <i>et al.</i> , 2006)		

Table A4.8. Surat Basin PAAS-normalised REE anomaly and ratio data*

Type	Sample #	Well	Formation	Depth (m unless marked ft)	La _{SN} /La _{SN} *	Ce _{SN} /Ce _{SN} *	Eu _{SN} /Eu _{SN} *	(La/Sm) _{SN}	(Tb/Yb) _{SN}	(Eu/Sm) _{SN}	(Pr/Yb) _{SN}	(Pr/Tb) _N	(Tb/Yb) _S
N/A	JCp1	N/A	(International coral standard)	N/A	1.91	0.74	1.21	0.9	0.91	1.35	0.43	0.47	0.91
Cement	10	Chinchilla 4	Hutton Sandstone	799.385	0.88	1.14	1.46	0.24	1.58	1.69	0.45	0.28	1.58
	14	Strathpine 1	Hutton Sandstone	500	1.08	1.05	1.3	0.57	2.38	1.31	1.57	0.66	2.38
	46	Strathpine 1	Walloon Coal Measures	270	1.18	1.1	1.35	0.36	1.44	1.44	0.6	0.42	1.44
	54	Moonie Corner 1	Walloon Coal Measures	1455	1.02	1.04	1.38	0.2	1.88	1.48	0.59	0.32	1.88
	55	Moonie Corner 1	Walloon Coal Measures	1497	0.91	1.05	1.27	0.19	2.6	1.34	0.88	0.34	2.6
	67	West Wandoan 1	Hutton Sandstone	800.70	0.99	1.09	1.24	0.71	2.09	1.19	1.96	0.94	2.09
	70	West Wandoan 1	Evergreen Formation	1056.10	1.12	1.11	1.56	0.92	3.9	1.48	4.09	1.05	3.9
	81	Yapunyah 1	Evergreen Formation	4993'8"	0.91	1	1.56	0.37	1.91	1.65	0.9	0.47	1.91
	85	Cameron 1	Springbok Sandstone	147.91	0.98	1.01	1.05	0.45	1.04	1.1	0.59	0.57	1.04
	86	Mitchell 2	Bungil Formation	69.43	1.16	0.91	1.18	1.78	2.07	1.13	3	1.45	2.07
	87	Mitchell 2	Bungil Formation	85.91	2.02	1.17	1.5	1.03	1.08	1.76	0.47	0.43	1.08
	263	Chinchilla 4	Walloon Coal Measures	580.73	1.17	1.02	1.82	0.92	1.72	1.82	1.51	0.88	1.72
	272	Chinchilla 4	Evergreen Formation	1143	1.05	0.99	1.97	0.55	2.42	2.04	1.46	0.6	2.42
278	Mitchell 2	Bungil Formation	82.81	1.56	1.09	1.46	0.98	0.89	1.56	0.55	0.61	0.89	
280	Mitchell 2	Evergreen Formation	825.53	1.86	1.14	1.07	0.37	1.95	1.06	0.81	0.41	1.95	
Vein	76	Chinchilla 4	Evergreen Formation	1032.68	1.54	1.17	1.66	0.79	1.28	1.81	0.69	0.53	1.28
	84	Cameron 1	Walloon Coal Measures	230	1.44	1.06	2.77	0.56	1.2	2.9	0.64	0.53	1.2
	156	Cameron 1	Walloon Coal Measures	230.7	1.73	1.08	3.3	0.81	0.99	3.55	0.53	0.54	0.99
	161	Chinchilla 4	Walloon Coal Measures	650.3	1.36	1.12	1.59	0.78	1.23	1.72	0.71	0.58	1.23
	279	Mitchell 2	Evergreen Formation	824.37	1.25	1.04	1.06	0.62	4.74	1.05	3.28	0.69	4.74
	281	Mitchell 2	Evergreen Formation	828.25	1.42	1.2	1.19	0.67	3.95	1.14	2.95	0.74	3.95
	282	Mitchell 2	Evergreen Formation	831.39	1.52	1.31	1.1	0.68	4.59	1.18	2.36	0.51	4.59
284	Chinchilla 4	Evergreen Formation	1032.84	1.1	1.17	1.16	0.53	3.64	1.17	2.37	0.65	3.64	
	*Cell colour legend: green fill >1.1, green writing 1.1-1.05, red writing 0.95-0.9, red fill <0.9				<1 indicates fluid experienced relatively oxidising conditions	>1 could indicate [SO ₄ ²⁻] >> [HS ⁻], and/or decomposition of plagioclase (Möller, 1983)	<1 may be indicative of metasomatism (Bau & Möller 1992)	>1 may be indicative of sorptive processes during REE mobilisation (Bau and Möller, 1992)	High ratio (>1) coupled with slightly elevated (Tb/Yb) _N could indicate hot reducing acidic hydrothermal solution (Bau & Möller 1992)	>1 LREE & <1 HREE positive anomalies. Neither Pr nor Yb behave anomalously (Lawrence <i>et al.</i> , 2006)	MREE positive anomaly if both (Pr/Tb) _N <1 (red) and (Tb/Yb) _N >1 (green), assuming no Tb anomaly (Lawrence <i>et al.</i> , 2006)		

Appendix 5: Fluid inclusion results

#82 Alton 3A: 6066'3" (Surat Basin)



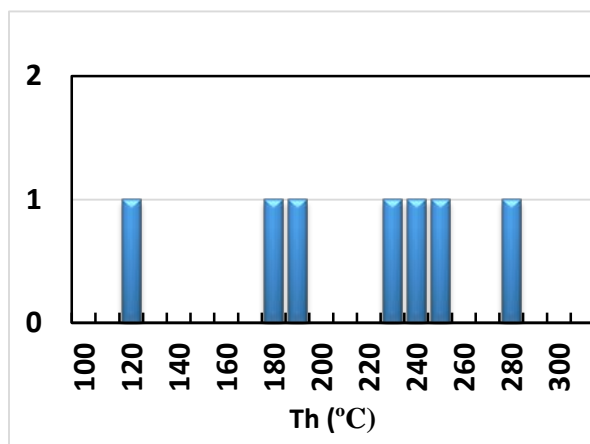
This sample from the Surat Basin was collected near an oil show, 100 feet above a minor coal occurrence. The sample contained relatively rare, very small ($< 2\mu\text{m}$ diameter) fluid inclusions in cloudy carbonate cement. Only a few inclusions were large enough for study. The inclusions formed both primary and secondary assemblages and were rounded to irregular in shape. The majority of inclusions were all-liquid although a few all-vapour inclusions (probably leaked) were also observed.

Homogenisation temperature was determined to be $< 70^\circ\text{C}$

Salinity could not be determined.

#85 Cameron 1: 147.91-148 m (Surat Basin)

This sample from the Springbok Sandstone in the Surat Basin contained calcite cement with siderite nodules up to 1 cm, both 10 m below and 15 m above a coal seam. The calcite cement contains small, wispy inclusion trails in which most of the fluid inclusions appear to have leaked. Some all-liquid inclusions were observed as well as some rare two-phase, liquid + vapour inclusions with approximately 10 vol.% vapour. The inclusions are primary and rounded to irregular in shape and range up to $5\mu\text{m}$ in diameter. Homogenisation temperatures for the two-phase inclusions are shown below.



Homogenisation temperatures for two-phase inclusions ranged from 119.5 to 273.5°C but the presence of all-liquid inclusions indicates a trapping temperature of $< 70^\circ\text{C}$.

Salinity of two-phase inclusions ranged from 0.7 to 4.0 wt.% NaCl eq.

#84 Cameron 1: 230-230.22 m (Surat Basin)

This sample from the Walloon Coal Measures contains calcite cement and veins, 2 m below and 5 m above the coal seams. The calcite cement consisted of bladed calcite crystals. Fluid inclusions were extremely rare but a few all-liquid inclusions were observed. These were primary inclusions ranging up to 10 µm in diameter with irregular to elongated shapes.

Homogenisation temperature was determined to be < 70°C

Salinity could not be determined.

#86 Mitchell 2: 69.43-69.52 m (Surat Basin)

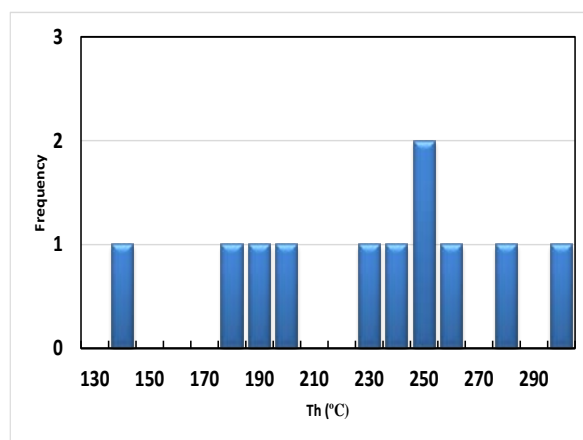
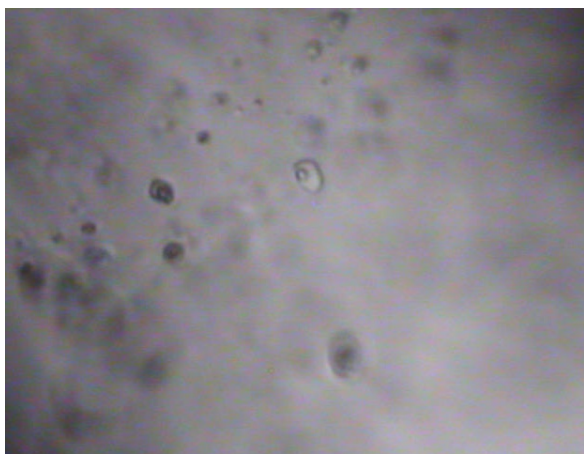
This interval of the Bungil Formation in the Surat Basin contains calcite cement, burrows filled with pyrite and plant fragments. The calcite cement contains small, primary, all-liquid fluid inclusions. They range in size up to 10µm diameter and are rounded to irregular in shape with some showing evidence of necking down.

Homogenisation temperature was determined to be < 70°C

Salinity could not be determined.

#88 Mitchell 2: 292.68-292.78 m (Surat Basin)

This sample from the Gubberamunda Sandstone in the Surat Basin contains 'mottled' calcite cement in minor finely laminated intervals. There are primary, two phase (liquid + vapour) fluid inclusions in the growth zones of crystals within the calcite cement. The fluid inclusions contain 10 – 20 vol.% vapour, range in size up to 10 µm and are rounded to irregular in shape.

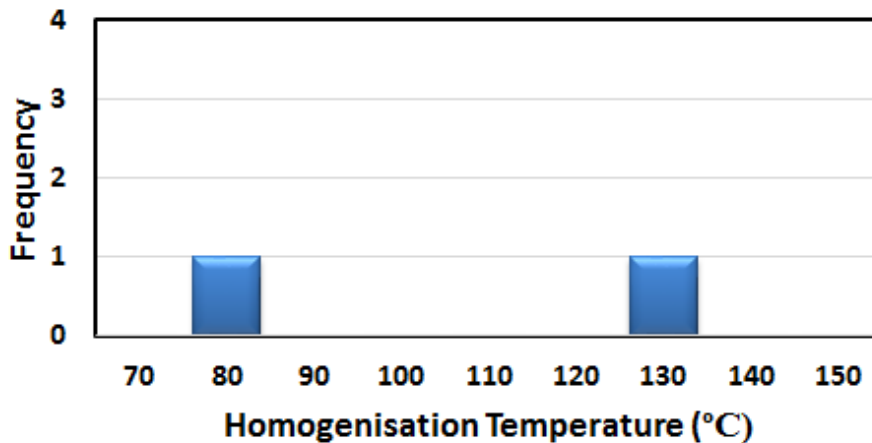


Homogenisation temperatures ranged from 130.0 – 299.1 °C with a mode at 250°C. Such high temperatures may suggest that this sample has been thermally re-equilibrated.

A single salinity measurement suggests the salinity was around 0.0 wt.% NaCl eq.

#83 Moonie 38 1727.72m (Surat Basin)

This sample contains rare, small (<5 micron), 2-phase aqueous inclusions in the calcite cement between quartz grains. These are primary inclusions with irregular to negative crystal shapes and may contain up to 10 vol.% vapour. Due to their small size no ice melting data was obtained and only two homogenisation temperatures were obtained. Both inclusions homogenised to liquid at 74.0 and 126.9 °C, respectively.



#80 Yapunyah 1 4970'7" (Surat Basin)

This sample also contains closely packed quartz grains with very little calcite cement. There are abundant large fluid inclusions in the quartz grains but no inclusions could be found in the calcite cement.

#81 Yapunyah 1 4994'1" (Surat Basin)

This sample contains closely packed quartz grains with very little calcite cement. Only a few, very small (<2 micron) were observed. They are primary with irregular to negative crystal shapes and appear to be all-liquid but the presence of vapour cannot be ruled out due to the poor optical quality of some grains. If the inclusions are all-liquid then this indicates trapping at temperatures below 70°C.

#127 Blackall #1 622.45 m (Eromanga Basin)

A subvertical carbonate fracture in the sandstone contains abundant solid inclusions, but only a few, rare, all-liquid fluid inclusions in growth zones or healed fractures in the carbonate grains. The inclusions are primary to pseudosecondary, rounded to irregular in shape and typically less than 10 microns diameter. As the majority of inclusions are all-liquid, this indicates trapping at temperatures below 70°C.

#90 Blackall #1 773.2 m (Eromanga Basin)

Most of the carbonate crystals in this sample appear to be stretched or deformed. This has destroyed most of the fluid inclusions and most of the remaining intact fluid inclusions are too small to study. The remaining inclusions are irregular shaped, small (< 2 micron), secondary inclusions. They appear to be all-liquid inclusions with a few rare inclusions containing up to 10 vol.% vapour. The presence of all-liquid inclusions would indicate trapping at temperatures below 70°C.

#154 Blackall 2: 314.47-314.48 m (Eromanga Basin)

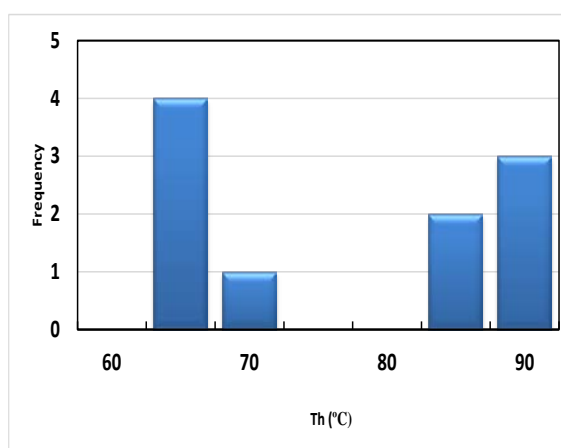
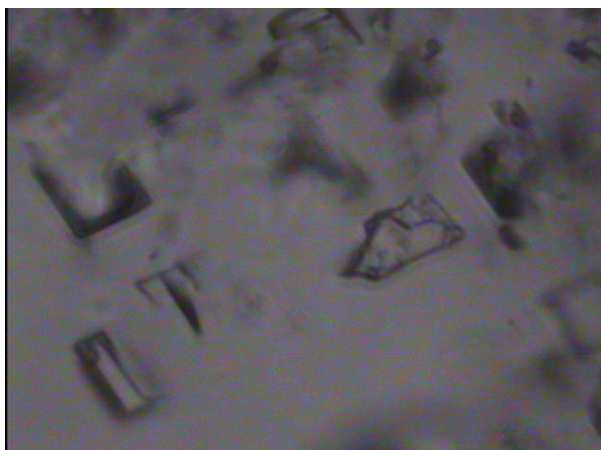
This interval of the Allaru Mudstone in the Eromanga Basin contained possible cone-in-cone and concretion calcite. The latter contains interlocking, anhedral crystals with dark, wispy fluid inclusions. Most of the fluid inclusions appear to be decrepitated but a few of the remaining inclusions are all-liquid. The inclusions are primary to pseudosecondary and irregular to elongated in shape and up to 20 µm in size.

Homogenisation temperature was determined to be below 70°C

Salinity could not be determined.

#98 Blackall 2: 660.38-660.54 m (Eromanga Basin)

This interval of the Toolebuc Formation in the Eromanga Basin contained calcite filled veins, cone-in-cone, slickensides, concretions and pyritised fossils. Only a ~10 mm wide calcite vein contained fluid inclusions suitable for study. A few, rare, liquid + vapour fluid inclusions were observed in the centre of the vein. These were primary, negative crystal to irregularly shaped inclusions with ~ 5 vol.% vapour and were up to 20 μm in size.



Homogenisation temperatures varied from 60.7 to 88.5 $^{\circ}\text{C}$ with trapping temperatures estimated to be $< 70^{\circ}\text{C}$.

Salinity measurements ranged from 0.0 to 1.7 wt.% NaCl eq.

#124 Connemara 1: 310.71-311 m (Eromanga Basin)

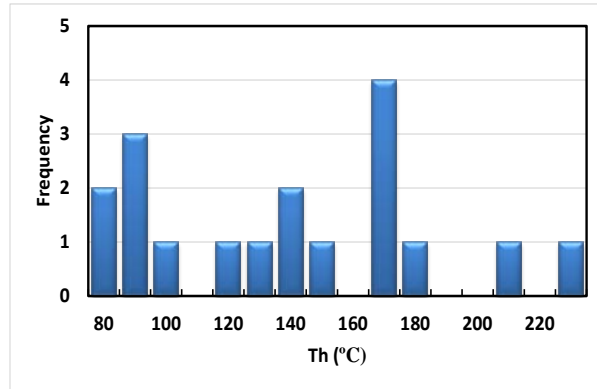
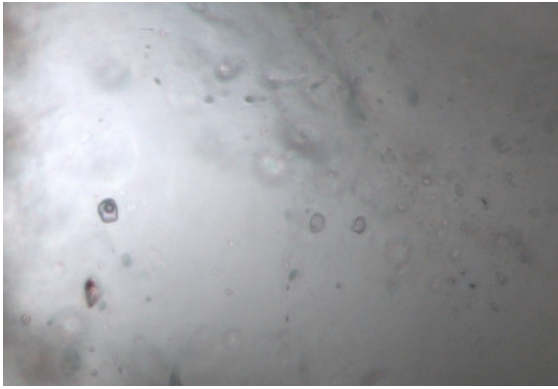
This interval of the Mackunda Formation in the Eromanga Basin contains calcite veining and cone-in-cone, and rare shells. The calcite veins contain very small, all-liquid fluid inclusions. They occur in crystal growth zones and hence are primary, range in size up to 5 μm and have irregular to negative crystal shapes.

Homogenisation temperature was determined to be $< 70^{\circ}\text{C}$.

Salinity could not be determined.

#103 Connemara 1: 942.17-942.37 m (Eromanga Basin)

This sample from the Westbourne Formation in the Eromanga Basin contains abundant calcite cement. Primary, two phase (liquid + vapour) inclusions and minor all-liquid inclusions occur in grains in the calcite cement. The inclusions range in size up to 10 μm , are mostly rounded and the two phase inclusions contain 5 – 10 vol.% vapour.



Homogenisation temperatures for the two phase inclusions ranged from 79.5 to 230 °C. However, the large spread of temperatures suggests re-equilibration of the fluid inclusions and the presence of all-liquid inclusions suggests a trapping temperature of < 70°C.

Final ice melting temperatures ranged from -19.6 to -22.6 °C which equates to salinities of 11.2 – 13.7 wt.% NaCl eq.

#105 Connemara 1: 946.24-946.34 m (Eromanga Basin)

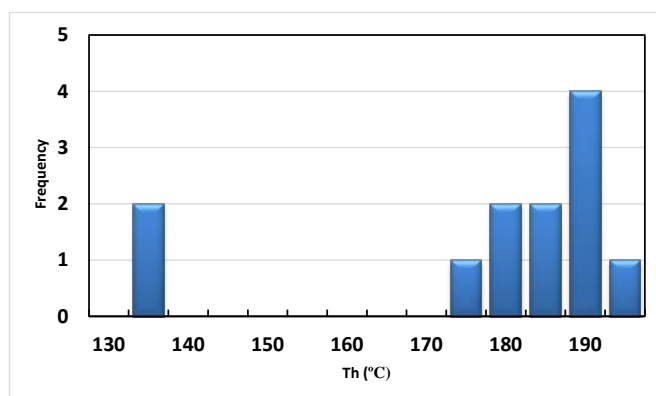
This interval of the Westbourne Formation in the Eromanga Basin contains calcite veining and cone-in-cone, cement, and shell fragments. The calcite cement contains rare all-liquid fluid inclusions and some liquid + vapour inclusions that likely result from post-entrapment re-equilibration. The all-liquid inclusions are primary and range in size up to 20 µm and have negative crystal to irregular shapes.

Homogenisation temperature was determined to be <70°C.

Salinity could not be determined.

#165 Dullingari 036: 4883'3" - 4883'4" (Eromanga Basin)

This sample from the Murta Formation in the Eromanga Basin contains oil and calcite cement, and is 350 feet below limestone. This sample had dark carbonate cement that made it difficult to observe the fluid inclusions. Some primary, two-phase (liquid + vapour) inclusions were observed. They ranged in size up to 5 µm and had negative crystal shapes.

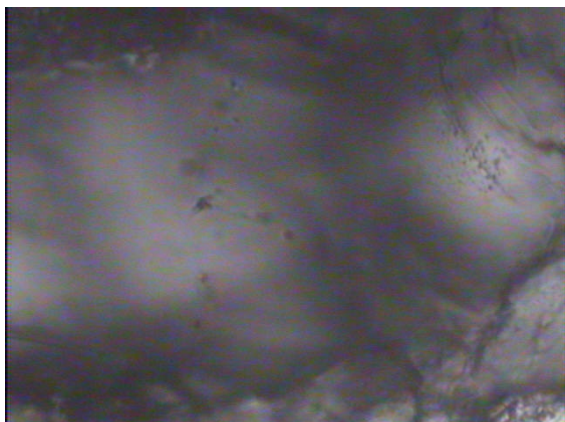


Homogenisation temperatures ranged from 131.8 - 191.3 °C. It is likely that this sample has undergone thermal re-equilibration and that trapping temperatures were around 130°C or less.

A single salinity measurement gave a value of 7.2 wt.% NaCl eq.

#167b Dullingari 037: 5065'8.5" - 5065'10.5" (Eromanga Basin)

This sample from the Murta Formation in the Eromanga Basin is a medium-grained sandstone with abundant calcite cement. Rare liquid + vapour inclusions are observed in the calcite cement. They are primary and range in size up to 15 μm and are irregular in shape and show signs of necking down.

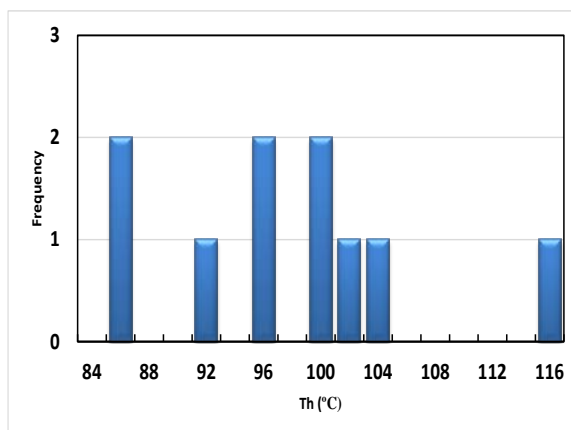
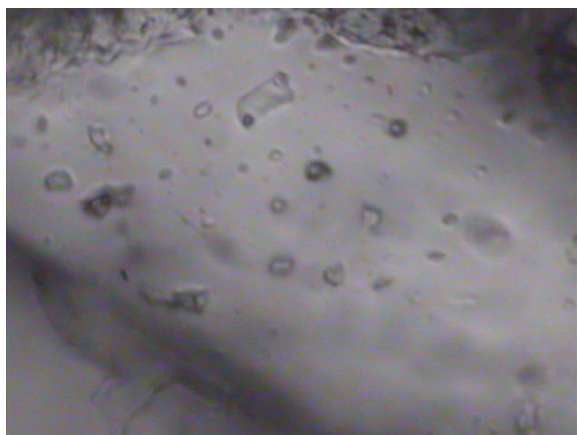


Only one homogenisation temperature was obtained at 184.8°C that must be viewed with caution in light of possible necking effects.

Salinity could not be determined.

#173 Dullingari 037: 5068'8" – 5069' (Eromanga Basin)

This sample from the Murta Formation in the Eromanga Basin consists of fine – medium grained sandstone with calcite cement. Rare two phase (liquid + vapour) fluid inclusions are observed in calcite crystals in lighter zones of the cement. Minor all-liquid inclusions are also present but these are thought to be in a metastable state. The primary inclusions range in size up to 10 μm diameter and are rounded to irregular in shape.

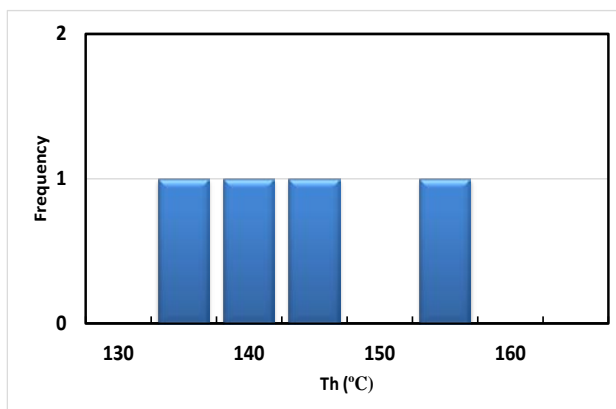
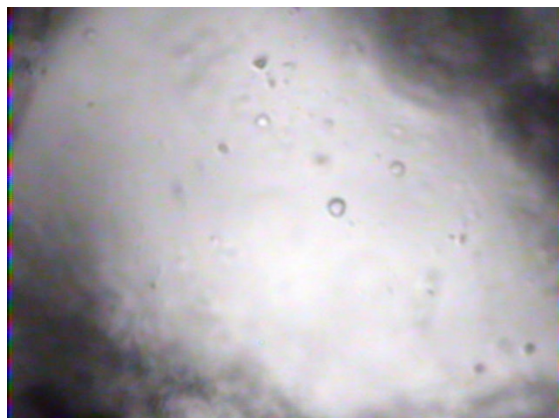


Homogenisation temperatures of the two phase inclusions range from 85.1 – 114.6 °C. Trapping temperatures are most likely below 105°C.

Final ice melting temperatures ranged from -19.5 to -16.8 that translated to salinities of 13.8 – 14.7 wt.% NaCl eq.

#171 Dullingari 039: 5024'9" - 5025'1.5" (Eromanga Basin)

This sample from the Murta Formation in the Eromanga Basin contains calcite cement, 70 feet above limestone. The calcite cement contains mostly all-liquid inclusions with some rare two phase, liquid + vapour inclusions. The inclusions are primary to pseudosecondary, range in size up to 5 µm and are rounded to irregular in shape.

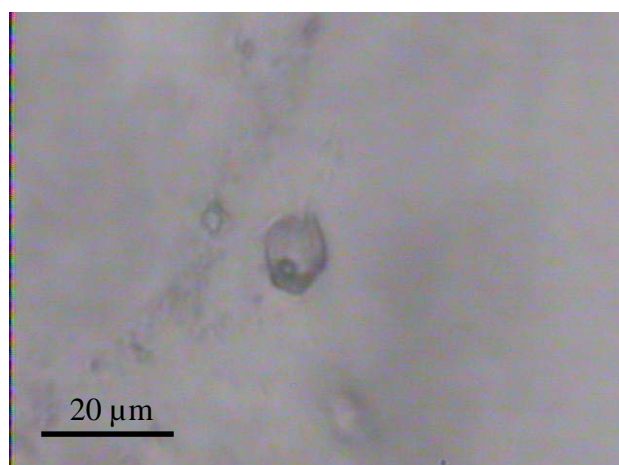


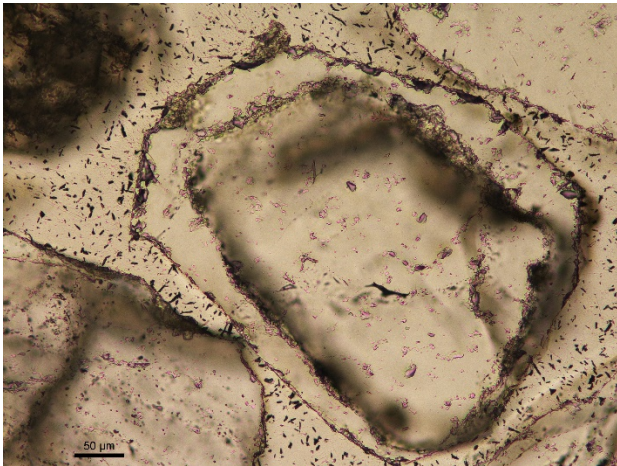
Homogenisation temperatures on two phase fluid inclusions ranged from 130.4 – 154.6 °C; however, as the majority of inclusions were all-liquid the trapping temperature is < 70°C.

Salinity could not be determined.

#189 Gidgealpa, Namur Sandstone: 5580' – 5590' (Eromanga Basin)

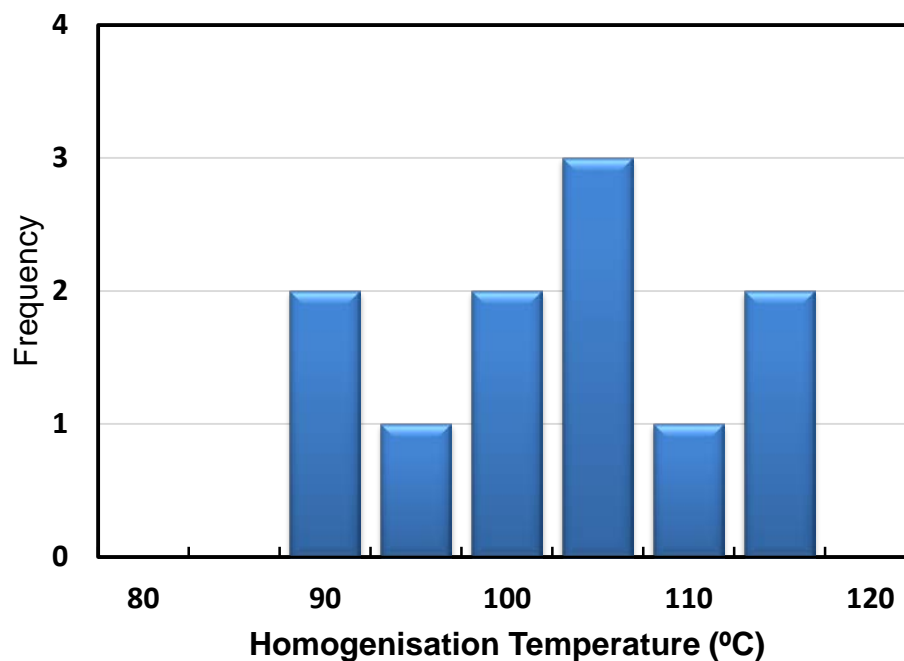
The quartz grains in this cuttings sample were irregular in shape with only a limited number having thin overgrowth bands. Unfortunately, this sample contained very little carbonate cement and no usable fluid inclusions could be found in the remaining cement. The overgrowths contained mostly liquid-only inclusions with rare two phase (liquid + vapour) inclusions. This may indicate that the liquid-only inclusions are in a metastable state and microthermometric data could only be obtained from the two phase inclusions. The fluid inclusions ranged in size up to 15 µm and were mostly irregular in shape. The two phase inclusions contained between 10 and 20 vol.% vapour. A few very rare fluid inclusions also contained an unidentified daughter crystal.





Overgrowth on a quartz grain
Primary, two phase, aqueous inclusion

A histogram of homogenisation temperatures for the two-phase inclusions is shown below.



Homogenisation temperatures for the two-phase inclusions ranged from 85.4 to 113.6 °C with a mode around 105°C. The presence of all-liquid inclusions may be due to metastability or may indicate the presence of a population of inclusions homogenising below 70°C. Therefore, the reported temperatures represent the highest possible homogenisation temperatures.

Salinity estimates were attempted but the inclusions showed metastable behaviour with ice melting temperatures above 0.0°C.

#78 Jackson South 2: 4279'6.5"-4279'9" (Eromanga Basin)

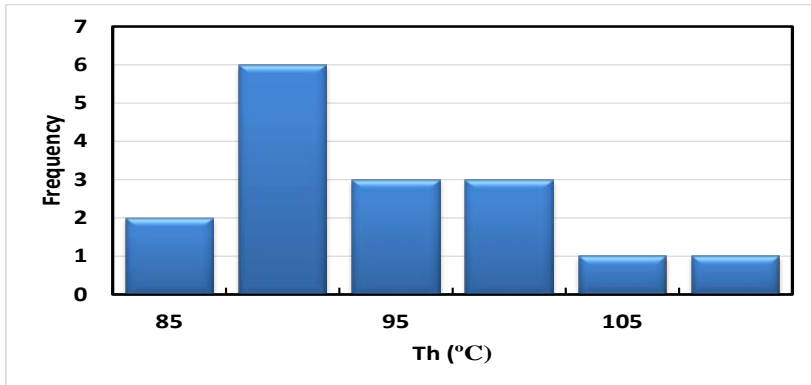
This sample from the Westbourne Formation in the Eromanga Basin contains oil stained, calcite cement, and calcite veins that have abundant, small, all-liquid aqueous and oil filled fluid inclusions. The inclusions are primary and range in size up to 5μm diameter and are rounded to irregular in shape.

Homogenisation temperature was determined to be < 70°C.

Salinity could not be determined.

#77 Jackson South 2: 4279'9"-4280'2" (Eromanga Basin)

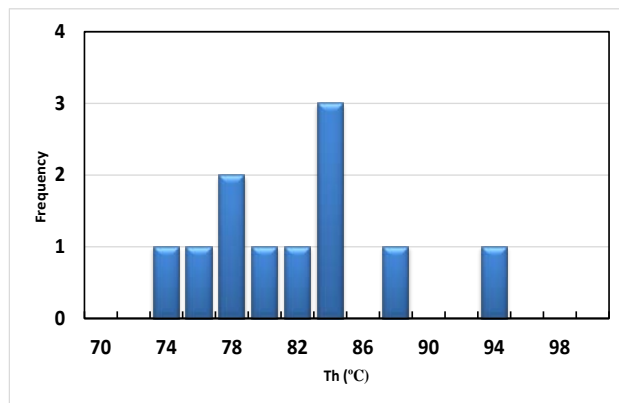
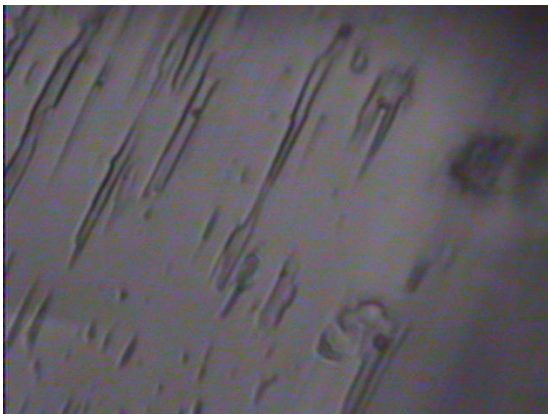
This sample from the Westbourne Formation in the Eromanga Basin contains oil stained calcite cement and veins. The calcite cement contains rare, very small, primary all-liquid and two phase (liquid + vapour) inclusions. The inclusions range in size up to 2 µm and are rounded to negative crystal in shape. The two phase inclusions contain ~5 vol.% vapour. The all-liquid inclusions may be in a metastable state.



Homogenisation temperatures for two phase inclusions ranged from 84.5 – 108.1 °C with a mode at 90°C. Salinity could not be determined.

#166 Jena 6: 3882'9" - 3882'11" (Eromanga Basin)

This sample from the Murta Formation in the Eromanga Basin contains oil stained, calcite cement, and calcite veins. Very rare, two phase (liquid + vapour) fluid inclusions were observed in a 3 mm wide calcite vein cross-cutting the sandstone. The primary inclusions were located close to the walls of the vein. They ranged in size up to 40µm diameter, were irregular to elongated in shape and contained ~5 vol.% vapour.

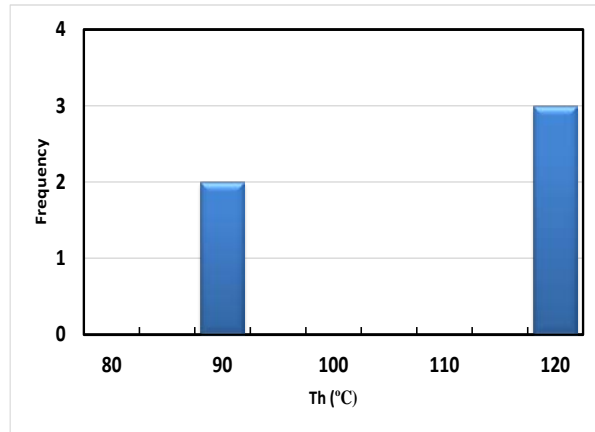
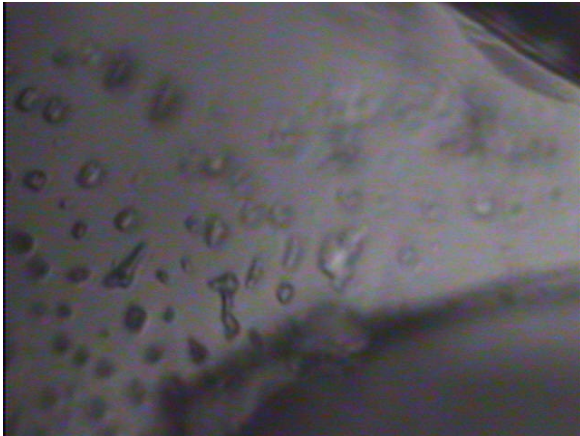


Homogenisation temperatures ranged from 72.4 - 93.8 °C with a mode at 84.0°C.

Freezing measurements were also conducted but all inclusions exhibited metastable behaviour with final ice melting above 0.0°C.

#108 Jundah 1: 905.65 m (Eromanga Basin)

This interval of the Hooray (Namur) Sandstone in the Eromanga Basin contains abundant calcite cement associated with calcite filled faults and other fractures and also cone-in-cone calcite. The cement contains sparse planar arrays of small, primary fluid inclusions in clear calcite crystals. The inclusions are mostly all-liquid with rare two phase (liquid + vapour) inclusions that may result from post entrapment modification. The inclusions are negative crystal to rounded in shape and range in size up to 10 µm diameter.



Homogenisation temperatures for the two phase inclusions ranged from 86.3 - 116.2°C but the presence of all-liquid inclusions indicates a trapping temperature of < 70°C.

Freezing measurements were also conducted but all inclusions exhibited metastable behaviour with final ice melting above 0.0°C.

#111 Jundah 1: 939.62-939.68m (Eromanga Basin)

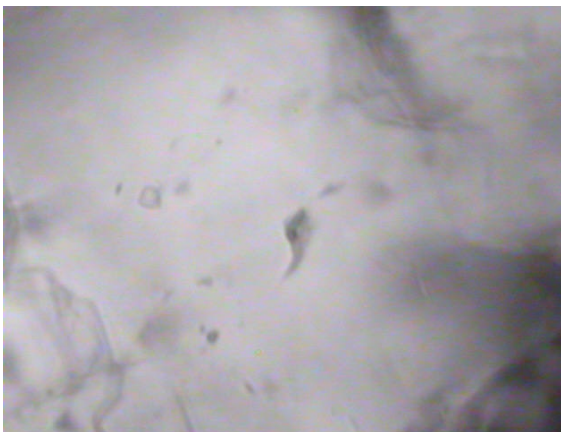
This sample from the Cadna-Owie Formation in the Eromanga Basin contains calcite cement associated with a shear-zone and some calcite veining. The calcite cement contained very small, primary fluid inclusions. The inclusions were rounded to irregular in shape and ranged in size up to 5 µm diameter.

Homogenisation temperature was determined to be < 70°C.

Salinity could not be determined.

#163 Marabooka 004: 3433' - 3433'6" (Eromanga Basin)

This sample from the Oodnadatta Formation in the Eromanga Basin is located 100 feet above and 350 feet below limestone and contains calcite cement and veins. The calcite veins contain very rare two phase (liquid + vapour) fluid inclusions. They are primary, range in size up to 5 µm diameter, are irregularly shaped and contain ~5 vol.% vapour.

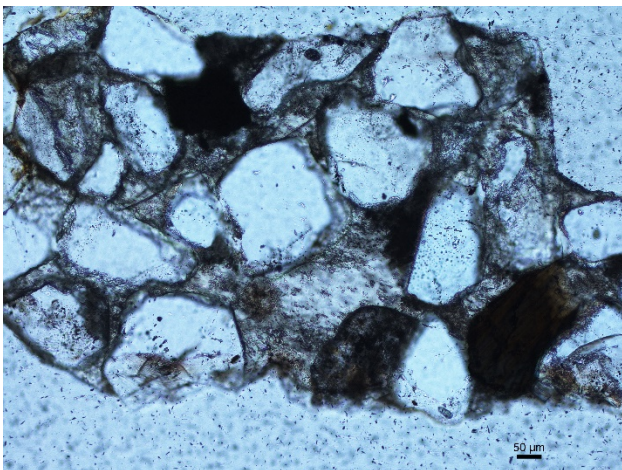


Only two homogenisation temperatures were obtained and they are 70.0 and 71.4 °C respectively.

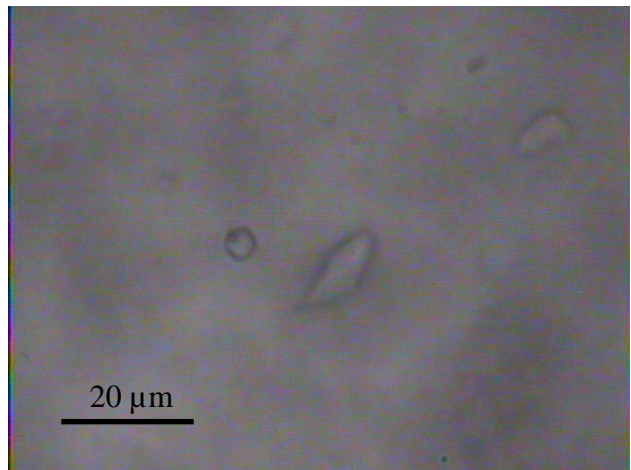
Salinity could not be determined.

#201 Muteroo 1, Namur Sandstone: 5290' – 5300' (Eromanga Basin)

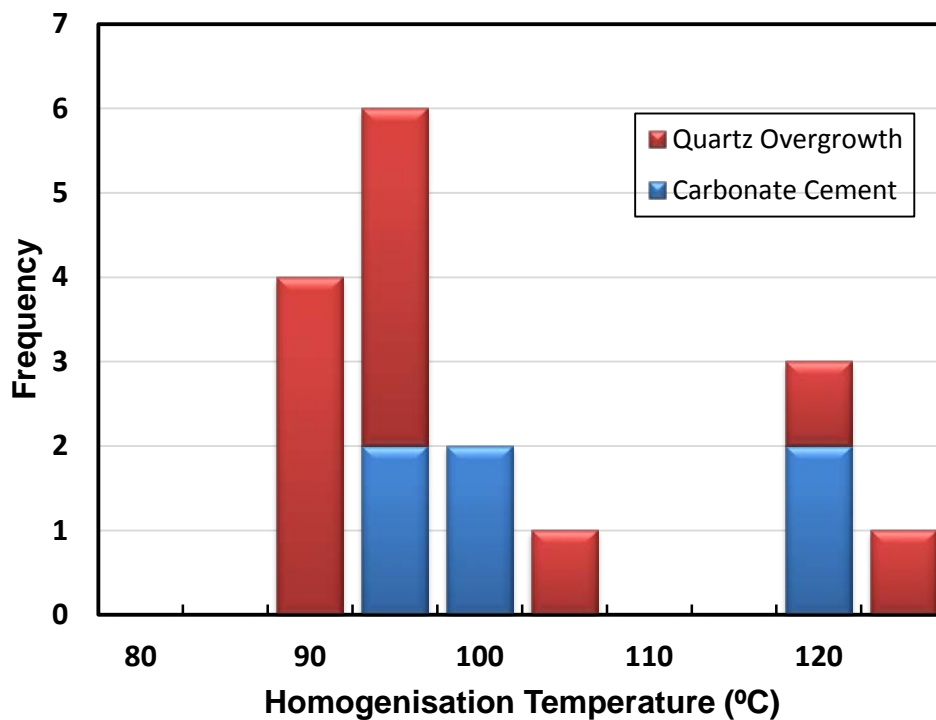
The carbonate cement was better preserved in this cuttings sample compared to the other two (#189 and #197), and contained several clusters of irregularly shaped quartz grains (< 500 µm diameter) with interstitial carbonate cement. Suitable fluid inclusions in the carbonate cement were rare but both liquid-only and aqueous two-phase inclusions were observed in the cement. They varied from rounded to irregular in shape and ranged in size up to 20 µm. Due to the scarcity of inclusions in the carbonate cement, a number of inclusions in the quartz overgrowths were also measured. Once again both liquid-only and aqueous, two phase inclusions were observed in the quartz overgrowths. They were also rounded to irregular in shape and ranged in size up to 30 µm.



Cluster of quartz grains with darker, interstitial carbonate cement.



Rounded two phase inclusion coexisting with larger liquid-only inclusion

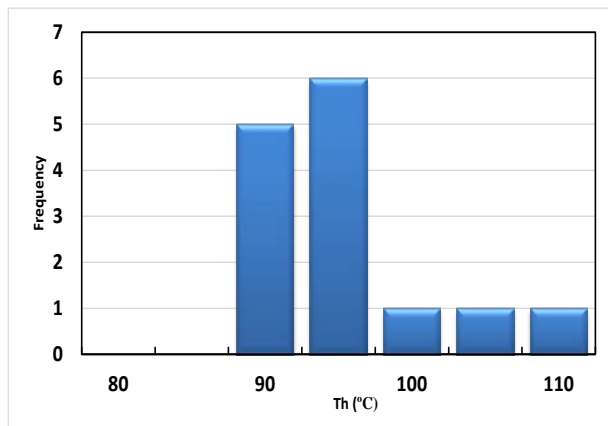


Homogenisation temperatures for inclusions in the carbonate cement are plotted in blue while those for inclusions in the quartz overgrowths are plotted in red. Homogenisation temperatures for all the two-phase inclusions ranged from 87.1 to 122.7 °C with a mode around 95°C. The presence of all-liquid inclusions may be due to metastability or may indicate the presence of a population of inclusions homogenising below 70°C. Therefore, the reported temperatures represent the highest possible homogenisation temperatures.

Most inclusions showed metastable ice melting behaviour but two inclusions in the carbonate cement exhibited an ice melting temperature of -0.3°C which equates to a salinity of 0.5 wt.% NaCl equivalent.

#172 Narcoonowie 004: 4382'5" - 4382'7" (Eromanga Basin)

This sample from the Murta Formation in the Eromanga Basin was positioned both 6 feet below and 6 feet above well-site logger-reported liquid oil occurrences and contains calcite cement. No suitable inclusions could be found in the calcite cement but co-existing quartz contained liquid + vapour and vapour-only fluid inclusions. The vapour-only inclusions may have resulted from leaking of inclusions during post-entrapment modifications. The inclusions are primary in crystal growth zones, range in size up to 20µm diameter and are irregular to rounded in shape. The two phase inclusions contain ~10 vol.% vapour.

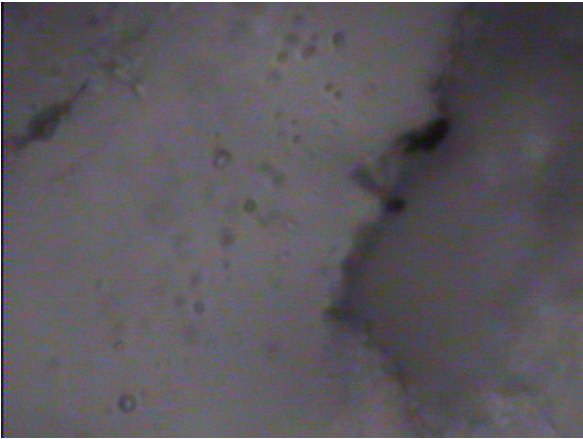


Homogenisation temperatures ranged from 86.0 - 109.6 °C with a mode at 95.0°C.

Salinity was not determined.

#164 Narcoonowie 004: 4395' - 4395'4" (Eromanga Basin)

This sample from the Murta Formation in the Eromanga Basin was located 5 feet below a well-site logger-reported oil occurrence and contains calcite cement and veins. There are sparse occurrences of small, all-liquid inclusions and aqueous inclusions containing what appear to be bitumen nodules in the calcite cement. The inclusions are primary, range in size up to 5µm and are mostly rounded in shape.

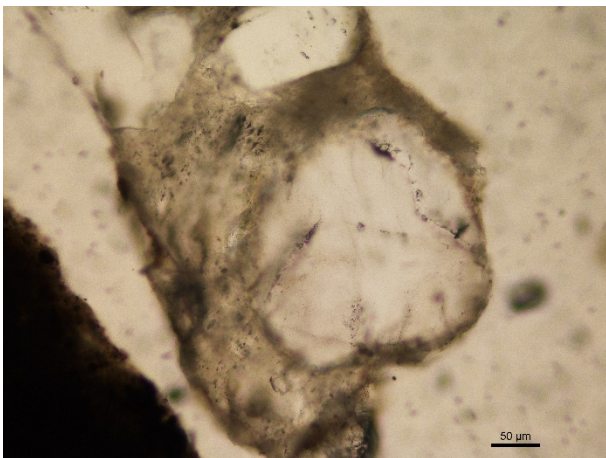


A single homogenisation temperature of 112.6°C was obtained from a two phase fluid inclusion but the dominance of all-liquid inclusions indicates a trapping temperature of < 70°C

Salinity could not be determined.

#197 Spencer West 1, Namur Sandstone: 5000' – 5010' (Eromanga Basin)

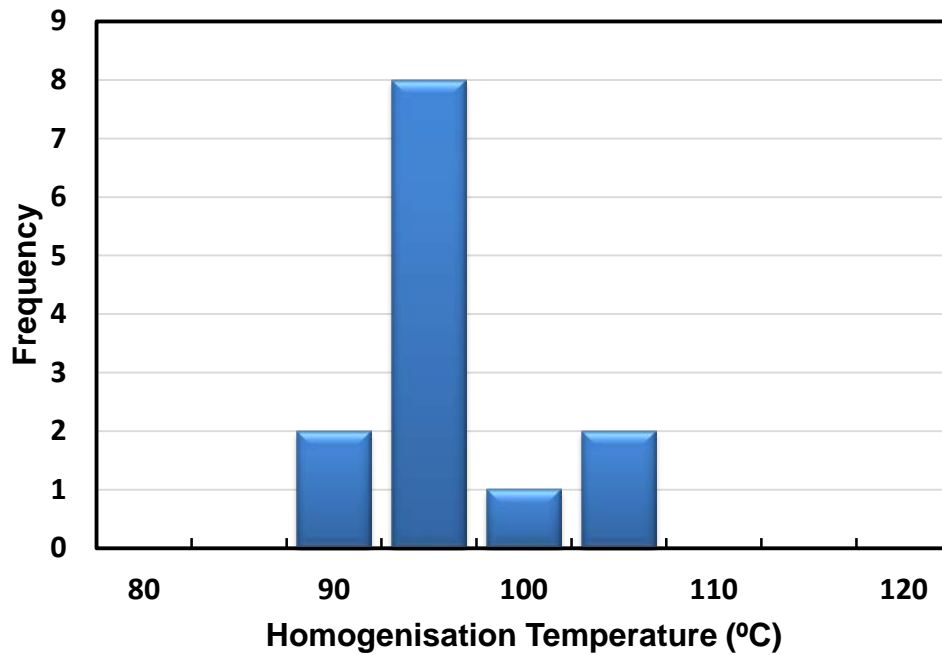
This cuttings sample contains irregular, small (< 500µm diameter) quartz grains with some cemented together by a brownish carbonate cement. The carbonate cement was cloudy and the fluid inclusions in this cement were too small to study by microthermometry. Therefore, all data for this sample were obtained from quartz overgrowths. Fluid inclusions in the overgrowths were irregular in shape and ranged in size up to 15µm. A mixture of liquid-only and two phase, aqueous inclusions were observed. The latter contained approximately 10 vol.% vapour.



Carbonate (darker brown) cementing quartz grains



Aqueous, two phase fluid inclusion and smaller liquid-only inclusions in quartz overgrowth

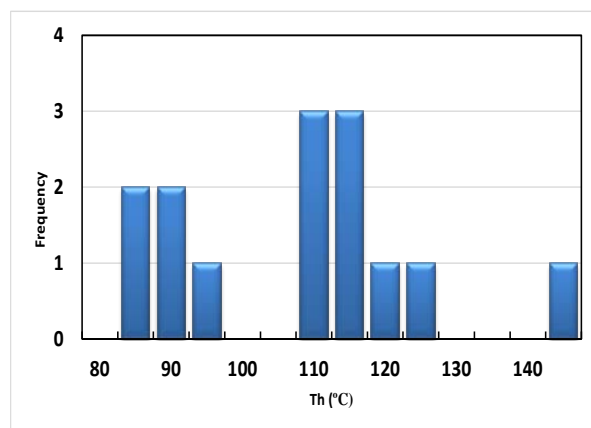


Homogenisation temperatures for the two-phase inclusions ranged from 87.3 to 101.5 °C with a mode around 95°C. The presence of all-liquid inclusions may be due to metastability or may indicate the presence of a population of inclusions homogenising below 70°C. Therefore, the reported temperatures represent the highest possible homogenisation temperatures.

Salinity could not be determined due to metastable ice melting behaviour.

#152 Thargomindah 1A: 966.86-967.12m (Eromanga Basin)

This sample from the Adori Sandstone in the Eromanga Basin contains calcite cement and veins. The calcite veins contain rare, primary, two phase (liquid + vapour) fluid inclusions. The inclusions range in size up to 30 µm diameter, are negative crystal to irregular in shape and contain ~5 vol.% vapour.

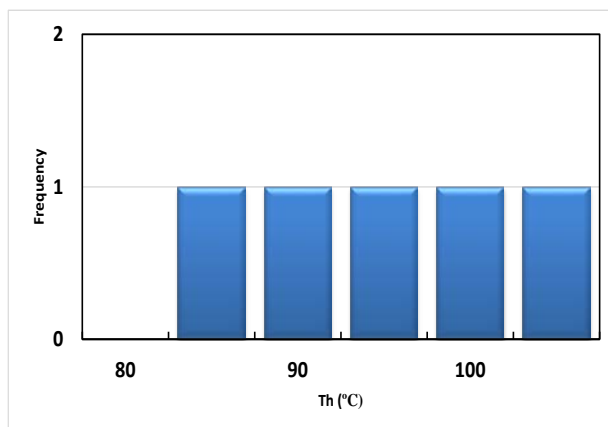


Homogenisation temperatures range from 82.1 - 144.0 °C. The higher temperatures may have resulted from thermal re-equilibration of the inclusions and therefore trapping temperatures are most likely less than 100°C.

Salinities ranged from 0.0 to 0.5 wt.% NaCl eq.

#118 Thargomindah 2: 956.38-956.44m (Eromanga Basin)

This sample from the Cadna-Owie Formation in the Eromanga Basin contains calcite cement and occurs just above a fault with offset of 1.3 m. The calcite cement contains rare, primary, two phase (liquid + vapour) inclusions. They range in size up to 5 µm diameter, are rounded to irregular in shape and contain 5 – 10 vol.% vapour.

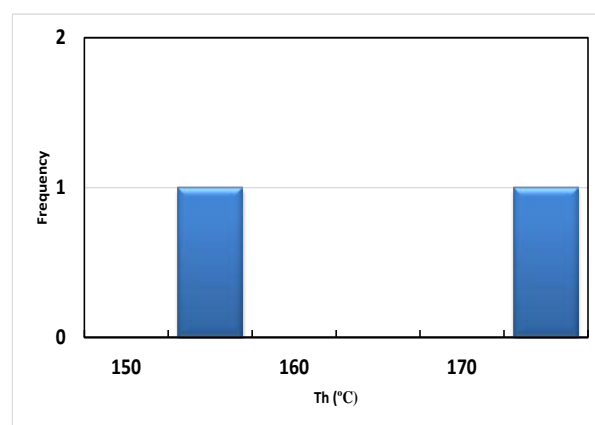


Homogenisation temperatures ranged from 81.1 – 104.6 °C.

Salinity could not be determined.

#168b Ulandi 5: 3914'10" - 3915'1" (Eromanga Basin)

This sample from the Cadna-Owie Formation in the Eromanga Basin contains oil shows and calcite cement. Clear calcite cement contains both all-liquid and two phase (liquid + vapour) fluid inclusions. The primary inclusions are located in the core of the clear calcite crystals, range in size up to 20 µm diameter and are mostly irregular in shape. The two phase inclusions contain ~10 vol.% vapour.

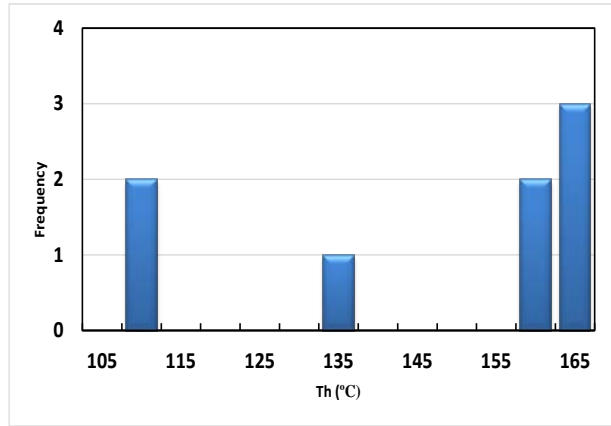
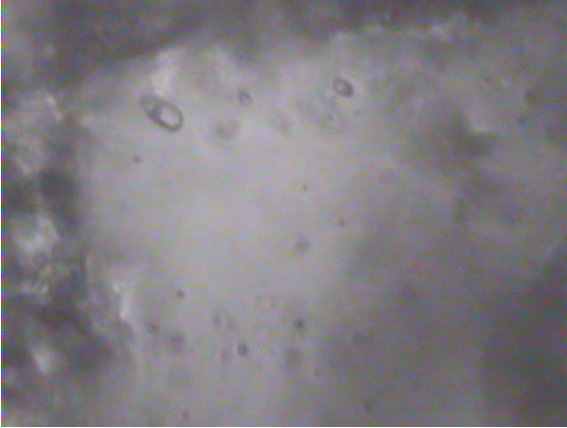


The homogenisation temperatures from two liquid + vapour inclusions were 151.2°C and 173.2 °C respectively. However, the presence of all-liquid inclusions indicates a trapping temperature of < 70°C.

A single salinity value of 5.8 wt.% NaCl eq. was obtained.

#8 Winna-1: 1008.08-1008.12 m (Eromanga Basin)

This sample from the Murta Formation in the Eromanga Basin contains good oil shows, moderate siliceous and strong calcite cement. There are occasional two phase (liquid + vapour) fluid inclusions in grains in the carbonate cement. The inclusions are primary, range in size up to 10 µm diameter and are rounded to irregular in shape.



Homogenisation temperatures range from 108.6 – 163.0 °C. The higher temperatures are likely due to post entrapment changes to the inclusions, and therefore, the trapping temperature is estimated to be 108.6°C. The salinity was not determined.

Appendix 6: FEI characterisation of samples WW1_Precipice_1212m and WW1_Hutton_724m pre and post batch reactor experiments

The full text of the FEI-LITHICON final report (29pp) is appended from the next page onwards.

PROJECT

Sample characterization before and after geochemical reactivity studies for ANLEC Project 7-1011-0189

<i>DATE</i> 24.12.2015	<i>DOCUMENT STATUS</i> FINAL
<i>FEI PROJECT NUMBER</i> VORT_3	<i>CLIENT REFERENCE</i>
<i>CLIENT</i> University of Queensland	<i>CLIENT CONTACT</i> s.golding1@uq.edu.au
<i>AUTHORS</i> Silvano Sommacal, Carley Goodwin, Julie Pearce	

FEI Trondheim AS

Stiklestadveien 1 N-7041 Trondheim
Norway
Tel +47 992 02 992

FEI Australia Pty Ltd

Suite 102 Level 1 73 Northbourne Ave Canberra ACT 2600
Australia
Tel +61 2 6173 6200

FEI Company (FEI Houston)

16700 Park Row Dr. Houston, TX 77084
USA
Tel +1 713 375 1313

FEI.com

Table of Contents

1	Executive summary	209
2	Project workflow	211
3	Results and Discussion	211
3.1	Scoping scan imaging in 3D by μCT	212
3.2	Before reaction imaging of sub-plug in 3D by μCT at the pore-scale	213
3.3	Segmentation of before reaction tomograms into X-ray distinct components and quantification in 3D	215
3.4	SEM imaging and mineral mapping by automated quantified SEM-EDS before reaction	217
3.5	Geochemical reactivity studies at University of Queensland	220
3.6	After reaction imaging of sub-plug in 3D by μCT at the pore-scale and mineral segmentation into X-ray distinct components	221
3.7	After reaction SEM imaging and mineral mapping by automated quantified SEM-EDS	223
3.8	Investigation and quantification in 3D of changes due to CO₂:brine:rock interactions	225
4	Conclusions	228

1 Executive summary

This project focussed on acquiring time series imaging of sample 724 from the Surat Basin West Wandoan 1 well Hutton Sandstone, 724m depth and of sample 1212 from the Precipice Sandstone (sampled at 1212m depth). The objective of this study was to time-lapse measure and characterise geochemical reactivity of core material from the Hutton Sandstone and a clean section of the Precipice Sandstone reservoir through micro-computed tomography (μ CT) 3D imaging, Scanning Electron Microscopy (SEM), and automated, quantified SEM-Energy Dispersive X-ray Spectroscopy (EDS) mineral mapping. This was performed before and after reaction with supercritical CO₂ and brine to investigate the potential for engineered mineral trapping.

This study investigated the reactivity to CO₂:brine of a) Hutton Sandstone with a low-salinity brackish water and traces of SO₂, and b) Precipice Sandstone with pure CO₂ and a high salinity brine. Experiment system conditions of 10-12MPa and 50-60°C were selected to simulate realistic in situ pressure-temperature conditions of the target carbon storage reservoir and seal formations within the Surat Basin, as detailed in the final report for ANLEC project 7-1011-0189.

Prior to experimentation, the core samples were digitally characterised in 3D by X-ray micro-computed tomography (μ CT) and the 3D μ CT images were registered into perfect geometric alignment with higher-resolution 2D SEM images and automated, quantified SEM-EDS (QEMSCAN®) mineral maps of the same samples. The samples were then reacted at University of Queensland before being imaged again and the two sets of before and after reaction images registered to one another to characterise the changes caused by geochemical reactions.

Sample 724 (West Wandoan 1 Hutton Sandstone from 724m depth) is a sub-arkosic sandstone with a high content of potentially reactive Fe-rich chlorite. To reduce the amount of trace or unclassified phase a mixed K-feldspar – chlorite phase was successfully quantified. Significant changes after reaction in porosity or mineral content were not detected in the sub-plug by μ CT or QEMSCAN®. No significant reduction in the chlorite content after reaction was measured; however, density changes indicated leaching of Fe from chlorite. Trace phases contained some Fe; however, precipitation of very small traces of siderite or Fe-oxides could not be identified or ruled out as the Fe could also have been measured from pre-existing chlorite.

Sample 1212 (West Wandoan 1 Precipice Sandstone from 1212m depth) is a clean, quartzose sandstone, medium to coarse grained. After reaction only very small amounts of calcite and dolomite precipitation were identified by QEMSCAN. Given the low content of reactive minerals in this core the precipitated carbonates were likely from Ca, Mg and bicarbonate sourced from the reaction brine.

2 Project workflow

For this project we adopted the same workflow that was previously designed and tested for ANLEC project 7-0311-0128, sub-project 5. Main steps of the workflow can be summarised as:

- 1) Scoping scan imaging in 3D by μ CT of the sections of core to investigate heterogeneity of features $>15\mu\text{m}$ in size and guide selection of region for sub-plug extraction;
- 2) Selection of location and drilling of one sub-plug from each off-cut for pore-scale imaging;
- 3) Imaging of sub-plugs in 3D by μ CT at the pore-scale before reaction;
- 4) Segmentation of 'before' tomograms into X-ray distinct components and quantification in 3D;
- 5) Trimming of one end of the sub-plugs within the imaged field-of-view for creation of a polished section;
- 6) Imaging of the polished section by SEM and registration of the high resolution 2D SEM image into the 3D tomogram to find the perfectly matching slice;
- 7) Automated, quantified SEM-EDS analysis of the same polished section to generate a mineral map and registration to the SEM image and the 3D tomogram;
- 8) Sending sub-plugs to UQ for geochemical reaction at reservoir temperature and pressure;
- 9) Imaging of sub-plugs in 3D by μ CT at the pore-scale after reaction and 3d:3d registration into perfect geometrical alignment to the 'before' tomogram;
- 10) Segmentation of 'after' tomograms into X-ray distinct components and quantification in 3D;
- 11) Trimming of the same end of the sub-plugs as in (5) within the imaged field-of-view, of the 'before' and 'after' tomograms, for creation of a polished section after reaction;
- 12) Imaging of the polished section by SEM and registration of the high resolution 2D SEM image into the 'before' and 'after' 3D tomograms to find the perfectly matching slice;
- 13) Automated, quantified SEM-EDS analysis of the same polished section to generate a mineral map and registration to the SEM image and the 'before' and 'after' 3D tomogram; and
- 14) Investigation and quantification in 3D of changes due to CO_2 :brine:rock interactions through digital comparison of the two registered 3D tomograms from (3) and (9).

Two sections of core, one from the Hutton Sandstone, the other from the Precipice Sandstone were sent to FEI, some basic information about these off-cuts is summarized in Table 37.

3 Results and Discussion

This section of the report is set-out to correspond to each of the imaging and analysis steps outlined in section 2.

3.1 Scoping scan imaging in 3D by μ CT

Imaging of the sections of core allowed the qualitative assessment of grain size, grain sorting, mineralogy, degree of pore-filling clay, and carbonate cement, and organic content. Scoping scan images were used to guide the coring (size and location) of sub-plugs to be extracted for high resolution imaging.

Vertically (X and Y) and horizontally (Z) oriented views of scoping scan tomogram images of samples 724 and 1212 are shown in Figure 60. A basic description of the samples based on visual inspection of the scoping scan images is provided in Table 37.

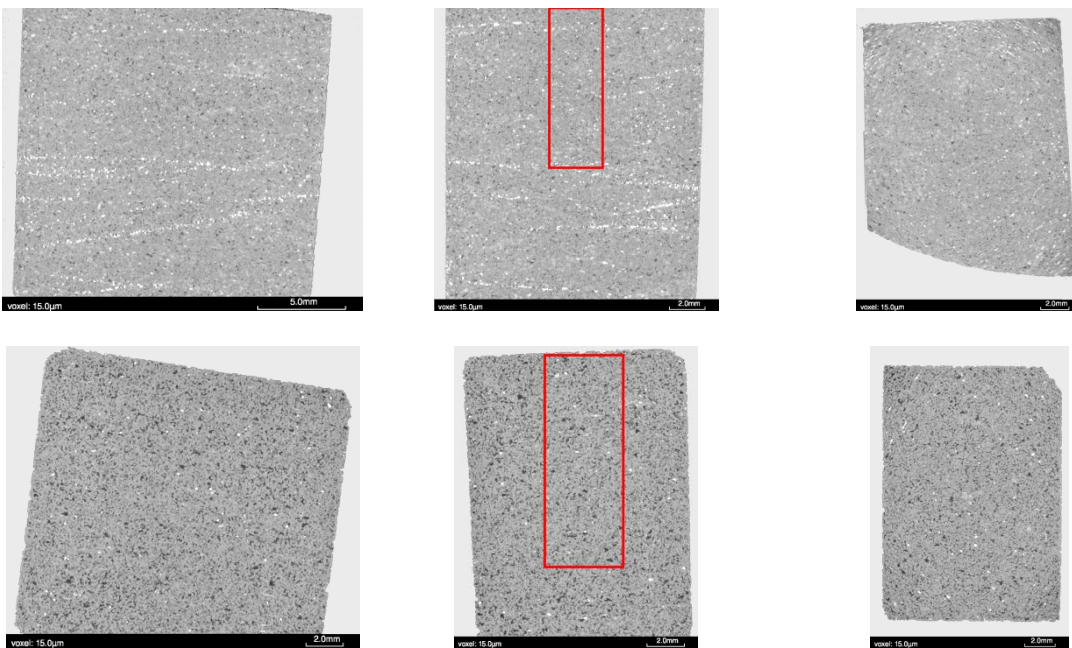


Figure 60: Tomogram images (X, Y, Z, left to right) from scoping scans of 724 (top) and 1212 (bottom) samples; red polygon indicates approximate location and size of sub-plug extracted for high resolution imaging study.

Table 37. Description of samples selected for geochemical reactivity study from scoping scan images.

Sample	Interval	Approx. off-cut size (mm)	Voxel size Scoping Scan image	Description
724	Hutton Sandstone	18 x 14 x 14	15µm	Moderately sorted medium to coarse-grained sandstone; abundant higher density grains and some open pores are present
1212	Precipice Sandstone	18 x 12 x 12	15µm	Moderately sorted medium to coarse-grained quartzose sandstone; abundant open pore space with some clay infilling and scattered heavy minerals.

Based on inspection of the 3D tomogram scoping scan images it was decided to core a $\approx 3 \times 9$ and a $\approx 4 \times 11$ mm sub-plug, respectively, from sample 724 and 1212.

3.2 Before reaction imaging of sub-plug in 3D by μ CT at the pore-scale

Imaging of the samples at the sub-plug scale allows the characterisation of pore-scale features.

Vertically (X and Y) and horizontally (Z) oriented views are shown in Figure 61 from tomogram high resolution sub-plug images of samples 724 and 1212. A basic description of the sub-plugs cored and some additional observations of the samples main textural / mineralogical features based on the visual inspection of the pore-scale tomograms are provided in Table 38.

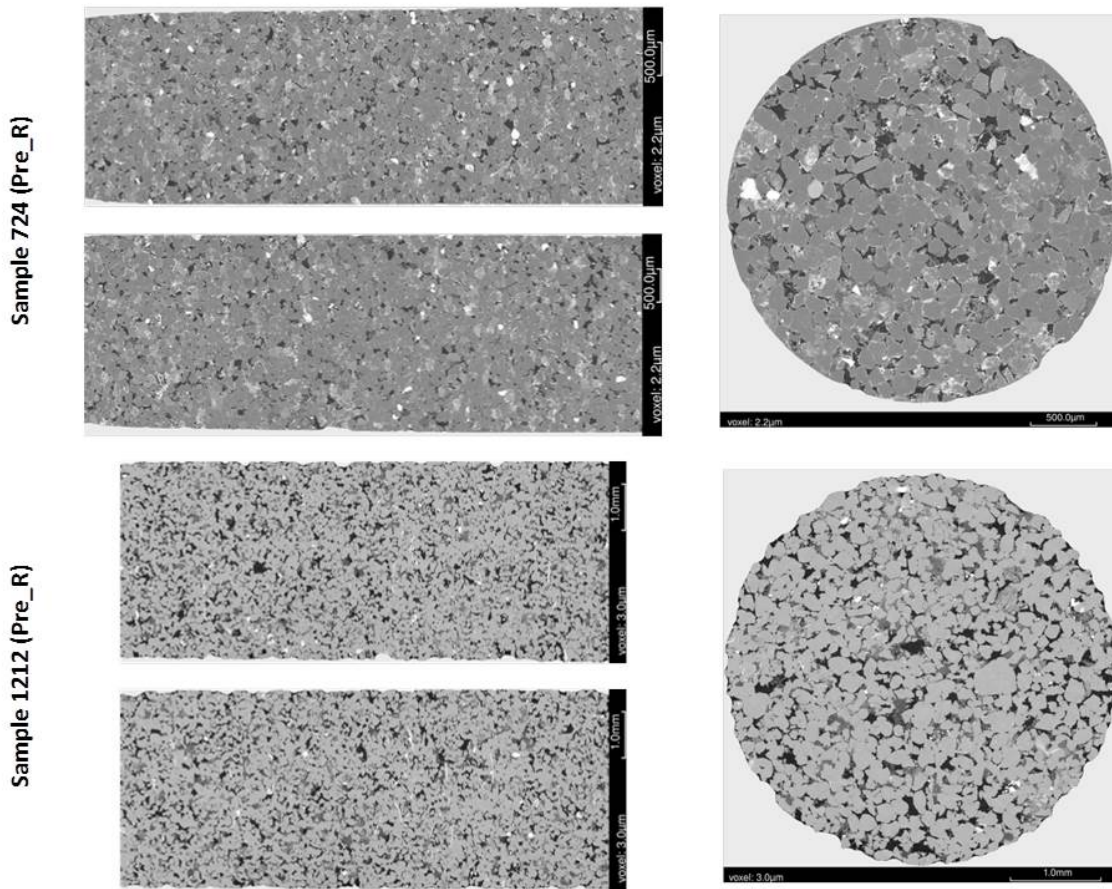


Figure 61: Vertical (X-top, Y-bottom) and horizontal (Z-right) plane images from high resolution 3D μ CT tomograms of sub-plugs 724 and 1212, before reaction.

Table 38. Description of samples selected for geochemical reactivity study from high resolution sub-plug images.

Sample	Sub-plug size (mm)	Voxel size sub-plug image	Additional observations
724	3 x 9	2.2 μ m	High density (Fe-rich) sheet silicates likely to be present as individual grains or pore-filling, pore-lining and/or pore-bridging phase. Large pores are present some of them partially when not almost completely filled in with low-density clay (probably kaolinite). Framework grains likely to be made of quartz and feldspar (both K- and Na- feldspar). Secondary porosity associated with weathered/altered framework grains is also present.
1212	4 x 11	3.0 μ m	Large pores are present with abundant clays of density either lower (likely kaolinite) or higher (likely illite and/or muscovite) than framework grains. Clays are pore-filling and to a lesser extent pore-bridging. Framework grains likely to be made mostly by quartz.

3.3 Segmentation of before reaction tomograms into X-ray distinct components and quantification in 3D

Segmentation of X-ray distinct components in the before reaction 3D tomograms has been performed for both 724 and 1212 samples (Figure 62).

This segmentation has allowed the quantification in 3D of X-ray distinct phases in the two samples, including open (i.e. resolved¹) pores, lower and higher density ‘clays’, main framework grain(s) and high density phases. Results of the segmentation are summarised in Table 39.

It has not, however, allowed the mapping and calculation of the sub-plugs total porosity as both samples contain a high proportion of pore-filling material with associated sub-resolution porosity which cannot be calculated by this technique alone. Ideally a well-separated multimodal distribution of the X-ray attenuation coefficients (grey-scale) gives an unambiguous phase assignment of the pore and various mineral phase peaks. For low permeability samples and/or samples with complex mineralogy and high clay content, the more complex lithology does not allow multiphase segmentation to distinguish sub-resolution micropores², which are associated with clay fractions, weathered framework grains or diagenetic cements (Knackstedt *et al.*, 2013).

¹ Resolved porosity indicates pores that are larger than the elemental volume for a tomogram, i.e. one voxel (3D pixel) in size.

² The term microporosity refers to pores that are smaller than one voxel, hence sub-resolution; the sum of the resolved and sub-resolution porosity is called the total porosity.

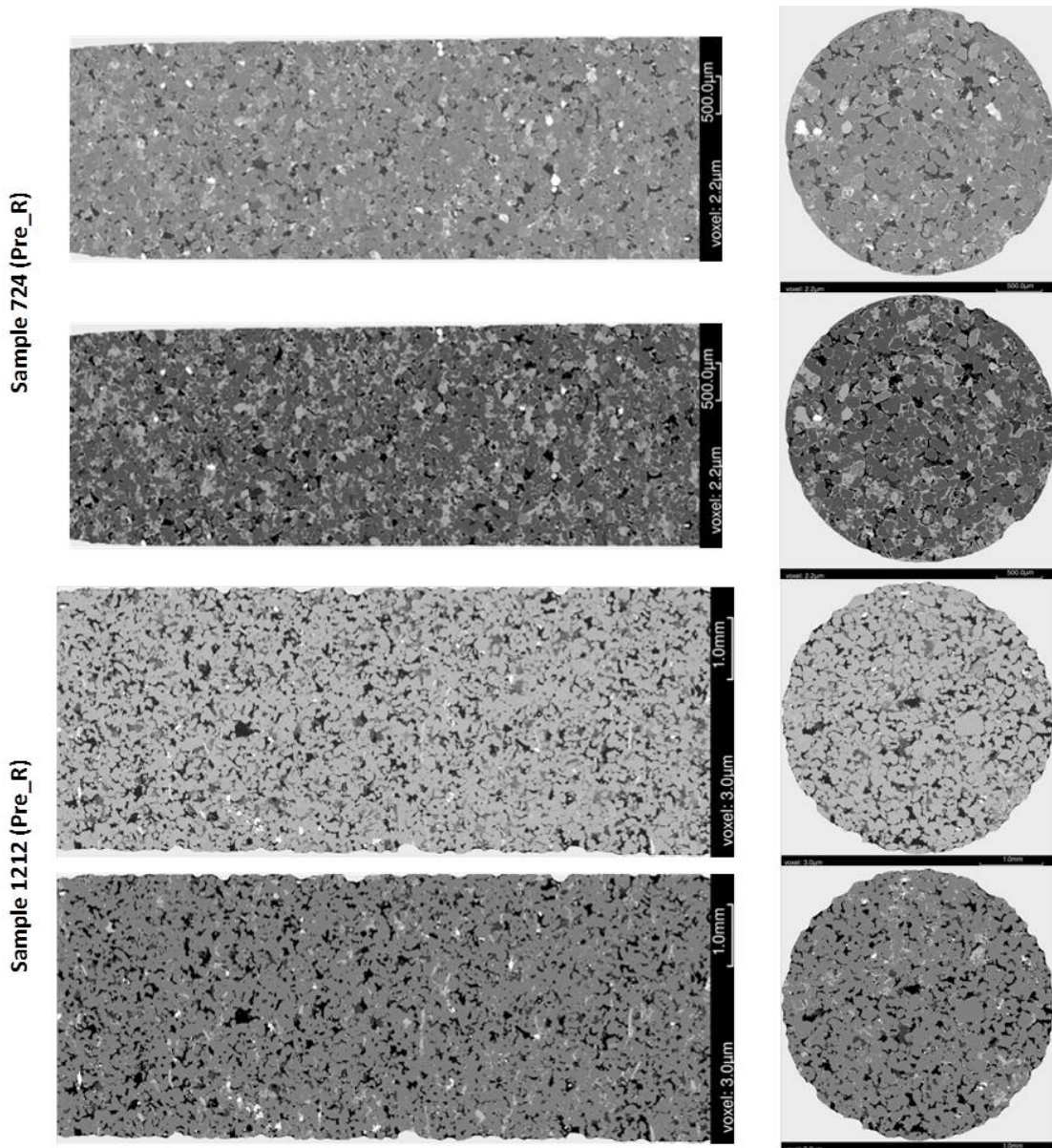


Figure 62: Sample 724 and 1212 vertical (X-left) and horizontal (Z-right) images from high resolution tomograms (row 1 & 3) and mineral segmented images (row 2 & 4), before reaction.

Table 39. Volume percentages of X-ray distinct components derived from segmentation of before reaction sub-plug scale images; where, Framework grain_1: mostly quartz + Na-plagioclase for 724, quartz for 1212; Framework grain_2: mostly K-feldspar; Lower density clay: mostly kaolinite; Higher density ‘clays’: mostly chlorite for 724, illite + muscovite for 1212; High density grain_1: mostly rutile; High density grain_2: mostly zircon.

Sample	Resolved porosity	Framework grain_1	Framework grain_2	Lower density Clay	Higher density ‘Clay’	High density Grain_1	High density Grain_2
724 (Pre_R)	6.85	54.85	11.5	4.8	21.6	0.2	0.15
1212 (Pre_R)	11.3	73.6	-	7.8	7.0	0.4	-

3.4 SEM imaging and mineral mapping by automated quantified SEM-EDS before reaction

Sub-plugs from samples 724 and 1212 have been cut horizontally along a nominated plane of interest located near one of the sub-plug’s end and within the field of view of the pre-reaction tomogram images, and polished to obtain a flat surface. The polished section was imaged by Scanning Electron Microscope (SEM) to investigate textures and secondary porosity below the resolution of the pore-scale CT images. The high resolution 2D SEM image has then been registered into the 3D tomogram to find the perfectly matching slice (Figure 63).

The same section as used for SEM analysis was then analyzed by QEMSCAN® for quantified in situ mineralogy. The analysis was undertaken using a QEMSCAN® instrument at ANU, Canberra. This instrument comprises a scanning electron microscope with four light-element, energy dispersive X-ray spectrometers (EDS). QEMSCAN® utilizes a software suite (iMeasure) controlling automated data acquisition. The mineral maps were registered to the corresponding SEM images and into 3D tomograms (Figure 63). Modal mineralogies for both samples are summarised in Table 40, where the mineral map legend is also shown.

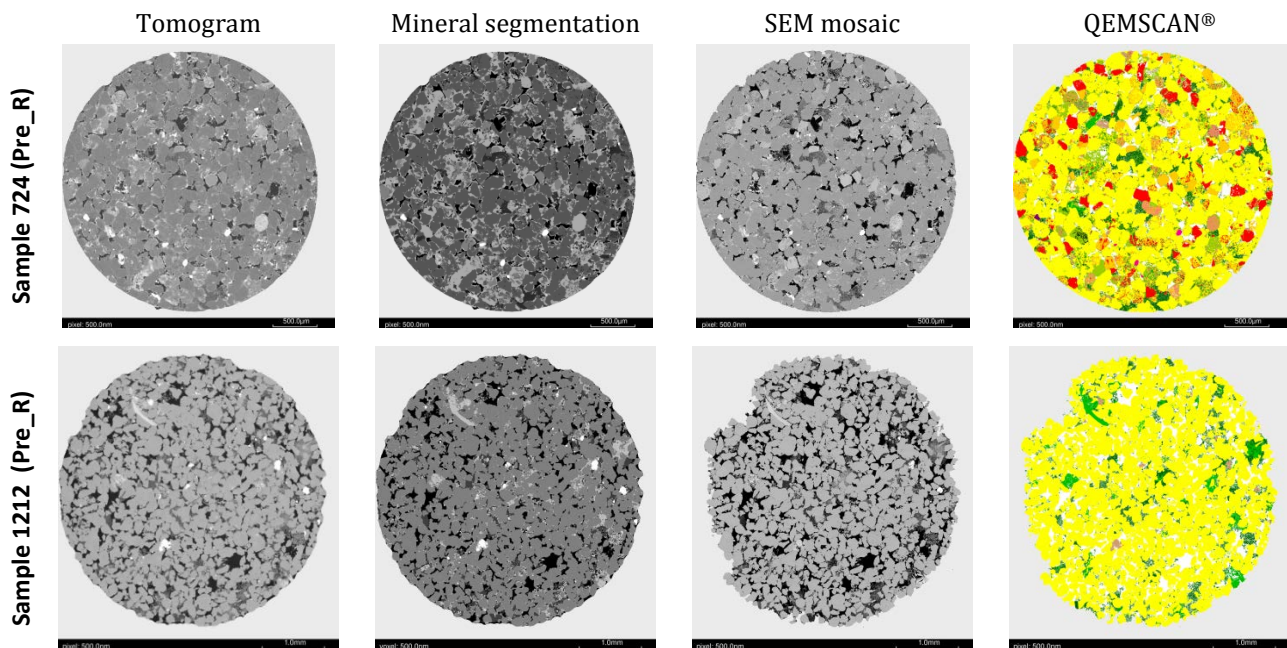
















Figure 63: SEM-registered images of samples 724 and 1212 from (left to right): tomogram, mineral segmentation, SEM and QEMSCAN® (see Table 40 for QEMSCAN® legend), before reaction.

QEMSCAN® is generally useful for gaining quantitative data on coarser grained rocks like sample 1212, while on very fine-grained or clay-rich lithologies similar to sample 724 it might be less useful because the interaction volume is too large to allow the accurate identification of minerals, often resulting in a higher proportion of unclassified minerals. In this specific case, however, we noticed that a large proportion of pixels originally identified as ‘unclassified’ had an elemental composition mostly consisting of K-Al-Si in various ratios which could be interpreted in most cases as a mixture of K-feldspar and chlorite minerals. Visual inspection of 2d:2d registered SEM and QEMSCAN® images would confirm the validity of this interpretation (Figure 64) and it was then decided to create a K-feldspar - chlorite mixture ‘phase’. As a result, the amount of unclassified pixels in sample 724 is quite low.

Table 40. Modal mineralogies (area%) of investigated polished sections of samples 724 and 1212, before reaction. QEMSCAN® legend is shown in the second column from left.

Mineral	QEMSCAN Legend	Sample 724 (Pre_R)	Sample 1212 (Pre_R)
Quartz		62.7	89.2
Alkali Feldspar		7.2	-
K Feldspar-Chlorite mixture		3.5	-
Plagioclase		7.4	-
Muscovite/Illite		1.35	3.5
Kaolinite		4.4	6.5
Chlorite		11.8	-
Calcite		-	-
Dolomite		-	-
Zircon		0.1	-
Rutile		0.8	0.7
Spinel		<0.1	-
Apatite		<0.1	-
Unclassified + traces		0.65	0.1
Total		100	100

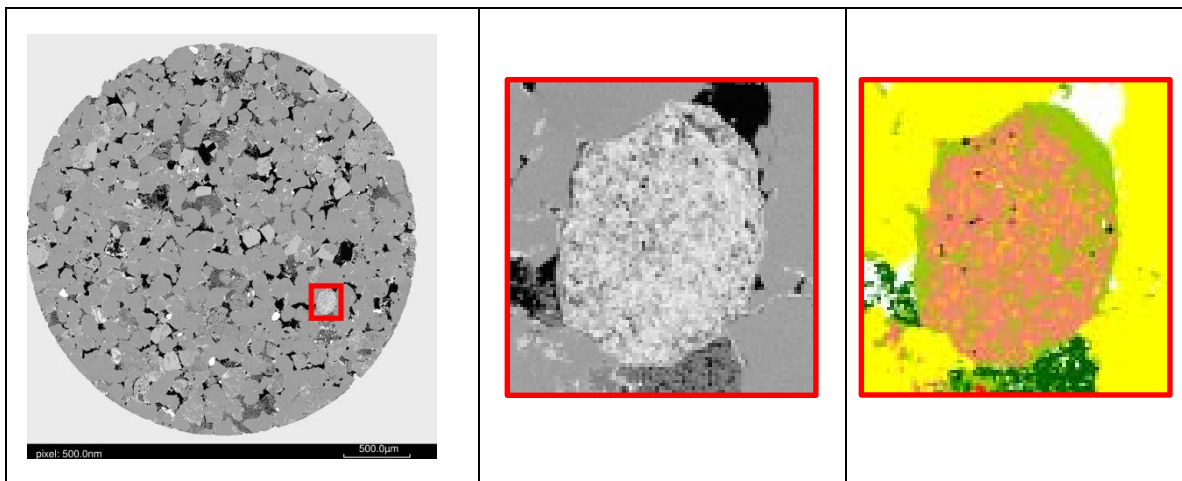


Figure 64: Sample 724: SEM image (left) and zoom-in area (centre) showing an altered K-feldspar grain; image to the right shows the grain's mineral map as analysed by QEMSCAN® (see Table 40 for mineral map legend); red polygon in left image shows location of zoom-in area.

Comparison between X-ray segmented phases (Table 39) and QEMSCAN® data (Table 40) of respective samples shows a good agreement. When comparing this data, it should be noted that the quantities listed in Table 40 represent the proportion of that mineral present in the 2D section that was investigated by QEMSCAN® (i.e. area%), whereas the quantities listed in Table 39 represent the proportion of that phase within the entire 3D sub-plug that was imaged by μ CT (i.e. volume%); furthermore, QEMSCAN® data does not include the amount of open pores.

In addition to the SEM mosaics shown in Figure 63, higher resolution SEM images were also collected. The purpose of these images was to identify and investigate phases most likely to show changes due to the reaction experiments such as high density (Fe-rich) minerals, loose grains and finer grained (usually pore-filling, -lining or bridging) material, and also to constrain the QEMSCAN® data processing.

Finally, information gained from analysis of the SEM and QEMSCAN® images was also very valuable in order to QC the outcome of the mineral segmentation process described in section 3.3.

3.5 Geochemical reactivity studies at University of Queensland

After the imaging program described in steps 1-4, the sub-plugs were posted to UQ for geochemical reactivity studies. There the sub-plugs were individually placed in Parr® reactor vessels (Figure 65) with supercritical CO₂ and water at 60°C and 12 MPa for ~2 months. Sample 724 was reacted in the presence of traces of SO₂ with a low salinity brine, and Sample 1212 was reacted in pure CO₂ with a high salinity and bicarbonate brine of complex chemistry, as described in detail in the accompanying final report for ANLEC project 7-1011-0189.

The sample was oven dried prior to shipping back to Canberra for post-reaction characterisation by μ CT imaging, SEM imaging, and QEMSCAN® analysis.

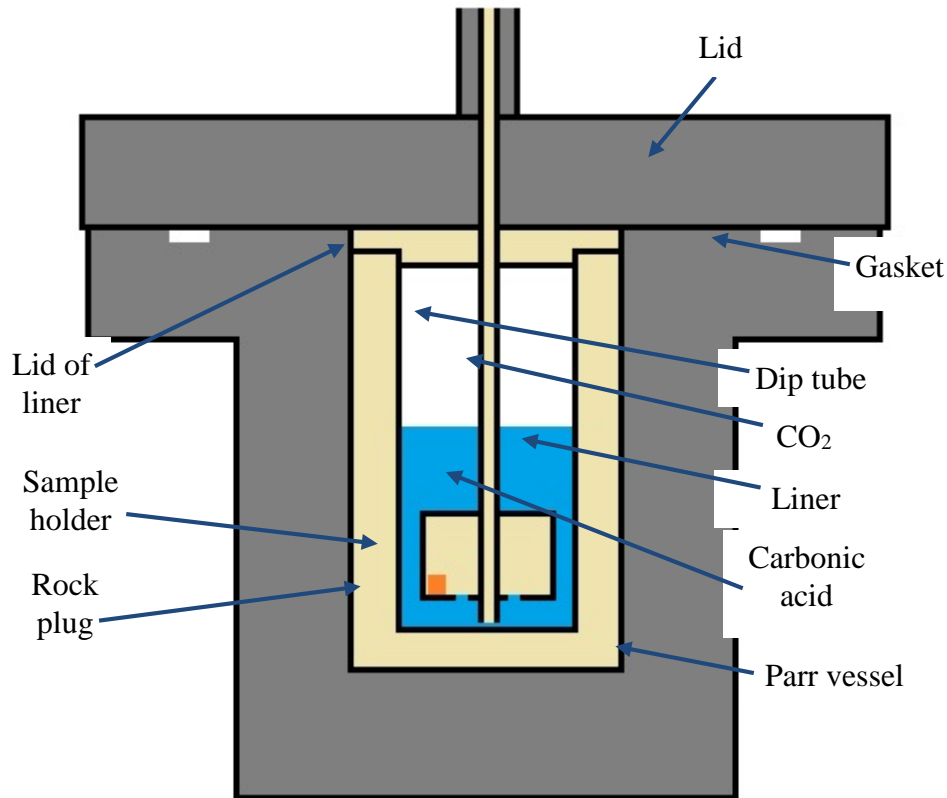


Figure 65: Diagram of the interior of the batch reactor vessel (Modified from Pearce *et al.*, 2015).

3.6 After reaction imaging of sub-plug in 3D by μ CT at the pore-scale and mineral segmentation into X-ray distinct components.

After reaction, sample 724 and 1212 sub-plugs were imaged by micro-CT as described in section 3.2 and for each sample the post-reaction tomogram was 3d:3d registered into perfect geometric alignment to the as-received state tomogram. The intensity histogram of the post-reaction tomogram was then normalized to the pre-reaction one so that same grains, if unaffected by reaction, would have an identical -or at least a very close- grey intensity value in both tomograms. Segmentation of X-ray distinct components in the after reaction 3D tomograms was then performed for the 724 and 1212 samples applying thresholds as close as possible to the thresholds used for the mineral segmentation of the pre-reaction images. This procedure allowed for a more direct and meaningful comparison between pre- and post-reaction mineral segmentation results (Table 41). Note that values shown in Table 41 have been calculated for the same 3d:3d registered volume of pre- and post-reaction sub-plug images, hence the slight difference with pre-reaction values shown in Table 39.

Vertically (X) and horizontally (Z) oriented views of high resolution 3D after reaction tomograms with the associated mineral segmented images are shown in Figure 66 for the two samples.

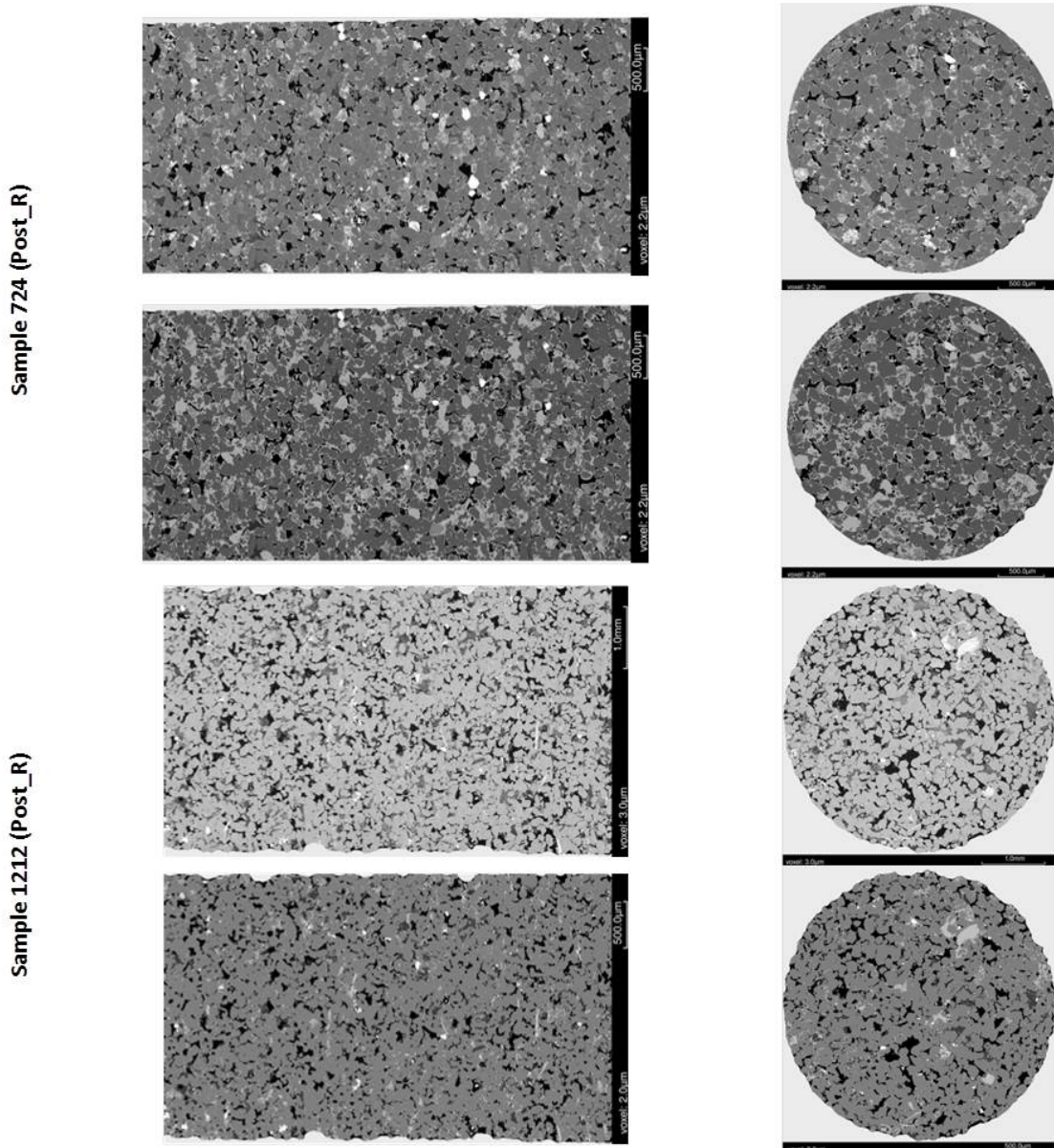


Figure 66: Sample 724 and 1212 vertical (X-left) and horizontal (Z-right) images from high resolution tomograms (row 1 & 3) and mineral segmented images (row 2 & 4), after reaction.

Table 41. Volume percentages of X-ray distinct components derived from segmentation of before and after reaction same volume of sub-plug scale images; where, Framework grain_1: mostly quartz + Na-plagioclase for 724, quartz for 1212; Framework grain_2: mostly K-feldspar; Lower density clay: mostly kaolinite; Higher density ‘clays’: mostly chlorite for 724, illite + muscovite for 1212; High density grain_1: mostly rutile; High density grain_2: mostly zircon.

Sample	Resolved porosity	Framework grain_1	Framework grain_2	Lower density Clay	Higher density ‘Clay’	High density Grain_1	High density Grain_2
724 (Pre_R)	7.0	54.95	11.6	4.45	21.6	0.2	0.1
724 (Post_R)	7.0	56.25	10.3	4.6	21.5	0.2	0.1
1212 (Pre_R)	11.1	73.3	-	8.0	7.2	0.45	-
1212 (Post_R)	11.4	73.4	-	7.7	7.1	0.45	-

Differences between pre- and post-reaction segmentation results are minimal and due probably mostly to minor differences between the normalized images gray intensities. It should also be noted that the distinction between Framework grain_1 and 2 is often not straightforward as the grey intensity values of the corresponding minerals (i.e. quartz, plagioclase and K-feldspar) in the tomogram images do partially overlap; in this case, for sample 724, by adding together the volume percentages of segmented Framework grain_1 and 2 one would obtain 66.55% for both the pre- and post-reaction images.

These results suggest that the reaction experiments are likely not to have caused significant detectable dissolution and/or precipitation of any major phase in either sub-plug, with no significant change in porosity.

3.7 After reaction SEM imaging and mineral mapping by automated quantified SEM-EDS

The after reaction sub-plugs from samples 724 and 1212 were cut horizontally along a nominated plane of interest located near the same sub-plug’s end where the polished section was created from the before-reaction samples (see section 3.4), so that the images (SEM and QEMSCAN®) that were subsequently acquired would as closely as possible represent a mirror-image of the plane previously investigated.

The new polished sections were imaged by SEM to investigate textures and secondary porosity below the resolution of the pore-scale CT images and then analyzed by QEMSCAN® for quantified in situ mineralogy.

The high resolution 2D SEM images have then been registered into the 3D pre- and post-reaction tomograms to find the perfectly matching slice, while the mineral maps were registered to the corresponding SEM images and then into the 3D tomograms too (Figure 67).

Modal mineralogies for the analyzed polished sections of the post-reaction samples are summarised in Table 42 where results of mineral analysis of the pre-reaction samples are also reported.

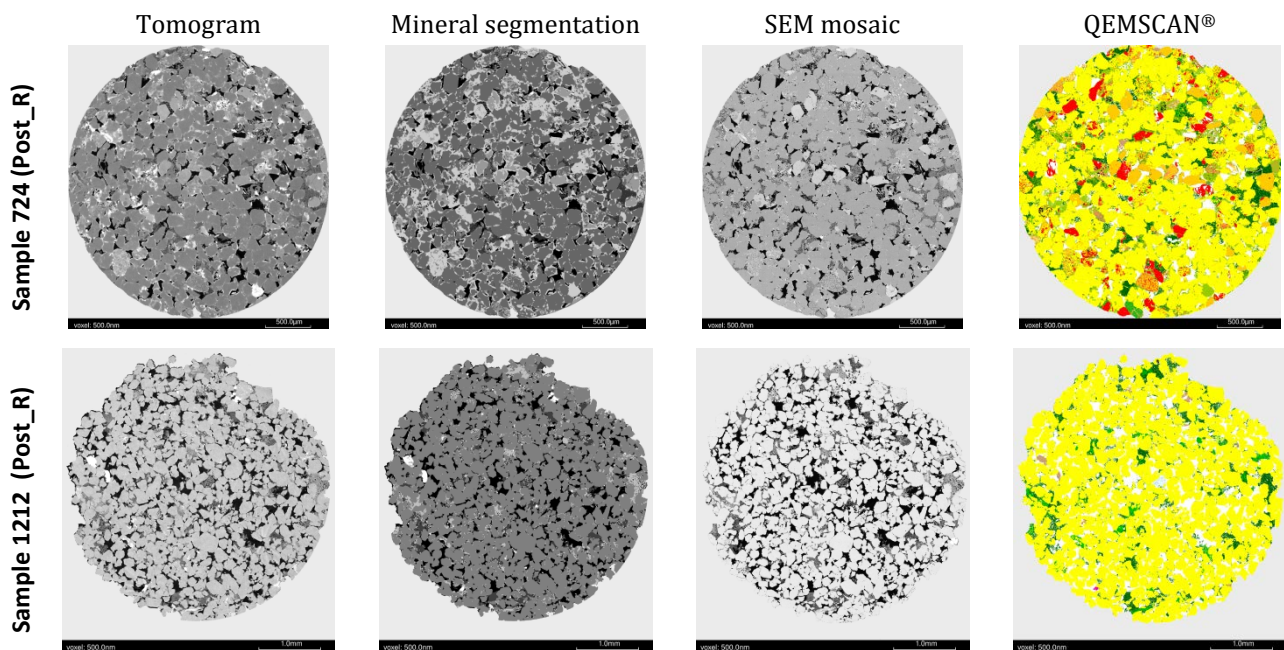
















Figure 67: SEM-registered images of samples 724 and 1212 from (left to right): tomogram, mineral segmentation, SEM and QEMSCAN® (see Table 42 for QEMSCAN® legend), after reaction.

Table 42. Modal mineralogies (area%) of investigated polished sections of samples 724 and 1212, before and after reaction. QEMSCAN® legend is shown in the second column from left. Note that the section investigated after reaction is not the same that was investigated before reaction.

Mineral	QEMSCAN Legend	Sample 724 (Pre_R)	Sample 724 (Post_R)	Sample 1212 (Pre_R)	Sample 1212 (Post_R)
Quartz		62.7	64.8	89.2	89.9
Alkali Feldspar		7.2	8.2	-	-
K Feldspar–Chlorite mixture		3.5	2.2	-	-
Plagioclase		7.4	5.3	-	-
Muscovite/Illite		1.35	1.2	3.5	2.2
Kaolinite		4.4	5.75	6.5	6.8
Chlorite		11.8	11.5	-	<0.1
Calcite		-	-	-	0.3
Dolomite		-	-	-	0.1
Zircon		0.1	<0.1	-	<0.1
Rutile		0.8	0.4	0.7	0.5
Spinel		<0.1	-	-	-
Apatite		<0.1	<0.1	-	-
Unclassified + traces		0.65	0.5	0.1	0.2
Total		100	100	100	100

3.8 Investigation and quantification in 3D of changes due to CO₂:brine:rock interactions

The 3d:3d registered before and after reaction tomograms of samples 724 and 1212 were analysed and compared to investigate and if/when possible quantify in 3D changes due to loss (dissolution) or gain (precipitation) of reactive minerals and/or movement and displacement of small grains and fine grained matter caused by the geochemical reactions with the carbonic acid formed in the reaction vessel.

Figures 68 and 69 show images of registered before and after reaction 3D tomograms of the two sub-plugs. A difference (before minus after) tomogram image was also created for both samples; differences, however, between tomograms in the pre- and post-reaction states were in general very small and for this reason images from the difference tomograms are here not shown. Instead for both samples some zoom-in images are shown that highlight what sort of differences were identified when comparing the before and after reaction tomograms.

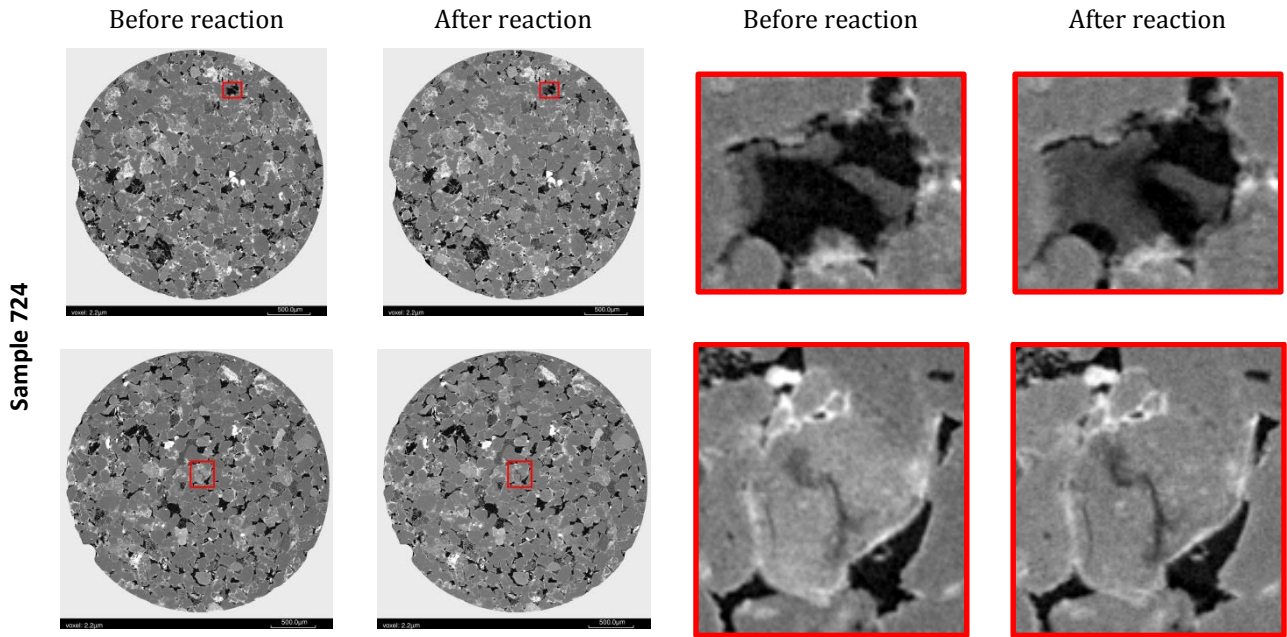


Figure 68: Sample 724: horizontal selected plane images (left) of before and after reaction tomograms and (right) zoom-in areas highlighting differences caused by reaction experiments; red polygon in left images shows location of zoom-in areas.

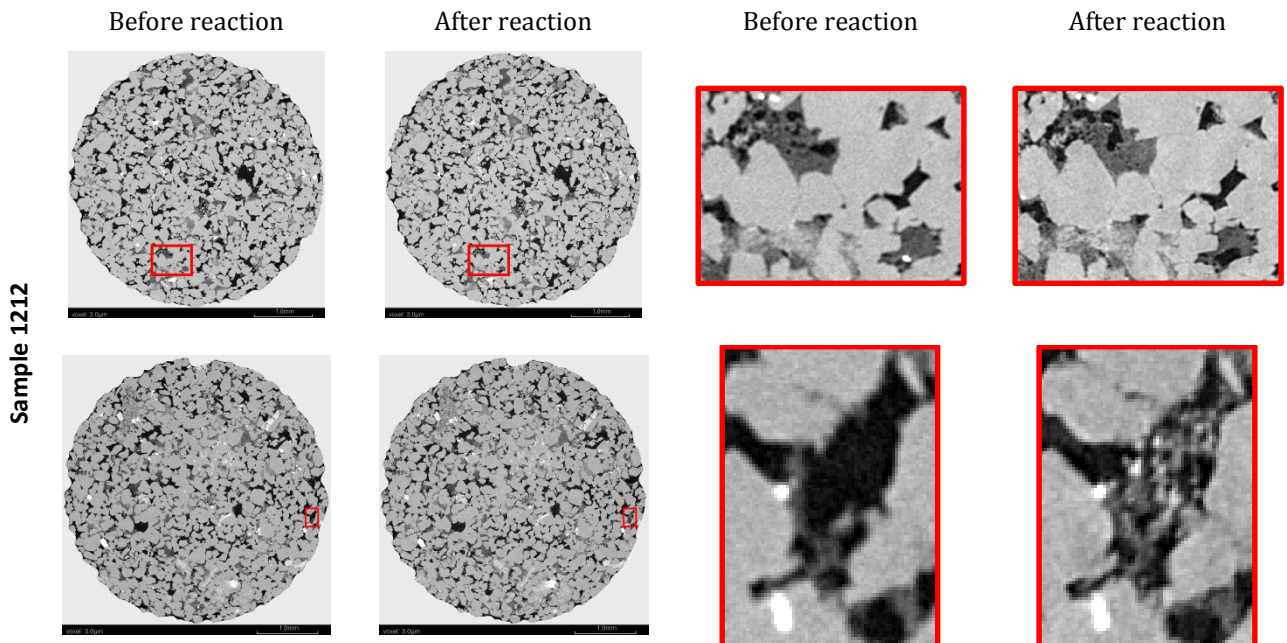


Figure 69: Sample 1212: horizontal selected plane images (left) of before and after reaction tomograms and (right) zoom-in areas highlighting differences caused by reaction experiments; red polygon in left images shows location of zoom-in areas.

Sample 724 (Hutton Sandstone) does not contain pore-filling calcite cement, which could partially dissolve during the reactivity experiments (e.g., Golab *et al.*, 2013), while it does contain considerable amount of potentially reactive Fe-rich chlorite. When chlorite is attacked by acid, leaching of cations often occurs (e.g., Fe, Mg, Al; Malmström *et al.*, 1996) and the chlorite's crystalline structure can be destroyed (Baker *et al.*, 1993). A slight decrease in density of solid material likely to be associated with Fe-rich chlorite has been detected in some of the post-reaction images (e.g., Fig. 68, bottom row images). It would seem that in those instances the chlorite might have lost some of its Fe³⁺ content due to reaction with the acid causing the decrease in density, this although without resulting in the creation of secondary porosity. Sampled geochemical reaction fluids did contain initially increasing concentrations of dissolved Fe up to ~85 mg/kg supporting this. Separately, some movement and/or displacement of matter (in general either fine-grained clay or small loose grains) has also been observed when comparing sample 724 pre- and post-reaction tomograms. Precipitation of small amounts of Fe bearing minerals (siderite or Fe-oxides) were observed on sister core blocks of 747 reacted with the sub-plug and analyzed by UQ. No mineral precipitation was however quantified in the sub-plug by QEMSCAN. The trace mineral content contained Fe-bearing minerals; however, it was not possible to determine if this was precipitated minerals or pre-existing fine grained Fe-chlorite. The amount of precipitated minerals may have been too low to detect or have not precipitated within the sub-plug pore space.

Sample 1212 (Precipice Sandstone) is about 73% by volume quartz and about 15% by volume clay/mica, with the remainder of the volume almost entirely occupied by porosity. This core sample does not contain sufficient reactive minerals to cause any detectable mineral dissolution, while also in this case movement and/or displacement of matter has been occasionally observed after reaction. Precipitation of very minor amounts of calcite and dolomite was quantified by QEMSCAN after reaction. Given the low reactivity of the minerals present in 1212, the calcite and dolomite likely precipitated from the ions present in the reaction brine. This is in agreement with calcite and dolomite precipitated on sister core blocks of 1212 and also a larger amount mainly precipitated in the reactor analyzed at UQ.

4 Conclusions

This study has confirmed the usefulness of digital core analysis to characterise the effects of geochemical reactions and textural changes in reservoir and seal / overburden lithologies as a result of CO₂:brine:rock interactions. Imaging and analytical techniques adopted in this study included the acquisition and registration of pre and post-reaction states 3D tomograms, SEM imaging (of a polished section in the field of view of the tomogram) and registration into the tomogram, and mineral mapping by QEMSCAN® (of the same polished section) and registration into the tomogram. The pore-scale imaging in 3D allowed the characterisation of pore-scale features and main structural and textural features, and the investigation of pore-filling material. The 3D tomograms were successfully segmented into resolved porosity and X-ray distinguishable minerals, their amounts calculated and compared between different states tomograms.

The 3d:3d perfect geometric alignment registration of before and after reaction tomograms allowed a direct comparison between the tomograms and the investigation and characterisation in 3D of their differences due to reaction with the carbonic acid at reservoir temperature and pressure.

In general differences between pre and post-reaction tomograms were very small and mostly the result of movement / displacement of small grains and / or fine-grained materials. No resolvable major mineral dissolution (loss of material) has been detected in either sample (with small changes in Hutton sample 747 possibly sample heterogeneity). Decreases in density in 747 were likely owing to Fe leaching from chlorite without quantifiable loss of material. Precipitation of small amounts of Fe bearing minerals (siderite or Fe-oxides) were observed on sister core blocks of 747 reacted with the sub-plug and analyzed by UQ. No mineral precipitation was however quantified in the sub-plug by QEMSCAN. The trace mineral content contained Fe-bearing minerals; however, it was not possible to determine if this was precipitated minerals or pre-existing fine grained Fe-chlorite. Very small traces of calcite and dolomite precipitated in sample 1212, likely originating from ions in the brine used in the experiment. This was in good agreement with characterisation of a sister core block and reaction water chemistry at UQ. No resolvable change in porosity was detected after reaction of Hutton sample 724, with a very slight potential increase in Precipice sample 1212 (which could also be from sample heterogeneity).

This study in combination with findings from previous works (e.g., Golab *et al.*, 2013c) confirmed that the unreactive, highly porous and permeable, sample of Precipice Sandstone here analysed would be a good CO₂ injection target. It also showed that small amounts of carbonates could precipitate in the pore space if brine containing dissolved Ca, Mg and bicarbonate were co-injected. It also showed that the sample 724 from the Hutton Sandstone formation, located almost 400m above the Precipice Sandstone sample, is unlikely to undergo significant changes in porosity or mineral content over short time scales at these conditions, should it ever be reached by the CO₂. However, some leaching of Fe from chlorite could make dissolved Fe available for mineral trapping over longer time scales. Previous work showed more significant changes (in terms of porosity and mineral content) in a calcite cemented Hutton core sample, where calcite dissolution was observed with pure CO₂, and additionally gypsum precipitation with higher concentrations of SO₂ and O₂ in the CO₂. The precipitation of gypsum has the potential to plug pores over longer time scales; however, this was not investigated. The potential movement of fine clay material observed in the samples could be an important observation in terms of changes in permeability if the displacement of fine matter causes blocking of pore throats. Determining permeability changes on reaction were however not within the scope of this project.

CO2CRC Limited

Level 1, 700 Swanston Street, bldg. 290

The University of Melbourne

Victoria 3010 Australia

p: +61 3 8595 9600

e: info@co2crc.com.au

www.co2crc.com.au



[Follow us on Twitter@CCS_research](https://twitter.com/CCS_research)

BUILDING A LOW-EMISSIONS FUTURE

